VERA MÓNICA LEMOS DA SILVA

LRH-1 SIGNALING AND CONTROL OF LIVER INTERMEDIARY METABOLISM: IMPACT ON NONALCOHOLIC FATTY LIVER DISEASE

Tese de Candidatura ao grau de Doutor em Biologia Básica e Aplicada submetida ao Instituto de Ciências Biomédicas Abel Salazar da Universidade do Porto

Orientador – Doutora Kristina Schoonjans
Categoria – Associate Professor
Afiliação – Institute of Bioengineering, École polytechnique fédérale de Lausanne

Co-orientador – Doutor Vítor Costa
Categoria – Professor Associado
Afiliação – Instituto de Ciências Biomédicas Abel Salazar, Universidade do Porto

Co-orientador – Doutor Pedro Gomes
Categoria – Post-doc, Professor Auxiliar Convidado
Afiliação – Facudade de Medicina, Universidade do Porto

All the experimental work presented here was conducted in the context of the Graduate Program in Areas of Basic and Applied Biology (GABBA) – 16th Edition at the École polytechnique fédérale de Lausanne (EPFL) and financially supported by the Portuguese Foundation for Science and Technology (FCT) – Fellowship #SFRH/BD/52046/2012 and Swiss National Science Foundation (31003A_1666695 and CRSII3_160798/1).

SWISS NATIONAL SCIENCE FOUNDATION

The following articles were used to write this thesis:

- Lemos V*, Stein S*, Xu P, Demagny H, Wang X, Ryu D, Jimenez V, Bosch F, Lüscher TF, Oosterveer MH, Schoonjans K. Impaired SUMOylation of nuclear receptor LRH-1 promotes nonalcoholic fatty liver disease. J Clin Invest. **2017** Feb 1;127(2):583-592. PMID: 28094767. **Chapter IV. original article in supplementary material.**
- Lemos V, Moullan N, Perino A, Sajic T, Jha P, Jimenez V, Aebersold R, Bosch F, Schoonjans K. Fasting-induced steatosis driven by loss of LRH-1 in the liver is rescued by SLC25A47. **In preparation. Chapter V. Original manuscript figures and details in supplementary material.**
- Lemos V, Moullan N, Perino A, Cirauqui N, Jimenez V, Dal Peraro M, Bosch F, Schoonjans, K. Liver-specific mitochondrial carrier SLC25A47 enhances fatty acid oxidation and is downregulated in NAFLD. **In preparation. Chapter V. Original manuscript figures and details in supplementary material.**

Other articles published during my PhD:

- Velazquez-Villegas L*, Perino A*, Lemos V, Zietak M, Nomura M, Pols TWH, Schoonjans K. TGR5 signaling promotes mitochondrial fission and beige remodeling of white adipose tissue. Nat Commun. **2017**. In press
- Item F, Wueest S, Lemos V, Stein S, Lucchini FC, Denzler R, Fisser MC, Challa TD, Pirinen E, Kim Y, *et al*. Fas cell surface death receptor controls hepatic lipid metabolism by regulating mitochondrial function. Nat Commun. **2017** Sep 7;8(1). PMID: 28883393.
- Gariani K, Ryu D*, Menzies KJ*, Yi HS, Stein S, Zhang H, Perino A, Lemos V, Katsyuba E, *et al*. Inhibiting poly ADP-ribosylation increases fatty acid oxidation and protects against fatty liver disease. J Hepatology. **2017**; 66(1):132-141. PMID: 27663419.
- Gariani K*, Menzies KJ*, Ryu D, Wegner CJ, Wang X, Ropelle ER, Moullan N, Zhang H, Perino A, Lemos V, *et al*. Eliciting the mitochondrial unfolded protein response by nicotinamide adenine dinucleotide repletion reverses fatty liver disease in mice. Hepatology. **2016**; 63(4):1190-204. PMID: 26404765.
- Stein S, Oosterveer MH, Mataki C, Xu P, Lemos V, Havinga R, Dittner C, *et al*. SUMOylation-dependent LRH-1/PROX1 interaction promotes atherosclerosis by decreasing hepatic reverse cholesterol transport. Cell Metabolism. **2014** Oct 7;20(4):603-13. PMID: 25176150.

*authors contributed equally

To my mother and grandmother, Isolina and Lucília…

Acknowledgements

Acknowledgements

In my last year in college to become a nutritionist, I got the chance to do scientific research for my internship together with the clinical part thanks to Prof. Alejandro Santos' advice. For this reason and first of all, I would like to leave my deep appreciation to Dr. Pedro Gomes with whom I got introduced to the scientific world. If it weren't for him, I wouldn't be here today because I would have never thought of doing research. I stayed with him even after I graduated, learning more and more and struggling together facing all difficulties to contribute to the metabolism field. He saw potential in me and advised me to pursue a carrier in science abroad in a competitive lab and therefore I am here.

Second of all, I would like to leave here a special thanks to Professor Kristina Schoonjans for taking me as a PhD student, her first exchange student. She gave me the opportunity to perform my thesis work on mitochondria and on metabolic diseases, letting me follow my ideas and guiding me to succeed on them.

I thank also Prof. Vítor Costa for having accepted being my mentor from UP. For his support and guidance through the years, even before I started my PhD.

I would also like to thank Professor Johan Auwerx since it was due to him that I came to this lab. He decided I was worth it and asked me to join the lab. It is also worth mentioning the insightful scientific discussions we got to have along the years that helped me to conduct my studies.

Sokrates (Soki), for all the advice and scientific discussions, for guidance and support and of course, for the work we shared together, side by side analyzing "brown things". If you see this you would say that it was not all scientific so I want to thank you also for your friendship and all the funny moments and relaxing times together. Cheers to that!

Pan, I couldn't include you just in a general thank you but of course in a personal one. You were one of the first that I became friends with especially from our LRH-1 team. We shared a lot scientifically and personally. I thank your support and advices; chats and confidentialities, gossips and memos and I hope our friendship forever holds.

Dongryeol, for all your wisdom and all the advices (and they were a lot). You always knew everything about everything and were always willing to help. My deep thanks to you and I hope everything will be bright in your future and full of success.

Pedro and Olli, no words can describe how much the lab misses you. You shared not only your scientific knowledge but especially your good humor and friendship, making it all easy to bare. Special thanks for all the good moments spent outside the lab.

Francesca, for all the times we spent together inside and outside the lab. For your laughter and your friendship I will be forever in your debt. You were a very recent but very significant additional asset in my life. Grazie mille!

Alessia, thanks for your inspiration, scientific help and endless friendship. You were always there when I needed ready to help and advice. Thanks for all the activities outside the lab and all the gifts for special occasions. I hope I will always have your friendship around!

Pooja, it was the nicest thing to have you next to me these past years. We learned a lot with each other. We struggled through R together and managed to succeed. Thanks for your kind words and inspiring laughter. I hope you fulfill all your dreams.

Norman, thank you so much for all your help. Without you, none of my mice would be ready for experiments. ☺ Furthermore, thanks for all the funny moments and good times during work time.

Thibaud, Roxanne, Sabrina, for all the technical help. You are the best technicians any lab could ever ask for. A very special extra one to thank Andréanne (Andie) for her friendship and very special laughter. I am very glad that you joined the lab and to have had you in the desk just in front of me. It was much more fun!

Charlotte, Vincenzo, Mario, Pirkka-Pekka, Davide, Dina, Melanie, Giovanni, Alexis, Laura, Marika for all the good times outside the lab. You definitely helped to improve the life in Lausanne and made it feel like home. And thanks to all the other past and present members of the lab for the help one way or another.

Lastly, but definitely not least, Elena and Adrienne. I cannot occupy a lot of my thesis space for acknowledgments otherwise I would have pages and pages of special and personal thanks to everybody and especially to you. All these years, the life in the lab was amazing due to all the special friends I made. You girls together with Alessia and Pan were my best friends, supporting and cheering me up, laughing with me. Thanks to all the girls' night out and the sushi nights. You will be forever with me.

To my fellow PhDs, GABBA16, all the thanks in the world for a very good start of the PhD life. All your help was crucial for a very motivated and excited first year of PhD.

Soraia, por seres a pessoa que és. És a minha melhor amiga e sempre me apoiaste nesta decisão apesar de isso significar a minha saída de Portugal. A partida não foi fácil e a distância não ajudou mas tudo superamos e a amizade persiste.

Obviamente que nada mesmo seria possível sem a ajuda dos meus pais, minha avó e irmã que sempre me motivaram a seguir os meus sonhos, portanto um grande obrigado pelo apoio e motivação.

Finally, I saved you for last Riccardo. The reason is obvious but worth emphasizing. You were my best surprise during the PhD. You helped me throughout the PhD life, encouraging me to surpass any difficult time. I thank you for that and for always being there for me, through the bad and good times. Hope it will continue forever.

Abstract

Abstract

Nonalcoholic fatty liver disease (NAFLD) is the most common liver disease in the western countries. The primary stage and therefore risk factor for NAFLD is an abnormal lipid accumulation in the liver, which is termed hepatic steatosis. Despite the high prevalence of NAFLD, there is no efficient treatment exist for this disease. Gaining insight into the molecular pathways and metabolic regulators involved in the development of NAFLD is hence a prerequisite to design and develop novel and effective therapeutic strategies.

In this thesis, we have established the role of the nuclear receptor LRH-1 as a key regulator in the development of NAFLD by regulating both *de novo* lipogenesis and fatty acid oxidation, pivotal pathways in hepatic lipid metabolism. We observed that increasing the transcriptional activity of LRH-1 under a refeeding condition led to SREBP-1c-dependent rise in the rate of fatty acid synthesis. On the other hand, loss of LRH-1 in the liver impaired fatty acid oxidation under fasting conditions. In turn both conditions led to hepatic steatosis. Moreover, two players in the above-mentioned phenotypes were identified as novel LRH-1 target genes, the oxysterol-binding protein OSBPL3 and the mitochondrial transporter SLC25A47.

Furthermore, diet-induced NAFLD models presented increased and decreased levels of OSBPL3 and SLC25A47, respectively, suggesting that targeting these two proteins could be effective in the treatment of NAFLD. Furthermore, we characterized the biological role of the poorly studied mitochondrial transporter, SLC25A47, and identified this protein as an important determinant of liver mitochondria function.

Collectively, these studies unveil the importance of fine-tuning LRH-1 expression/activity to prevent the development of complex diseases such as NAFLD. Additionally, this thesis work highlights SLC25A47 as a novel target to treat or prevent NAFLD. Further studies will be required to fully understand the therapeutic significance of these druggable targets.

Resumo

Resumo

A doença do fígado gordo não alcoólico (DFGNA) é a doença do fígado mais comum nos países ocidentais. O primeiro estágio e portanto fator de risco para DFGNA é a acumulação anormal de lípidos no fígado, chamada de esteatose hepática. Apesar da elevada prevalência, atualmente não há nenhum tratamento eficiente para esta doença. Ganhar mais conhecimento sobre as vias e reguladores metabólicos que estão envolvidos no desenvolvimento da DFGNA é então um pré-requisito para planear e desenvolver estratégias terapêuticas novas e eficazes.

Nesta tese, nós estabelecemos o papel do receptor nuclear LRH-1 como um regulador metabólico essencial no desenvolvimento da DFGNA ao regular tanto a síntese de lípidos como a oxidação dos ácidos gordos, vias metabólicas fundamentais no metabolismo lipídico hepático. Nós observamos que aumentando a atividade de transcrição de LRH-1 numa condição de realimentação (saciedade) levou a um aumento da síntese de lípidos dependente de SREBP-1c. Por outro lado, a perda de LRH-1 no fígado sob jejum comprometeu a oxidação dos ácidos gordos na mitocôndria. Ambas situações levaram a esteatose hepática. Além disso, dois intervenientes nestes fenótipos foram identificados como genes alvo da atividade de transcrição de LRH-1, a proteína de ligação a oxisteróis OSBPL3 e o transportador mitocondrial SLC25A47.

Modelos de DFGNA induzidos por dietas apresentam níveis aumentados e diminuídos de OSBPL3 e SLC25A47, respetivamente, sugerindo que desenvolver compostos que atuem sobre estas proteínas poderão ser eficientes no tratamento de DFGNA. Adicionalmente, nós caracterizamos o papel biológico de SLC25A47, um transportador mitocondrial muito pouco estudado até agora, e identificamos esta proteína como um determinante da função mitocondrial hepática.

Coletivamente, estes estudos desvendam a importância de "afinar" corretamente a expressão/atividade de LRH-1 para prevenir o desenvolvimento de doenças complexas como a DFGNA. Mais ainda, o trabalho nesta tese destaca SLC25A47 como um novo alvo para tratar ou prevenir DFGNA. Estudos adicionais são necessários para compreender o significado terapêutico destas proteínas.

List of abbreviations

List of abbreviations

1CC – one-carbon cycle
ABC – ATP binding cassette
ADP – adenosine diphosphate
AF2 – activation factor 2
ALAT – alanine aminotransferase
Alb - albumin
APO – apoliprotein
APR – acute phase response
ASAT – aspartate aminotransferase
ATGL – adipocyte TG hydrolase
ATP – adenosine triphosphate
BA – bile acids
BN-PAGE - blue native- polyacrylamide gel electrophoresis
BSEP – bile acid export pump (ABCB11)
CD36 – fatty acid translocase
ChD – choline-deficient diet
ChREBP - carbohydrate response element-binding protein
CI-V – mitochondrial complexes I-V
CMV - cytomegalovirus
CoQ - coenzyme Q
Cyt c – cytochrome c
DBD – DNA-binding domain
ddH_2O - double-distilled water
DLPC - dilauroyl phosphatidylcholine
DNL – *de novo* lipogenesis
ER – endoplasmic reticulum
ES – embryonic stem cells
ETC – electron transport chain
eWAT – epididymal white adipose tissue
FA – fatty acids
$FADH_2$ - flavin adenine dinucleotide reduced form
FAO – fatty acid oxidation
FASN – fatty acid synthase
FBS – fetal bovine serum

FFA – free fatty acids
FLI – fatty liver index
Ftz-F1 - fushi tarazu factor 1
G6P – glucose-6-phosphate
GCK – glucokinase
GEO – gene expression omnibus
GGT - gamma-glutamyl-transferase
GNMT - glycine-n-methyltransferase
H&E – Hematoxylin and Eosin staining
HCC - hepatocellular carcinoma
HDL – high-density lipoprotein
HNF4 - hepatocyte nuclear factor-4
HSL – hormone-sensitive lipase
IMM – inner mitochondrial membrane
IMS – intermembrane space
KO – knockout
KRAP - ki-ras-induced-induced actin-interacting protein
LAP- lipid accumulation product
LBD – ligand binding domain
LCAD - long chain acyl-CoA dehydrogenase
LRH-1 - liver receptor homolog-1
LXR - liver X receptor
MCAD - medium-chain acylcoenzyme-A dehydrogenase
MCD – methionine and choline deficient diet
MCs – mitochondrial carriers
MDR2 – multidrug resistance 2
MRI - magnetic resonance imaging
mRNA – messenger ribonucleic acid
MRP3 – multidrug resistance protein 3
mtDNA – mitochondrial DNA
MTTP - microsomal TG transfer protein
NAD - nicotinamide adenine dinucleotide
NADH - nicotinamide adenine dinucleotide reduced form
NAFLD - nonalcoholic fatty liver disease
NASH - nonalcoholic steatohepatitis
NRs – nuclear receptors

OCR – oxygen consumption rate
OMM – outer mitochondrial membrane
ON - overnight
OXPHOS – oxidative phosphorlylation
PC – phosphatidylcholine
PGC-1α - peroxisome proliferator-activated receptor γ-coactivator-1α
PKA – Protein kinase A
PNPLA3 - Patatin-like phospholipase domain containing 3
PROX1 - prospero homeobox protein 1
PS – penicillin- streptomycin
PTM – post-translational modifications
RER – respiratory exchange ratio
ROS – reactive oxygen species
RXR – retinoid X receptor
SAM - S-adenosylmethionine
SCAFI – supercomplex assembly factor I
SCD-1 – stearoyl-CoA desaturase-1
SCs – supercomplexes
SEM – standard error of the mean
SLC – solute carrier
SLC25A47 – solute carrier family 25 member 47
SR-BI - scavenger receptor class B type I
SRC-2 - steroid receptor coactivator-2
Srebf1, SREBP1 – sterol element binding protein 1
SUMO-1 – small ubiquitin-like modifier
T2DM - type 2 diabetes mellitus
TCA – tricarboxylic acid cycle
TG – triglycerides
UCP1 – uncoupling protein 1
VLCAD – very long chain acyl-CoA dehydrogenase
VLDL – very low density lipoproteins

Table of Contents

Table of Contents

“Metabolites, after all, are the ultimate molecular arbiters of biological function…“

Jeffrey Perkel

Chapter I

General Introduction

Section 1

Nonalcoholic Fatty Liver Disease and its determinants

Chapter I General Introduction

I. Section 1 Nonalcoholic fatty liver disease

I.1.1 NAFLD and obesity

From hunter-gatherers to farmers where food availability to survive was inconsistent and unpredictable, humans nowadays are facing a massive overnutrition. More and more the production of calories at low cost sustains the increase of the new world epidemic called obesity. Excessive consumption of calories has become a global phenomenon (Figure I.1). Currently, it is estimated that worldwide there are about 2 billion (34% of men and 35% of women) overweight and over 600 million (10% of men and 13% of women) obese adults with body mass indices over 30kg/m^2 (World Health Organization).

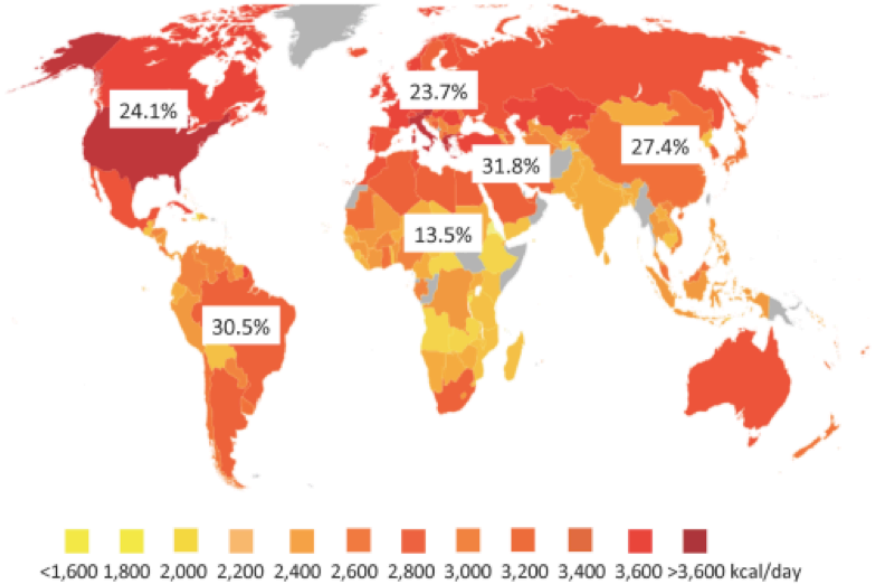

Figure I.1. World caloric intake distribution and prevalence (%) of non-alcoholic fatty liver disease (NAFLD) (1).

Considering human biology and the path that we have trailed since pre-historical times, one can easily state that the human organism is not ready to cope with these overfeeding patterns. The resulting excess in body fat is the main trigger for metabolic disturbances that culminate in several diseases (Figure I.2). Being one of the obesity-associated morbidities, nonalcoholic fatty liver disease (NAFLD) is the most common liver disease and its prevalence increases with the growing obesity epidemic. NAFLD is now regarded as the liver manifestation of the metabolic syndrome.

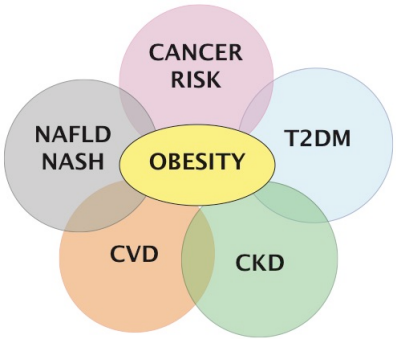

Figure I.2. Medical complications related to obesity.
NAFLD, nonalcoholic fatty liver disease; NASH, nonalcoholic steatohepatitis; CVD, cardiovascular disease, CKD, chronic kidney disease; T2DM, Type 2 *Diabetes Mellitus*.

I.1.2 Definition of NAFLD

NAFLD is a spectrum of disorders, of which the earliest stage is characterized by the deposition of lipid droplets within the cytoplasm of the hepatocytes (hepatic steatosis – fatty liver). The progressive fat accumulation increases the susceptibility to hepatocyte damage and inflammation, a condition termed nonalcoholic steatohepatitis (NASH) that can progress to cirrhosis and may ultimately lead to hepatocellular carcinoma (HCC) (2-4) (Figure I.3).

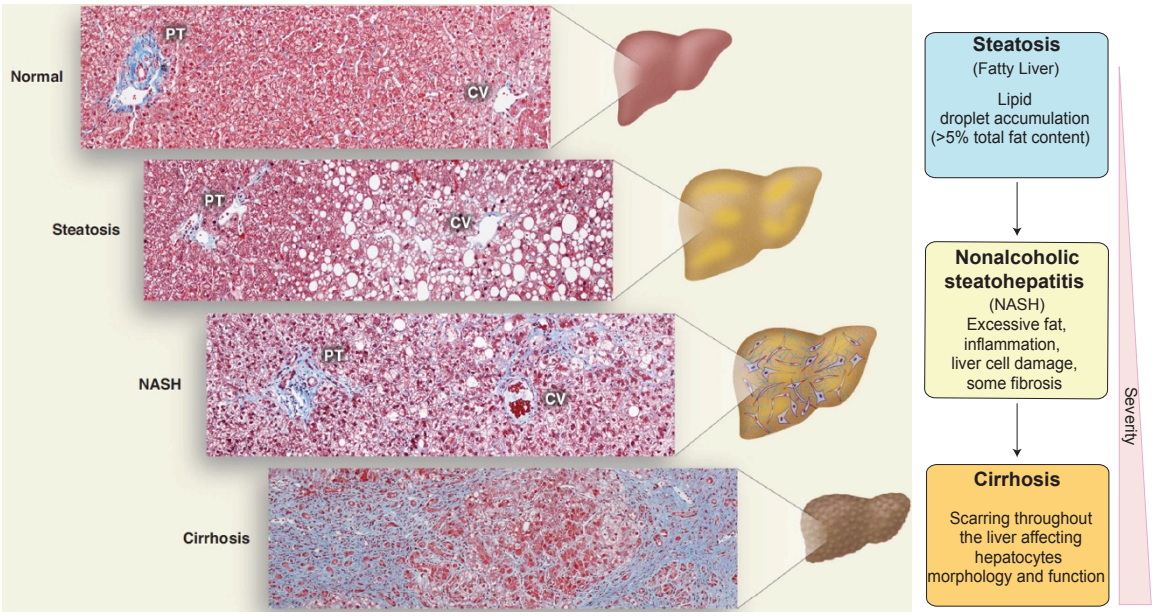

Figure I.3. The disease spectrum of NAFLD. Adapted from (2)

Each stage within this disease has its own features (Figure I.3). While the first manifestation of the disease is mainly represented by lipid accumulation (steatosis), the next stages comprise a whole rearrangement of structure and

compromised liver function. Inflammation, cell damage, fibrosis, along with excessive fat accumulation, characterizes NASH. Cirrhosis is the most severe stage of NAFLD and can be distinguished by a pronounced scarring of the tissue (fibrosis) that alters the whole morphology and polarization/zonation of the hepatocytes.

I.1.3 Prevalence and risk factors of NAFLD

NAFLD is a complex disease that affects almost one third of the adult population worldwide, however, its prevalence is not fully predicted by the total caloric intake (Figure I.1) (1). This emphasizes the complexity of NAFLD and it hints at the importance of factors other than body mass index or daily caloric excess in the pathophysiology of NAFLD. Of interest, multiethnic population-based studies showed that NAFLD varies in prevalence among ethnic groups, with African Americans having the lowest (24%) and Hispanics the highest (45%) prevalence (5, 6), validating genetic susceptibility as an important contributing factor. Hepatic steatosis, NASH, and cirrhosis cluster in families, with the heritability of NAFLD being estimated to be ~39% (7).

Although single-gene mutations cause rare forms of severe steatosis, the increased prevalence of NAFLD in the general population over the past 30 years is due to changes in the quantity and composition of food. Diets high in fat are major contributors to NAFLD but carbohydrates in general and fructose in particular, play important roles as well. Fructose is a highly lipogenic sugar found in food and beverages consumed worldwide. Glucose and fructose differ in several ways. Fructose is poorly absorbed in the small intestine and is cleared from the blood in the liver on the first pass and metabolized in the hepatocytes. The mechanism of transport and utilization are independent of insulin action and phosphofrutokinase regulation step (8-10). The action of frutokinase is also 10 times faster than glucokinase (GCK) and hexokinase leading to the accumulation of fructose-1-phosphate in the liver and a rapid drop of ATP levels. Fructose-1-phosphate can then be converted into substrates for gluconeogenesis, glycolysis and *de novo* lipogenesis (DNL) in a relatively unregulated fashion (9). Therefore, high fructose intake leads to increased hepatic lipogenesis rapidly promoting lipid accumulation.

Due to the close association of NAFLD with the presence and severity of obesity, studies in morbidly obese people (BMI> 35kg/m^2) undergoing bariatric

surgery reported the incidence of NAFLD of 91% (11). 70% of type 2 diabetes mellitus (T2DM) patients present NAFLD (12) (Figure I.4). This rising trend of NAFLD is alarming, and it is of particular concern in the pediatric population where studies in children have verified a general prevalence of 3% that increases to 53% in obese children (13).

Besides race and ethnicity, genetic variations and concomitant presence with other metabolic disturbances, gender (31% men vs 16% women) and age (46% in geriatric population) also seem to predispose to NAFLD (14).

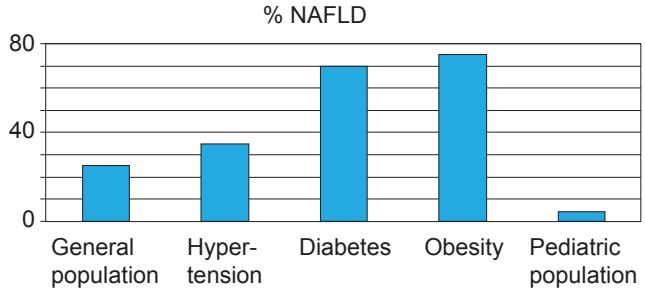

Figure I.4. Prevalence of NAFLD. Adapted from (13).

I.1.4 Diagnosis of NAFLD

Analysis of liver biopsies has been proven to be the most effective method to diagnose fatty liver, however, it is a very invasive method to be applied in human diagnostics. Moreover, they are discretionary in nature and rely on histological scoring. Thus, several non-invasive diagnostic methods for NAFLD and NASH have been introduced recently in human studies. Non-invasive radiological methods used to assess the prevalence of fatty liver include magnetic resonance imaging (MRI) and ultrasonography (15-17). Other studies rely on the monitoring of the liver enzymes, alanine aminotransferase (ALAT) and aspartate aminotransferase (ASAT) in the blood, as non-invasive indicators of NAFLD (18-20). Finally, classification protocols exist based on measured clinical variables, such as Fatty Liver Index (FLI) composed of BMI, waist circumference, triglycerides (TG) and gamma-glutamyl-transferase (GGT) (21), and Lipid Accumulation Product (LAP) with waist circumference and fasting TG (22).

Although these methods have been applied to diagnose this liver condition, NAFLD is often an asymptomatic disease in which blood tests may be completely normal. Furthermore, radiological methods are known to be sensitive only when more than one third of the liver is affected by steatosis (13). These facts have made studies on prevalence of NAFLD very difficult emphasizing how underestimated the prevalence of NAFLD may be. Therefore and since invasive

liver biopsies are still the only method to accurately diagnose NAFLD, there is an urgent need to find novel biomarkers that could surpass this diagnostic challenge, ultimately leading to better and earlier treatment.

I.1.5 Natural history of NAFLD

The long-term prognosis of NAFLD largely depends on the stage of the disease, ranging from mild to very severe (Figure I.5). On the other hand, NAFLD has a good short-term prognosis. From patients presenting simple hepatic steatosis, only 12-40% will develop NASH with early fibrosis in 8 to 13 years. 13% of patients presenting with NASH will develop cirrhosis and/or evidence of hepatic decompensation in the same time period. While about 50% of patients presenting cirrhosis will require a liver transplant or die from liver failure, 7% will develop HCC within 10 years (Figure I.5). For this reason, the described relation between HCC, obesity and diabetes can only be partly explained by NAFLD (23).

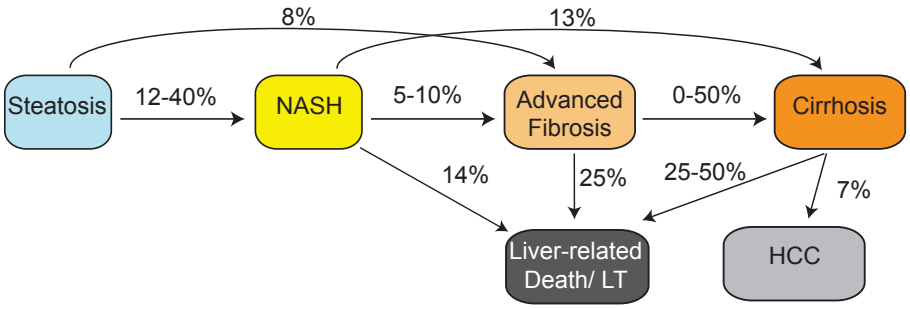

Figure I.5. Natural history of NAFLD over 8-13 years.
NASH, nonalcoholic steatohepatitis; HCC, hepatocellular carcinoma; LT, Liver Transplant. Adapted from (13).

I.1.6 Pathogenesis of hepatic steatosis

In the course of evolution, TG have turned into the preferred and most reliable source of stored energy as a mean to cope with variations in energy demand and availability. TG provide the greatest amount of energy (9 kcal/g) compared to other macronutrients, proteins and carbohydrates, and their hydrophobic nature allows efficient accumulation and storage without engendering osmotic effects on the cell. TG are primarily stored in adipocytes but can accumulate in other cell types upon specific and unusual conditions. For instance, migratory birds accumulate TG in their liver (*fois gras*) as a preparation for their seasonal flights. Humans also accumulate TG in their liver after caloric excess; however, this condition has no physiological advantage. Because the liver does not serve as a prime location for fat storage, the steady state concentration of hepatic TG is low

under physiological conditions. TG are assembled *via* ester bonds between fatty acids and glycerol. Hepatic TG formation relies on the supply of fatty acids from three sources: diet, adipose tissue or *de novo* synthesis (Figure I.6).

The excessive accumulation of TG in the liver is a consequence of an imbalance between the acquisition and disposal of fatty acids (FA). Increased hepatic uptake of adipose tissue or diet-derived fatty acids, defective breakdown via β-oxidation, reduced very-low density lipoproteins (VLDL)-triglyceride secretion or induced activity of master regulators of DNL, such as the transcription factor sterol element binding protein 1 (SREBP-1) and carbohydrate responsive element-binding protein (ChREBP), are factors that contribute to the development of steatosis (2) (Figure I.6).

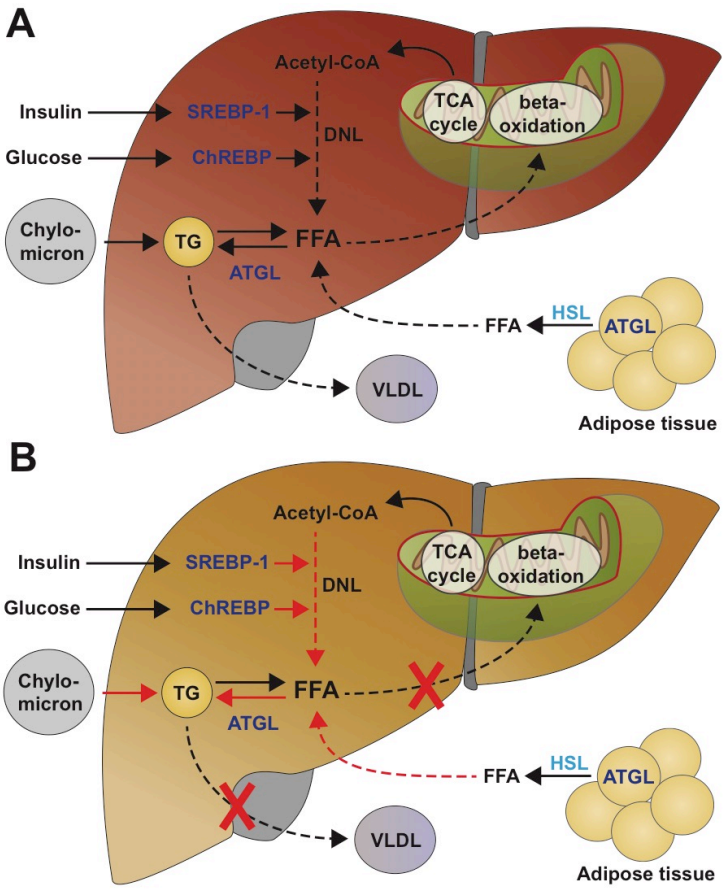

Figure I.6. Metabolic pathways impacting on NAFLD.
(**A**) Normal liver. (**B**) Liver with NAFLD. DNL, *de novo* lipogenesis; TG, triglycerides; TCA cycle, tricarboxylic acid cycle; FFA, free fatty acids; VLDL, very low density lipoproteins; ATGL, adipose triglyceride lipase; HSL, hormone sensitive lipase. Adapted from (2).

I.1.6.1 Source of FA in the liver

Chylomicrons

After eating, dietary fat is hydrolyzed to fatty acids and monoacylglycerols by

intestinal lipases and then absorbed by the enterocytes. Here, they can be re-esterified and packed into chylomicron lipoprotein particles for distribution to the other tissues. There has been an increased awareness about the importance of the fed-state events in the development and/or exacerbation of many diseases. Indeed, postprandial hypertriglyceridemia poses as an independent risk factor for coronary atherosclerosis, obesity, T2DM and NAFLD (24). Data are emerging to show that a significant source of the liver TG derive from dietary lipids. Diets high in fat content have long been associated with obesity and NAFLD (25). Using multiple stable isotopes followed by liver biopsies, it was calculated that 8-12% of meal-TG reach the liver in healthy patients after a single meal, and that in patients with NAFLD a greater burden (10-16%) of dietary TG is taken up by the liver in the postprandial state (24). This could be due to lower peripheral clearance of the dietary lipids in NAFLD and increased fatty-acid transport proteins (FATPs and fatty acid translocase or CD36) in the liver (26).

De novo lipogenesis

High insulin levels and increase substrate availability by carbohydrate feeding promotes *de novo* synthesis of fatty acids from acetyl-CoA in liver cells. Insulin is responsible for the induction of SREBP1c gene expression and activity through the liver X receptor (LXR) transcriptional regulation and through signaling involving RAC-beta serine/threonine-protein kinase (AKT2) and the mechanistic target of rapamycin (mTOR) (27). SREBP1c in turn drives the expression of genes involved in lipogenesis, such as fatty acid synthase (*Fasn)* and stearoyl-CoA desaturase-1 (*Scd-1*) (28). Glucose also promotes DNL by activating the transcription factor ChREBP (29, 30). Hepatic ChREBP activation requires GCK-dependent glucose metabolism, with glucose-6-phosphate being the major signaling metabolite responsible for ChREBP activation (31). The unique glucose-sensing ability of this transcription factor is further emphasized by the fact that several independent glucose metabolites, such as xylulose-5-phosphate, fructose-2,6-bisphosphate, acetyl-CoA and *O*-linked β-*N*-acetylglucosaminylation, can activate hepatic ChREBP (30). ChREBP stimulates the expression of several genes in the fatty acid biosynthetic pathway. In addition, ChREBP increases expression of liver pyruvate kinase, thus providing more substrate for FA and TG synthesis (29). An increase in DNL has been considered an important contributing factor to NAFLD development (32, 33). In fact, DNL is 5-fold greater in NAFLD than in normal livers and it fails to increase postprandially, a pattern present in healthy

individuals (32). In turn, inhibition of ChREBP and SREBP1c-stimulated lipogenesis has proven efficient in decreasing hepatic steatosis (34-36).

Lipolysis

During fasting, rising levels of glucagon and epinephrine stimulate TG hydrolysis from its storage in the adipose tissue. Adipocyte triglyceride lipase (ATGL) and hormone-sensitive lipase (HSL) are key enzymes involved in this mobilization (37). Free fatty acids (FFA) are then released into circulation, mostly bound to albumin and delivered to the liver. FATPs and CD36 are key contributors to the transmembrane process of fatty acid uptake (38). In the liver, FFA are converted into fatty acyl-CoAs and oxidized in the mitochondria, re-esterified into TG and stored or secreted in VLDL. Of all the FATPs isoforms, FATP5 is liver-specific and genetic ablation of this transporter decreases the rates of fatty acid uptake (39). Humans with NAFLD have higher hepatic CD36 levels (40). Congenital generalized lipodystrophy is invariably associated with severe hepatic steatosis (41). Insulin resistance that is largely associated with obesity can favor hepatic FA overload due to dysfunctional adipose tissue with increased lipolysis (42).

Patatin-like phospholipase domain containing 3 (PNPLA3, adiponutrin) is consistently associated with NAFLD and is one of the most common genetic variants triggering this condition (6). PNPLA3 is a member of the PNPLA family, most closely related to ATGL (PNPLA2). PNPLA3 is highly expressed in adipose tissue and liver and is transcriptionally regulated by insulin through a signaling cascade that includes LXR and SREBP1c (43). The frequency of this genetic variant accounts for the degree of susceptibility to this pathological condition that differs between Hispanics, African Americans and Europeans (6).

Despite the role of ATGL in increasing lipolysis and consequent FA delivery to the liver, Jha *et al* demonstrated that lack of ATGL in the liver increases the susceptibility to diet-induced NAFLD by promoting hepatic inflammation (44), emphasizing the complexity and difficulty of intervention to counteract the development of this disorder.

I.1.6.2 Disposal of FA from the liver

VLDL secretion

Hepatic TG leave the liver through assembly into VLDL for lipid fuel

distribution to peripheral tissues. Any mutations that would affect proteins or other constituents affecting the production or secretion of VLDL can lead to hepatic steatosis. The structural protein Apolipoprotein B (APOB) and microsomal TG transfer protein (MTP) responsible for adding TG into nascent VLDL are two examples of proteins whose mutations trigger steatosis. Indeed, individuals with a mutation in APOB protein have lower secretion of VLDL from the liver and a three-fold increase in hepatic steatosis compared to healthy subjects (45). Moreover, studies have reported that dysfunctional VLDL synthesis and release may be a key factor in the establishment and progression of NASH, this being decreased in patients with NAFLD (46). A structural component of cellular membranes, a metabolic substrate for other lipids and a ligand for nuclear receptors such as LRH-1, phosphatidylcholine (PC), is also a very important component of VLDL (47). Diets deficient in methionine and choline affect the secretion of VLDL leading to hepatic steatosis and more advanced stages of NAFLD (48).

Fatty Acid Oxidation

FA undergo mitochondrial β-oxidation to produce acetyl-CoA that can be further processed in the citric acid cycle and feed the electron transport chain (discussed in the next section) (49). Fatty acid oxidation (FAO or β-oxidation) itself also renders nicotinamide adenine dinucleotide (NADH) and flavin adenine dinucleotide ($FADH_2$) that can increase oxidative phosphorylation. FA need to be activated by coenzyme A (CoA) and then enter the mitochondria in a carnitine-dependent manner. Carnitine palmitoyltransferase-1 (CPT-1), present in the outer mitochondrial membrane, catalyzes the formation of Acyl-Carnitines and represents the first and rate-limiting step for FAO (49). Then, CoA replaces again carnitine inside the mitochondria before proceeding with β-oxidation. Several enzymes are responsible for the sequential break down of long chain acyl-CoAs to several Acetyl-CoA, NADH and $FADH_2$. FAO poses as one of the main sources of fatty acid disposal, converting them into energy. Mitochondrial dysfunction, on the other hand, can lead to the dysregulation of this process or to incomplete β-oxidation with consequent accumulation of FA (50). Defects in the enzymes required for oxidation of FA in the mitochondria by β-oxidation also cause hepatic steatosis (41). Hepatic lipid accumulation is a common feature in patients with fatty acid oxidation disorders, including deficiency of medium-chain acylcoenzyme-A dehydrogenase (MCAD), long chain acyl-CoA dehydrogenase

deficiency (LCAD), very long-chain acyl-CoA dehydrogenase (VLCAD), long-chain 3-hydroxyacyl-CoA dehydrogenase (LCHAD) or mitochondrial trifunctional protein (TFP) (51).

Section 2

Mitochondria as the hub of intermediary metabolism

Chapter I General Introduction

I. Section 2 Mitochondria as the hub of intermediary metabolism

I.2.1. Introduction on Mitochondria

Mitochondria are eukaryotic bean-shaped organelles comprised of double and functionally distinct membranes (inner mitochondrial membrane-IMM and outer mitochondrial membrane-OMM), intermembrane space (IMS) and matrix compartments (Figure I.7). The endosymbiotic theory states that mitochondria arose from an *alpha-proteobacterium* engulfed by an eukaryotic progenitor that survived endocytosis and became incorporated in the cytosol (52). One of the remnants of this former life is the presence of a genome (mitochondrial DNA, mtDNA), organized into discrete nucleoids in the matrix that bears more sequence resemblance to its prokaryotic precursor than to its eukaryotic host.

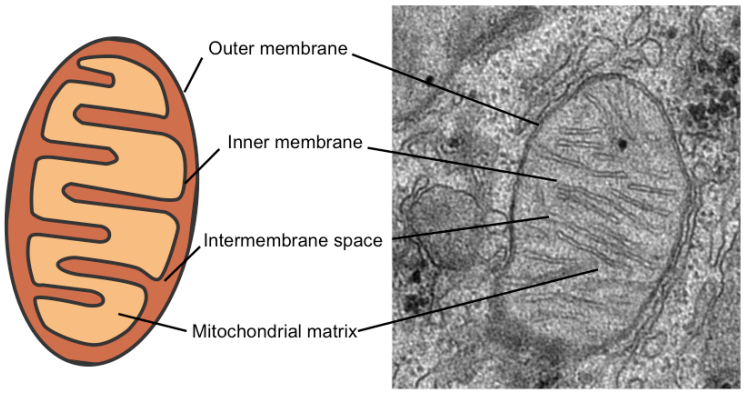

Figure I.7. Structure of a mitochondrion.

The mitochondrial genome consists of a circular, double-stranded DNA molecule that is 15,000-17,000 base pairs long encoding thirty-seven genes. Twenty-four encode the translational machinery of the mtDNA itself (22 tRNAs and 2 rRNAs) and 13 genes encode for the electron transport chain complexes subunits (53). In mammals, mtDNA inheritance is exclusively maternal being the paternal mtDNA actively destroyed after fertilization by autophagy (54).

Mitochondria are iconic structures in biochemistry and cell biology that caught the attention of scientists quite recently (Figure 1.8). Being first called by Altman “bioblasts”, mitochondrial biology has undergone major transformations probably unforeseen by the bioenergeticists who unveiled many of the mysteries of this organelle. Several scientists who contributed to the understanding of mitochondrial structure and function have been awarded a Nobel Prize emphasizing the importance of these findings (Figure 1.8). Indeed the simplistic

concept of mitochondria as discrete, kidney bean-shaped energy factories has given rise to that of a dynamic network that moves, fuses, divides and directs a plethora of functions central to life (53).

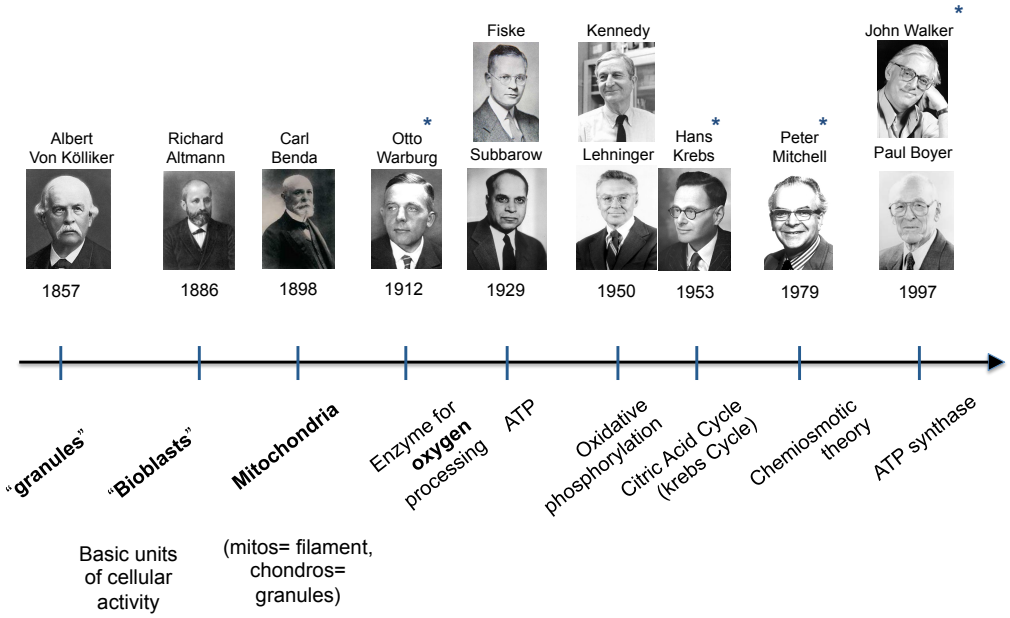

Figure I.8. History of mitochondria.
Timeline of important breakthroughs related to mitochondria from its first discovery to the scrutiny of its constituents and main functions, depicting the main scientists who played a part in it. * Nobel prize winners

Mitochondria are essential to metabolic homeostasis. In addition to converting nutrient flux into the energy molecule adenosine triphosphate (ATP), mitochondria generate intermediates for biosynthesis, reactive oxygen species (ROS) that serve as secondary messengers to mediate signal transduction and metabolism and play fundamental roles in fatty acid oxidation and apoptosis (55). Furthermore, mitochondria are able to integrate metabolism with signaling transduction, cell cycle, development and stress responses (53).

Importantly, it has increasingly become clear that mitochondrial dysfunction underlies more than 50 inborn errors of metabolism (56, 57); strongly contributes to common diseases, including type 2 diabetes (58), neurodegenerative diseases (59), and cancer (60); and is essential to the aging process (61, 62).

I.2.2. Mitochondria as metabolic signaling centers

Mitochondria are best known for the production of ATP via oxidative phosphorylation (OXPHOS). In the mitochondrial matrix, enzymes of the tricarboxylic acid cycle (TCA) generate electron carriers (NADH and $FADH_2$) that

donate electrons to the IMM-localized electron transport chain (ETC). The ETC comprises four protein complexes (I-IV), which through sequential redox reactions pump protons to the IMS. The two electron carrier molecules are ubiquinone [also known as coenzyme Q (CoQ) or ubiquinol when in the fully reduced state (CoQH2)] and cytochrome c (cyt c). The proton gradient generated by complex I, III and IV drives the rotation of a fifth complex (complex V) leading to phosphorylation of adenosine diphosphate (ADP), hence called ATP synthase (Figure 1.9).

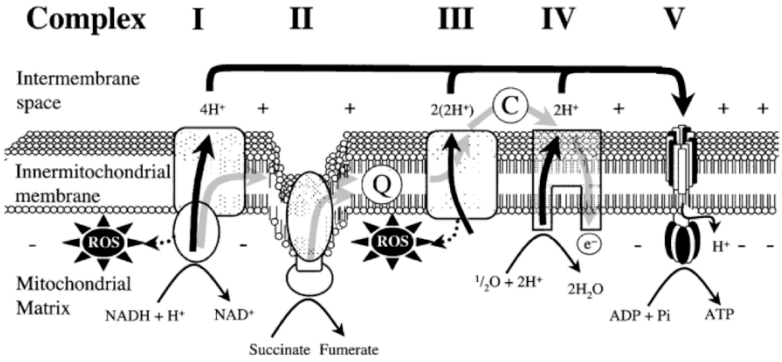

Figure I.9. Mitochondrial inner membrane complexes. Adapted from (64).

Beyond ATP production, the IMM-proton gradient generates an electrochemical potential that is a vital feature of this organelle. Any change in membrane potential affects other essential mitochondrial functions, such as mitochondrial import (63).

These paramount organelles are not just the main source of energy in the cells but also the main source of ROS, including superoxide and hydrogen peroxide. Mitochondria require about 85% of oxygen consumed by cells and complex IV reduces it into water using electrons that stem from NADH and $FADH_2$ and are transported in the respiratory chain (Figure 1.9). Complexes I and III are responsible for the generation of ROS as an inevitable byproduct that can damage lipids, DNA and proteins if not neutralized (65). Although mitochondria are exposed to constant generation of ROS, the mitochondrial antioxidant defense system, namely glutathione, glutaredoxin, thioredoxin and manganese superoxide dismutase, prevents oxidative damage generated during normal aerobic metabolism (66). Independent from its detrimental effects, ROS also coordinates several physiological processes and influences homeostatic signaling pathways to control cell proliferation, differentiation and adaptive stress responses (55). When the burden of ROS production surpasses the antioxidant capacity, cellular oxidative stress increases. Mitochondria have been intensively

studied in the context of ROS biology and its link to diseases associated with mitochondrial dysfunction, like neurodegeneration (67).

Mitochondria also house parts of the lipid metabolism, including fatty acid oxidation; are involved in pyrimidine and bile acids biosynthesis; and regulate levels of amino acids, metabolites and cofactors such as NAD^+, important for key metabolic players such as sirtuins (class III deacetylases) (53, 68) (Figure I.10). Moreover, mitochondria play a pivotal role in iron metabolism, synthesizing heme and Fe-S clusters machinery (essential components of oxygen carriers), hemoglobin and DNA repair. Additionally, mitochondria buffer the second messenger calcium (Ca^{2+}) hence coordinating its distribution from the plasma membrane and ER (53).

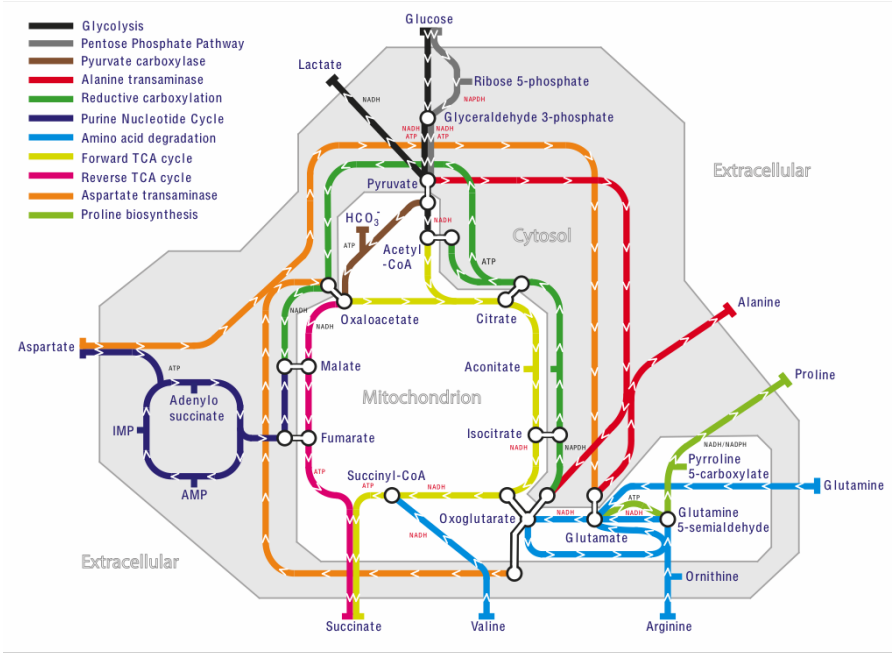

Figure I.10. Metabolic pathways.
Representation of metabolic pathways occurring within the cell, depicting the central role of mitochondria. (Mitochondrial Biology Unit, MRC, UK).

Supercomplexes as highly organized ETC

Mitochondrial electron transport chain was first seen as respiratory components that were more or less rigidly held together in a framework that would ensure the electron transport and proton gradient formation (solid model) (69). This model inspired the introduction of "oxysome" defined as "a functional unit for electron transfer and oxidative phosphorylation" (Figure 1.11) (70). However, the observation that isolated and reconstituted mitochondrial complexes are still functional led to the description of the fluid model, also known as random collision model (Figure 1.11) (71). During the last decade,

these models have been nevertheless the subjects of debate especially because they cannot explain the phenotypic consequences observed upon mitochondrial dysfunction. A prominent example of this is complex III deficiency that leads not only to the loss of complex III activity but also of complex I (72).

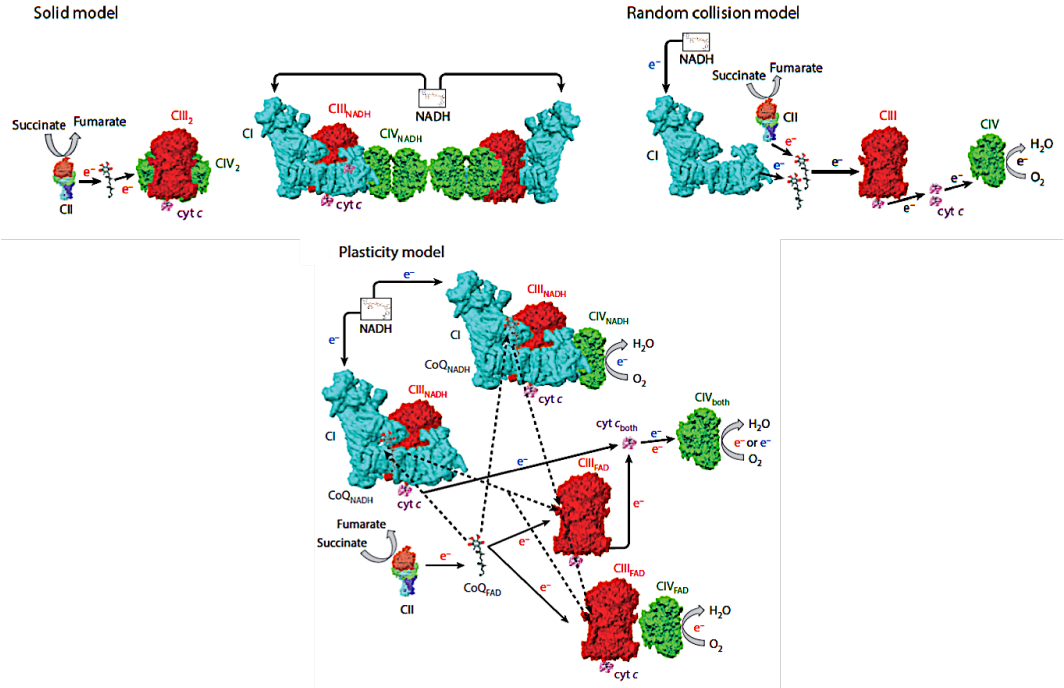

Figure I.11. Models (solid, random collision and plasticity) of the organization of the electron transport chain.

The respiratory chain components are represented as opaque surfaces from their structural models and their colors are maintained throughout the schemes. Solid lines indicate the preferential routes for electrons. The plasticity model proposes that the CoQ and cyt c segmentation is incomplete and, therefore, the pools are promiscuous (dotted lines). This is promoted by the dissociation of the supercomplexes or just the escape of CoQ and cyt c from the assembled complexes. Adapted from (73).

The fluid model has become the textbook definition for the respiratory chain until the first blue native-polyacrylamide gel electrophoresis (BN-PAGE) was performed on isolated digitonin-permeabilized bovine mitochondria (74). The presence of the individual mitochondrial complexes in these gels was accompanied with some higher molecular weight bands indicating comigrating complexes (later called supercomplexes, SCs). The existence of supercomplexes was challenged by all the other model's defenders stating that these were nothing but technical artifacts due to the sample preparation and use of detergents. However, laboratories working with mitochondria from diverse organisms (yeast, plants, vertebrates and invertebrates) found supercomplexes by BN-PAGE that were remarkably similar with a limited number of possible combinations between CI, CIII and CIV (Figure 1.11). Additionally, different detergents allowed the same visualization of supercomplexes. Final confirmation

was obtained when critical factors and conditions affecting superassembly were defined (e.g. assembly factors, mitochondrial shape, lipid composition of the IMM) (73). Single particle electron cryo-microscopy (cryo-EM) has led to a rise in relatively high-resolution structural models of the mammalian respirasome (arrangement of CI, CIII and CIV) (75, 76).

The organization of the mitochondrial ETC into SCs increases the efficiency of the electron flux through the channeling of substrates and CoQ and cyt c pools, optimizing the use of available substrates and allowing for private electron pathways (Figure 1.11). Moreover, CI and CIII interactions minimizes ROS production (77).

Nevertheless, the characterization of supercomplexes did not invalidate the functionality of individual complexes. Mitochondrial complexes are equally functional in free form and when incorporated into superassemblies. In fact, a screening study demonstrated a mutation of the supercomplex assembly factor 1 (SCAFI) in a very common laboratory mouse strain, C57Bl/6J, which renders it inactive preventing complex IV assembly into supercomplexes. These animals without functional SCAFI are healthy but lack the refinement of their bioenergetics performance (78).

Mitochondrial inner membrane transporters as the gatekeepers of mitochondrial metabolism

Lipid membranes that delineate cells and certain organelles within the cell act as selective barriers and provide separation of pathways and specific processes through compartmentalization. The channeling of metabolites across compartments relies on specific transporters and channels. To achieve this purpose, a myriad of proteins is expressed, correctly folded and targeted to their final location.

The OMM, which encloses the entire organelle, has a 1:1 protein-to-phospholipid ratio similar to that of the plasma membrane (79). Voltage-dependent anion channels called porins are integrated in the OMM, making this membrane permeable to solutes up to 5kDa. Larger proteins can enter the mitochondria if an N-terminus signaling sequence is recognized by translocase of outer membrane (TOM). In contrast, the IMM has a very high ratio protein-to-phospholipid (3:1), similar to that of bacteria, comprising about 1/5 of the total protein content in a mitochondrion. IMM has also a distinct lipid composition that may vary between cell types. In pig heart, phosphatidylethanolamine (PE) is the

most abundant (37%), followed by PC (26.5%), while OMM is richer in PC (56%) than PE (28%). Additionally, the IMM is rich in an unusual phospholipid called cardiolipin (25.4%) which seems absent in the OMM (79). Cardiolipin has been shown to interact with mitochondrial respiratory complexes and substrate carrier proteins affecting mitochondrial bioenergetics (80). These features make the IMM selectively permeable to maintain efficient oxidative phosphorylation and membrane potential. The need to import substrates and cofactors and export products is overcome by a superfamily of mitochondrial carriers (MCs), in mammals called solute carrier family 25 (SLC25) (Figure I.12A) (81).

SLC25 comprises a family of nuclear-encoded proteins that are mostly localized in the inner mitochondrial membrane and transport numerous metabolites, nucleotides, cofactors and inorganic anions in and out the mitochondria (Figure I.12B) (81). Out of around 53 members of this family, only few exceptions have been identified to be located in outer mitochondrial membrane (82, 83) and peroxisome (84). Some SLC25 have been identified and extensively studied, such as uncoupling protein-1 (UCP1 or SLC25A7) and ATP/ADP carrier protein 1 (AAC, SLC25A4), others are still orphan transporters and their function still needs to be characterized (Figure I.12A).

Although they transport a wide variety of solutes, all SLC25 members have a common 3-fold repeated signature motif: three tandemly repeated homologous domains of about 100 amino acids in length with two hydrophobic transmembrane segments (α-helices) connected by a long hydrophilic matrix loop. Both N- and C-termini are located in the intermembrane space (Figure I.12C). Due to the plethora of molecules transported into and out of the mitochondria, MCs are involved in many important metabolic pathways, such as oxidative phosphorylation, citric acid cycle, fatty acid oxidation, amino acid degradation, gluconeogenesis, lipogenesis, transfer of reducing equivalents, synthesis and breakdown of mitochondrial DNA, RNA and proteins, urea cycle, heme synthesis, ketone body production and utilization, modulation of the nucleotide and deoxynucleotide pools, heat production, Ca^{2+} cell signaling and necrotic and apoptotic cell death (Figure I.12C) (81, 85).

In many respects, the integrity of the membranes represents a critical element to cellular individuality, as does the preservation and transmission of the genetic information (86). The regulation of the transport of metabolites of intermediary metabolism across the membranes is key to a cell's physiology and is the gatekeeper of its interface with the environment. Despite this central role and the

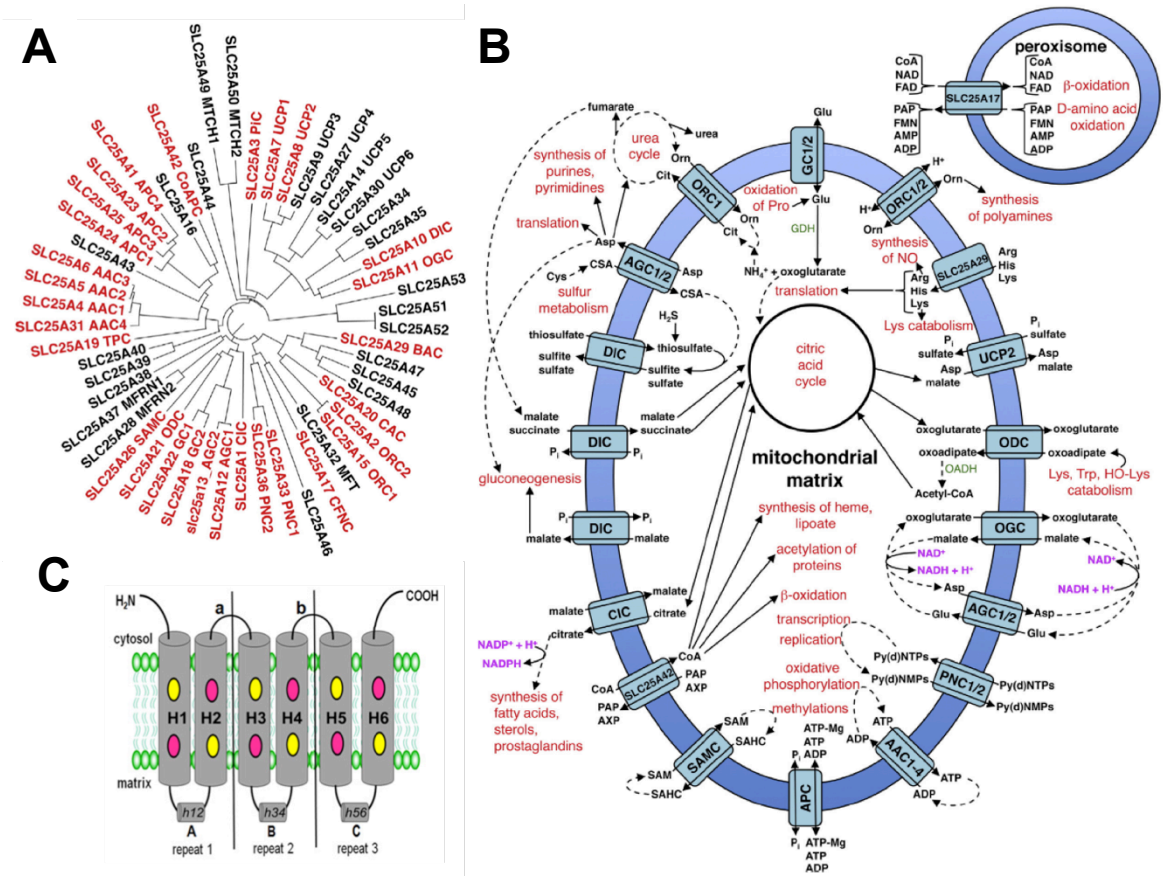

Figure I.12. SLC25 superfamily of mitochondrial transporters.
(**A**) Phylogenetic tree of human mitochondrial carriers (MCs, SLC25). The names of MCs and their acronyms are found on the terminal nodes with members that have been biochemically characterized represented in red. (**B**) Structural model of signature motif in the structure of SLC25 members. A, B, C, long matrix loops. a, b, short cytosolic loops. (**C**) Role of human SLC25 members. Processes are indicated in red whereas enzymes are abbreviated in green: GDH, glutamate dehydrogenase; OADH, 2-oxoadipate dehydrogenase. AXP, adenine nucleotides; CSA, cysteinesulfinate; HO-Lys, hydroxylysine; ADP, adenosine 3',5'-diphosphate; SAM, S-adenosylmethionine; SAHC, S-adenosylhomocysteine. Dashed arrows indicate several steps. Adapted from (81, 87).

fact that around 10% of our genome encodes for transport-related functions, transporters are still understudied and poorly understood, with SLCs in particular being the most neglected group of genes in the human genome (88). Most of SLCs carry small organic molecules and this feature is privileged with respect to small-molecule druggability (89). There are already some SLCs being targeted by drugs in active development in clinical trials. Given the therapeutical relevance of these transporters, more has to be learned about the orphan SLC25 members and their role in metabolic diseases.

I.2.3. Mitochondrial dysfunction as a determinant in NAFLD

One of the main functions of the liver is to coordinate and fine-tune the energy demands of peripheral tissues. The metabolic flexibility of hepatocytes is

surprisingly high but can be disrupted upon metabolic stress. For instance, in the context of obesity and insulin resistance, significant alterations occur favoring hepatic triglyceride accumulation (90). Recent evidence suggests that liver mitochondria and its oxidative metabolism undergo an adaptive program in response to hepatic steatosis (50). Importantly, the adaptation and remodeling of mitochondrial bioenergetics is central to NAFLD (90). Recent studies demonstrated that simple steatosis triggered by either plasma or diet FFA and/or DNL correlates with increased mitochondrial function (91-93). Fatty acid degradation, TCA cycle, oxidative phosphorylation and ketogenesis work together to maintain mitochondrial homeostasis in a compensatory effort to dispose excess acyl-CoA (90-93). A "chronic" nutritional overload in turn leads to a failure in these mechanisms with concomitant decrease in mitochondrial function and energetics (90). More importantly, this mitochondrial (dys)function can dictate the disease progression (50, 90). Dysfunctional mitochondria are associated with lipotoxicity due to incomplete/reduced fatty acid oxidation. This then leads to the accumulation of acyl-carnitines, ceramides and diacylglycerols that can trigger inflammatory responses, key feature of NASH, a more advanced stage of NAFLD (94). Although in NASH mitochondrial ETC and ATP synthesis is lower and ketogenesis is impaired, hepatic TCA cycle remains upregulated as a futile attempt to sustain the high energy demanding anabolic processes during states of caloric excess (94). This persistent upregulation of the TCA oxidative flux together with the accretion of a variety of lipotoxic metabolites may underlie the potent mitochondrial milieu featuring NASH, fueling ROS production and hastening inflammation.

Acknowledging the pivotal role of mitochondria in NAFLD has led to the interest of targeting this organelle to reduce hepatic steatosis and/or halt disease progression. Gariani *et al*. showed that the improvement of mitochondrial function by treating mice with NAD^+ boosters, Nicotinamide Riboside (NR) or poly ADP-ribose polymerase inhibitors (PARPi), while on a high-fat high-sucrose diet (HFHS) was sufficient to prevent the development of NAFLD (95, 96). Moreover, modulation of key regulatory mitochondrial proteins expression, such as phosphoenolpyruvate carboxykinase (PEPCK) or mitochondrial pyruvate carrier (MPC), prevented hepatic inflammation triggered by high-fat diet (HFD) and reversed NASH and advanced fibrosis, respectively (97, 98). Additionally, liver-specific mitochondrial uncoupler therapy led to improvements in hepatic

steatosis paralleled with ameliorated metabolic parameters, such as plasma glucose, insulin and inflammation markers (99, 100).

Further identifying mitochondrial defects and/or major alterations during the development of NAFLD will unravel important and promising novel therapeutic agents/targets to manage NAFLD.

Section 3

LRH-1 in Health and Disease

Chapter I General Introduction

I. Section 3 LRH-1 in Health and Disease

I.3.1 Liver receptor homolog-1 in control of liver metabolic pathways

The adequate control of metabolic pathways is of extreme importance to accommodate systemic fuel requirements and availability. Nuclear receptors and their coregulators have been shown to play a key role in the transcriptional regulation of metabolic players expression integrating the responses to cellular nutrient and energy status (103). Liver receptor homolog-1 (LRH-1; also known as nuclear receptor subfamily 5 group A member 2, NR5A2) is a member of the nuclear receptors (NRs) superfamily. NRs are one of the largest families of transcription factors comprising 48 members divided into seven subfamilies (NR0-NR6) (101, 104). Based on its functions and/or localization and due to the fact that different groups have isolated and characterized LRH-1 independently, it is also known as fushi tarazu factor 1 (Ftz-F1) (105-110), pancreas homolog receptor 1 (111), α-fetoprotein transcription factor (112), human B1-binding factor (113) and CYP7A1 promoter binding factor (114). Similar to other NRs, LRH-1 has a conserved modular structure (Figure I.13) that includes the A/B domain; the highly conserved DNA-binding domain (DBD or C domain); the ligand-binding domain (LBD or E domain), which contains an equally conserved

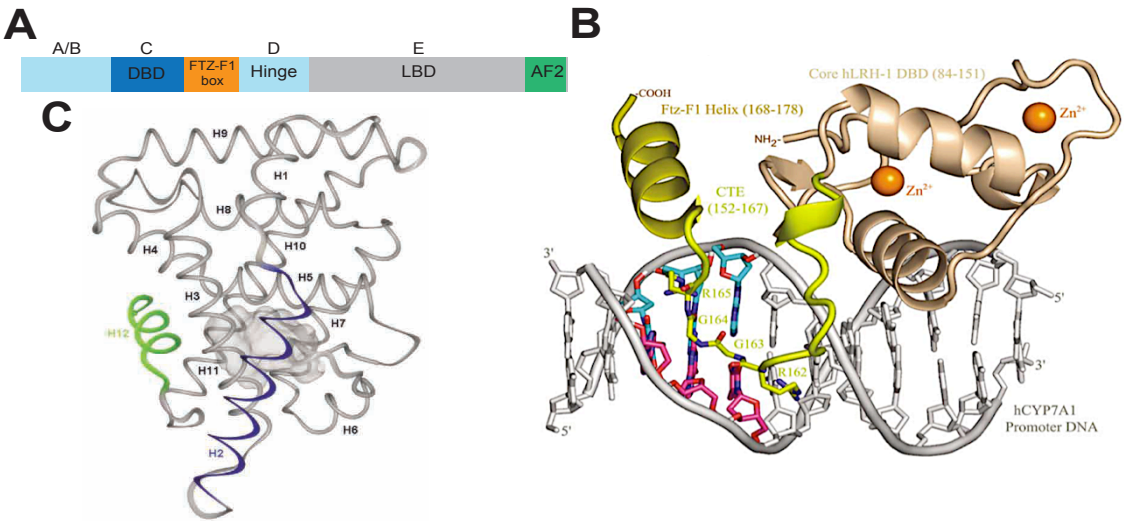

Figure I.13. Structure of LRH-1.
(**A**) Structure of LRH-1 protein depicting the A/B, DNA-binding (DBD), Ftz-F1, Ligand-binding (LBD) and activation function-2 (AF-2) domains. (**B**) Structure of the hLRH-1 DBD-DNA complex demonstrating the importance of Ftz-F1 box for this interaction. CTE, C-terminal extension. (**C**) Empty ligand-binding pocket of mLRH-1 is shown in gray. Helix 12 (H12, green) determines the active state of a nuclear receptor. The extended NR5A-specific H2 (blue) provides an additional layer to the canonical LBD fold and stabilizes the active position of H12 in the LRH-1 crystal structure. Adapted from (101, 102).

ligand-dependent activation function 2 (AF2) motif that mediates coactivator interaction; and the D domain, which serves as a flexible hinge between DBD and LBD (Figure 1.13A). Members of the NR5A or Ftz-F1 subfamily contain an additional Ftz-F1 box between the C and DE domains that confers high affinity to the DNA as monomers (Figure 1.13B). This hallmark feature of the NR5A subfamily distinguishes them from most NRs that form either homodimers (e.g. estrogen receptors) or heterodimers with retinoid X receptor (RXR or NR2B1) to bind DNA in the promoter region of their target genes (104). The crystal structure of hLRH-1 DBD obtained in complex with hCYP7A1 gene promoter demonstrated that the packing of the Ftz-F1 helix against the DBD is crucial for LRH-1 transcriptional regulation (Figure 1.13B) (102). Furthermore, crystal structure of the mouse LRH-1 LBD confirmed a stable monomer but with an empty ligand-binding pocket (Figure 1.13C), suggesting that LRH-1 acts without ligand binding rendering it constitutively active (101). The dispensable activation of LRH-1 by ligand binding emphasizes the importance of interactions with activators or repressors, and posttranslational modifications (PTM), such as phosphorylation, acetylation, ubiquitination and SUMOylation, to fine-tune the activity of LRH-1 (115-118). While phosphorylation enhances LRH-1 activity, reversible covalent modification by small ubiquitin-like modifier-1 (SUMO-1) protein, or SUMOylation, in specific lysine residues by E3-SUMO ligases reduces its transcriptional activity (117-119).

LRH-1 is then an orphan member of the Ftz-F1 subfamily based on its constitutive activity and the absence of established physiological ligands. However, more recent studies have revealed that phospholipid species, including phosphatidyl glycerol, phosphatidyl ethanolamine and phosphatidyl choline, as well as the second messengers phosphatidyl inositols, can bind to the ligand binding pocket of LRH-1 (120-122). Importantly, studies specifically with the phospholipid dilauroyl phosphatidylcholine (DLPC) have identified it as a potent ligand of LRH-1 (123, 124). Numerous synthetic agonists and antagonists of LRH-1 have been described (125-129), indicating the nuclear receptor is a druggable target.

LRH-1 is mainly expressed in tissues of the enterohepatic axis, exocrine pancreas and ovaries, where it has a plethora of biological functions in development, differentiation and metabolism (130) (Figure I.14). LRH-1 can replace *Oct4* in the generation of pluripotent stem cells from somatic cells (131) implicating LRH-1 in the control of stemness and pluripotency (132, 133). In the

pancreas, LRH-1 is essentially required for adequate production and secretion of the pancreatic digestive juice (134, 135). LRH-1 is a key player in female reproduction by regulating steroidogenesis (136-139), ovulation (140) and gestation (141). Moreover, LRH-1 has been associated with cell proliferation (142-144), immunity response (145), hepatic endoplasmic reticulum (ER) stress resolution (146) and different cancers including intestinal (147), pancreatic (143), breast (142) and liver cancer (148).

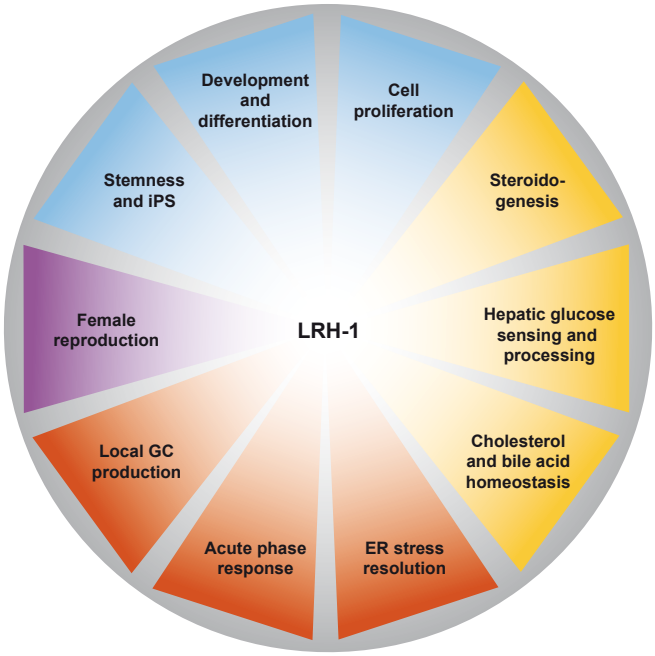

Figure I.14. Overview of the functions of LRH-1.
Metabolic Processes; Adaptive Stress Responses; Female Reproduction; Stemness, Development and Proliferation. Adapted from (130).

I.3.2 LRH-1 is central in Liver Metabolism

Different metabolic pathways take place in the liver, including glucose, fatty acids (FA), cholesterol, bile acids (BA) and ketone bodies production and processing. Hepatocytes also exhibit immunoregulatory responses to several stress stimuli activating the hepatic acute phase response. LRH-1 plays a crucial role in many of the above-mentioned pathways presenting a complex regulatory circuit (Figure I.15).

Bile Acid Homeostasis

The synthesis and excretion of BA comprise the major pathway of mammalian cholesterol catabolism. Through this pathway, the hydrophobic cholesterol is

converted to a readily excreted water-soluble bile acid (149). Besides being fundamental for intestinal lipid absorption, BA are very important signaling molecules having a role in the regulation of glucose, lipid and energy homeostasis (150). This process involves many enzymes mainly expressed in the liver. *Cyp7a1* and *Cyp8b1*, which are two important genes encoding enzymes fundamental for BA synthesis, were amongst the first LRH-1 target genes identified (114, 151). For this reason, LRH-1 has been placed as a master regulator of BA homeostasis. SHP, an atypical member of the nuclear receptor family that lacks a DNA-binding domain (152, 153), competes with peroxisome proliferator-activated receptor γ-coactivator-1α (PGC-1α) to bind the AF2 domain of LRH-1 in the liver and modulate the expression of *Cyp7a1* (154) (Figure I.15).

Importantly, liver-specific *Lrh-1* knockout (KO) mice have altered bile acid composition with reduced ratio of cholic acid and its amino acid conjugate taurocholic acid to muricholic acid and ursodeoxycholic acid. This effect is attributed to the marked reduction of CYP8B1, but not CYP7A1 (155-157). Notably, this altered BA composition leads to a compromised intestinal lipid absorption and enhances the fecal excretion of lipids (155, 157). In addition to controlling BA biosynthesis, LRH-1 also activates the transcription of the bile salt

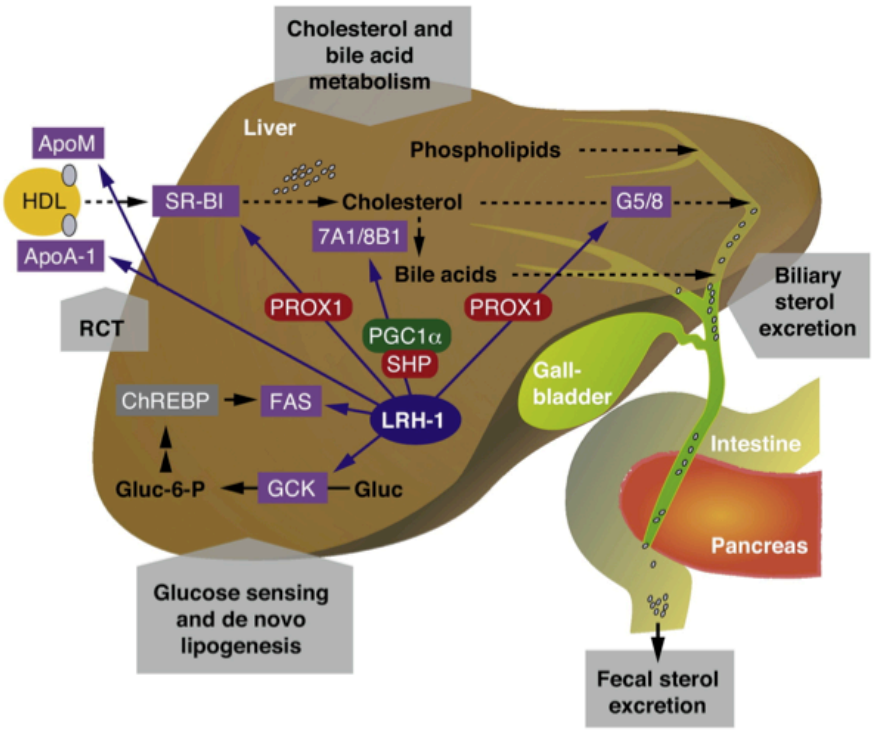

Figure I.15. Scheme representing the main hepatic functions of LRH-1.
RCT, reverse cholesterol transport; HDL, high-density lipoprotein; SR-BI, Scavenger receptor class B1; G5/G8, ABCG5/ABCG8; 7A1/8B1, CYP7A1/CYP8B1; FAS, fatty acid synthase. Corepressors are illustrated in red, coactivators in green. Adapted from (130).

export pump (BSEP, *Abcb11* gene) in hepatocytes that encodes a transporter responsible for the canalicular secretion of BA from the liver (158). Furthermore, LRH-1 controls multidrug-resistance protein 3 (MRP3) expression in hepatocytes preventing hepatocellular injury induced by BA during cholestasis (159). MRP3 exports BA from enterocytes and hepatocytes into the bloodstream, thereby preventing BA intracellular accumulation.

Reverse cholesterol transport

The transport of excessive cholesterol from the peripheral tissues back to the liver and its eventual excretion in the bile is an anti-atherogenic mechanism, referred to as reverse cholesterol transport (RCT). LRH-1 governs the expression of genes involved in this process hence being involved in cholesterol homeostasis, including scavenger receptor class B type I (SR-BI) (160), ATP binding cassette (ABC) half-transporters ABCG5 and ABCG8 (161), apolipoprotein A1 (APOA1) (162), and apolipoprotein M (APOM) (163). Transcriptional regulation of SR-BI receptors, APOA1 and APOM increases the transfer of mature high-density lipoprotein (HDL) particles from plasma into hepatocytes facilitating cholesterol clearance (160, 162, 163). ABCG5/8 limits intestinal absorption and facilitates extrahepatic cholesterol efflux avoiding sterol accumulation (161). A recent study from our lab reported that SUMOylation of LRH-1 promotes its interaction with prospero homeobox protein 1 (PROX1) and leads to the transrepression of hepatic RCT genes such as *Scarb1*, *Abcg5*, and *Abcg8* (119). Of interest, a single point mutation in the *Lrh*-1 gene rendering a non-SUMOylatable form of LRH-1 (LRH-1 K289R mouse model) in an atherosclerosis-prone background displayed increased biliary sterol excretion and RCT decreasing the development of atherosclerosis (119). These studies emphasize LRH-1 as a relevant pharmacological target for atherosclerosis, which is the primary cause of myocardial infarction and stroke in humans.

Methyl-pool Homeostasis

Proper liver function also relies on a tight balance of labile methyl groups, present in choline, betaine, methionine and folate, which can supply for the synthesis of S-adenosylmethionine (SAM) in the one-carbon cycle (1CC). SAM acts as the reactive methyl donor in all necessary pathways, being the second most common enzymatic cofactor after ATP (47, 164). Besides the production of SAM, the 1CC falls at the crossroads of multiple other anabolic pathways, including

amino acids, purine and thymidine, phospholipids and the antioxidant glutathione synthesis, and homocysteine remethylation (47, 164). Moreover, gene expression can be directly affected by 1CC since histone and DNA methylation are sensitive to SAM levels. The production of phosphatidylcholines (PCs), which are ligands for LRH-1, also consume a significant amount of labile methyl groups. Moreover, a recent report identified LRH-1 as an essential element for methyl-pool homeostasis in the liver by transcriptionally regulating *glycine-n-methyltransferase* (*Gnmt*) and biliary phospholipid floppase *multidrug resistance 2* gene (*Mdr2*) (165). Upon hepatic loss of LRH-1, a blunted expression of GNMT and MDR2 favors an increase in the SAM/SAH ratio and a decrease in biliary PC secretion (165). Consequently, *Lrh-1* liver specific KO mice fed a normal diet display similarities to WT mice fed a methionine and choline deficient (MCD) diet that harshly depletes methyl groups. On the other hand, the higher SAM levels present in *Lrh-1 -/-* mice makes them resistant to MCD detrimental effects, still presenting hepatic steatosis but being protected from hepatitis (165).

Hepatic Acute Phase Response

Upon inflammatory stimuli due to injury, infection or chronic metabolic stress, immune cells secrete several cytokines into the bloodstream. In turn, the liver integrates this signal activating the hepatic acute phase response (APR) (166). This response comprises the induction and secretion of a number of acute phase proteins into the plasma for the restoration of homeostasis. As described above, SUMOylation of hepatic LRH-1 leads to the recruitment of different co-repressors. Binding of SUMOylated LRH-1 to the nuclear receptor corepressor 1 and histone deacetylase 3 (NCOR1/HDAC3) complex via G protein pathway supressor 2 (GPS2) mediates the induction of acute phase response genes (118, 167). Furthermore, LRH-1 exerts anti-inflammatory roles in the liver by inducing the expression of interleukin-1 receptor antagonist (IL-1RA), a robust inhibitor of IL-1 signaling (168).

Glucose and fatty acid metabolism

The concentration of glucose in the blood determines its availability to the liver. During the post-prandial phase, which lasts about 2h after a meal, glycaemia rises and the liver takes up approximately 10-25% of this glucose (30). Once inside the hepatocytes, glucose is phosphorylated to glucose-6-phosphate (G6P) by GCK and this constitutes the initial postprandial glucose-sensing

component that coordinates hepatic glucose metabolism. G6P can have multiple biochemical fates, including glycolysis, pentose phosphate pathway and glycogen synthesis (30). LRH-1 has also emerged as an important player in hepatic glucose sensing and intermediary metabolism by directly regulating *Gck* (169). Under postprandial conditions, liver-specific *Lrh-1* KO mice display reduced availability of G6P, the end product of GCK, leading to reduced glycogen synthesis, glycolysis, and DNL (169). Reduced G-6-P in turn limits the nuclear translocation and consequent activation of the hepatic ChREBP (Figure I.16). Moreover, LRH-1 acts a competence factor for LXR potentiating the expression of its target genes, such as *Fasn* (170). These studies pinpoint LRH-1 as a pivotal regulatory element for proper integration of postprandial glucose and lipid metabolism.

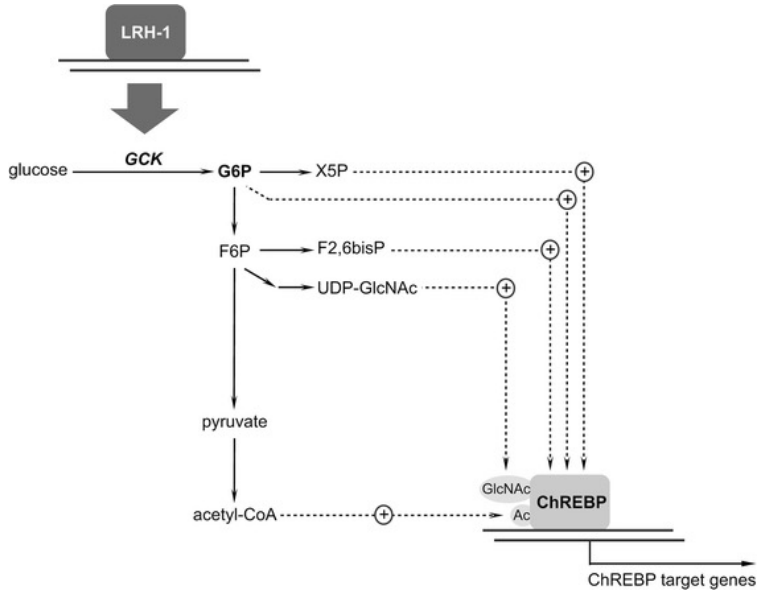

Figure I.16. LRH-1 regulates central glucose-sensing system in the liver.
LRH-1 transcriptionally regulates glucokinase (GCK) impacting on glucose-6-phoshphate (G6P) levels and therefore activation of carbohydrate response element binding protein (ChREBP). Acetyl-CoA, acetyl-coenzyme A; F2,6bisP, fructose-2,6-bisphosphate; F6P, fructose-6-phosphate; UDP-GlcNAc, UDP-N-acetylglucosamine; X5P, xylulose-5-phosphate. Adapted from (30).

I.3.3 LRH-1 and metabolic disorders

Metabolic functions of LRH-1 have also been described in obese and diabetic mouse models. LRH-1 activator DLPC improves glucose homeostasis and decreases hepatic steatosis in diet-induced and genetically obese and diabetic mice (124). The improvement in glucose tolerance and insulin resistance was not accompanied by a change in body weight and was lost upon liver-specific *Lrh-1* deletion (124). On the other hand, heterozygous *Lrh-1*+/-mice have a mild but

significant body weight gain when exposed to a high-fat diet, without changes in glucose or insulin tolerance (171). Furthermore, targeted deletion of *Lrh-1* results in fatty liver in mice (146). 1CC has multiple links to lipid accumulation in the liver. Both SAM and PC are closely correlated with hepatic lipid accretion. SAM directly regulates gene expression through methylation, whereas PC is important for VLDL assembly and secretion (172) and activation of SREBP-1-dependent lipogenesis (173). The complex relation of LRH-1 with the 1CC impacts in the development of hepatic steatosis in mice fed a MCD diet (165).

Considering the plethora of metabolic functions LRH-1 coordinates in the liver (Figure I.15, I.16), one might envision a putative role for LRH-1 in NAFLD. Importantly, several pathways that can lead to lipid accumulation are regulated by LRH-1. Identifying the interplay of LRH-1 in NAFLD will aid in understanding the pathogenesis of this disease.

Chapter II

Research Aims

Chapter II Research aims

Although liver diseases in general, and NAFLD, in particular, are an emerging public health problem, there are no significant advances in treatment. Understanding the pathogenesis of NAFLD is thus crucial for unraveling new therapeutic avenues.

The adequate control of liver metabolic pathways is pivotal to prevent lipid dysregulation. The nuclear receptor LRH-1 with its high expression in the hepatocytes and its important role in the transcriptional regulation of metabolic players makes it an excellent target to asses the contribution of different metabolic pathways to the development of NAFLD.

With the general goal of providing more insight into this complex disease and identifying potential biomarkers and/or future therapeutic targets, we focused our work on the role of LRH-1 in coordinating hepatic lipid metabolism. To achieve this, we took advantage of both loss and gain-of-function of LRH-1 models together with different nutritional cues (refed and fasted) and diets (diet-induced NAFLD). Within this overarching aim, the specific aims were the following:

1) To assess the regulatory role of LRH-1 in hepatic lipogenesis using a selective gain-of-function *knock-in* mouse model achieved by compromised SUMOylation at LRH-1 K289 residue – **Chapter IV**.

2) To identify the repercussions of increased LRH-1 transcriptional activity in the development of NAFLD – **Chapter IV**.

3) To determine the contribution of LRH-1 for proper mitochondrial function during fasting with a hepatocyte-specific *knockout* mouse model – **Chapter V**.

4) To characterize SLC25 member 47 mitochondrial transporter as a potential target for hepatic steatosis alleviation - **Chapter V**.

Some additional results are presented in **Chapter VI** to support previous work and serve as a basis for future studies to complete the scientific work presented here. A general conclusion and future perspectives are included in **Chapter VII** to integrate the studies performed and highlight subsequent ones.

Chapter III

Material and Methods

Chapter III Material and Methods

Lrh-1$^{hep-/-}$ mouse model generation. For the generation of *Lrh-1* floxed (*Lrh-1* L2/L2) mice, genomic DNA covering the *Lrh-1* locus (NCBI Gene ID: 26424) was amplified from the 129/Sv strain by using high-fidelity PCR. The resulting DNA fragments were assembled into the targeting vector and electroporated into 129Sv embryonic stem (ES) cells. After selection and verification of karyotype several correctly targeted ES cell clones were injected into blastocysts from C57BL/6J mice. These blastocysts were transferred into pseudo-pregnant females, resulting in chimeric offspring that were mated to female C57BL/6J mice that express the Flp recombinase under the control of the ubiquitous cytomegalovirus (CMV) promoter. Offspring that transmitted the mutated allele, in which the selection marker was excised, and that lost the Flp transgene (*Lrh-1* +/L2 mice) were selected, mated with albumin-Cre mice (The Jackson Laboratory), and then further intercrossed to generate hepatocyte-specific LRH-1 KO (Alb-Cre; *Lrh-1* $^{hep-/-}$) and wildtype littermates (*Lrh-1* $^{hep+/+}$) mice.

LRH-1 K289R mouse model generation. To generate LRH-1 K289R mice, gDNA covering the *Lrh-1* gene was amplified from the C57BL/6J strain by using high-fidelity PCR. The point mutation of interest (AAG -> AGG) was introduced by PCR. The amplified DNA fragments were ligated into the targeting vector with a floxed Neo cassette (Institut Clinique de la Souris, Strasbourg). The construct was then electroporated into C57BL/6N ES cells. After selection, karyotype-verified ES cell clones were injected into blastocysts from BALB/c mice. These blastocysts were transferred to pseudo-pregnant females. Chimeric offspring were mated to female C57BL/6J mice expressing the Cre-recombinase under the control of the CMV promoter to delete the Neo cassette. Offspring transmitting the mutated allele, in which the selection marker was excised, and that lost the Cre transgene (*Lrh-1* L-/+ mice) were selected and inbred with to obtain *Lrh-1* L-/L- (LRH-1 K289R) mice. LRH-1 K289R and LRH-1 WT mice were backcrossed for 6-7 generations onto commercial C57BL/6J purchased from the Jackson Laboratory.

Animal studies. Congenic male C57Bl/6J LRH-1 WT or LRH-1 K289R (119), as well as C57Bl/6J *Lrh-1* $^{hep-/-}$ and *Lrh-1* $^{hep+/+}$ mice (174) and WT C57BL/6J (Janvier Labs) were housed with ad libitum access to food and water and kept under a 12h dark/12h light cycle.

Chapter IV studies: For fast-refeeding protocols 12 to 16-week-old male mice were initially fasted for 24 hours, followed by refeeding for 12 hours (8 pm to 8 am), 6 hours (2 am to 8 am), or 2 hours (6 am to 8 am), and finally sacrificed together at 8 am to avoid confounding effects of the circadian rhythm. To induce a chronic hepatic steatosis, male mice were fed ad libitum with a HFHS diet (TD.08811, Harlan Laboratories) for 17 weeks and sacrificed at 9 am. To study the APR, male mice fed a chow diet received an intraperitoneal injection of either 500 μl PBS or 40 μg LPS dissolved in 500 μl PBS. Mice were sacrificed 2.5 hours post injection and tissues collected.

Chapter V studies: For fed-fasted protocols, 8- to 10-week-old male mice were fasted overnight (12h). To induce hepatic steatosis, male mice were fed ad libitum one week after AAV8 injections with either a choline-deficient diet, 20% Lard diet (TD.170068, Teklad Custom Diet, Envigo) for 4 weeks and sacrificed under normal fed condition or HFHS for 7 weeks and sacrificed after an ON fasting. The diet-induced NAFLD model found in Figure V.8A, C57Bl/6J mice were fed HFHS diet for 18 weeks to develop NAFLD/NASH as described previously (95).

Respiratory exchange ratio (RER) was assessed using comprehensive lab animal monitoring system (CLAMS) one week before mice were sacrificed. Food intake was assessed over two days and normalized per day.

All animal procedures were approved by the Swiss authorities (Canton of Vaud, animal protocols ID #2380, #2561 and #2768, #3187, #3221) and performed in accordance with our institutional guidelines.

In vivo siRNA transfection. siRNA sequences are listed in the Supplemental table S4. 3 nmol HPLC-purified siRNAs (Microsynth) were tail-vein injected into each recipient mice using *in vivo*-JetPEI (Polyplus) according to the manufacturer's instructions. Mice were fast-refed as described above and sacrificed 2 days post injection.

Adenoviral infection. The Osbpl3 cDNA was cloned into a pENTR/D-TOPO plasmid (Invitrogen; the Topo primer is listed in Table 3) and then subcloned in the pAd/CMV-DEST plasmid (Invitrogen). After linearization with PacI, the construct was transfected into HEK 293A cells to produce the adenoviruses. Mice were tail-vein injected with Ad-gfp or Ad-Osbpl3, PFU 2.5 x 10^9, fast-refed as described above and sacrificed 3 days post injection.

AAV8 injections. The Osbpl3-siRNA sequence (Table 4) was engineered to create a pre-miRNA sequence targeting Osbpl3, which was cloned into an AAV vector construct driven by the liver-specific hAAT promoter. Slc25a47 cDNA was subcloned from a pCMV6-mSlc25a47 (Origene MC212109) into an AAV vector driven by hAAT promoter. AAV8-hAAT-mirOsbpl3 and AAV8-hAAT-mSlc25a47 were generated, titrated as described previously (175, 176), and injected into the jugular vein under isoflurane anesthesia (5×10^{11} vg and 1×10^{12} vg respectively). For mirOsbpl3 experiments, two weeks after the injection, mice were fasted for 24 hours followed by 6 hours refeeding, then sacrificed and tissues were snap-frozen. For Slc25a47 experiments, five weeks after injection, mice were sacrificed after overnight fasting and tissues harvested. For the choline-deficient diet protocol, 3 weeks after the viral particles injection, mice were fed the diet for 4 weeks more before sacrifice.

Immunohistochemistry. Liver tissue was fixed overnight in phosphate-buffered 10% formalin and embedded in paraffin, sectioned in 4 μm and stained for hematoxylin/eosin (H&E). Immunohistochemistry was performed to stain collagen with Sirius Red and CD45-positive cells using rat anti-CD45 antibody (eBioscience, no. 30-F11). Liver pieces were frozen while embedded in optimum cutting temperature (OCT) and later cut into 8-μm-thick serial cryosections for Oil-red O staining to visualize neutral lipids.

Cell culture and LXR agonist treatment. Hepatocyte (AML12, and Hepa 1.6) and non-hepatocyte (HeLa) cell lines were obtained from American Type Culture Collection (ATCC) and kept in culture under standard conditions (37°C, 5% CO_2, humidified incubator). DMEM with glucose (4.5 g/l), 10% fetal bovine serum (FBS) and penicillin-streptomycin (10 mg/ml) was used for Hepa 1.6 and HeLa cells. DMEM/F12 (Ham mixture) with 10% FBS, 400 μl of gentamicin solution (50 mg/ml, Sigma), 100mM dexamethasone and insulin, transferrin and selenium supplement (Roche) was used for AML12 cells. Hepa 1.6 or AML-12 cells were treated with 1 μM of GW3965 (Selleckchem), a dual LXR-α and LXR-β agonist, for 6 hours in full medium.

Immunofluorescence. AML12 cells were transfected using JetPEI® DNA transfection reagent (Polyplus transfection) for 24h with pCMV6-m*Slc25a47*mycDDK (Origene, MC212109) or pCMV6-empty-flag plasmids.

Immunofluorescence was then performed using FLAG antibody (Sigma, F1804) in goat serum (3% in TBS).

Subcellular fractionation of liver tissues and Western blotting. To perform subcellular fractionation for protein enrichment, 50 to 100 mg of liver pieces were incubated in 400μl of hypotonic buffer (10mM HEPES-KOH pH 7.4, 10mM KCl, 1.5mM $MgCl_2$, 0.5mM DTT, protease and phosphatase inhibitor cocktails (Roche)) and lysed with 10 strokes in a Dounce homogenizer. The supernatant fraction containing mainly cytoplasmic proteins was collected after centrifugation (1,400 x g for 5 min, 4˚C), and the pellets were washed twice with hypotonic buffer. The pellets were resuspended in 100-200 μl of hypertonic buffer (50mM Tris-HCl pH 7.4, 150mM NaCl, 0.1 % NP-40, protease and phosphatase inhibitor cocktails) for 30 min on ice. The supernatant containing mainly nucleoplasm and membrane fractions was collected by centrifugation (2,000 x g for 5 min, 4˚C), and the remaining insoluble pellet containing mainly chromatin was resuspended in 100 μl of hypertonic buffer and sonicated. For whole protein lysates, cells or tissues were homogenized with RIPA buffer (50mM Tris-HCl pH7.4, 150mM NaCl, 0.1% SDS, 0.5% sodium deoxycholate, 1% NP-40, 2 mM EDTA and 50 mM NaF) supplemented with 1 mM PMSF and protease and phosphatase inhibitor cocktails (Roche), sonicated and centrifuged full speed for 15 min, 4˚C. Before running SDS-PAGE, protein lysates were boiled for 5 min 95˚C. Following proteins were used for Western blotting on **Chapter IV**: using anti-Hsp90, anti-SREBP-1 and anti-P62 (BD Biosciences no. 610418, 557036, and 610497), anti-OSBPL3 (Novus Biologicals, no. NBP-155151), anti-FASN (Abcam, no. ab22759), anti-SCD1 (Thermo Fisher, no. A13996), anti-alpha-TUBULIN, anti-PARP1 and anti-beta-ACTIN (Santa Cruz, no. sc-5286, sc-7150 and sc-47778). Anti-SREBP-1, anti-P62, and anti-PARP1 were blotted on nuclear/membrane fractions, all other antibodies on cytoplasmic fractions. Additional antibodies used for mitochondrial studies (**Chapter V**): anti- OPA1 (BD Biosciences no. 612606); anti-SLC25A47, PINK1 (Novus Biologicals, NB100-5783, BC100-494); anti-TOMM20, TOMM40 (Santa Cruz, sc-11415, sc-11414); anti-VDAC, PGC-1α, OxPhos, SDHA and NDUFS3 (Abcam, ab14734, ab54481, ab110413, ab14715, ab14711); anti-HSP60 (Enzo Life Science, ADI-SPA-806).

Proteomics. SWATH-mass spectrometry (SWATH-MS) was used to quantify proteins with good reproducibility and quantification accuracy on liver lysates from *Lrh-1* $^{hep-/-}$ and *Lrh-1* $^{hep+/+}$ mice as described previously (177).

Gene expression and analysis. RNA was extracted from the livers using TRIZOL (Invitrogen) and purified with the RNeasy cleanup kit for microarray analysis (Qiagen). For RT-qPCR, cDNA was generated using the QuantiTect® Reverse Transcription Kit (Qiagen), and analyzed by Q-PCR using a LightCycler® 480 Real-Time PCR System (Roche) and the primers listed in supplementary tables. Expression data were normalized to 36b4 or B2m mRNA levels. Microarray analysis was performed using the Affymetrix MouseGene 1.0 ST array and normalized using the Robust Multi-array Average (RMA) method. All microarray data presented from our study are accessible at the NCBI gene expression omnibus (GEO) database (GSE89877). For mtDNA/nDNA ratio, genomic DNA was extracted from liver tissues using NucleoSpin Tissue (Macherey-Nagel) and qPCR was performed for the expression analysis of 16S (mitochondrial) normalized to HK2 (nuclear gene).

Bioinformatic analysis. Liver microarray data (Affymetrix Mouse Gene 1.0 ST) from a BXD mouse genetic reference population (178) fed normal chow diet and sacrificed under fasting conditions were analyzed for correlations with *Slc25a47* transcript expression using the GeneNetwork program (http://www.genenetwork.org). Raw microarray data are also publicly available on Gene Expression Omnibus (GEO; http://www.ncbi.nlm.nih.gov/geo) under the accession number GSE60149. Significant top 20 correlating genes ($p<1x10^{-8}$) were plotted in a network using Cytoscape v3.4.0 (179). Gene/Protein/Pathway enrichment analysis was performed with DAVID Bioinformatic Resources (https://david.ncifcrf.gov/) using respective background lists (180, 181). *Mus musculus* protein sequence alignments and phylogenetic tree were designed using Geneious v10.2 (http://www.geneious.com) (182). SLC25A47 protein sequence was aligned with SLC25A45, A48, A20, A29, A2 and A15, being the closest homologs considering both phylogenetic trees of *Mus musculus* and *Homo sapiens*. *Mus musculus Slc25* family of transporters expression profiles was obtained from Expression Atlas (https://www.ebi.ac.uk/gxa/home/, reference: 22012392) (183). All heat maps were generated using heatmap.2 including dendogram per row or using GENE-E

(http://www.broadinstitute.org/cancer/software/GENE-E/index.html), where rows were clustered using the 'one minus Pearson correlation' metric. Color code represents row z-score. Corrgrams were made using corrgram function in R.

Homology modeling. The mitochondrial ADP/ATP carrier (AAC or SLC25A4, PDB ID 1OKC) was the first SLC25 structurally characterized. The HHPred server (doi: 10.1093/nar/gki408) identified this carrier as the best hit for performing homology modeling of the SLC25A47 protein, with E-values of $4.3x10^{-55}$. Using the sequence alignment provided by the HHPred server, structural models for the SLC25A47 protein were created with the Modeller program, version 9.13 (doi: 10.1002/0471250953.bi0506s15). 100 models were created for each conformation (template), using the default optimization and refinement protocol, and for each conformation, the model with the lowest DOPE score was selected.

Chromatin immunoprecipitation (ChIP)-PCR. ChIP analysis was performed as described previously with minor modifications (119). ChIPed DNA was purified using the PCR clean-up extraction kit (Macherey-Nagel), after which qPCR was performed as described previously (155). Data were normalized to the input (Fold differences=$2^{-(Ct\text{-}sample\ -\ Ct\text{-}input)}$). ChIP primer sequences are listed in supplementary tables. For LXR ChIP assays an anti-LXRα antibody (Abcam, no. ab41902) was used. For LRH-1 ChIP experiments, a custom LRH-1 antibody was generated. A synthetic peptide ([H]-QEQSNRNRQEKLSAFG-[NH2]) was used to immunize two rabbits (AbFRONTIER). The antiserum with the highest ELISA titer was selected and used in ChIP experiments. The pre-immunization serum from the same rabbit was used as a negative control.

Mitochondrial Isolation and digitonin-permeabilization assay. Mitochondria were isolated from the livers or cells as described in the literature (184). Briefly, livers or cells were homogenized in mitochondria isolation buffer (IBc) that contains 10ml of 0.1M Tris-MOPS, 1ml of EGTA/Tris and 20ml of 1M sucrose, up to 100 ml with distilled water, adjusting pH to 7.4. Homogenates are then centrifuged at 600-800g, 10 minutes at 4˚C to discard the debris leaving mitochondria in the supernatant. Next, we spin down the supernatant at 7,000-10,000 x g for 10 minutes at 4˚C to pellet the mitochondria. The pellets were washed once with 1ml IBc. The mitochondria pellet was resuspended in RIPA buffer for western blot or in mir05 for the assessment of respiration or Ibc buffer

for digitonin-permeabilization assay. For the latter, isolated mitochondria were incubated for 15 minutes on ice with an increasing concentration of digitonin in 100 μl mitochondrial isolation buffer as described before (185). The pellet was recovered by centrifugation (13,000 g, 10 minutes, 4˚C).

Oxygen consumption assessment with Oxygraph. Liver tissue was homogenized using Mitochondrial Respiration Medium (mir05) containing EGTA 0.5mM, $MgCl_2.6H_2O$ 3mM, Taurine 20mM, KH_2PO_4 10mM, HEPES 20mM, D-Sucrose 110mM, BSA essentially fatty-acid free 1g/l, Lactobionic Acid 60mM, pH 7.1. Oxygen consumption rate was assessed in liver homogenates or isolated mitochondria in mitochondrial Respiration Medium (mir05: EGTA 0.5mM, $MgCl_2.6H_2O$ 3mM, Taurine 20mM, KH_2PO_4 10mM, HEPES 20mM, D-Sucrose 110mM, BSA essentially fatty-acid free 1g/l, Lactobionic Acid 60mM, pH 7.1) by High Resolution Respirometry (Oxygraph 2k, Oroboros Instruments) following manufactures' instructions. For the Substrate-Uncoupler-Inhibitor Protocol (SUIT) compounds were added into the 2ml-chamber. Compounds used: Succinate (10mM), CI-inhibitor Rotenone (0.1 μM) and ADP+Mg^{2+} (1.25mM) for $State_{3ADP}$ respiration; FCCP (titration of 1μl each from 1mM stock) for maximal respiration, Oligomcyin (2 μg/ml) for uncoupled respiration. For fatty acid oxidation (FAO) assay, Palmitoyl-Carnitine (50μM) and Octanoyl-Carnitine (0.2mM) were used in the presence of ADP. Malate was added to sustain fatty acid degradation avoiding Acetyl-CoA accumulation. Full liver homogenates were used to assess $State_{3ADP}$ and FAO. Isolated mitochondria were used to assess coupled and uncoupled respiration.

Oxygen consumption assessment with Seahorse XF96. Cells were plated in a Seahorse Bioscience XF96-well plate (Agilent Technologies) 2 days before the experiment. The day after, cells were transfected as indicated in Immunoflouorescence section above. One day later and 30 minutes before the Seahorse run, cells were treated with Forskolin 20 μM and the plate was placed in a 37˚C incubator without CO_2. FCCP (10μM) was then injected and oxygen consumption recorded.

Blue Native Polyacrylamide Gel Electrophoresis (BN-PAGE). Blue Native Polyacrylamide Gel Electrophoresis was performed as previously described (186). Briefly, 50 μg of mitochondria were gently ressuspended in 5μl NativePAGE

sample buffer 4x, 8μl 5% digitonin (Thermo Fisher Scientific) and 7μl water mix (8g/g digitonin/protein ratio). After staying on ice for 20 min, mitochondria were centrifuged for 10 min, 20,000 x g at 4˚C. 2 μl of Coomassie Blue G-250 sample additive were then added to the supernatant and samples were loaded into a Native-PAGE gradient gel (3-12%). The run was performed using Dark Blue Cathode Buffer (0.044 g Coomassie Brilliant Blue G-250 in 220ml NativePAGE anode buffer) (Thermo Fisher Scientifc) for 30 min at 150V. Next, Dark Blue Cathode Buffer was replaced by a Light Blue Cathode Buffer (dilution of 1:10 of Dark Blue Cathode Buffer) and the run proceeded for 1hour at 250V. Using iBlot gel transfer device (Invitrogen), the gel was transferred onto a PVDF membrane and blotted with OxPhos antibody cocktail (Thermo Fisher Scientific, cat. no. 45-7999), and anti-MTCO1 antibody (Abcam, cat. no. ab14705).

Clear-Native PAGE and In-Gel-Activity. To perform in-gel activity, the procedure to follow is very similar to BN-PAGE (186), differences being the amount of digitonin used and the cathode buffer during the electrophoresis run. 50 μg of mitochondria were ressuspended in 5μl NativePAGE sample buffer 4x, 4μl 5% digitonin (Thermo Fisher Scientific) and 11μl water mix (4g/g digitonin/protein ratio). For the run, light blue cathode buffer (1:10 dilution of the Dark Blue Buffer described above) was used for 30 minutes at 150V and then changed to clear NativePAGE running buffer to avoid excessive blue color of the Coomassie dye on the gel, which interferes with the color of the activity detected. The run proceeded for 150 minutes at 250V. After the run, the gel was incubated with Complex IV substrate solution: 50mg diaminobenzidine (DAB), 100mg cytochrome c and 90ml 50 mM phosphate buffer pH 7.4 to 10 ml with ddH_2O. Then, the same gel was washed with water and incubated with complex I substrate solution: 40 μl 1M Tris-HCl, pH 7.4, 2mg NADH, 50mg Nitrotetrazolium Blue chloride (NTB) to 20ml with bisdistiled ddH_2O. Another gel is needed to check complex II activity with complex II substrate solution: 200μl 1M sodium succinate, 25mg Nitrotetrazolium Blue chloride (NTB), 8μl 250mM phenazine methosulfate (prepare 250mM stock in DMSO), 50μl 1M Tris-HCl to 10ml with ddH_2O. Reactions were stopped with 10% acetic acid wash for 5 min followed by water for 5 min more. Gels were scanned at different time points of incubation to follow kinetics of the signal before saturation. Quantification of the bands obtained through in *in-gel* activity was performed with ImageJ (1.47v) using coomassie blue band as a loading control.

ATP quantification. Cell or liver lysates were prepared by homogenization with RIPA buffer (see above recipe), sonicated and centrifuged full speed for 15 min at 4˚C. Supernatant was used for ATP quantification and Citrate synthase activity assay. ATP was quantified with CellTiter-Glo® Luminescent Cell Viability Assay (Promega). 10µl of each sample were diluted with 90µl PBS in a 96-well plate. Then, 100µl of CellTiter-Glo® Reagent were added in each well, plate was incubated for 5 min at room temperature protected from light and luminescence was read.

Oleic acid oxidation assessment. A piece of 100–200 mg liver tissue was homogenized in sodium chloride-Tris-EDTA buffer, centrifuged at 420×*g* for 10 min at 4 ˚C, and the supernatant was incubated for 40 min at 37 ˚C in a reaction mixture containing ^{14}C-radiolabeled oleic acid, 2 mM ATP, 0.5 mM dithiothreitol, and measured for acid-soluble metabolites and trapped CO_2 as described previously (187).

Lipid analyses and plasma parameters. Hepatic lipids were extracted according to the Bligh & Dyer protocol (188). TG, FFA and cholesterol contents in plasma and/or hepatic lipid fractions were quantified using enzymatic assays (Roche). To asses fatty acid synthesis rates *in vivo*, mice received sodium [1-^{13}C] acetate via their drinking water (2%) 24 hours prior to sacrifice. FA derived from hepatic lipid extracts were liberated, derivatized, and subjected to GC-MS analysis in order to calculate the fractional synthesis rates from the incorporation of ^{13}C-acetate as described previously (189). Hepatic acylcarnitines were determined by tandem mass spectrometry (190). ASAT and ALAT concentrations in blood were determined using standard clinical chemistry methods.

VLDL secretion assay and glucose-6-phosphate quantification. The VLDL secretion assay was performed as described previously (189). 13-week-old male LHR-1 K289R or LRH-1 WT mice were subjected to the fasting-refeeding protocol and treated with 50 mg/ml Poloxamer-407 (Sigma Aldrich, no. 16758) 8 hours after refeeding was initiated. Blood samples were collected once before and every hour after Poloxamer treatment to determine the triglyceride content. Glucose-6-phosphate content was determined using enzymatic assays as described previously (174).

Ex vivo lipolysis assessment. Fresh epididymal white adipose tissue explants (~20mg) from *Lrh-1* $^{hep-/-}$ and their WT littermates were washed in PBS and incubated in a 96-well plate with low glucose DMEM supplemented with 2% BSA with and without forskolin (10 μM, positive control) for one hour at 37°C. Subsequently, tissues were transferred into a new 96-well with fresh media (with and without forskolin) for an additional hour. Supernatant was used to quantify the presence of glycerol and FFA using Free glycerol Reagent (Sigma, F6428) and NEFA-HR(2) (Wako Diagnostics), respectively. Tissue was dissolved in 0.3N NAOH/ 1% SDS at 60°C for protein quantification and normalization of the results.

Statistics. Data are expressed as mean ± S.E.M. Comparison of differences between two groups was assessed using unpaired two-tailed Student's t-tests. Multiple group comparisons were assessed by ANOVA analysis and Bonferroni post-hoc t-tests. Differences under $p < 0.05$ were considered statistically significant (* $p < 0.05$, ** $p < 0.01$, *** $p < 0.001$). Other symbols may be used for different group comparisons but they will be specified on the legends.

Chapter IV

A SUMO-dependent LRH-1/OSBPL3 pathway promoting NAFLD

Chapter IV A SUMO-dependent LRH-1/OSBPL3 pathway promoting NAFLD

IV.1 Introduction

In the liver, LRH-1 is an important regulator of glucose, cholesterol and bile acid metabolism (130). Liver-specific *Lrh-1* knockout mice display reduced glycolytic flux and *de novo* lipogenesis secondary to impaired GCK activity (174). On the other side, treatment of mice with the LRH-1 agonist, DLPC, protects animals from developing NAFLD and insulin resistance in genetic and dietary models of diabesity (123, 124). To address this apparent contradictory role of LRH-1 in hepatic triglyceride metabolism, we chose to study lipogenesis in our recently described *Lrh-1* K289R knockin mouse model (LRH-1 K289R mice), which displays selective gain-of-function of LRH-1 as a result of impaired SUMOylation at K289 (119).

In this study, we demonstrate that LRH-1 K289R induces the expression of oxysterol binding protein-like 3 (OSBPL3, encoded by *Osbpl3,* also known as *Orp3*), which in turn promotes the posttranslational activation of SREBP-1. As a consequence, LRH-1 K289R mice display increased *de novo* lipogenesis upon refeeding in comparison with WT mice. In fact, compared to LRH-1 WT mice, this chronic lipogenic stress promotes NAFLD in LRH-1 K289R mice accompanied by early signs of NASH when exposed to a lipogenic high-fat, high-sucrose (HFHS) diet.

IV.2 Results

Increased hepatic SREBP-1 processing in LRH-1 K289R mice

In order to evaluate the role of an LRH-1 SUMO-defective pathway on intermediary liver metabolism, we subjected LRH-1 K289R mice, which exhibit partial gain-of-function of LRH-1, and control LRH-1 wildtype (WT) mice (119) to fasting-refeeding challenges, in which mice were fasted and then refed for a period of 6 hours. We then evaluated the expression of metabolic genes in refed livers of both genotypes using microarray analysis. Interestingly, the expression of many SREBP-1 target genes was increased in 6-hour-refed LRH-1 K289R compared to LRH-1 WT livers, whereas SREBP-2 targets were not altered (Figure IV.1A). Although no changes in Srebf1 mRNA (Figure IV.1B) or uncleaved precursor SREBP-1 (Figure IV.1C) could be observed between both genotypes,

refed LRH-1 K289R livers displayed significantly more of the cleaved and transcriptionally active SREBP-1 protein in comparison to the LRH-1 WT livers (Figure IV.1C), indicating that the posttranslational processing and maturation of SREBP-1 is increased in LRH-1 K289R mice.

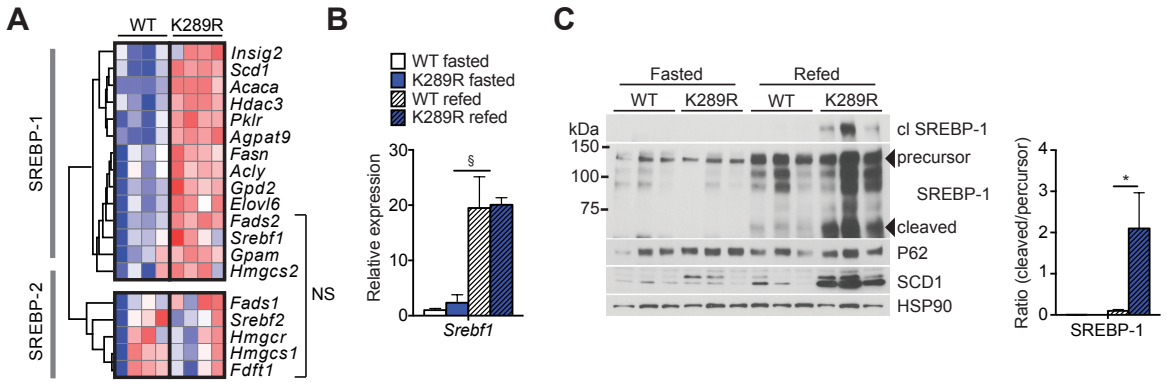

Figure IV.1. The posttranslational processing and maturation of SREBP-1 is increased in LRH-1 K289R mice.

(**A**) Heat map showing the expression of genes involved in *de novo* fatty acid and cholesterol synthesis in refed WT and K289R mice, depicting SREBP-1 and SREBP-2 target genes; (**B**) Hepatic mRNA expression of Srebf1 in K289R and WT mice. (**C**) Left, Immunoblots of precursor and cleaved (cl) SREBP-1, SCD1, HSP90, and P62 in hepatic lysates of WT or K289R livers. Right, graph displaying the ratio of cleaved to precursor SREBP-1. $^{§}P < 0.001$ refed relative to fasted mice.

We then performed acute insulin challenges as well as shorter 2-hour refeeding experiments to analyze if early signaling events could explain the increased SREBP-1 activity. Insulin did not induce an additional increase in AKT phosphorylation or a consistent induction of early response genes, such as activating transcription factor 3 (*Atf3*) or early growth response 1 (*Egr1*) (Figure IV.2A, B) (175, 176) in LRH-1 K289R versus LRH-1 WT livers. Similarly, we did not observe differences in *Srebf1a* and *Srebf1c* expression in 2-, 6-, or 12-hour-refed LRH-1 K289R and LRH-1 WT mice (Figure IV.2C). Taken together these data suggest that LRH-1 K289R induces SREBP-1 signaling primarily at the posttranscriptional level independent of early insulin-AKT signaling.

Enhanced de novo lipogenesis in LRH-1 K289R mice

To verify whether the increased expression of lipogenic genes is accompanied by hepatic fat accumulation, we next quantified hepatic triglyceride content in LRH-1K289R and LRH-1 WT mice. The content of neutral lipids and triglycerides was significantly increased in LRH-1 K289R compared to LRH-1 WT livers upon refeeding (Figure IV.3A, B). Of note, plasma triglycerides and free fatty acids did

not show significant alterations between LRH-1 K289R and LRH-1 WT mice (Figure IV.3C, D).

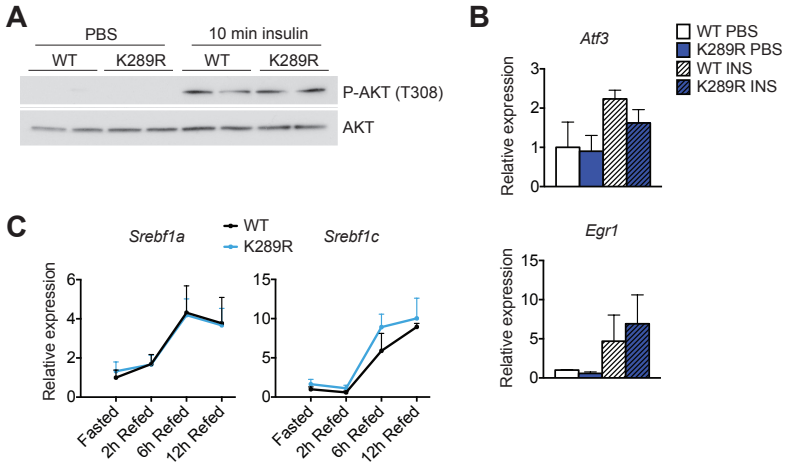

Figure IV.2. LRH-1 K289R mice do not show changes in the early insulin response.
(**A**, **B**) Phospho and total AKT immunoblots (**A**), and mRNA expression of early response genes (**B**) in livers from fasted WT or K289R mice that were injected with PBS or insulin 10 min prior to sacrifice. (**C**) Hepatic expression of the two *Srebf1* isoforms, *Srebf1a* and *Srebf1c*, in fasted and refed WT and K289R mice.

To verify whether the enhanced expression of lipogenic genes translates into increased *de novo* lipogenesis, animals received ^{13}C-acetate prior to sacrifice to quantify *de novo* lipogenesis (174). In line with the increased lipogenic gene expression, *de novo* synthesis of palmitate (C16:0), stearate (C18:0) and oleate (C18:1) was significantly higher in LRH-1 K289R compared to LRH-1 WT livers (Figure IV.4A-C). Of note, chain elongation of pre-existing fatty acids was not altered between the two genotypes (Figure IV.4D, E). Collectively these data show that LRH-1 K289R mice display increased *de novo* lipogenesis and enhanced

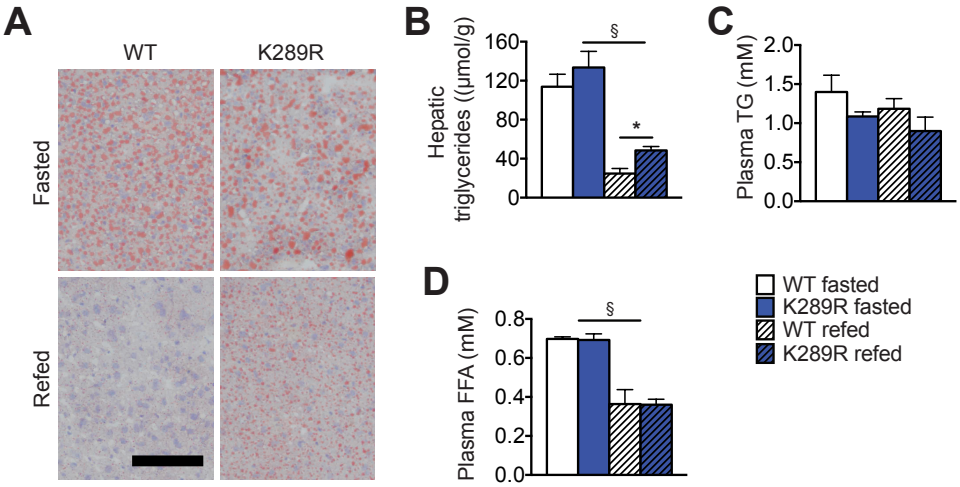

Figure IV.3. LRH-1 K289R mice display hepatic steatosis.
(**A**) Representative images of liver sections of K289R or WT mice stained with Oil-red O to visualize neutral lipids. Scale bar, 200 µm. (**B**) Quantification of hepatic triglyceride content in WT and K289R mice. (**C**, **D**) Plasma triglyceride (TG, **C**) and free fatty acid (FFA, **D**) contents in WT and K289R mice. $^{§}P < 0.001$ refed relative to fasted mice.

activation of SREBP-1 likely contributes to this process.

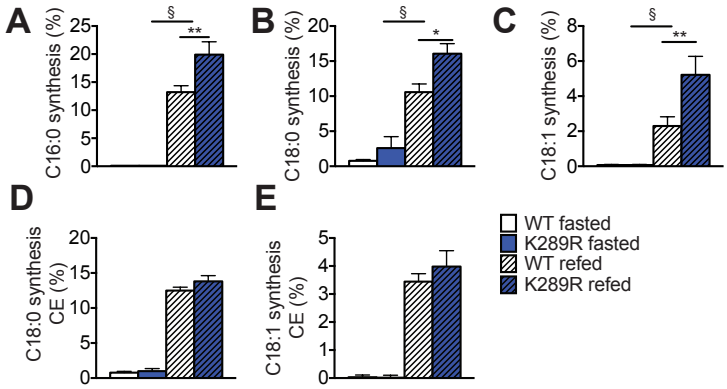

Figure IV.4. LRH-1 K289R mice display increased *de novo* lipogenesis.
(**A**-**C**) Fractional *de novo* synthesis rates of palmitate (**A**), stearate (**B**) and oleate (**C**) in WT and K289R mice. (**D**, **E**) Fractional chain elongation (CE) of pre-existing palmitate to hepatic stearate (**D**) and oleate (**E**). $^{\S}P < 0.001$ refed relative to fasted mice.

SUMOylation-defective LRH-1 drives the expression of oxysterol binding protein-like 3 (Osbpl3)

We next analyzed the transcriptome of livers from refed LRH-1 K289R and LRH-1 WT mice, and searched for transcripts that are linked to SREBP-1 processing. One of the top hits on the list of genes that was increased in LRH-1 K289R compared to LRH-1 WT livers corresponded to *Osbpl3* (*Orp3* gene), a member of a class of lipid transfer proteins recently implicated in the shuttling of lipids between the plasma and endoplasmic reticulum membrane (191-193). The expression of *Osbpl3*, and to a lesser extent *Osbpl1a*, was robustly induced in LRH-1 K289R livers while that of most other OSBP family members did not differ between the two genotypes (Figure IV.5A). Of interest, overexpression of certain oxysterol binding proteins has been suggested to increase SREBP-1 processing and hepatic lipogenesis (194). Analysis of livers of LRH-1 K289R versus LRH-1 WT mice confirmed the enhanced expression of *Osbpl3* during fasting and refeeding (Figure IV.5B-D), while the expression of other OSBP family members did not differ between the two genotypes (Figure IV.5E). Notably, the expression of *Osbpl3* is high during fasting and then reduced upon refeeding (Figure IV.5B). This postprandial suppression of *Osbpl3* mRNA expression was also observed upon overexpression of *Osbpl3* in mice using an adenovirus (Figure IV.5F),

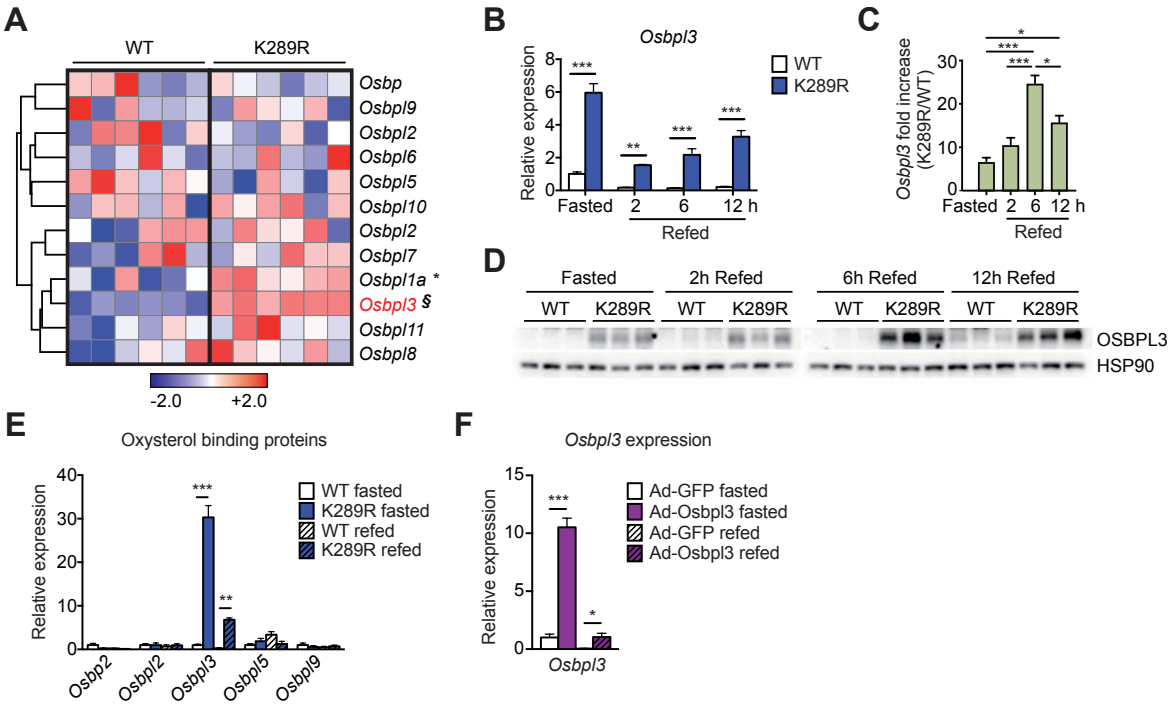

Figure IV.5. SUMOylation-defective LRH-1 drives the expression of *Osbpl3*.
(**A**) Heat map showing the hepatic expression of oxysterol binding protein family members in WT and K289R mice. (**B**, C) Expression of *Osbpl3* mRNA in hepatic lysates of fasted and refed WT and K289R mice (**B**), and the fold change between the genotypes (**C**). (**D**) Expression levels of OSBPL3 protein in hepatic lysates of fasted and refed WT and K289R mice. (**E**) Hepatic mRNA expression of oxysterol binding protein family members in fasted or 6-hour-refed K289R and WT mice. (**F**) *Osbpl3* expression in hepatic lysates of fasted or refed mice infected with Ad-GFP or Ad-OSBPL3. $^{§}P = 2 \times 10^{-7}$ relative to WT.

suggesting that during the refed state *Osbpl3* is regulated by post-transcriptional mechanisms occurring independently of LRH-1. Despite this feeding-dependent regulation of the mRNA, hepatic *Osbpl3* mRNA levels are consistently higher in the LRH-1 K289R mice in all nutritional states, but particularly high in the 6-hour-refeeding condition (Figure IV.5C), and these differences are translated into similar changes at the protein level (Figure IV.5D).

To investigate whether *Osbpl3* is directly controlled by LRH-1, we first analyzed the *Osbpl3* genomic region in available ChIP-Seq data for potential LRH-1 binding sites (195, 196). We identified three main sites from the ChIP-Seq data from Holmstrom *et al.* (sites 1-3, (195)) and three additional sites with an LRH-1 consensus sequence close to one of the transcription start sites of the *Osbpl3* gene (sites 4-6) were identified by computational analysis (Figure IV.6A). We then performed site-specific ChIP analysis to evaluate if these sites are bound by LRH-1 in fasted and refed mice. LRH-1 was recruited at different sites in both nutritional conditions (Figure IV.6B, C), suggesting that *Osbpl3* is a direct LRH-1 target gene.

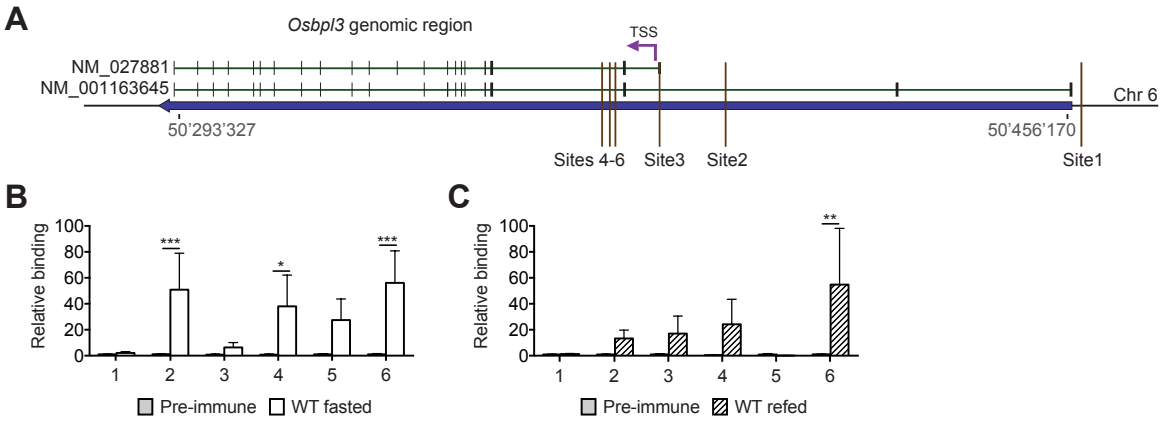

Figure IV.6. *Osbpl3* is a direct LRH-1 target gene.
(**A**) Scheme showing the genomic area containing the *Osbpl3* gene and the sites used for ChIP-qPCR experiment (mouse genome assembly mm10). (**B**, **C**) Binding of LRH-1 to the different *Osbpl3* promoter sites assessed by ChIP analysis using genomic DNA from fasted WT (**B**) and refed WT livers (**C**).

Based on the fact that LRH-1 and LXR have been shown to crosstalk in the regulation of hepatic acute phase response proteins (118, 167) and that various LRH-1 target genes, including lipogenic genes, are co-regulated by members of the LXR subfamily (170, 197, 198), we assessed the possibility that the LRH-1 mutant may modulate the recruitment of LXRα to its target genes, *Abca1*, *Chrebp*, and *Srebf1*. Although recruitment of LXRα was detected on these promoters in the genomic lysates of LRH-1 K289R and LRH-1 WT livers, no differences were observed between both genotypes, suggesting that LXRα binding is not altered due to the LRH-1 K289R mutation (Figure IV.7A). Furthermore, Hepa 1.6 and AML-12 cells treated with the LXR agonist GW3965 did not alter *Osbpl3* expression (Figure IV.7B, C), indicating that *Osbpl3* expression is not regulated by LXR.

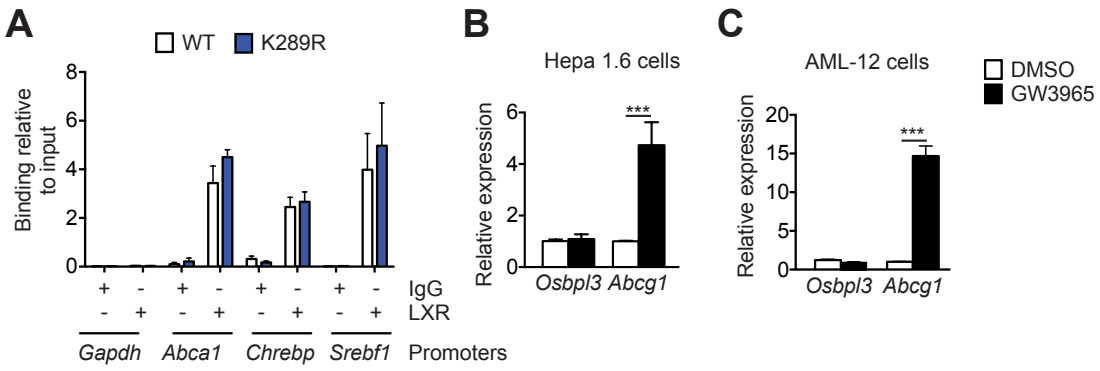

Figure IV.7. Crosstalk between LXR and LRH-1 pathways.
(**A**) LXR chromatin immunoprecipitation on hepatic lysates from WT and K289R mice. (**B**, **C**) Expression of *Osbpl3* and *Abcg1* in Hepa 1.6 (**B**) or AML-12 (**C**) cells upon treatment with the LXR agonist GW3965.

Osbpl3 silencing rescues the steatotic phenotype of LRH-1 K289R mice

To establish whether the increased expression of OSBPL3 in LRH-1 K289R livers

is causatively linked to the exacerbated *de novo* lipogenesis, we performed *in vivo* overexpression and silencing experiments. Adenoviral overexpression of OSBPL3 increased SREBP-1 cleavage in refed LRH-1 WT mice (Figure IV.8A), suggesting that elevated OSBPL3 levels promote SREBP-1 activation. We next silenced *Osbpl3* in LRH-1 K289R mice using siRNAs in LRH-1 K289R mice under fast-refeeding conditions. The hepatic mRNA expression of *Osbpl3* showed a clear trend of effective silencing (Figure IV.8B), while *Srebf1* expression was not altered (Figure IV.8C). Importantly, we observed a robust decrease in OSBPL3 protein, along with a reduction in the maturation of SREBP-1, and a blunted expression of the FASN transcript and protein in the livers of refed LRH-1 K289R mice treated with *siOsbpl3* (Figure IV.8D, E). We next assessed the effect of *Osbpl3* silencing under normal fed conditions.

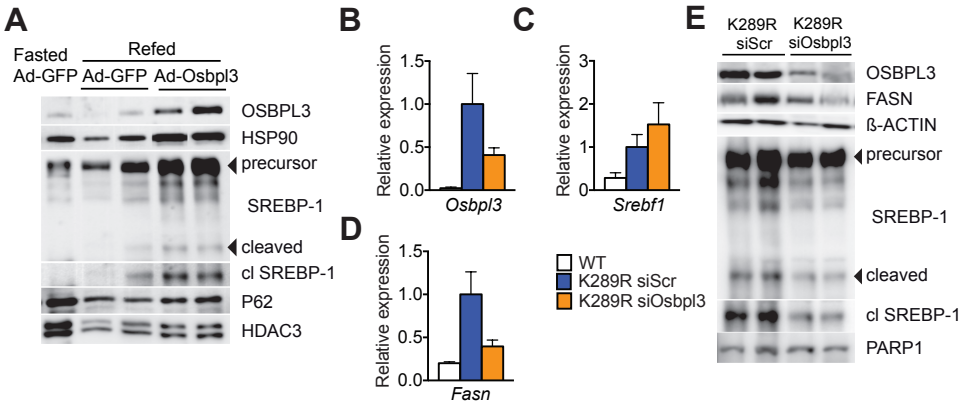

Figure IV.8. OSBPL3 promotes the maturation of SREBP-1.
(**A**) Immunoblots of OSBPL3, HSP90, precursor and cleaved (cl) SREBP-1, P62, and HDAC3 in hepatic lysates of fasted or refed WT + Ad-GFP or refed WT + Ad-OSBPL3 livers. (**B**, **C**) Hepatic mRNA expression of *Osbpl3* (**B**) and *Srebf1* (**C**) in refed K289R and WT mice. (**D**) Immunoblots of OSBPL3, FASN, β-ACTIN, precursor and cleaved (cl) SREBP-1, and PARP1 in hepatic lysates of refed K289R siScr or K289R siOsbpl3 livers. (**E**) Hepatic mRNA expression of *Fasn* in refed WT, K289R siScr or K289R siOsbpl3 mice.

Western blot analysis revealed reduced OSBPL3 expression (Figure IV.9A), and a robust decrease in the lipogenic proteins FASN and SCD-1 in *ad libitum* fed LRH-1 K289R mice treated with *siOsbpl3* compared to control mice (Figure IV.9A). Of interest, expression of the lipogenic enzymes, acetyl-Coenzyme A carboxylase alpha *(Acaca), Fasn,* stearoyl-Coenzyme A desaturase 1 *(Scd1), and* glycerol-3-phosphate acyltransferase *(Gpam),* was often normalized to values observed in LRH-1 WT mice (Figure IV.9B), suggesting that *Osbpl3* silencing rescues the lipogenic phenotype of LRH-1 K289R mice. In line with the reduced expression of lipogenic genes, *Osbpl3* silencing also decreased hepatic triglyceride and neutral lipid content (Figure IV.9C). As an additional approach to silence *Osbpl3*, we injected mice with an AAV8 viral vector containing a miRNA targeting *Osbpl3* in

the liver. Here again, we observed a robust silencing of *Osbpl3,* which was accompanied by the suppression of *Fasn* and a striking reduction of hepatic lipid droplets (Figure IV.9D-F).

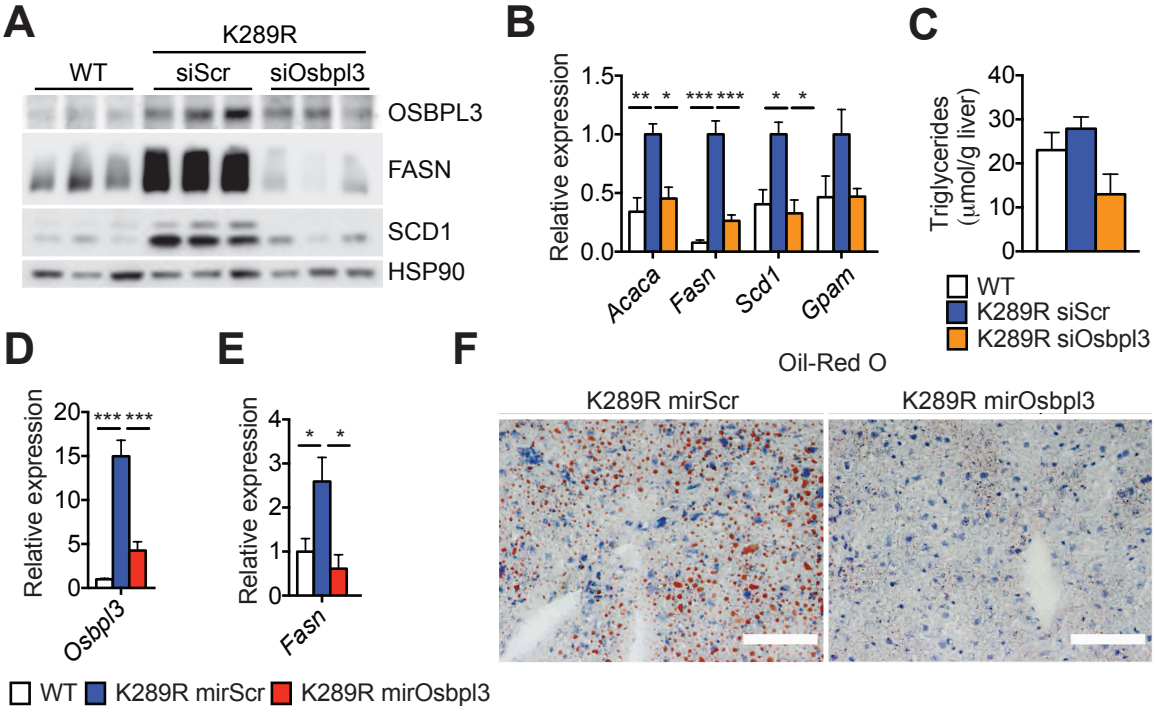

Figure IV.9. *Osbpl3* silencing rescues the lipogenic phenotype of LRH-1 K289R mice. (**A**) Hepatic expression of OSBPL3, FASN, SCD1, and HSP90 in livers of ad libitum fed WT, K289R siScr or K289R siOsbpl3 mice. (**B**) Hepatic mRNA expression of genes involved in de novo lipogenesis in ad libitum fed WT, K289R siScr or K289R siOsbpl3 mice. (**C**) Quantification of hepatic triglycerides in hepatic lipid extracts from ad libitum fed WT, K289R siScr or K289R siOsbpl3 mice. (**D**, **E**) Hepatic mRNA expression of *Osbpl3* (**D**) and *Fasn* (**E**) in 6-hours refed WT, K289R or K289R mirOsbpl3 mice. (**F**) Representative Oil-red O stainings in liver cryosections from refed K289R mirScrambled or K289R mirOsbpl3 mice. Scale bar, 100 µm.

Finally, we also examined whether other mechanisms, directly or indirectly regulated by LRH-1, may contribute to the lipogenic phenotype. Of interest, both hepatic glucose-6-phosphate content (174) and VLDL secretion (199) were unchanged between LRH-1 K289R and LRH-1 WT mice (Figure IV.10A-C), making it unlikely that these processes account for the exacerbated lipid accumulation in the liver.

Altogether these data suggest that the LRH-1-OSBPL3 signaling axis contributes to the increased maturation of SREBP-1, the induction of lipogenic enzymes, and the hepatic accumulation of triglycerides observed in LRH-1 K289R mice.

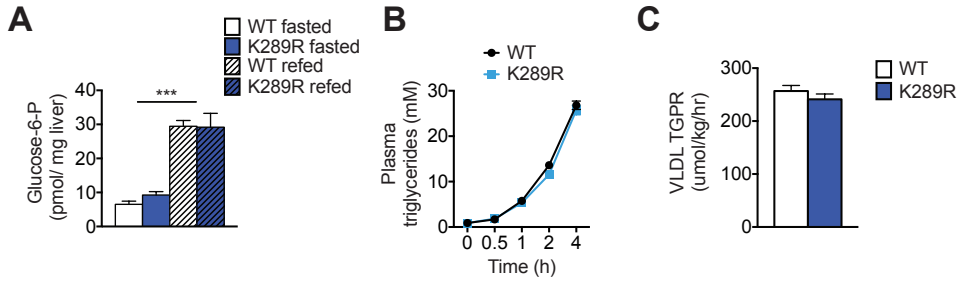

Figure IV.10. No change in glucose-6-phosphate production and VLDL secretion in LRH-1 K289R mice.

(**A**) Quantification of glucose-6-phosphate (glucose-6-P) in hepatic lysates of fasted or refed WT and K289R mice. (**B**, **C**) Plasma triglyceride synthesis over time (**B**), and triglyceride production rate (TGPR) in WT and K289R mice (**C**).

LRH-1 K289R mice are prone to develop NAFLD upon lipogenic diet feeding

Excessive *de novo* lipogenesis contributes to the development of NAFLD, a condition that can eventually progress to NASH (2, 4). In order to investigate if LRH-1 affects the development of NAFLD, LRH-1 K289R and LRH-1 WT mice were fed a highly lipogenic high-fat high-sucrose (HFHS) diet or a chow diet for 17 weeks, and then sacrificed under normal fed conditions. Stainings of hepatic sections with hematoxylin and eosin (H&E) and oil red O revealed that LRH-1 K289R mice develop a stronger steatotic phenotype compared to LRH-1 WT mice fed a HFHS diet (Figure IV.11A). While plasma cholesterol levels were unchanged (Figure IV.11B), triglyceride content in plasma (Figure IV.11C) or in VLDL fractions (Figure IV.11D) was reduced in HFHS-fed LRH-1 K289R mice. This reduction was accompanied with a robust accumulation of hepatic triglycerides (Figure IV.11E), as well as an induction of plasma levels of the enzymes alanine transaminase (ALAT) and aspartate aminotransferase (ASAT) in the HFHS-challenged LRH-1 K289R mice (Figure IV.11F, G). Similar to our earlier observations in normal chow diet conditions (Figure IV.5A-D), *Osbpl3* mRNA and OSBPL3 protein were significantly induced in LRH-1 K289R compared to LRH-1 WT mice fed a HFHS diet (Figure IV.11H, I), while the expression of other *Osbp* genes did not differ between the genotypes (Figure IV.11J).

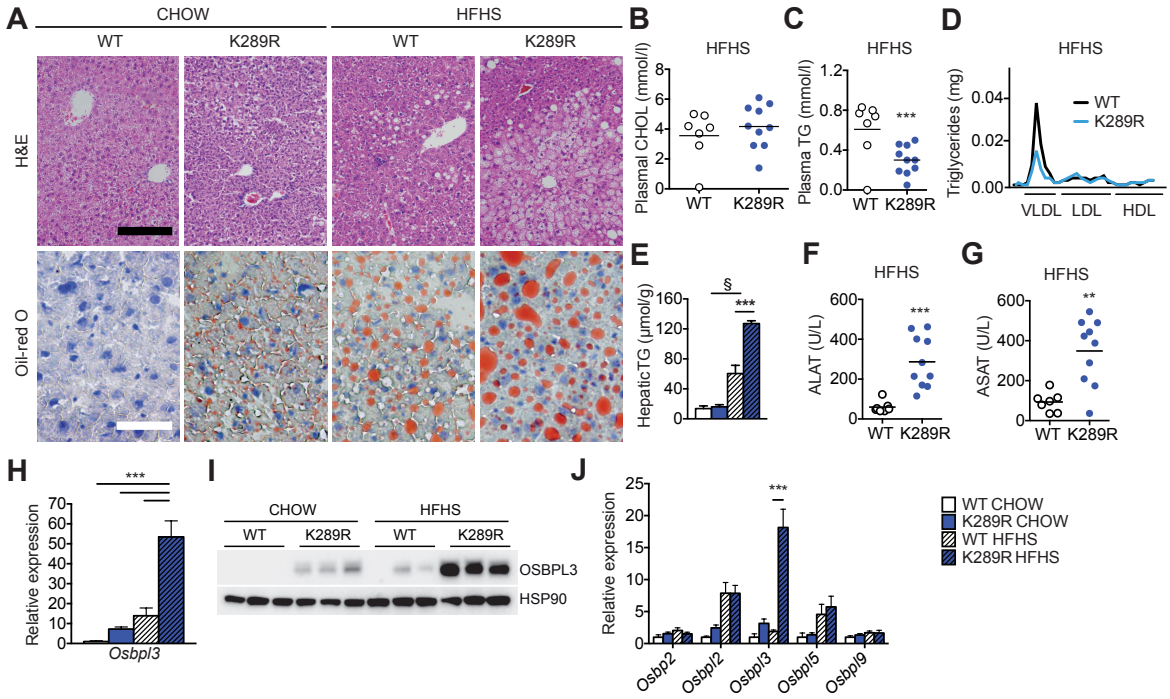

Figure IV.11. LRH-1 K289R mice develop NAFLD upon HFHS diet feeding.

(**A**) Representative images of liver sections of K289R or WT mice stained with hematoxylin and eosin (H&E) or Oil-red O to visualize the tissue structure and neutral lipids, respectively. Black scale bar, 200 µm; White scale bar, 50 µm. (**B**, **C**) Plasma cholesterol (**B**) and triglycerides (**C**) levels in WT and K289R mice fed a HFHS diet. (**D**) Triglyceride content in lipoprotein subfractions. (**E**) Quantification of triglyceride content in hepatic lipid extracts in WT and K289R mice. (**F**, **G**) Plasma levels of alanine transaminase (ALAT, **F**) and aspartate aminotransferase (ASAT, **G**) in mice fed a HFHS diet. (**H**, **I**) Expression of OSBPL3 mRNA (**H**) and protein (**I**) level in livers of WT and K289R mice fed chow and HFHS diets. (**J**) Hepatic mRNA expression of oxysterol binding protein family members in K289R and WT mice upon chow or HFHS feeding. $^{§}P < 0.001$ refed relative to fasted mice.

The development of hepatic steatosis in mice is known to be highly heterogeneous (200). Therefore we analyzed the data from a study in which mice were fed a chow or high-fat diet, and then classified according to the development of NAFLD/NASH into low-fat low (LFL) responders, low-fat high (LFH) responders, high-fat low (HFL) responders, and high fat high (HFH) responders (200). Interestingly, the expression of *Osbpl3* was significantly induced in the HFH responders along with markers of inflammation and necrosis (Figure IV.12A), and was by far the most strikingly increased *Osbp* among all family members (Figure IV.12B). We also analyzed *OSBPL3* expression in two cohorts of NAFLD/NASH patients. In the first cohort livers were categorized as mild or advanced NAFLD (Figure IV.13A) (201). In the second study, subjects had livers ranging from healthy controls to steatosis and further to NASH (Figure IV.13B) (202). *OSBPL3* expression was low in healthy livers, but increased in advanced stages of NAFLD/NASH and clustered with markers of fibrosis, suggesting that OSBPL3 could be a novel biomarker for advanced liver diseases, such as NASH.

Taken together, these data show that *Osbpl3* is significantly increased in LRH-1 K289R mice as well as in mice and humans with NAFLD/NASH.

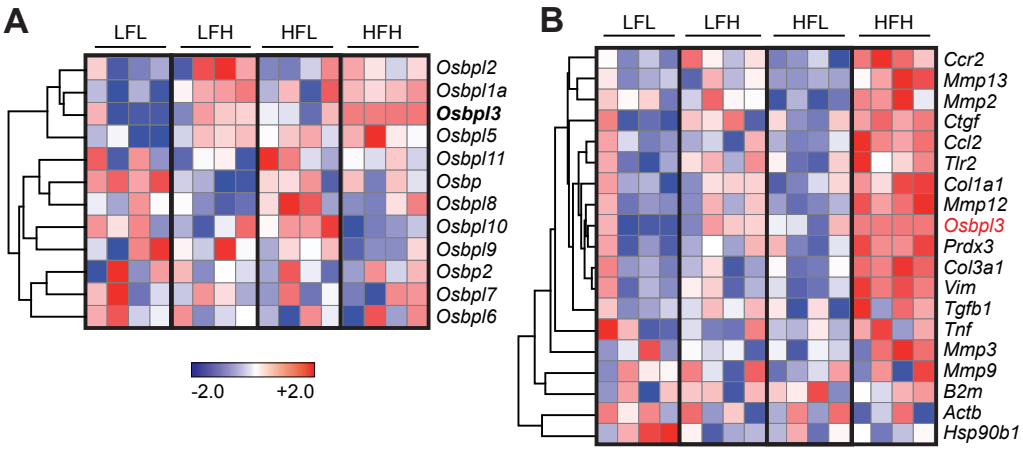

Figure IV.12. *Osbpl3* is significantly induced in high-fat diet responders and clusters with inflammation and fibrosis markers.

(**A**, **B**) Heat map displaying the expression of all *Osbps* (**A**) or of *Osbpl3* as well as markers of matrix degradation, fibrosis, and inflammation (**B**) in mice that were classified as into low-fat low (LFL) responders, low-fat high (LFH) responders, high-fat low (HFL) responders, and high fat high (HFH) responders according to the development of NAFLD/NASH upon chow or high-fat diet feeding.

LRH-1 K289R mice display increased inflammation and early signs of fibrosis in response to lipogenic diet feeding

Given the strong steatotic phenotype and the high levels of ALAT and ASAT markers in LRH-1 K289R mice fed a HFHS diet, as well as the clustering of *Osbpl3* with genes involved in inflammation and fibrosis in mice and humans with NAFLD, we next analyzed inflammatory and fibrotic markers in LRH-1 K289R and LRH-1 WT mice. Stainings of hepatic sections with Sirius Red and CD45 revealed that in contrast to LRH-1 WT mice, LRH-1 K289R mice develop small fibrotic lesions and accumulate CD45-positive immune cells upon HFHS feeding (Figure IV.14A). Moreover, LRH-1 K289R livers displayed higher levels of the inflammatory genes tumor necrosis factor alpha (*Tnfα*), monocyte chemoattractant protein-1 (*Mcp1* or *Ccl2*), and macrophage inflammatory protein-1 alpha (*Mip1α* or *Ccl3*) (Figure IV.14B), indicating increased inflammation in livers of HFHS-fed LRH-1 K289R mice.

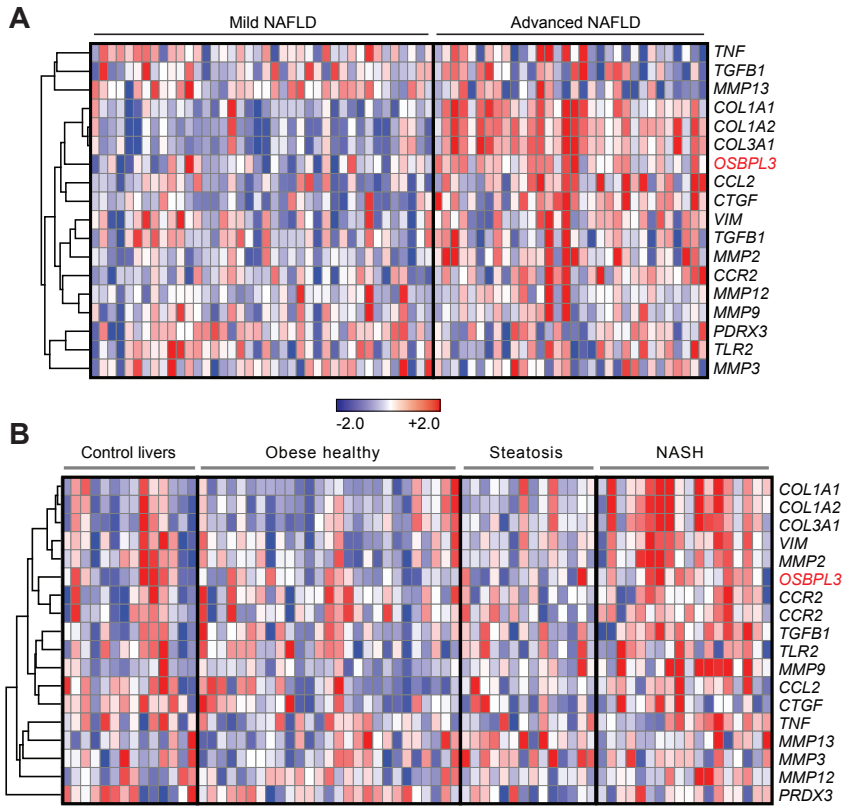

Figure IV.13. *Osbpl3* is increased in advanced stages of NAFLD/NASH.
(**A**) Expression of *OSBPL3* and markers of matrix degradation, fibrosis, and inflammation in transcriptomic data from human patients that were categorized for mild or advanced NAFLD. (**B**) Expression of *OSBPL3* and markers of matrix degradation, fibrosis, and inflammation in transcriptomic data from human subjects that had livers ranging from healthy controls to steatosis and further to NASH.

The expression of matrix metalloproteinases (MMPs), such as *Mmp2* and *Mmp13*, as well as early markers of fibrosis, such as alpha-1 type I collagen (*Col1a1*) and transforming growth factor beta-1 (*Tgfb1*), was also elevated in LRH-1 K289R in comparison to LRH-1 WT mice fed a HFHS diet (Figure IV.14C, D). Hepatic stellate cells are the primary hepatic cell type promoting fibrogenesis (203). The expression of different hepatic stellate cell markers, such as desmin (*Des),* glial fibrillary acidic protein (*Gfap*), and reelin (*Reln*), was also increased in HFHS-fed LRH-1 K289R compared to LRH-1 WT mice (Figure IV.14E), suggesting that HFHS-treated LRH-1 K289R mice exhibit early signs of NASH.

Previous studies showed that LRH-1 and the SUMOylation machinery might affect the hepatic acute phase response (APR) (118, 167, 168). While induction of the APR by short exposure of lipolysaccharide (LPS) led to reduced hepatic expression of C-reactive protein (*Crp)* and *Tnf* in LRH-1 K289R compared to LRH-1 WT mice, it did not alter the hepatic expression of other APR and inflammatory genes (Figure IV.15A). Moreover, no difference in plasma IL-6, MCP-1 (CCL-2) or TNF-α could be observed in LPS challenged LRH-1 K289R and LRH-1 WT mice

(Figure IV.15B), suggesting that the APR is likely not driving the observed inflammatory phenotype in our NAFLD-model.

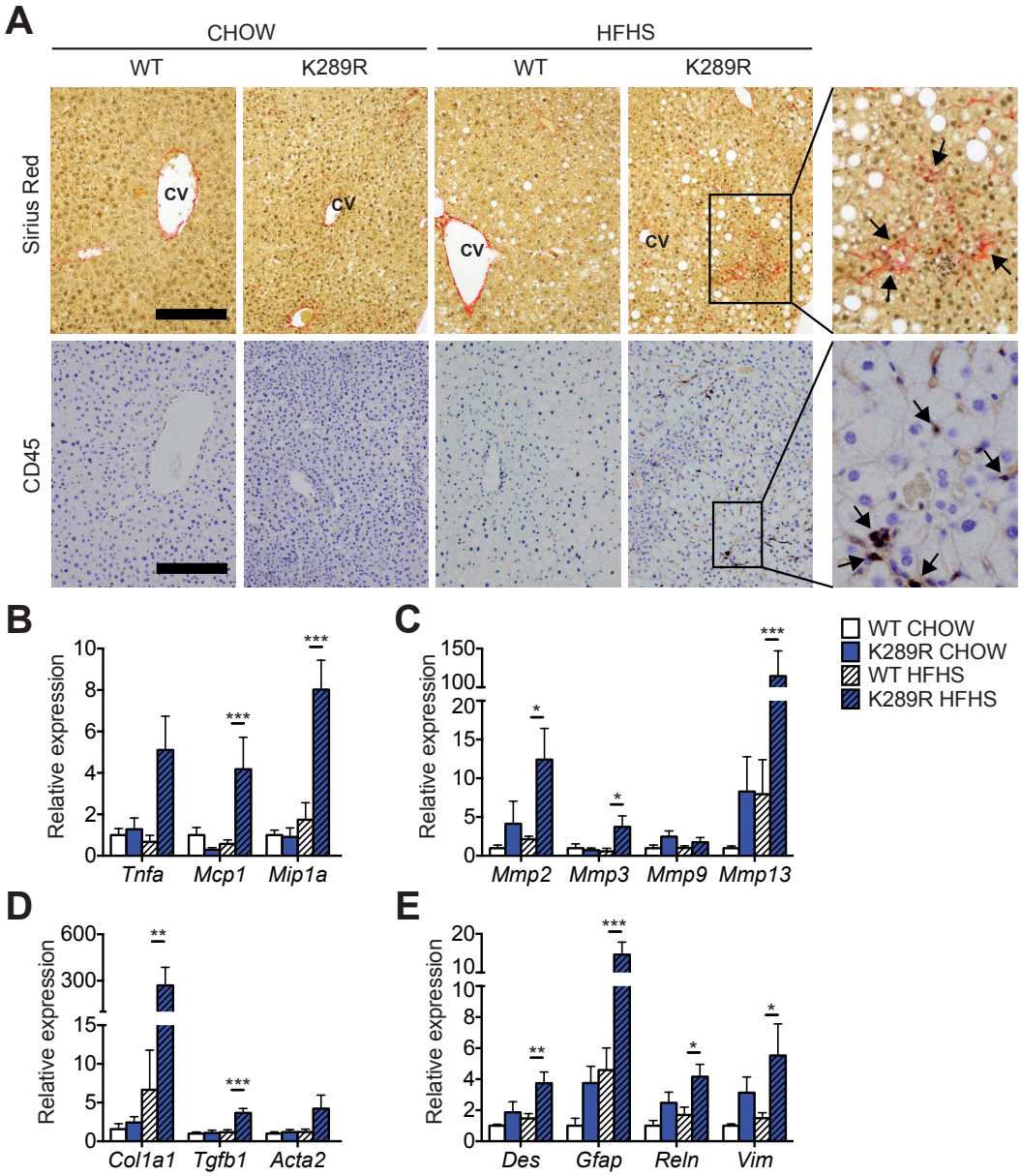

Figure IV.14. LRH-1 K289R mice display increased inflammation and early signs of fibrosis upon HFHS diet feeding.

(**A**) Representative images of liver sections of K289R or WT mice stained with Sirius Red or CD45 to visualize collagen depositions and CD45-positive cells, respectively. Scale bars, 200 µm; CV, central vein. (**B** - **E**) Hepatic mRNA expression of genes involved in inflammation (**B**), matrix degradation (**C**), fibrosis (**D**), and stellate cells (**E**) in K289R and WT mice.

Taken together, these data show that SUMOylation-defective LRH-1 promotes the development of NAFLD and displays early signs of NASH in mice fed a HFHS diet. This process is at least partially driven by the LRH-1-OSBPL3 signaling axis, which contributes to increased maturation of SREBP-1, the induction of lipogenic enzyme expression and hepatic triglyceride accumulation in LRH-1 K289R mice (Figure IV.16)

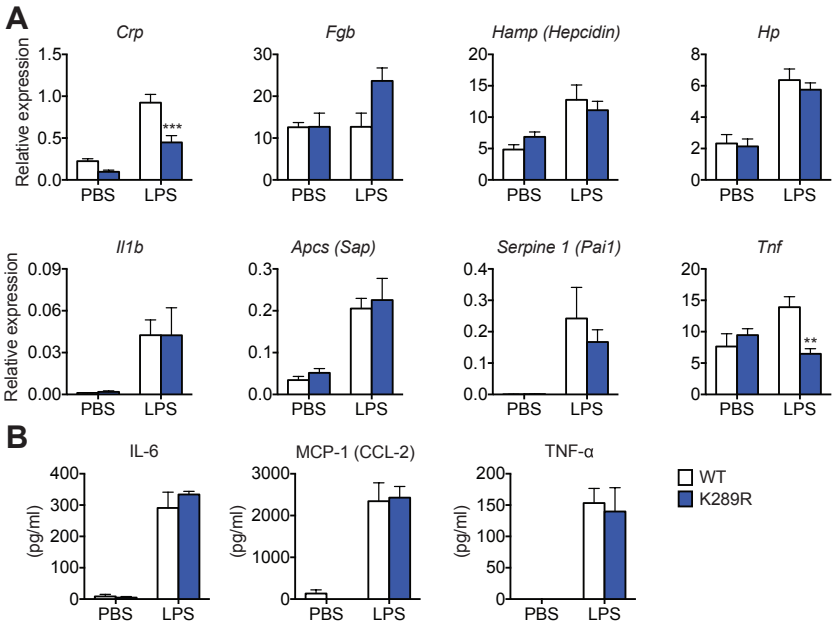

Figure IV.15. Hepatic acute phase response in LRH-1 WT and K289R mice.
(**A**) Hepatic expression of the indicated acute phase response genes in WT and K289R mice that were challenged with either PBS or lipopolysaccharide (LPS) for 2.5 hours. (**B**) ELISA assays to determine the plasma content of IL-6, MCP-1 or TNF-α.

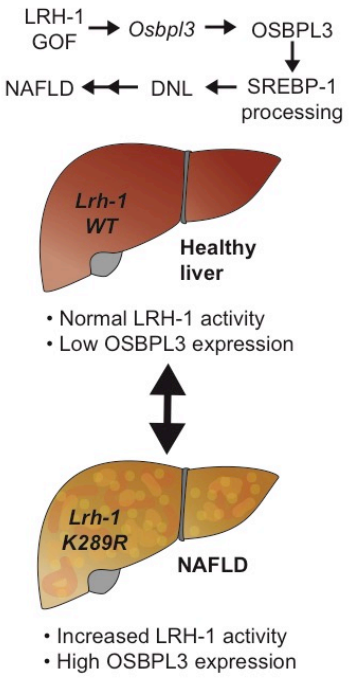

Figure IV.16. Graphical presentation depicting how the LRH-1/OSBPL3 axis drives the accumulation of hepatic lipids.

IV.3 Discussion

In this study, we analyzed the contribution of a selective LRH-1 gain-of-function on hepatic *de novo* lipogenesis and fatty liver development and identified *Osbpl3* as a critical component in the regulation of this process. While the hepatic

expression of *Osbpl3* is normally low in mice under basal conditions, LRH-1 K289R mice express high levels of this specific OSBP family member. Consistent with our observations, the analyses of independent mouse and human transcriptomic datasets revealed that *Osbpl3* expression is often induced in NAFLD/NASH. Our work furthermore strengthens the putative role of OSBPL3 in SREBP-1 maturation. As a consequence, LRH-1 K289R mice display increased *de novo* lipogenesis and accumulation of triglycerides upon refeeding in a manner that is independent of enhanced LXRα recruitment or activity. Importantly, silencing of OSBPL3 *in vivo* reverts the increased lipogenesis observed in these animals. Moreover, when exposed to a lipogenic HFHS diet, LRH-1 K289R mice develop NAFLD accompanied by early signs of NASH, most likely as a consequence of chronic fat accumulation (2, 4).

The excessive accumulation of hepatic lipids and increased *de novo* lipogenesis could also have other causes. A previous study using liver-specific *Lrh-1* knockout mice showed that LRH-1 promotes glucokinase expression, hence regulating glycolysis and *de novo* lipogenesis (174). However, we did not observe a difference in hepatic glucose-6-phosphate content between LRH-1 WT and LRH-1 K289R mice, suggesting that the selective gain-of-function of LRH-1 driven by the K289R mutation does not increase substrate availability for the glycolytic pathway. Based on the finding that the primary corepressor of LRH-1 affects microsomal triglyceride transfer protein levels and consequently hepatic VLDL-triglyceride secretion (199), we also performed *in vivo* VLDL-secretion assays, but could not detect any difference between refed LRH-1 K289R and LRH-1 WT mice. Finally, LRH-1 SUMOylation has been linked to the induction of the hepatic acute phase response (118, 167, 168), which could explain the excessive inflammation observed in the livers of mice receiving a chronic HFHS diet. To study the acute phase response *in vivo*, we challenged LRH-1 WT and LRH-1 K289R mice with lipopolysaccharide for 2.5 hours. Besides the reduction in *Crp* and *Tnf*, the inflammatory signature was comparable between the genotypes, suggesting that the exacerbated inflammatory phenotype of the LRH-1 K289R mice is most likely not driven by changes in the APR.

While the induction of SREBP-2 processing has been well described, the mechanisms that trigger SREBP-1 processing are less well understood (28). Insulin receptor-AKT-mTOR signaling is considered as one of the main pathways triggering SREBP-1 signaling (204). A recent study showed that insulin promotes SREBP-1 activation and *de novo* lipogenesis via mTORC1-dependent

and -independent mechanisms (205). Others proposed that while insulin signaling is required for SREBP-1 activation in insulin-resistant conditions, it is not critical to induce the feeding-dependent induction of SREBP-1 under physiological conditions (206, 207). In breast epithelial cells the expression of oncogenic forms of the PI3K or K-Ras are sufficient to induce SREBP-1 maturation and *de novo* lipogenesis through induction of mTOR signaling (208). Whereas these and many other studies demonstrate that the expression of *Srebf1* and the posttranslational maturation of SREBP-1 can be triggered by insulin signaling, other downstream or parallel pathways exist. One recent example is the induction of SREBP-1 processing upon depletion of phosphatidylcholine, whose synthesis is dependent on S-adenosylmethionine, a methionine derivative that is generated in the one-carbon cycle (173). We did not observe a difference in AKT phosphorylation between LRH-1 WT and LRH-1 K289R mice, suggesting other signaling pathways to induce the processing of SREBP-1. Indeed, our current study highlights the existence of an alternative mechanism of SREBP-1 activation involving a SUMO-dependent LRH-1/OSBPL3 pathway.

The first oxysterol binding proteins were identified, purified and cloned in the 1980s (209-211). Recent studies suggest that OSBPs act as sterol transfer and/or sensor proteins that may also play important roles in cell signaling (212, 213). OSBPL3, a member of subfamily III, contains a conserved sterol-binding OSBP homology domain (OHD) as well as a phosphatidylinositol lipid species-binding pleckstrin homology (PH) domain and two 2-phenylalanines in an acidic tract (FFAT) domains that bind to the vesicle-associated membrane protein-associated (VAMP-associated) protein (VAP) (212, 214, 215). Recently, it has been shown that this last interaction can activate R-RAS, thus reorganizing the actin cytoskeleton and affecting cell polarity and cell-cell adhesion (216). Future studies will be necessary to dissect the exact mechanisms by which OSBPL3 modulates SREBP-1 processing, but its association with the ER could indicate a possible site of regulation.

In addition to the identification of OSBPL3 as a target of LRH-1, our study also highlights the existence of complex regulatory mechanisms to which OSBPL3 is subjected. We observed a discrepancy between mRNA and protein levels of OSBPL3 between fasting and refed conditions despite its persistent increase in LRH-1 K289R mice. The marked reduction in mRNA levels upon refeeding was also noticed when OSBPL3 was overexpressed using an adenovirus, indicating that additional posttranscriptional mechanisms independent of LRH-1 regulate

the expression of OSBPL3. Moreover, while the expression of OSBPL3 is low in healthy livers, it is increased in NAFLD, suggesting that this protein could be a novel biomarker for NAFLD.

In this study, we described a novel function of LRH-1 in the development of fatty liver disease. It is noteworthy that other nuclear receptors also contribute to the development of NAFLD by affecting steatosis, glucose homeostasis, inflammation and/or fibrosis in the liver. For instance, while activation of LXRs or pregnane x receptor (PXR) promote lipogenesis and the development of NAFLD, activation of other nuclear receptors such as peroxisome proliferator-activated receptors (PPARs) or farnesoid X-activated receptor (FXR) has opposite effects (reviewed in (217)). Clinical trials performed in NASH patients using PPARγ or FXR agonists showed that the beneficial effects observed on hepatic steatosis and inflammation were accompanied by adverse effects on obesity and hypercholesterolemia, respectively (218, 219), highlighting the functional complexity of nuclear receptors (217). Therefore, the development of drugs targeting specific nuclear receptors targets, such as OSBPL3, might provide alternative therapeutic options for treating NAFLD.

Chapter V

SLC25A47 as a novel determinant in hepatic steatosis

Chapter V SLC25A47 as a novel determinant in hepatic steatosis

V.1 Introduction

In recent years, LRH-1 has emerged as an essential regulator of the hepatic glucose-sensing system. *Lrh-1* liver-specific knockout (*Lrh-1* $^{hep-/-}$) mice fail to adequately induce glycolysis, glycogen synthesis and DNL in response to a standardized meal (169). In contrast to its role in postprandial hepatic metabolism, the physiological role of LRH-1 in the fasted state is still largely unknown. Furthermore, the impact of LRH-1 on mitochondria, key organelles in times of scarcity of nutrients, is largely unexplored. We hence decided to explore the role of LRH-1 in the fasted liver and its influence on mitochondrial function.

Mitochondria are essential organelles for metabolic homeostasis being the prime location for FA oxidation and therefore lipid disposal. Their oxidative capacity and flexibility to environmental and/or endocrine signals are crucial for NAFLD and dictates the disease progression (50).

SLC25 are mitochondrial transporters responsible for the import and export of almost all metabolites, cofactors and anions to and from mitochondria (81). Due to the plethora of molecules transported, SLC25 members are involved in many metabolic pathways, including oxidative phosphorylation, citric acid cycle and FA degradation (81, 87). Targeting mitochondria in general or SLC25 family members in particular could thus prove an efficient tool for NAFLD treatment (88).

In this chapter, we demonstrate that mice lacking LRH-1 in hepatocytes present mitochondrial dysfunction exacerbated by fasting challenge. As a consequence, *Lrh-1* $^{hep-/-}$ mice display fasting-induced steatosis. Finally, the expression of *Slc25a47* is regulated by LRH-1 and its recovery in LRH-1-deleted livers rescues the steatotic phenotype (**section V.2.1)**. Moreover, we identified a novel liver-specific mitochondrial transporter (SLC25A47) that is induced upon fasting and improves mitochondrial FA oxidation. The identification of SLC25A47 as a pivotal player in oxidative catabolism proved to be also beneficial in the context of NAFLD, a condition in which this transporter is normally downregulated (**section V.2.2)**.

V.2. Results

V.2.1 Fasting-induced steatosis driven by the loss of LRH-1 in the liver is rescued by SLC25A47

Lrh-1 $^{hep-/-}$ mice display fasting-induced steatosis

In the liver, the fasted and fed states are examples of physiological conditions that differ significantly in biochemical responses. To explore the putative involvement of LRH-1 in liver intermediary metabolism during fasting, we subjected mice with a somatic deletion of LRH-1 in hepatocytes (*Lrh-1* $^{hep-/-}$) (169) and their control littermates (*Lrh-1* $^{hep+/+}$) to an overnight (ON) fasting challenge. Interestingly, fasting caused a robust lipid accumulation in the liver of *Lrh-1* $^{hep-/-}$ mice (Figure V.1A) compared to *Lrh-1* $^{hep+/+}$ littermates. Fasting-induced steatosis was accompanied by a higher liver mass in *Lrh-1* $^{hep-/-}$ mice but not by changes in body weight and eWAT mass (Figure V.1B-D). To further verify the content of lipids in the liver, we quantified hepatic TG levels and confirmed lipid accumulation (Figure V.1E) in the liver of fasted *Lrh-1* $^{hep-/-}$ mice. Of note, plasma FA and TG did not show any significant alterations between the two genotypes (Figure V.1F, G), making it unlikely that decreased VLDL secretion in the liver could account for the steatotic phenotype.

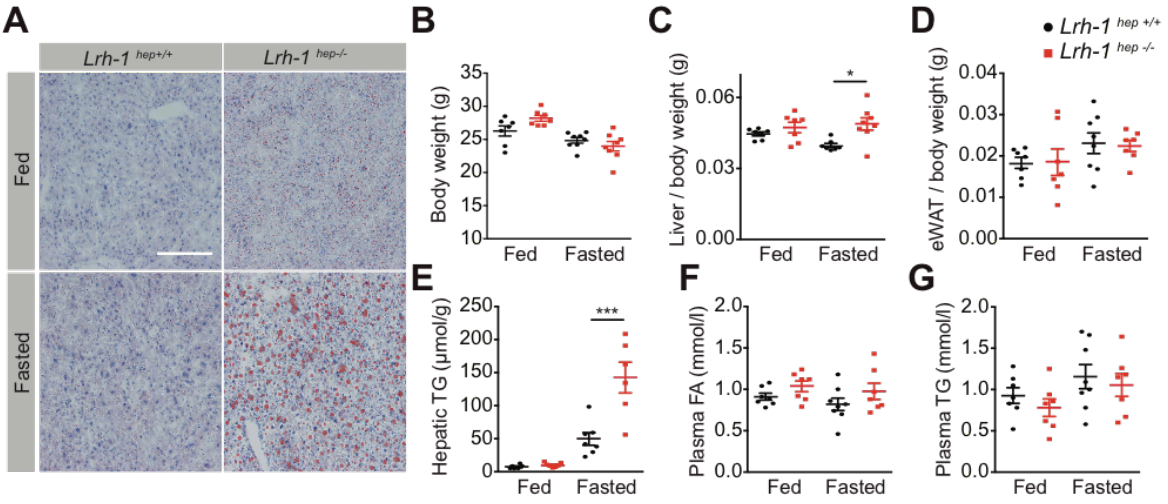

Figure V.1. *Lrh-1* $^{hep-/-}$ mice display fasting-induced steatosis.
(**A**) Representative oil red O stainings of *Lrh-1* $^{hep+/+}$ and *Lrh-1* $^{hep-/-}$ mice in fed and fasted conditions to visualize neutral lipids. Scale bar: 200 µm (**B-D**) Body weight (**B**), liver (**C**) and epididymal white adipose tissue (eWAT) mass (**D**) of fed and fasted *Lrh-1* $^{hep+/+}$ and *Lrh-1* $^{hep-/-}$ mice. (**E**) Quantification of hepatic triglyceride (TG) in lipid extracts of fed and fasted *Lrh-1* $^{hep+/+}$ and *Lrh-1* $^{hep-/-}$ mice. (**F**, **G**) Plasma free fatty acids (FA, **F**) and TG (**G**) levels in fed and fasted *Lrh-1* $^{hep+/+}$ and *Lrh-1* $^{hep-/-}$ mice.

Lrh-1 $^{hep-/-}$ *mice display mitochondrial dysfunction*

Excessive hepatic lipid accumulation during fasting can be due to a dysregulation of several processes, including adipose tissue lipolysis or hepatic fatty acid oxidation (2). To test if increased adipose tissue lipolysis accounts for the observed hepatic lipid overload in the *Lrh-1* $^{hep-/-}$ livers, we next performed an *ex vivo* lipolysis assay. Free fatty acids and glycerol release in the medium from adipose explants was not significantly changed between *Lrh-1* $^{hep-/-}$ and *Lrh-1* $^{hep+/+}$ mice (Figure V.2A, B), while there was a significant stimulation after forskolin treatment, indicating equal lipolysis rate.

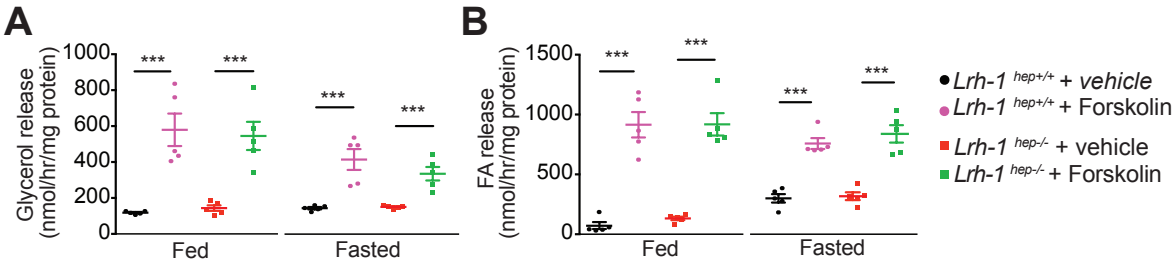

Figure V.2. *Lrh-1* $^{hep-/-}$ mice don't present altered white adipose tissue lipolysis rate.

(**A**, **B**) *Ex vivo* lipolysis-associated glycerol (**A**) and free fatty acids (FA, **B**) released from *Lrh-1* $^{hep+/+}$ and *Lrh-1* $^{hep-/-}$ white adipose tissue explants.

We then decided to evaluate the capacity of hepatic mitochondrial activity in these animals. First, we performed microarray analysis in the liver of fasted *Lrh-1* $^{hep+/+}$ and *Lrh-1* $^{hep-/-}$ mice. Liver transcriptome analysis exhibited an important representation of the transcripts for mitochondrial proteins (14%) among the most significantly altered genes upon loss of LRH-1 (Figure V.3A, shown in red). More importantly, gene ontology (GO: cellular compartment) showed mitochondria as the top compartment where genes downregulated in LRH-1-deficient livers are mostly located (Figure V.3B). The most significantly downregulated mitochondrial genes are depicted in Figure V.3C. In addition, we performed proteomics in the liver of *Lrh-1* $^{hep+/+}$ and *Lrh-1* $^{hep-/-}$ mice. KEGG pathway analysis of all the proteins downregulated in *Lrh*-1 $^{hep-/-}$ livers revealed fatty acid degradation as one of the most significant pathways affected by the lack of LRH-1 (Figure V.3D).

High-resolution respirometry using either succinate and rotenone ($State_{3ADP}$, Figure V.4A) or fatty acid oxidation (FAO) substrates (fatty acyl-carnitines, Figure V.4B) in the presence of ADP revealed that loss of LRH-1 in hepatocytes is associated with lower hepatic mitochondrial oxygen consumption rate (OCR).

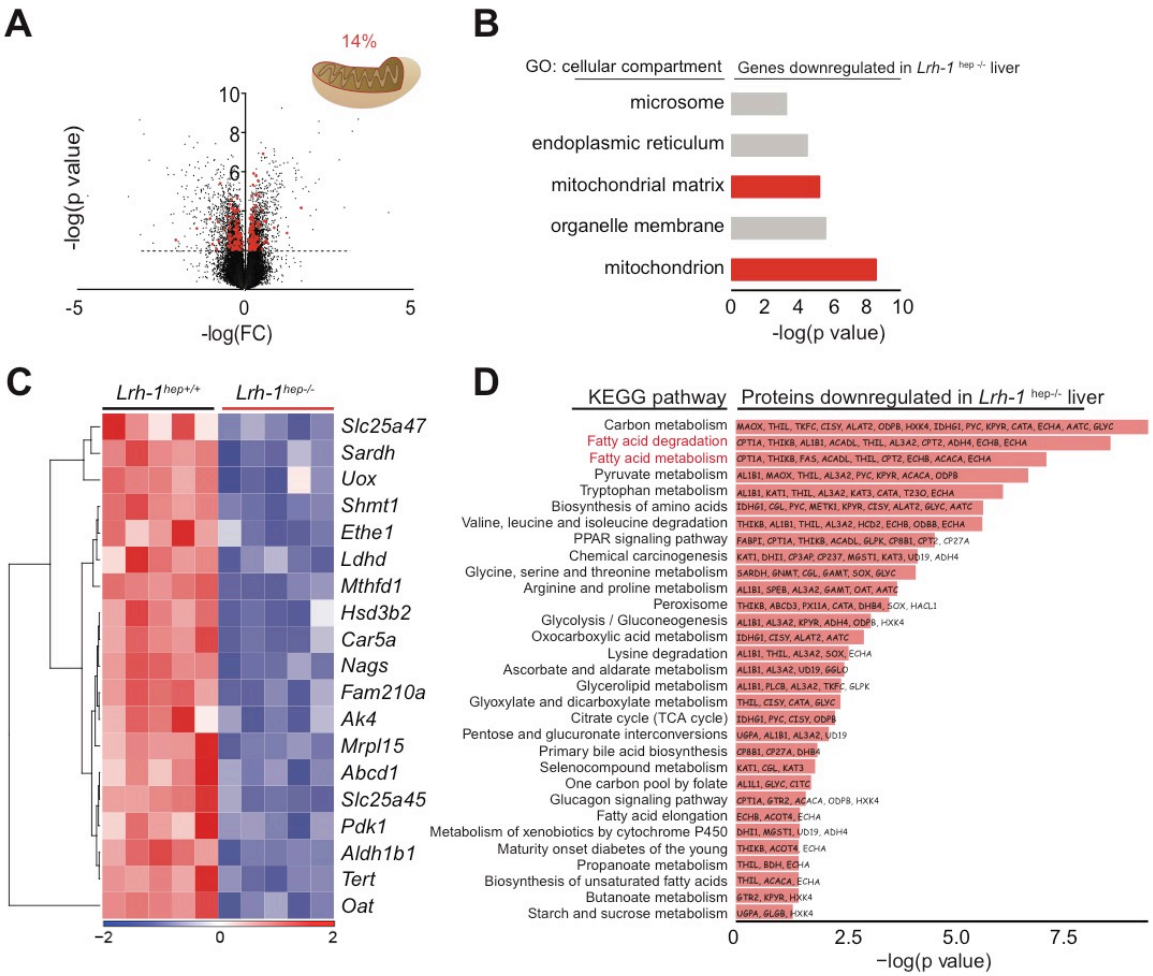

Figure V.3. LRH-1 regulates mitochondrial proteins transcripts.
(**A**) Vulcano plot depicting in red the significant representation of mitochondrial transcripts among all genes in fasted *Lrh-1* $^{hep+/+}$ and *Lrh-1* $^{hep-/-}$ mice liver microarray. FC, fold-change (WT/KO). (**B**) Gene ontology (GO, cellular compartment) of genes downregulated in livers from fasted *Lrh-1* $^{hep-/-}$ in comparison with *Lrh-1* $^{hep+/+}$ mice. (**C**) Heat map of the most significant downregulated mitochondrial genes (from **B**) in fasted *Lrh-1* $^{hep-/-}$ livers, FC>1.4 and $P<1x10^{4}$. (**D**) Pathway enrichment analysis (KEGG) of proteins downregulated in *Lrh-1* $^{hep-/-}$ livers.

Furthermore, oleic acid oxidation was significantly reduced in the liver of *Lrh-1* $^{hep-/-}$ mice (Figure V.4C). In line with these observations, *Lrh-1* $^{hep-/-}$ mice showed an accumulation of hepatic acyl-carnitines when compared to those in the liver of *Lrh-1* $^{hep+/+}$ mice (Figure V.4D). This reduction in fatty acid oxidation was accompanied by lower levels of hepatic ATP in *Lrh-1* $^{hep-/-}$ mice (Figure V.4E), suggestive of reduced substrate utilization to energy conversion. In parallel to the reduced mitochondrial OCR, expression and activity of the mitochondrial complexes were decreased in the liver of *Lrh-1* $^{hep-/-}$ mice, especially CII (Figure V.4F-H). Together these data indicate that LRH-1-deficient livers display mitochondrial dysfunction that makes them inefficient in producing sufficient energy from the substrates available during a fasting condition.

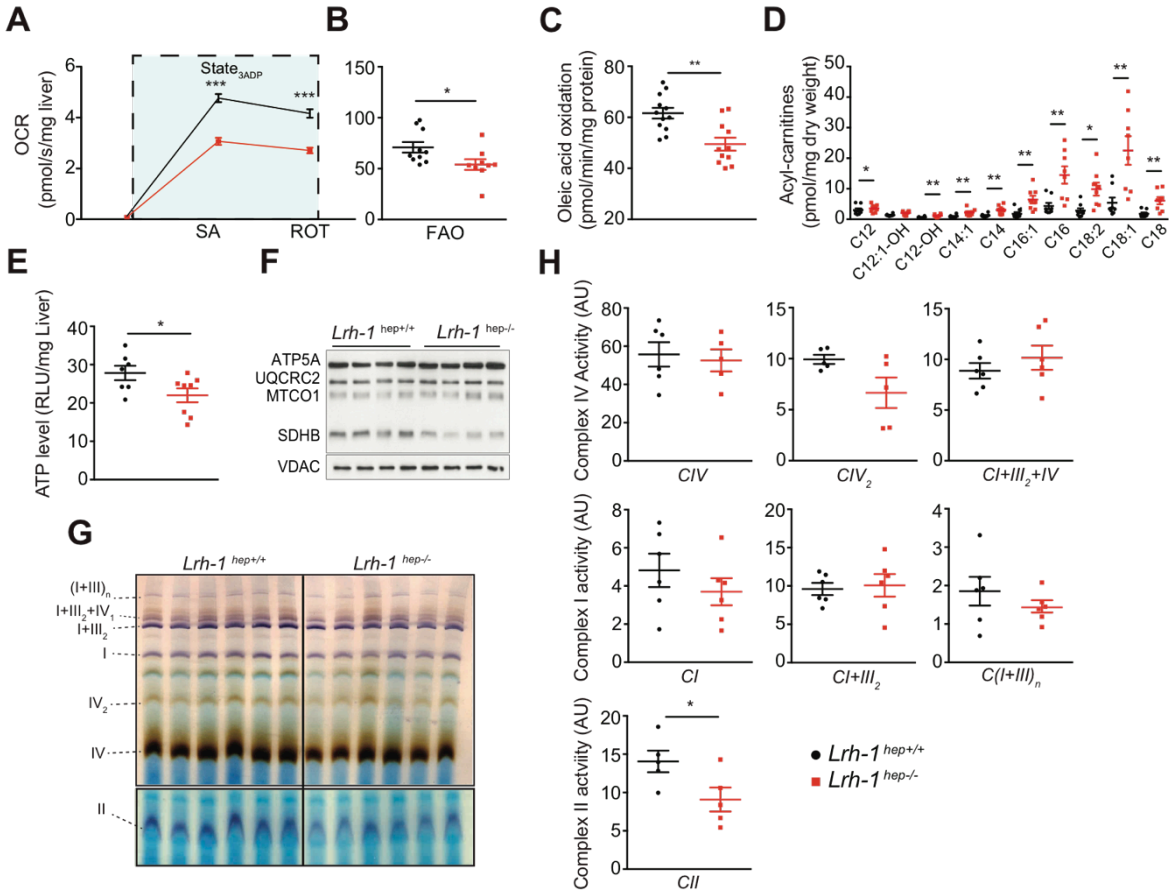

Figure V.4. ***Lrh-1*** $^{hep-/-}$ **mice display mitochondrial dysfunction.**
(**A**) Oxygen consumption rate (OCR) of fresh liver homogenates from fasted *Lrh-1* $^{hep+/+}$ and *Lrh-1* $^{hep-/-}$ mice by high-resolution respirometry in the presence of succinate, ADP (SA) and rotenone (ROT) - State$_{3ADP}$. (**B**) OCR of fresh liver homogenates from fasted *Lrh-1* $^{hep+/+}$ and *Lrh-1* $^{hep-/-}$ mice in the presence of fatty acid oxidation (FAO) substrates, palmitoyl- and octanolyl-carnitine, and ADP. (**C**) Oleic acid oxidation assay in the liver of fasted *Lrh-1* $^{hep+/+}$ and *Lrh-1* $^{hep-/-}$ mice. (**D**) Liver acyl-carnitines content in fasted *Lrh-1* $^{hep+/+}$ and *Lrh-1* $^{hep-/-}$ mice. (**E**) Hepatic ATP level of fasted *Lrh-1* $^{hep+/+}$ and *Lrh-1* $^{hep-/-}$ mice. (**F**) Immunoblots of mitochondrial complexes subunits ATP5A (CV), UQCRC2 (CIII), MTCO1 (CIV), SDHB (CII) and VDAC as a loading control in isolated mitochondria from fasted *Lrh-1* $^{hep+/+}$ and *Lrh-1* $^{hep-/-}$ livers. (**G**) *In-gel* activity of mitochondrial complexes (I, II and IV) from *Lrh-1* $^{hep+/+}$ and *Lrh-1* $^{hep-/-}$ fasted liver mitochondria. Complex I (purple); Complex IV (brown); complex II (blue). (**H**) Quantification of the bands in **G** normalized to coomassie blue staining bands.

LRH-1 drives the expression of Slc25a47

Mitochondrial solute carriers (SLC25) are very important for mitochondrial metabolism allowing the shuttling of substrates and products through the IMM thus establishing the communication between cytosol and mitochondria (81). Since LRH-1 deficient livers have compromised substrate utilization by the mitochondria, we next sought to verify whether any SLC25 family member is affected by the loss of LRH-1 in the liver. Since *Slc25a47* is significantly downregulated in *Lrh-1* $^{hep-/-}$ livers (Figure V.3C), we decided to further explore the molecular link between LRH-1 and *Slc25a47*. Intriguingly, *Slc25a47* is downregulated in a similar manner as LRH-1 target genes such as *Nr0b2*, *Cyp8b1*

and Gnmt (Figure V.5A) indicating that this carrier could be directly regulated by LRH-1. Analysis of livers of *Lrh-1* $^{hep-/-}$ mice confirmed the decreased expression of *Slc25a47* at both transcript (Figure V.5B) and protein level (Figure V.5C). To investigate whether SLC25A47 is directly controlled by LRH-1, we analyzed the *Slc25a47* genomic region in available ChIP-seq data for potential LRH-1 binding sites (196). We identified 3 significant peaks with an LRH-1 consensus-binding site, one being close to the transcriptional start site of the *Slc25a47* gene (Figure V.5D, black arrow). We then performed site-specific ChIP-qPCR analysis to evaluate whether the site with the most significant peak is bound by LRH-1 (black arrow). LRH-1 was recruited at the *Slc25a47* promoter region when using liver chromatin from *Lrh-1* $^{hep+/+}$ mice (Figure V.5E). However, loss of LRH-1 binding was observed when using LRH-1-deficient livers (Figure V.5E), suggesting that *Slc25a47* is a direct LRH-1 target gene.

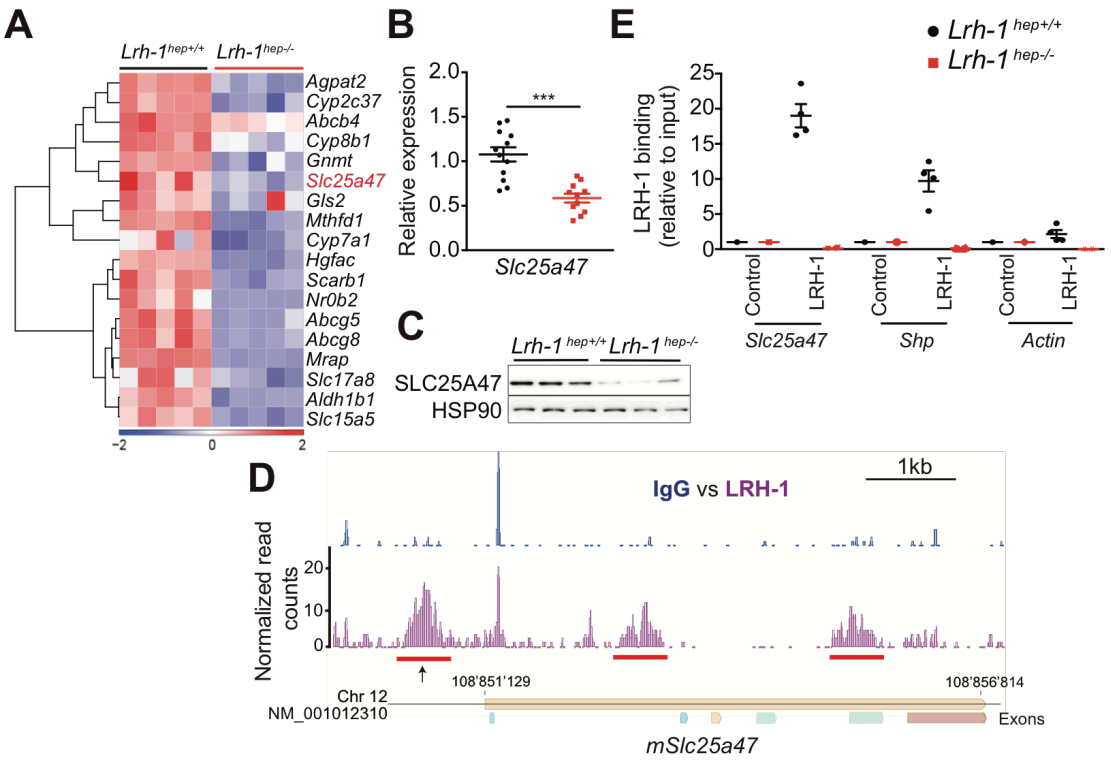

Figure V.5. *Slc25a47* is a direct target of LRH-1 transcriptional regulation.
(**A**) Heat map depicting LRH-1 target genes expression between fasted *Lrh-1* $^{hep+/+}$ and *Lrh-1* $^{hep-/-}$ livers. Normalized values are in log_2 scale. (**B**, **C**) *Slc25a47* gene (**B**) and protein (**C**) expression levels in the liver of fasted *Lrh-1* $^{hep+/+}$ and *Lrh-1* $^{hep-/-}$ mice. (**D**) University of California at Santa Cruz (UCSC) genome browser (mm9) view displaying the occupancy of mouse *Slc25a47* by LRH-1 and IgG (196). Significant peaks are underlined in red. (**E**) Binding of LRH-1 to *Slc25a47* promoter region as assessed by Chip analysis using genomic DNA from *Lrh-1* $^{hep+/+}$ and *Lrh-1* $^{hep-/-}$ livers.

Slc25a47 rescue in Lrh-1 hep-/- mice reverses fasting-induced lipid accumulation in the liver

Overexpression of *Slc25a47* in HepG2 cells has been suggested to decrease lipid accumulation (220). Based on the previous observations, we hence hypothesized that overexpression of hepatic *Slc25a47* may counteract the lipid accumulation observed in the liver of *Lrh-1* hep-/- mice. To explore this possibility, we performed rescue experiments using AAV8 viral vector-mediated gene transfer in *Lrh-1* hep-/- mice and sacrificed the mice under fasting conditions five weeks later (Figure V.6A). *Slc25a47* expression levels increased specifically in the liver of AAV8-*Slc25a47* transduced *Lrh-1* hep-/- mice (Figure V.6B), but not in other

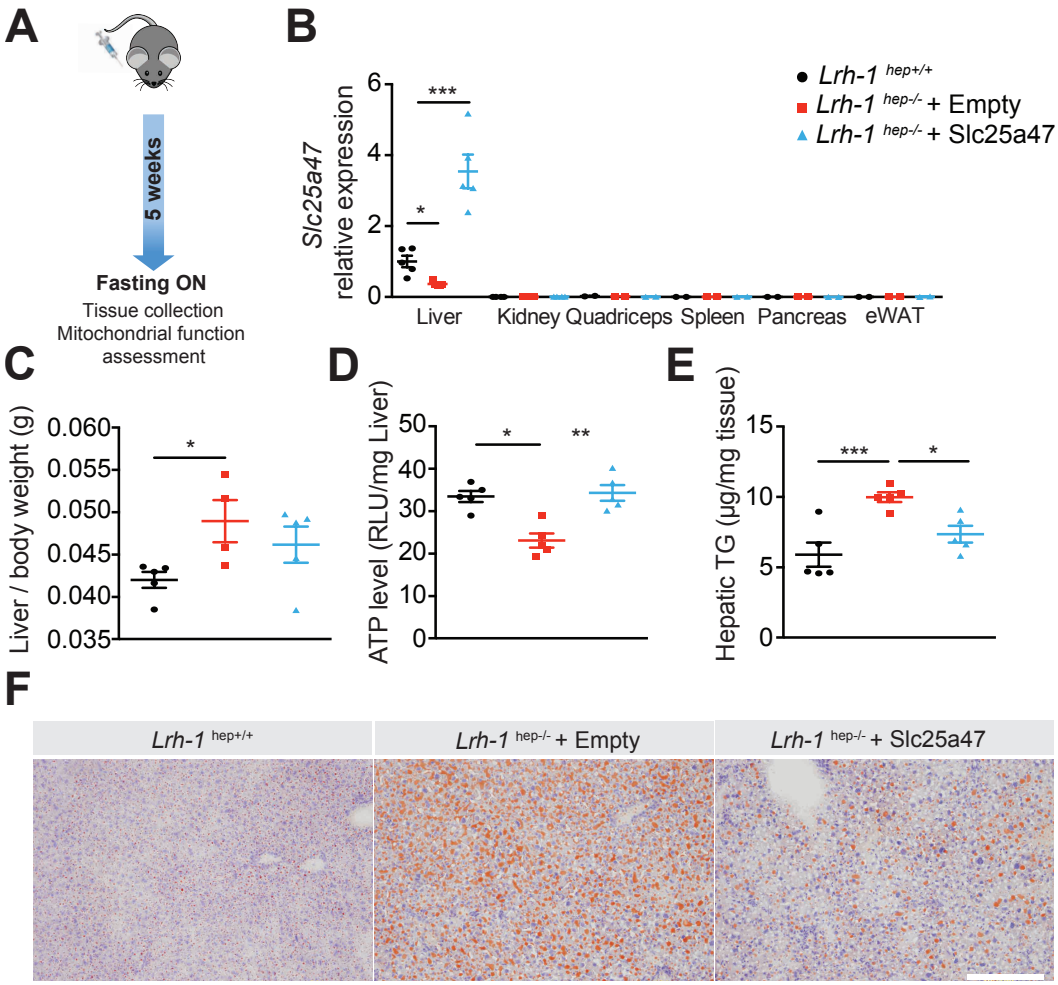

Figure V.6. *Slc25a47* rescues the steatotic phenotype of *Lrh-1* hep-/- fasted livers.
(**A**) Scheme showing experimental design for *in vivo* AAV8-mediated gain-of-function of SLC25A47 in mice. (**B**) Gene expression of *Slc25a47* in *Lrh-1* hep+/+ and *Lrh-1* hep-/- mice transduced with AAV8-Empty or AAV8-Slc25a47. (**C**) Liver weight of *Lrh-1* hep+/+ and *Lrh-1* hep-/- mice transduced with AAV8-Empty or AAV8-Slc25a47. (**D-E**) Hepatic ATP level (**D**) and triglyceride (TG) content (**E**) of *Lrh-1* hep+/+ and *Lrh-1* hep-/- mice transduced with AAV8-Empty or AAV8-Slc25a47. (**F**) Representative oil red O stainings in the liver of *Lrh-1* hep+/+ and *Lrh-1* hep-/- mice transduced with AAV8-Empty or AAV8-Slc25a47.

tissues. Overexpression of *Slc25a47* showed a trend to decrease the liver mass of fasted *Lrh-1* $^{hep-/-}$ mice (Figure V.6C). Importantly, ATP levels were recovered to the values observed in *Lrh-1* $^{hep+/+}$ mice in *Slc25a47*-overexpressing *Lrh-1* $^{hep-/-}$ mice (Figure V.6D). Strikingly, both staining of liver sections with oil red O and quantification of TG content revealed that *Slc25a47* upregulation in *Lrh-1* $^{hep-/-}$ mice decreased significantly the hepatic lipid accumulation (Figure V.6E, F).

To assess if hepatic OCR was increased in *Slc25a47*-rescued LRH-1-deficient livers independent on the number of mitochondria, we assessed OCR in isolated mitochondria from the livers of these animals. Oxygen consumption rate ($State_{3ADP}$) was significantly improved in *Lrh-1* $^{hep-/-}$ mice after *Slc25a47* expression recovery (Figure V.7A). Consistent with enhanced mitochondrial respiration,

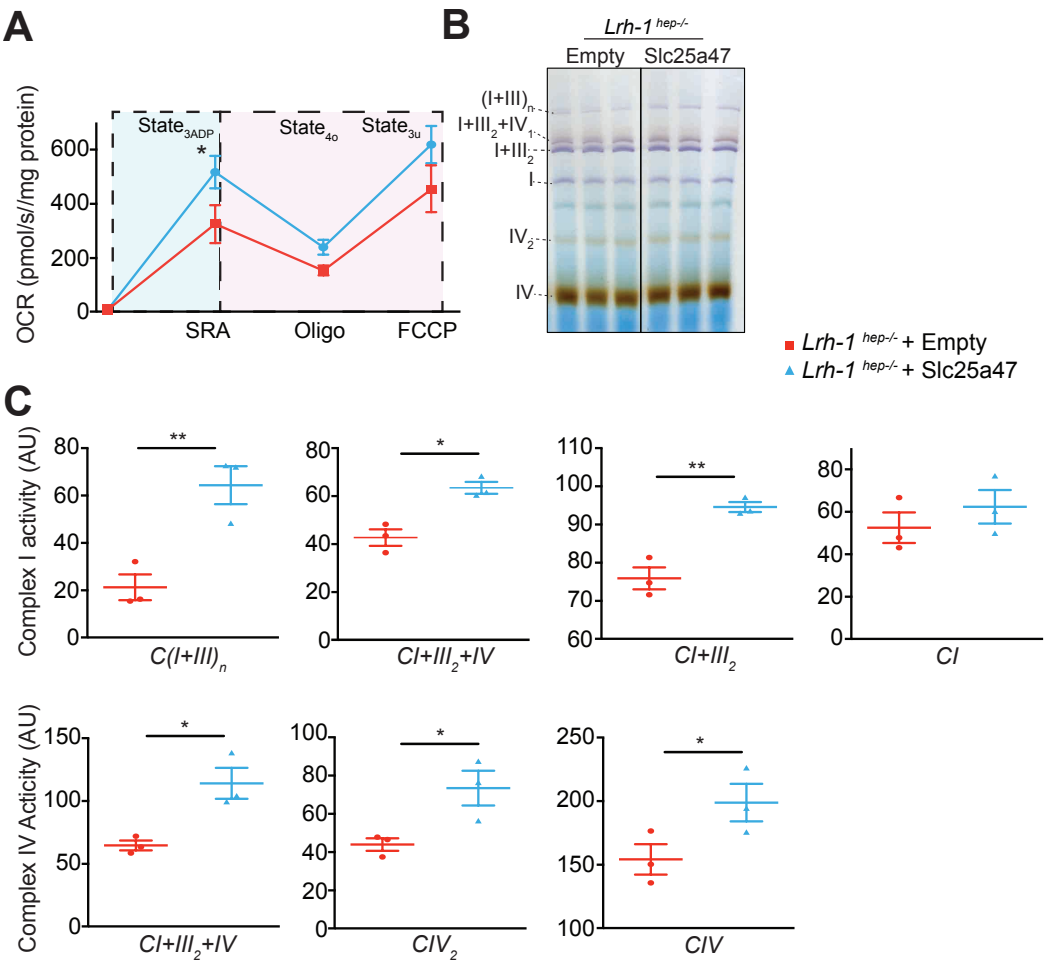

Figure V.7. *Slc25a47* improves mitochondrial function in *Lrh-1* $^{hep-/-}$ livers.
(**A**) Oxygen consumption rate (OCR) in liver mitochondria of *Lrh-1* $^{hep-/-}$ transduced with AAV8-Empty or AAV8-Slc25a47 by high-resolution respirometry in response to substrates (succinate, rotenone and ADP – SRA, $State_{3ADP}$), oligomycin (Oligo, $State_{4o}$) and the uncoupler carbonyl cyanide-4-(trifluoromethoxy)phenylhydrazone (FCCP, $State_{3u}$) in freshly isolated liver mitochondria from AAV8-empty and AAV8-Slc25a47 transduced *Lrh-1* $^{hep-/-}$ mice. (**B**) *In-gel* activity of mitochondrial complexes (I, II and IV) from *Lrh-1* $^{hep+/+}$ and *Lrh-1* $^{hep-/-}$ fasted liver mitochondria. Complex I (purple); Complex IV (brown). (**C**) Quantification of the bands in (**B**) normalized by coomassie blue staining bands.

mitochondrial complexes activity was also increased after *Slc25a47* overexpression in *Lrh-1* $^{hep-/-}$ mice in comparison with *Lrh-1* $^{hep-/-}$ mice transduced with control viral particles (Figure V.7B, C).

Taken together, these data show that reconstitution of *Slc25a47* in *Lrh-1* $^{hep-/-}$ livers is sufficient to rescue the steatotic phenotype induced upon fasting by improving mitochondrial function.

V.2.2 Liver-specific mitochondrial carrier SLC25A47 enhances fatty acid oxidation and is downregulated in NAFLD

Slc25a47 is a liver-specific mitochondrial inner membrane carrier

Despite the clear importance of SLC25 (88), there is a clear negligence in their characterization as shown in the phylogenetic tree of the family represented in Figure V.8.

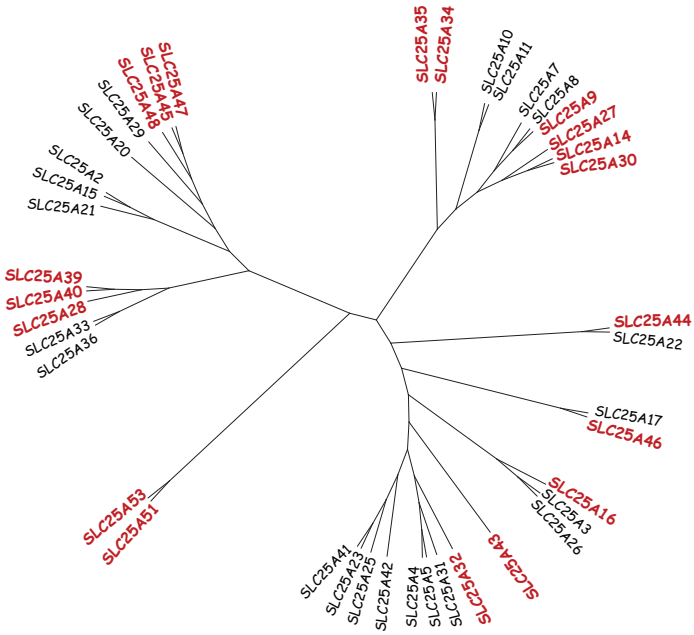

Figure V.8. Phylogenetic tree of mouse SLC25 family members.
Uncharacterized members are represented in red.

Slc25a47 is still one of the members that is not characterized (Figure V.8) we thus decided to further understand its function. Gene expression profiling of the entire mouse *Slc25* family members depicted *Slc25a47* as the most expressed solute carrier in the liver (Figure V.9A). Moreover, its expression both at the mRNA and protein level is liver-specific, as confirmed by RT-qPCR and immunoblotting (Figure V.9B, C). Also when checked in over 50 human tissues,

SLC25A47 is only confined in the liver (accessible on https://www.gtexportal.org/home/).

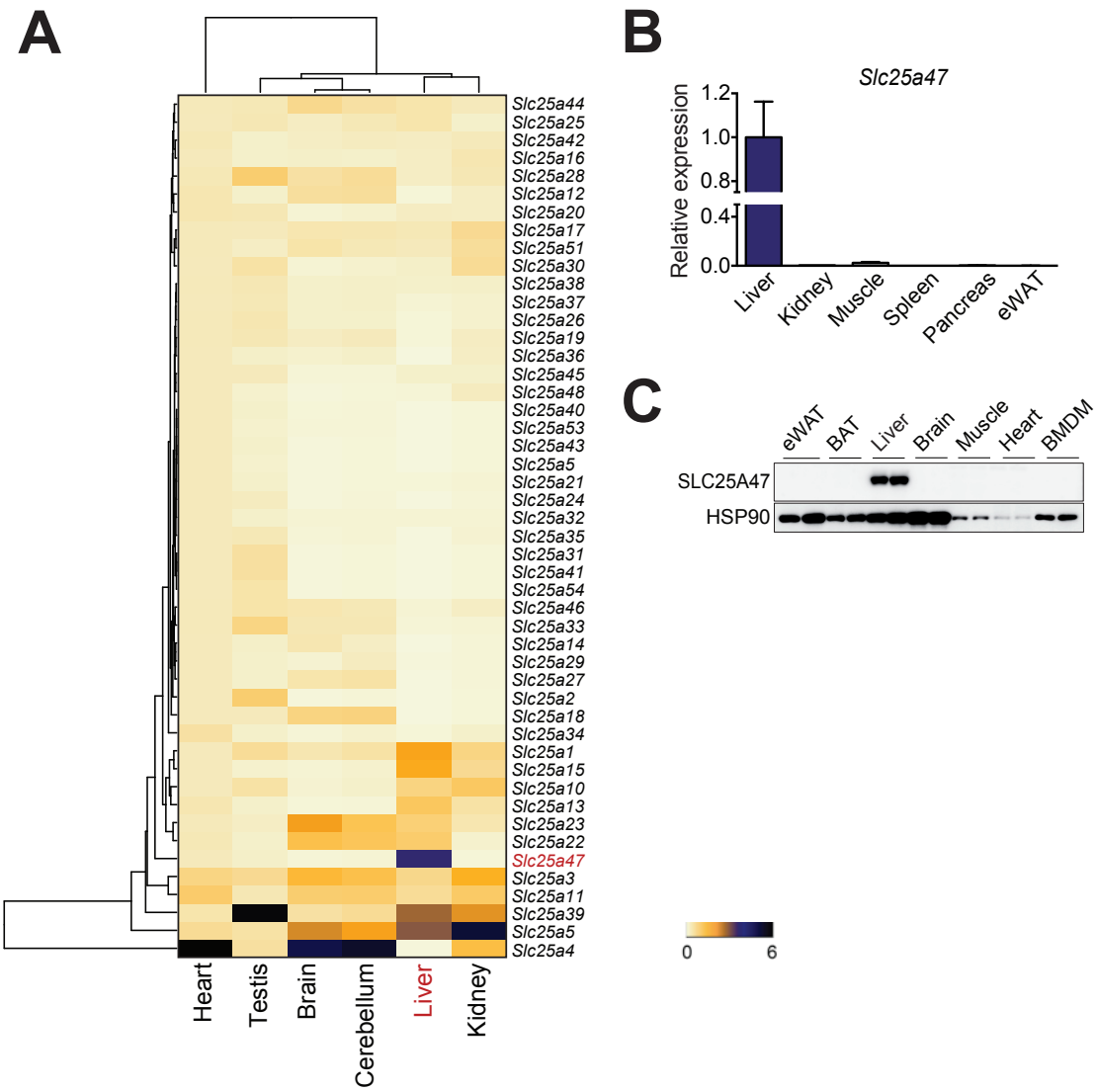

Figure V.9. *Slc25a47* mitochondrial transporter is liver-specific.
(**A**) Heat map depicting relative mouse *Slc25* family transcripts abundance in heart, testis, brain, cerebellum, liver and kidney. (**B**, **C**) Expression level of *Slc25a47* transcript (**B**) and protein (**C**) levels in different mouse tissues.

SLC25 transporters are mostly located in the IMM. However some SLC25 family members have been exceptionally identified in the OMM, we next decided to confirm the IMM localization of SLC25A47. Permeabilization of mitochondria with increasing amounts of digitonin releases mitochondrial proteins from the OMM, IMS and then IMM in a concentration dependent-manner. This assay confirmed the detection of SLC25A47 in the inner mitochondrial membrane (Figure V.10A). Immunofluorescence of alpha mouse liver 12 (AML12) cells overexpressing Flag-tagged SLC25A47 additionally confirmed the staining of this transporter in a mitochondria-shaped network (Figure V.10B).

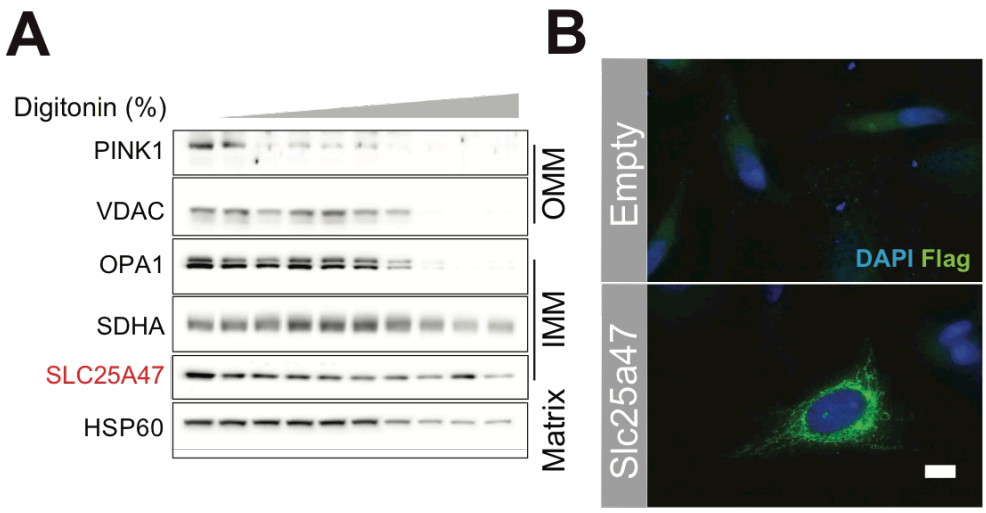

Figure V.10. SLC25A47 is localized in the inner mitochondrial membrane.
(**A**) Immunoblots of SLC25A47 in liver mitochondria lysates after permeabilization with increasing amount of digitonin. PINK1 and VDAC for the OMM, OPA1 and SDHA for the IMM and HSP60 for the matrix are used as controls. (**B**) FLAG immunofluorescence staining of alpha mouse liver 12 (AML12) cells overexpressing FLAG-tagged SLC25A47. DAPI is used to stain nuclei. Scale bar: 10 μm.

To gain more insight into the function of the orphan SLC25A47, we followed the same strategies as the ones applied to discover the function of other SLC25 family members. First, phylogenetic clustering of a particular carrier with others of known function can provide clues to be tested. Therefore, we assessed sequence similarity between SLC25A47 and its closest members of the family, SLC25A45, SLC25A48, SLC25A29, SLC25A20, SLC25A15 and SLC25A2 (Figure V.8), some of which with known functions. Although SLC25A47 is very conserved among species (~90% similar, Figure V.11A), protein sequence alignment indicated only about 30% similarity between SLC25A47 and its closest homologs (Figure V.11B), indicating that SLC25 family is more similar in structure rather than sequence. Moreover, one portion of the protein sequence of SLC25A47 could not be found in the other transporters (Figure V.11B, evidenced with a black rectangle), highlighting another unique feature of SLC25A47. The mitochondrial ADP/ATP carrier (AAC or SLC25A4, PDB ID 1OKC) was the first SLC25 structurally characterized (221) and after that the structure of other SLC25 family members has been obtained using it as a model. Homology modeling of SLC25A47 to AAC revealed this distinctive portion of the protein in a matrix-localized loop (Figure V.11C), suggesting that this part of the sequence is exceptional even when comparing to other members of the family. Furthermore, the model emphasizes a positively charged core within the protein, suggesting that the solutes transported are most likely negatively charged (Figure V.11C,

representation on the right).

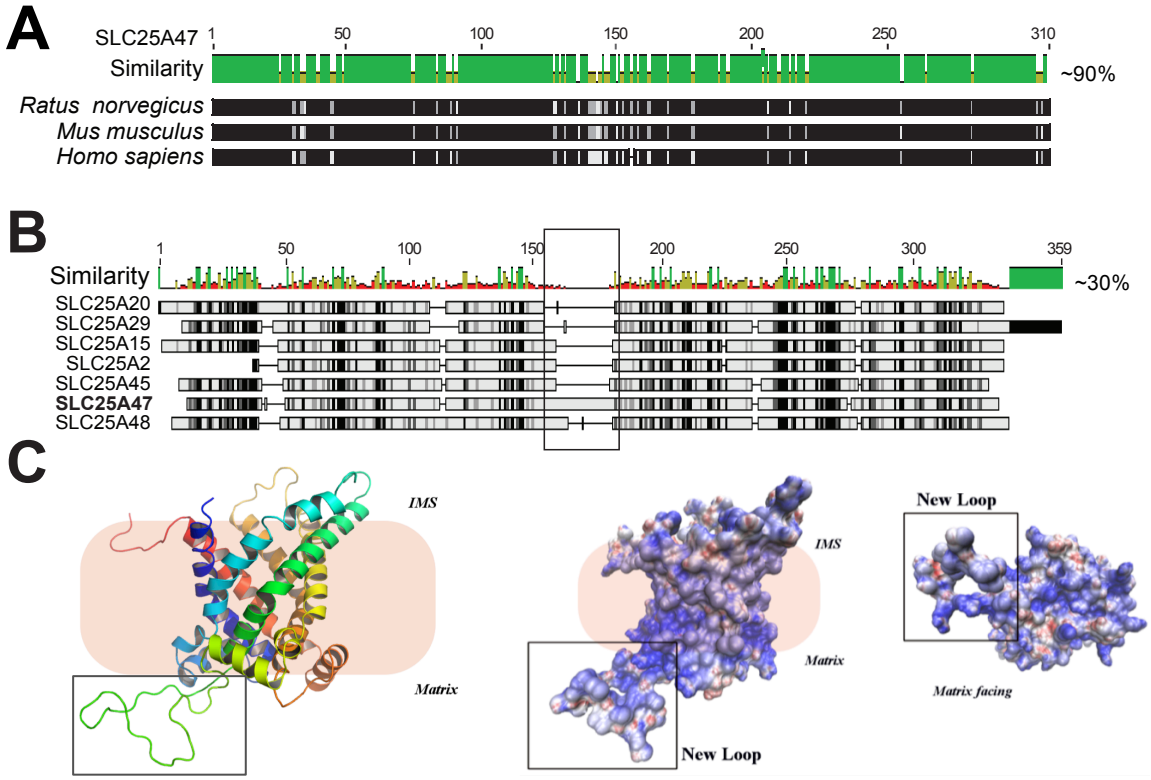

Figure V.11. SLC25A47 presents a unique loop in the mitochondrial matrix side.
(**A**, **B**) Protein alignment of SLC25A47 within species (**A**) and between SLC25A47 and its closest homologs (**B**). Similarity color code: green, high homology; red, low homology. (**C**) 3-D structure of SLC25A47 depicting the new loop. Color code for the amino acids charge: blue, positive; white, neutral; red, negative. Black rectangle emphasizes the loop specific to SLC25A47.

Together, these data identify SLC25A47 as a liver-specific inner mitochondrial membrane carrier whose exclusive distribution and unique features suggest a crucial role for liver function.

Slc25a47 is induced upon fasting

Since the function of SLC25A47 is unknown, we decided to take advantage of published datasets to evaluate if the fasting/feeding cycle influences *Slc25a47* gene expression. Genome binding/occupancy for active transcription (222) and microarray analysis (223) throughout the diurnal cycle of the mouse liver demonstrated that *Slc25a47* is a fasting-induced gene, with higher Pol II occupancy during the day (Zeitgeber Time 2 - ZT2, Figure V.12A) and peak of expression after an over day fasting (Figure V.12B). To verify the induction upon fasting at the mRNA level, we evaluated hepatic *Slc25a47* in mice after a 24h-fasting and confirmed a 5-fold upregulation (Figure V.12C).

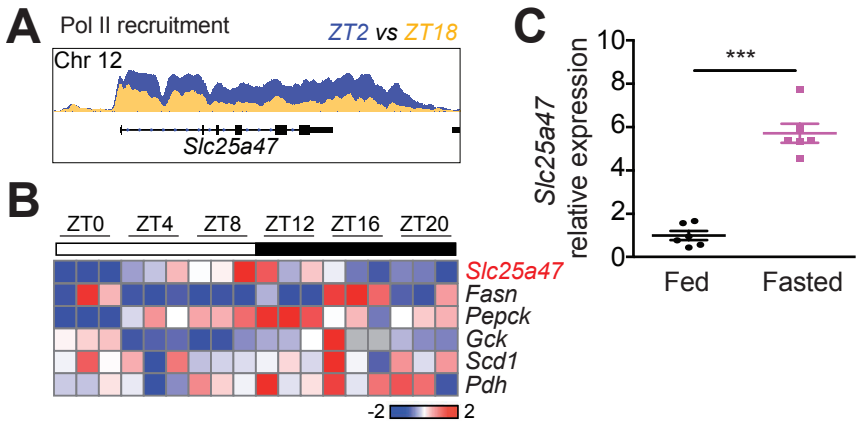

Figure V.12. *Slc25a47* is induced upon fasting.
(**A**) Representation of *Slc25a47* genomic area binding/occupancy by Pol II assessed by Chip-seq (222) at ZT2 (9 AM) and ZT18 (1AM). (**B**) Heat map displaying the expression of genes important under fed and fasted conditions during circadian rhythm (223). (**C**) Gene expression analysis of *Slc25a47* in the liver of fed and 24h-fasted mice (7am-7am).

The increase in *Slc25a47* mRNA levels in response to fasting suggests that this carrier could be linked to catabolic pathways transporting solutes that promote the mobilization of energy sources. Accordingly, we found that *Slc25a47* correlates positively with genes involved in fatty acid degradation and PPAR signaling in fasting livers of the BXD mouse genetic reference population (178) (Figure V.13A, B). On the contrary, lipid biosynthesis pathways were amongst the ones in which the genes correlating negatively with *Slc25a47* are enriched (Figure V.13C). Taken together these data indicate that this novel unknown mitochondrial carrier is induced upon fasting and positively linked to oxidative catabolism.

SLC25A47 *improves mitochondrial function*

Until now, the most successful strategy employed to identify substrate specificity of solute carriers with unknown function consists in reconstitution of recombinant protein into liposomes followed by radioactive transport assays, herein referred to as the "expression–purification-reconstitution-assay" (EPRA) method (87). Unfortunately, the reconstitution of SLC25A47 in liposomes turned out to be technically challenging due to the high content of cysteine residues in this transporter, resulting in disulfide bond formation and compromised native protein folding. Consequently, we focused on addressing the repercussions of *Slc25a47* gene manipulation *in vivo* to better understand its function.

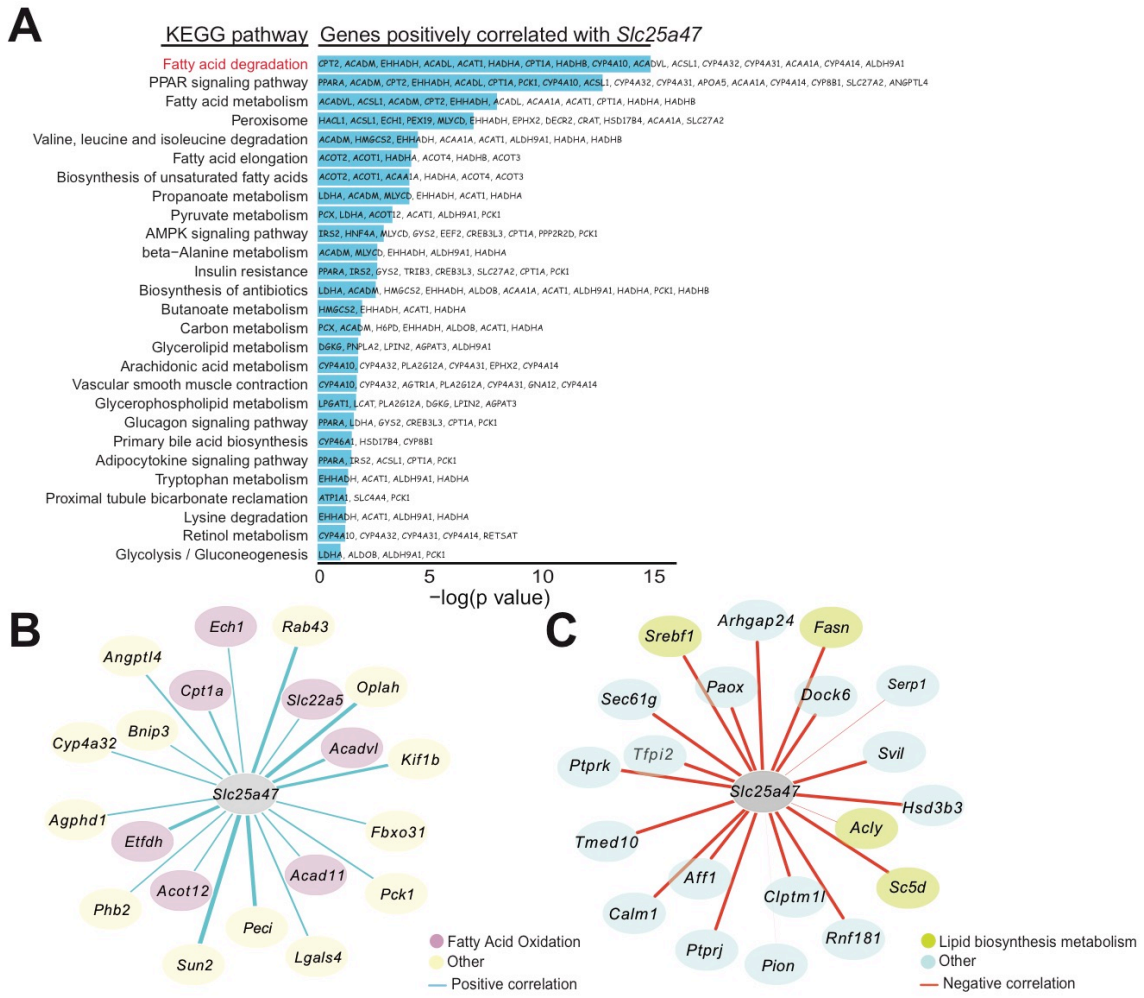

Figure V.13. Hepatic *Slc25a47* positively correlates to fatty acid degradation.
(**A**) Pathway enrichment (KEGG) of genes positively correlating with *Slc25a47* using 42 BXD mouse strains fed chow diet and sacrificed under fasting. (**B**, **C**) Correlation network (pearson's r) between *Slc25a47* and top 20 most significantly correlating genes, positively (blue) and negatively (red). Thickness of the line is associated with higher significance.

To achieve this, we enhanced hepatic *Slc25a47* expression levels *in vivo* as described above (Figure V.6A). AAV8-Slc25a47 transduced mice didn't present any changes in body weight or liver and epididymal white adipose tissue (eWAT) mass (Figure V.14A, B). Hepatic gene expression analysis demonstrated that *Slc25a47* was upregulated in the liver together with important mitochondrial regulators, including mitochondrial transcription factor A (*Tfam*), peroxisome proliferator-activated receptor gamma coactivator 1-alpha (*Pgc1a)* and nuclear respiratory factor-1 (*Nrf-1)* (Figure V.14C). Accordingly, *Slc25a47* overexpression increased mitochondrial respiration, as well as respiratory complex activity and expression (Figure V.14D-F), especially the supercomplex $I+III_2+IV_1$ (the respirasome), indicating that SLC25A47 could influence supercomplex formation.

Western blot analysis revealed increased expression of mitochondrial CI (NDUFB8, NDUFS3, CIII (UQCRC2) and CIV (MTCO1), along with the mitochondrial protein VDAC (Figure V.14G).

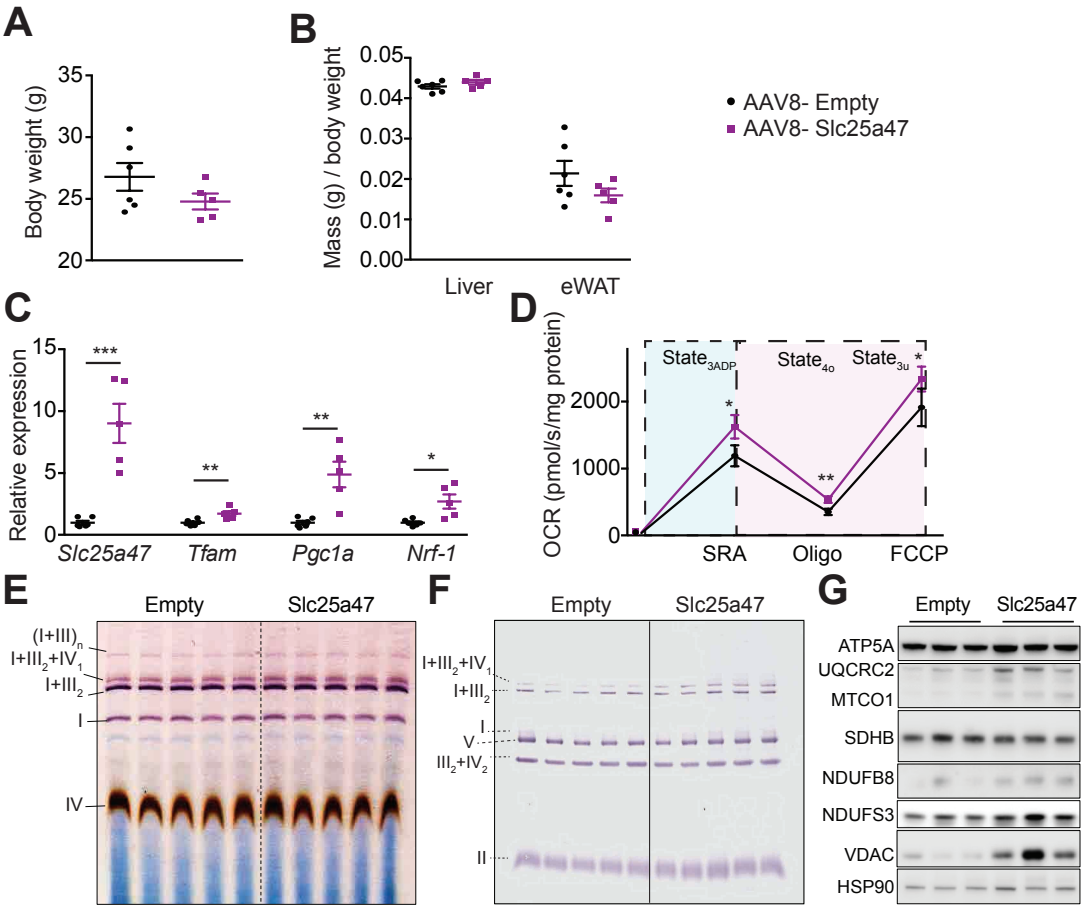

Figure V.14. SLC25A47 enhances mitochondrial function.
(**A**, **B**) Body weight (**A**), liver and epididymal white adipose tissue (eWAT) mass (**B**) of mice transduced with *Slc25a47* or control viral vectors. (**C**) Gene expression of mitochondria-related genes, *Tfam*, *Pgc1a* and *Nrf-1* in AAV8-Empty and AAV8-Slc25a47 transduced livers. (**D**) Oxygen consumption rate (OCR) in response to substrates (succinate, rotenone and ADP – SRA, State$_{3ADP}$), oligomycin (Oligo, State$_{4o}$) and the uncoupler carbonyl cyanide-4-(trifluoromethoxy)phenylhydrazone (FCCP, State$_{3u}$) in freshly isolated liver mitochondria from AAV8-Empty and AAV8-Slc25a47 transduced mice. (**E**, **F**) *In-gel* activity (CIV and CI, **E**) and Immunoblot (**F**) of mitochondrial complexes in AAV8-Empty and AAV8-Slc25a47 transduced liver mitochondria after blue-native polyacrylamide gel electrophoresis (BN-PAGE). CI activity (purple); CIV activity (brown). (**G**) Immunoblots of mitochondrial complexes subunits ATP5A (CV), UQCRC2 (CIII), MTCO1 (CIV), SDHB (CII), NDUFB8 and NDUFS3 (CI), and mitochondrial protein VDAC. HSP90 was used as loading control.

Next, we decided to verify whether SLC25A47 activity could be further potentiated. The additional 30 amino acid-long stretch of SLC25A47 that defines a mitochondrial loop (Figure V.11B, C) can be a possible regulation site dictating the opening of the channel. With this hypothesis, we aimed at assessing phosphorylation sites in this loop that could regulate SLC25A47 activity. Since SLC25A47 is important for oxidative catabolism during fasting, we decided to search for possible protein kinase A (PKA) phosphorylation sites in this loop. We

found a very particular and known consensus sequence for PKA phosphorylation (R-R-X-S/T) (224) for serine 137 (S137) within the unknown loop (Figure V.15A). This sequence is conserved for SLC25A47 within species but not present in any of SLC25A47 homologs, not even the closest A45 and A48 (Figure V.15A, B). The location of S137 within the loop can be seen in Figure V.15C.

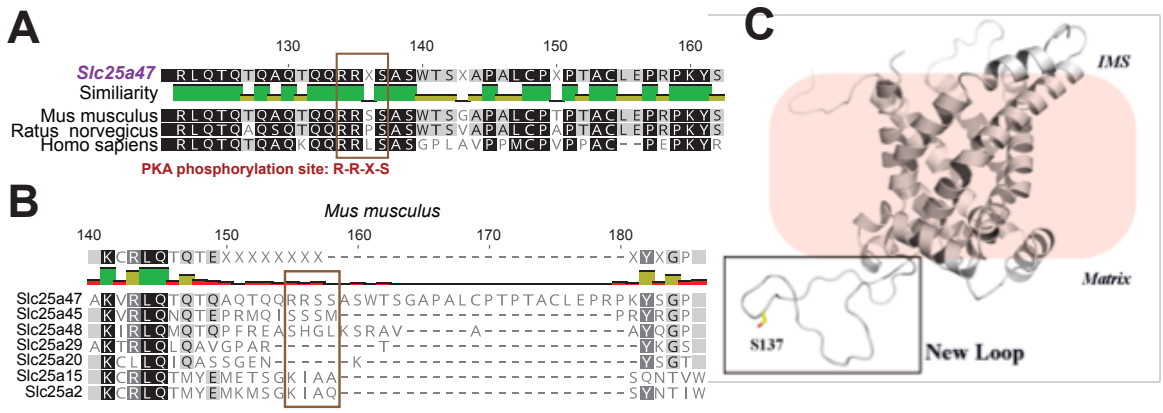

Figure V.15. SLC25A47 presents an unknown loop that could be a possible point of regulation.

(**A**) Amino acid sequence alignment of the extra loop of SLC25A47 between species. PKA consensus phosphorylation site is indicated inside a rectangle. (**B**) Protein alignment between the loop region of SLC25A47 and its closest homologs. (**C**) Structure of SLC25A47 depicting the new matrix loop in which serine 137 (S137) can be phosphorylated by PKA.

As PKA is activated by an increase in cellular cAMP levels, we next treated AML12 cells transfected with either empty or *Slc25a47* vector with the adenylyl cyclase activator forskolin (20 μM) or vehicle just before measuring oxygen consumption in the Seahorse. Forskolin is very commonly used in biology to raise cellular cAMP levels (225). Maximum respiration was increased upon *Slc25a47* overexpression and forskolin pre-treatment, indicating that mitochondrial function was further enhanced in *Slc25a47*-overexpressing cells with forskolin (Figure V.16). This observation suggests that SLC25A47 could be phosphorylated by PKA upon rising of cAMP levels leading to increased transport activity. During fasting cAMP levels are known to rise in many tissues, including the liver (226, 227). Our results further strengthen the role of SLC25A47 during fasting and suggest that post-translational modifications, such as

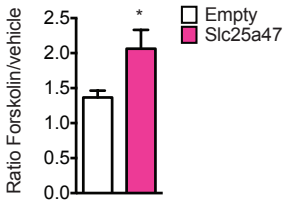

Figure V.16. Forskolin further enhances mitochondrial maximum respiration upon *Slc25a47*-upregulation in AML12 cells.

phosphorylation, can modulate its activity leading to improved mitochondrial response to nutritional cues.

Collectively, these data show that *Slc25a47* is an unknown transporter with unique features that boost mitochondrial function.

Slc25a47 is downregulated in NAFLD

Mitochondrial dysfunction contributes to the development of NAFLD (49, 90). Since SLC25A47 improves mitochondrial function under normal physiological conditions, we decided to evaluate the potential role for this carrier as a mitochondrial enhancer under pathological conditions, such as NAFLD. We first started by asking if *Slc25a47* expression is altered in NAFLD and if the presence of this carrier could be associated with a better prognosis. Analysis of the liver transcriptome of mice fed a chow diet versus mice fed a HFHS diet (NAFLD model (95)) revealed a significant downregulation of *Slc25a47* in the disease state (Figure V.17A). Moreover, mouse liver lipid species recently identified as biomarkers pro- and anti-NAFLD (unpublished data) correlated negatively and positively with *Slc25a47*, respectively (Figure V.17B). Together these two observations indicate that *Slc25a47* could potentially protect from the deleterious effects of NAFLD.

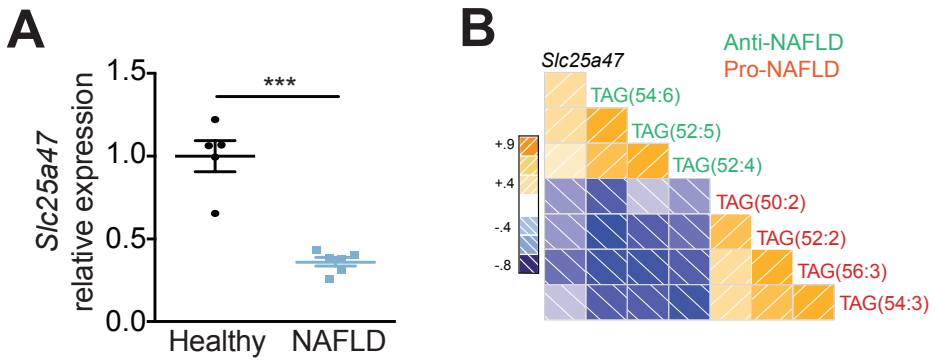

Figure V.17. *Slc25a47* is downregulated in NAFLD.
(**A**) Liver gene expression of *Slc25a47* in diet-induced NAFLD model (high-fat, high-sucrose diet for 18 weeks). Mice fed a chow diet are depicted as "healthy". (**B**) Corrgram (pearson's r) of *Slc25a47* with hepatic lipid species assigned as anti- and pro-NAFLD.

Slc25a47 enhances fatty acid oxidation in NAFLD model decreasing hepatic lipid accumulation

To confirm the protective effect of SLC25A47 against hepatic steatosis and since *Slc25a47* is decrease upon HFHS diet feeding, we fed mice HFHS for 7 weeks after AAV8-Slc25a47 transduction. In agreement with our hypothesis, H&E staining of the livers of HFHS-fed *Slc25a47*-overexpressing mice revealed less

lipid droplets (Figure V.18A), demonstrating a strong protection against hepatic steatosis formation. TG quantification confirmed a significant decrease in the lipid accumulation resultant of HFHS-feeding in AAV8-Slc25a47 transduced livers (Figure V.18B).

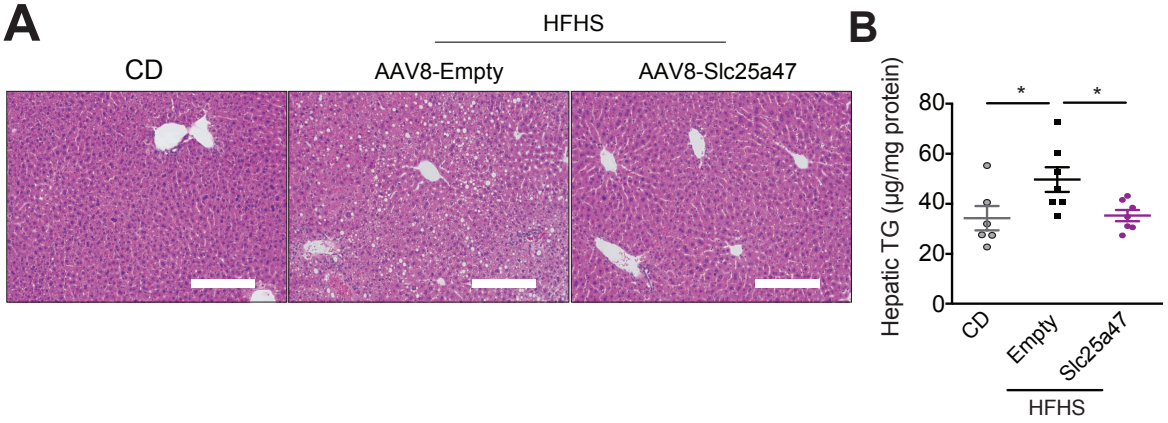

Figure V.18. *Slc25a47* decreases lipid accumulation in NAFLD model.
(**A**) Representative images of liver sections of AAV8-Empty and AAV8-Slc25a47 transduced mice fed high fat high sucrose (HFHS) diet for 7 weeks stained with hematoxylin and eosin (H&E) to visualize the tissue structure. Scale bar, 200 µm. (**B**) Hepatic triglyceride (TG) content of HFHS-fed AAV8-Empty and AAV8-Slc25a47 transduced mice.

To investigate whether overexpression of *Slc25a47* protects mice from hepatic steatosis in another diet-induced NAFLD model, C57BL/6J mice transduced with AAV8-*Slc25a47* were fed a choline-deficient diet (ChD) for 4 weeks (Figure V.19A). ChD-feeding was chosen based on the fact that this diet, in contrast with methionine-choline deficient diet, a well-known model of NAFLD, promotes hepatic TG accumulation without triggering body weight loss (48). Indirect calorimetry one week before mice were euthanized showed a low (~0.8) respiratory exchange ratio (RER) in accordance with more fatty acid utilization (Figure V.19B). Surprisingly, upregulation of *Scl25a47* in the liver was sufficient to further decrease the RER, indicative of improved fatty acid oxidation (Figure V.19B). *Slc25a47* was efficiently overexpressed in the liver of mice transduced with AAV8-Slc25a47 viral particles (Figure V.19C). There were no differences in food intake nor effects on body weight as well as liver and white adipose tissue mass (Figure V.19D-F). The latter observation suggests that enhanced lipolysis was not the main source of fatty acids being extensively used in the *Slc25a47*-overexpressing livers. While plasma TG levels showed a tendency to be increased in mice transduced with AAV8-*Slc25a47*, plasma free FA were increased in the *Slc25a47*-overexpressing mice (Figure V.19G, H), presumably indicating that FA are not accumulating in the liver.

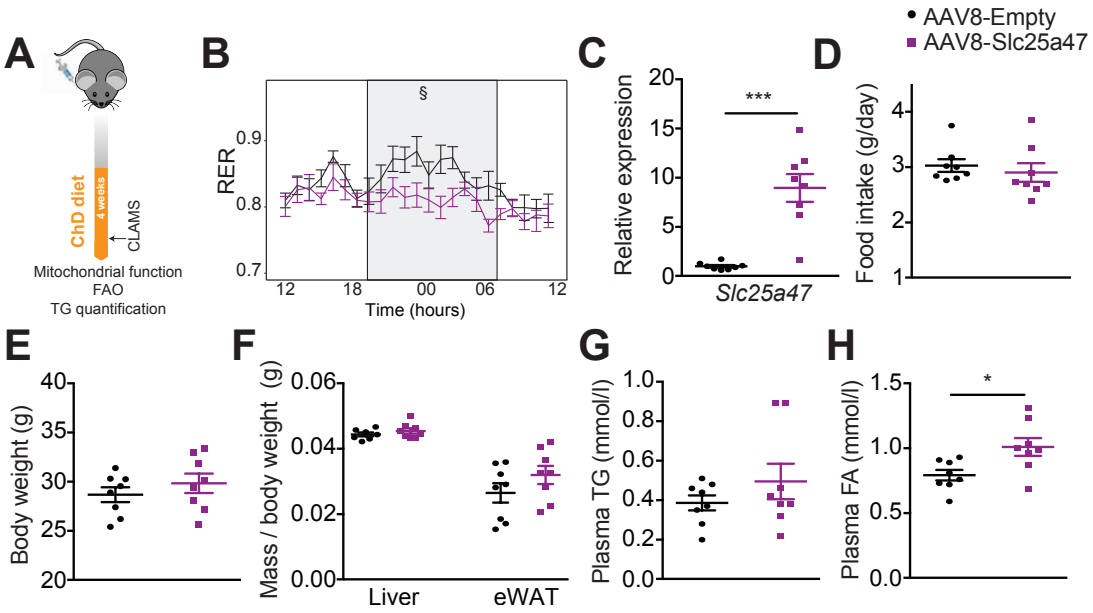

Figure V.19. Hepatic *Slc25a47* overexpression increases respiratory exchange ratio and shifts fuel utilization.

(**A**) Scheme demonstrating experimental design for AAV8-Empty and AAV8-Slc25a47 *in vivo* transduction in mice fed choline-deficient diet (ChD) for 4 weeks. (**B**) Respiratory exchange ratio (RER) measured through indirect calorimetry (24h) in ChD-fed AAV8-Empty and AAV8-Slc25a47 transduced mice one week before sacrifice. (**C**) *Slc25a47* gene expression in ChD-fed AAV8-Empty and AAV8-Slc25a47 transduced livers. (**D**) Food intake per day of ChD-fed AAV8-Empty and AAV8-Slc25a47 transduced mice. (**E**, **F**) Body weight (**E**) and liver and epididymal white adipose tissue (eWAT) mass (**F**) in ChD-fed AAV8-Empty and AAV8-Slc25a47 transduced mice. (**G**, **H**) Plasma triglyceride (TG, **G**) and free fatty acids (FFA, **H**) content in ChD-fed AAV8-Empty and AAV8-Slc25a47 transduced mice. §adjusted p-value<0.05, relative to the night period.

Consistent with what we observed in mice fed a normal chow diet, mitochondrial OCR was dramatically increased in ChD-fed *Slc25a47*-overexpressing livers compared to control mice (Figure V.20A). Moreover, fatty acid oxidation substrates in the presence of ADP were used to reveal enhanced fatty acid oxidation capacity in the livers where *Slc25a47* was boosted (Figure V.20A, B), observation that coincides with the RER previously assessed (Figure V.19B). Consequent to enhanced mitochondrial respiration, we observed increased ATP levels in *Slc25a47*-upregulated livers (Figure V.20C). mtDNA/nDNA ratio exhibited increased mitochondrial content in ChD-fed *Slc25a47*-overexpressing livers (Figure V.20D). Consistent with improved fatty acid oxidation, hepatic TG content showed a clear tendency to be decreased in *Slc25a47*-overexpressing livers (Figure V.20E).

Taken together, these data demonstrate that SLC25A47 ameliorates mitochondrial function enhancing fatty acid oxidation hence reversing hepatic lipid accumulation associated with NAFLD.

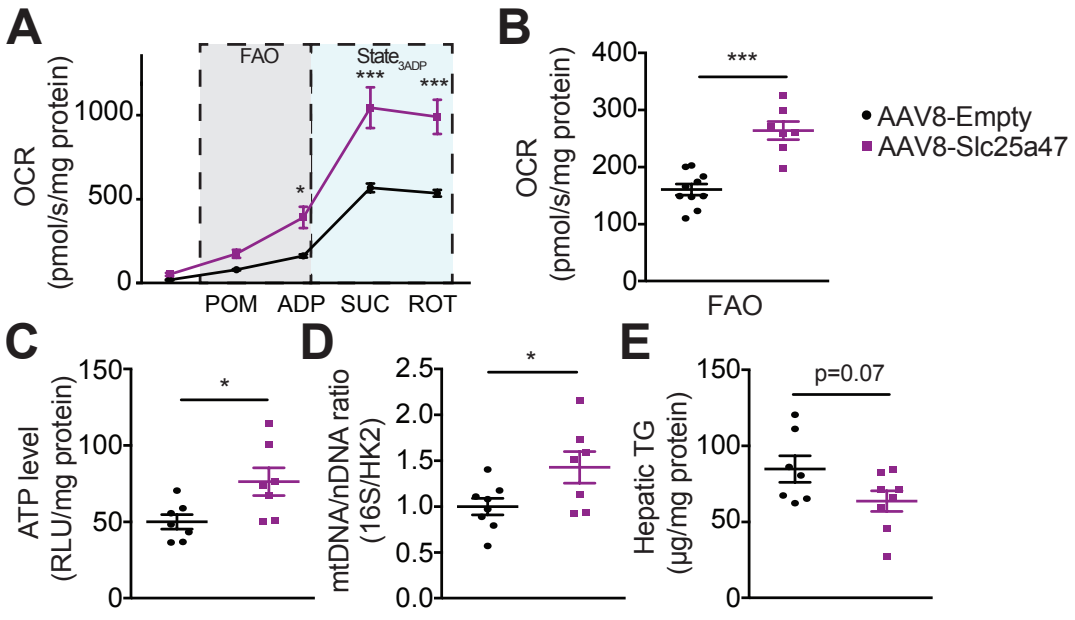

Figure V.20. Hepatic *Slc25a47* enhances fatty acid oxidation in NAFLD model.
(**A**) Oxygen consumption rate (OCR) of fresh liver homogenates from choline-deficient diet (ChD)-fed AAV8-Empty and AAV8-Slc25a47 transduced mice. Fatty acid oxidation (FAO) substrates (palmitoyl- and octanoyl-carnitine with malate to sustain FAO, POM) were added in the presence of ADP, followed by succinate (SUC) and rotenone (ROT) to achieve State3ADP (**B**) Quantification of FAO-driven respiration assessed in (A). (**C**, **D**) Hepatic ATP level (**C**) and mtDNA/nDNA ratio (16S/HK2, **D**) of ChD-fed AAV8-Empty and AAV8-Slc25a47 transduced mice. (**E**) Hepatic triglyceride (TG) content of ChD-fed mice transduced with either AAV8-Empty or AAV8-Slc25a47.

V. 3 Discussion

Hepatic LRH-1 is an established transcriptional regulator of glucose, cholesterol and bile acid metabolism (104, 155-157, 169). Here, we report that LRH-1 regulates liver lipid metabolism during the fasted state. Loss of LRH-1 in hepatocytes impairs mitochondrial fatty acid oxidation eliciting fasting-induced steatosis. Furthermore, we identified a mitochondrial carrier SLC25A47 as a direct target of LRH-1. More importantly, reconstitution of SLC25A47 in the livers of *Lrh-1* $^{hep-/-}$ mice enhanced mitochondrial function and reversed lipid accumulation observed in the livers of these animals. Additionally, we identified this novel transporter as a liver-specific inner mitochondrial membrane carrier, which is upregulated during fasting and improves fatty acid oxidation. We also demonstrated that the unique features of SLC25A47 go well beyond its liver specificity. Indeed our studies revealed that SLC25A47 is endowed with a distinctive 3-D structure displaying a long loop in the matrix side that could be crucial for the modulation of the channel activity. Our work furthermore strengthens the putative role of SLC25A47 in NAFLD. Consistent with our hypothesis, the analysis of independent hepatic transcriptomics and lipidomics revealed that *Slc25a47* is often decreased in NAFLD and positively correlates with

anti-NAFLD lipid biomarkers. Moreover, when exposed to steatotic diets, *Slc25a47*-overexpressing mice displayed improved mitochondrial function with enhanced fatty acid oxidation leading to decreased hepatic TG content (Figure V.21).

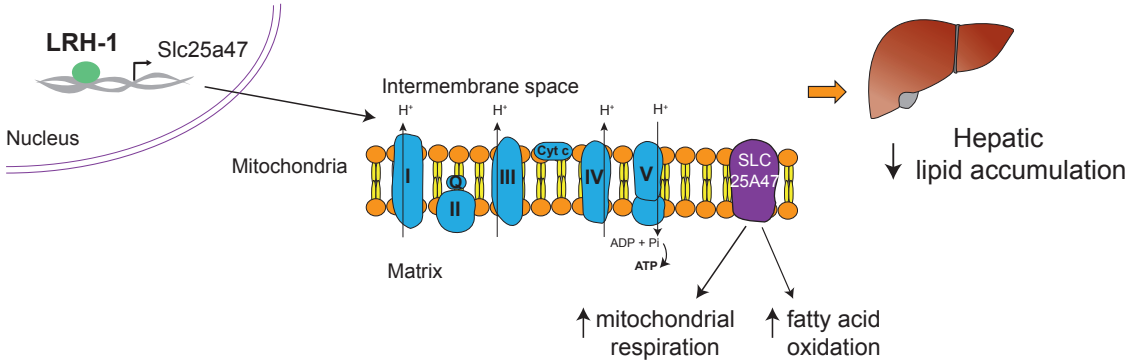

Figure V.21. Graphical presentation showing how LRH-1 regulates *Slc25a47* leading to normalization of lipid accumulation by enhancing the breakdown of fatty acids.

The liver plays a crucial role in metabolic homeostasis meeting systemic fuel requirements by coordinating the synthesis, storage, breakdown, and redistribution of nutrients (228). The excessive accumulation of lipids in the livers of *Lrh-1* $^{hep-/-}$ mice could be due to a dysregulation of one or more of these processes. Hepatic steatosis during a fasting condition rules out excessive TG from the diet delivered by chylomicrons to the liver as the main cause. Furthermore, our laboratory previously identified *Gck* as a target gene of LRH-1 (169). As a consequence, *Lrh-1* $^{hep-/-}$ mice display decreased DNL rates thus not explaining the hepatic steatosis observed. During fasting, the lack of insulin action promotes adipose tissue lipolysis, condition that when exacerbated is unequivocally linked to hepatic lipid overburden (41). However, we did not observe a difference in WAT mass nor in glycerol or FA released from white adipose tissue explants of *Lrh-1* $^{hep-/-}$ when compared to WT littermates. Although the prime repressor of LRH-1, SHP, is known to affect VLDL-triglyceride secretion from the liver (199), we could not detect any significant difference in the level of plasma TG, indicating that TG are not being differently retained in the liver of LRH-1-deficient mice.

In this study, we show that LRH-1 is important for proper mitochondrial function by regulating mitochondrial transcripts. Compromised fatty acid oxidation associated with mitochondrial dysfunction favors lipid accumulation. In addition to several proteins involved in fatty acid degradation being affected in *Lrh-1* $^{hep-/-}$ livers, we detected a severe reduction in CII expression (SDHB) and

activity, mitochondrial complex which is especially active during fasting when fatty acids are the primary substrate for energy production (229). Of all the proteins significantly altered, SLC25A47 stood out as one of the most downregulated mitochondrial proteins in the liver of *Lrh-1* $^{hep-/-}$ mice. Other mitochondrial carriers are known to be important for fatty acid oxidation such as SLC25A20 (carnitine-acyl-carnitine transferase, CACT) and SLC25A29 (CACT-like) (230, 231). However, besides the fact that afterwards SLC25A29 was shown not to have acyl-carnitine/carnitine transferase activity (232), both transporters are not abundantly expressed in the liver (81). Moreover, the expression of *Slc25a20* and *Slc25a29* was not altered in *Lrh-1* $^{hep-/-}$ livers.

Still very little is known about the interactions between mitochondria and the cytosol. In 1965 (233, 234), pioneering studies suggested the existence of an ADP/ATP antiporter system embedded in the mitochondrial membrane whose sequence (235) and structure (221) was resolved later on. Since then, several other members of the SLC25 transporter family have emerged as gatekeepers of metabolites distribution between cellular compartments (81). SLC25 is a large family of nuclear-encoded mitochondrial inner membrane transporters. Out of the 53 members, only a few of them have been identified to be located in the OMM (82, 83) and peroxisomes (84). Our study identified SLC25A47 as an inner mitochondrial membrane carrier involved in fatty acid oxidation. *Slc25a47* was first cloned and identified in 2004 (236), being also called hepatocellular carcinoma-downregulated mitochondrial carrier protein (HDMCP), however, no studies on *Slc25a47* and liver cancer were ever published. Jin *et al.* later reported two studies on *Slc25a47* proposing that this carrier could have a role in hepatic steatosis (220, 237). However, these two studies present contradictory results, emphasizing the need for confirmation and further studies to support a role for SLC25A47 in NAFLD.

Unfortunately, we could not rule out if the positive effect SLC25A47 has in FAO is due to the transport of fatty acyl-carnitines inside mitochondria for β-oxidation or if it is indirect through the transport of co-factors or other metabolites that favor FAO. The inability to reconstitute SLC25A47 in liposomes has hampered thorough characterization of its transport activity. Additionally, the increase in mitochondrial function by SLC25A47 could be accounted by a rise in mitochondrial content. We did observe augmented mtDNA content but the dynamic process of mitochondrial biogenesis is difficult to determine since it is usually also coordinated with the renewal of existing mitochondria through

mitophagy (238). Nevertheless, the beneficial influence of SLC25A47 in mitochondrial function was still observed in isolated mitochondria, which pinpoints this transporter as a potential target for drug discovery to treat/prevent hepatic mitochondrial disorders.

Our results demonstrate SLC25A47 being involved in oxidative catabolism. In accordance to this, it was recently demonstrated that *Slc25a47* is one of the main genes upregulated in the liver when lipolysis, fatty acid degradation and ketogenesis are activated by FXRα2 (239). Furthermore, single-cell RNA-seq performed to demonstrate the zonation of gene expression in the liver dividing the metabolic labor proved *Slc25a47* localization in the portal node (240). The portal node is the most oxygenated area where enzymes for gluconeogenesis, ureagenesis, FAO and OXPHOS are located (240). The distinctive loop SLC25A47 presented outside the inner membrane could provide an opportunity for PTM to modulate its activity. We showed that there is a consensus phosphorylation site for PKA within the mitochondrial loop and that forskolin (cAMP booster, activating PKA) further enhanced mitochondrial respiration upon *Slc25a47* overexpression. PKA has been found in the mitochondrial matrix where it phosphorylates mitochondrial proteins, regulating ATP production (241). Although PKA is a valid candidate for SLC25A47 activation, other PTM such as acetylation/deacetylation could occur. The fasting-responsive mitochondrial sirtuin 3 (SIRT3) is a vey interesting contender for SLC25A47 deacetylation and activation. The liver of mice lacking SIRT3 displays accumulation of acyl-carnitines and TG during fasting associated with decreased levels of fatty acid oxidation (187). Further studies are needed to confirm the control over SLC25A47 activity by PKA and SIRT3.

Our studies in isolated mitochondria also demonstrated that SLC25A47 increases the expression and activity of mitochondrial complexes and supercomplexes, suggesting that this transmembrane carrier influences supercomplex formation. For example, SLC25A47 could interact with supercomplex assembly factors (78) or change mitochondrial ultrastructure determining cristae shape that is known to affect assembly and stability of supercomplexes (242). This latter could be accomplished by interaction with cristae-associated proteins, such as OPA-1 (242) or as a consequence of SLC25A47-mediated solute transport affecting membrane fluidity. Nevertheless, SLC25A47 beneficial effect on supercomplex assembly and activity impacts on the organization of electron flux between the mitochondrial complexes, optimizing the utilization of available substrates. Further studies using *Slc25a47*

KO mice will help to address the physiological and therapeutical role of this carrier.

In this study, we described that loss of function of LRH-1 promotes the development of fasting-induced hepatic steatosis. On **Chapter IV**, we showed that LRH-1 selective gain-of-function favors the development of NAFLD by a different mechanism. This contradictory role of LRH-1 in this disorder emphasizes the intricacy of targeting a nuclear receptor for the treatment of complex diseases. Other nuclear receptors that also contribute to the development of NAFLD have failed to show beneficial effects without adverse effects on clinical trials (218, 219). Therefore, the development of drugs targeting specific nuclear receptor targets, such as SLC25A47, might provide alternative therapeutic options for treating NAFLD.

Chapter VI

Additional results

Chapter VI Additional results

VI.1 High levels of *Slc25a47* are associated to enhanced metabolic rate and decreased hepatic steatosis

SLC25A47 is a novel mitochondrial transporter that is highly and specifically expressed in the liver. Although the cognate solutes are still unknown, we showed its function is tightly linked with mitochondrial FAO (**Chapter V**). While further attempting to characterize the physiological role, thus relevance, of SLC25A47 in the liver, we sought to evaluate its liver expression profile in different publically available datasets in GEO. We found four different datasets were *Slc25a47* was significantly changed as depicted in Figure VI.1.

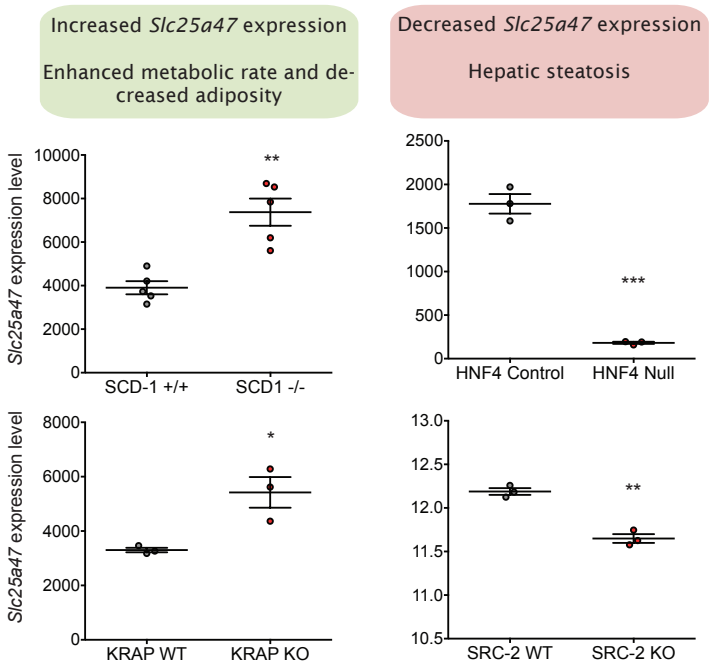

Figure VI.1 *Slc25a47* expression profiles show a beneficial role of this transporter for liver function.
Slc25a47 expression profiles as obtained from stearoyl-CoA desaturase-1 (SCD-1) (243), ki-ras-induced-induced actin-interacting protein (KRAP) (244), hepatocyte nuclear factor-4 (HNF4) (245) and steroid receptor coactivator-2 (SRC-2) (246) knockout (KO) liver transcriptomes.

Stearoyl-CoA desaturase (SCD-1) is a key lipogenic enzyme that is responsible for the synthesis of monounsaturated fatty acids, lack of which was reported to protect mice from obesity through enhanced oxygen consumption and energy expenditure. In SCD-1 KO mice, lipid oxidation genes are upregulated while other lipid synthesis genes are downregulated (243). Ki-ras-induced actin-interacting protein (KRAP) is a protein associated with the cytoskeleton that was described as being related to cancer. Mice lacking KRAP displayed enhanced metabolic rate

and decreased adiposity paralleled by a downregulation of fatty acid synthesis genes in the liver (244). In both models, *Slc25a47* expression levels are heightened. On the other hand, hepatocyte nuclear factor-4 (HNF4) steroid receptor coactivator-2 (SRC-2) KO mice present low levels of hepatic *Slc25a47*. SRC-2 stimulates liver fatty acid degradation and down-regulates cholesterol and steroid biosynthetic pathways (246). HNF-4 is a crucial hepatic transcription factor responsible for liver identity by orchestrating the hepatocyte gene expression program (245). HNF4 alpha liver-specific KO mice display severe hepatomegaly and hepatic steatosis (247). Taken together, the expression profiles where *Slc25a47* is significantly changed point to a beneficial role of this mitochondrial carrier in the liver.

Together these data corroborate the results presented on Chapter V indicating that *Slc25a47* is a hepatocyte marker with a vital role in maintaining proper liver function, loss of which is related to hepatic steatosis.

VI.2 SLC25A47 as the hepatocellular carcinoma-downregulated mitochondrial protein (HDMCP)

The data obtained so far have demonstrated SLC25A47 as important for proper liver function. Further proof of that is the fact that SLC25A47 is downregulated in liver cancer (hepatocellular carcinoma, HCC). For this reason, the name hepatocellular carcinoma downregulated carrier protein (HDMCP) has been proposed for this transporter, however no publication corroborates this information. To determine the validity of this nomination and to gain further insight into the vital role of this transporter, we decided to use datasets of HCC in humans to evaluate *Slc25a47* expression profile (248). As the liver loses its characteristic morphology and progresses through the pathological stages of HCC, *Slc25a47* expression levels are decreasing, being practically lost in advanced HCC (Figure VI.2A, B). This observation validates our previous hypothesis that SLC25A47 is a marker of normal liver. Moreover, these results show that hepatitis C virus (HCV)-induced HCC presents the same *Slc25a47* repression pattern derived from HCC from the metabolic disturbances associated with NAFLD progression (Figure VI.2B).

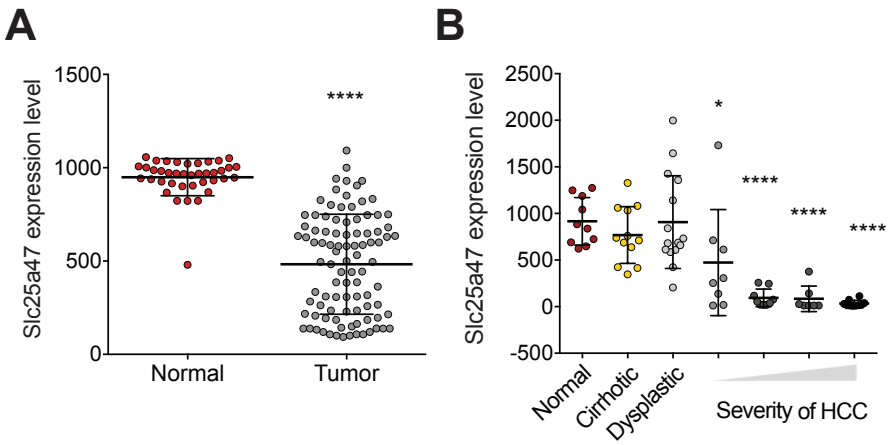

Figure VI.2 *Slc25a47* is downregulated in hepatocellular carcinoma (HCC) in an increasing severity manner.

(**A**) Hepatic SLC25A47 gene expression profile in HCC-patients, GSE45436, Wang *et al*, unpublished data. (**B**) Hepatic SLC25A47 gene expression profile of hepatitis C-infected patients representing the stepwise carcinogenic process from preneoplastic lesions (cirrhotic and dysplasia) to advanced HCC, GSE6764 (248).

Using the dataset of HCV-induced HCC where *Slc25a47* declines as disease progresses, we next assessed hepatic gene expression and pathway analysis of genes with the same or opposite profile as *Slc25a47.* In line with our previous analysis (Figure V.13), *Slc25a47* positively correlates with genes involved in fatty acid degradation (Figure VI.3A), presenting the same pattern of downregulation as fatty acid degradation enzymes (Figure VI.3B). Indicative of a possible tumor suppressor role of SLC25A47 that is consistent with its downregulation in liver cancer, *Slc25a47* correlated negatively with genes involved in cell cycle and DNA replication, common features of cancer cells (Figure VI.3C).

It is known that cancer cells rely more on glycolysis to obtain energy with concomitant lactate production (249). Therefore it is expected that fatty acid degradation is one of the metabolic pathways repressed as HCC becomes more aggressive. Taken together these data confirm that SLC25A47 is critical for liver function and identity, and its loss is associated with hepatocellular carcinoma.

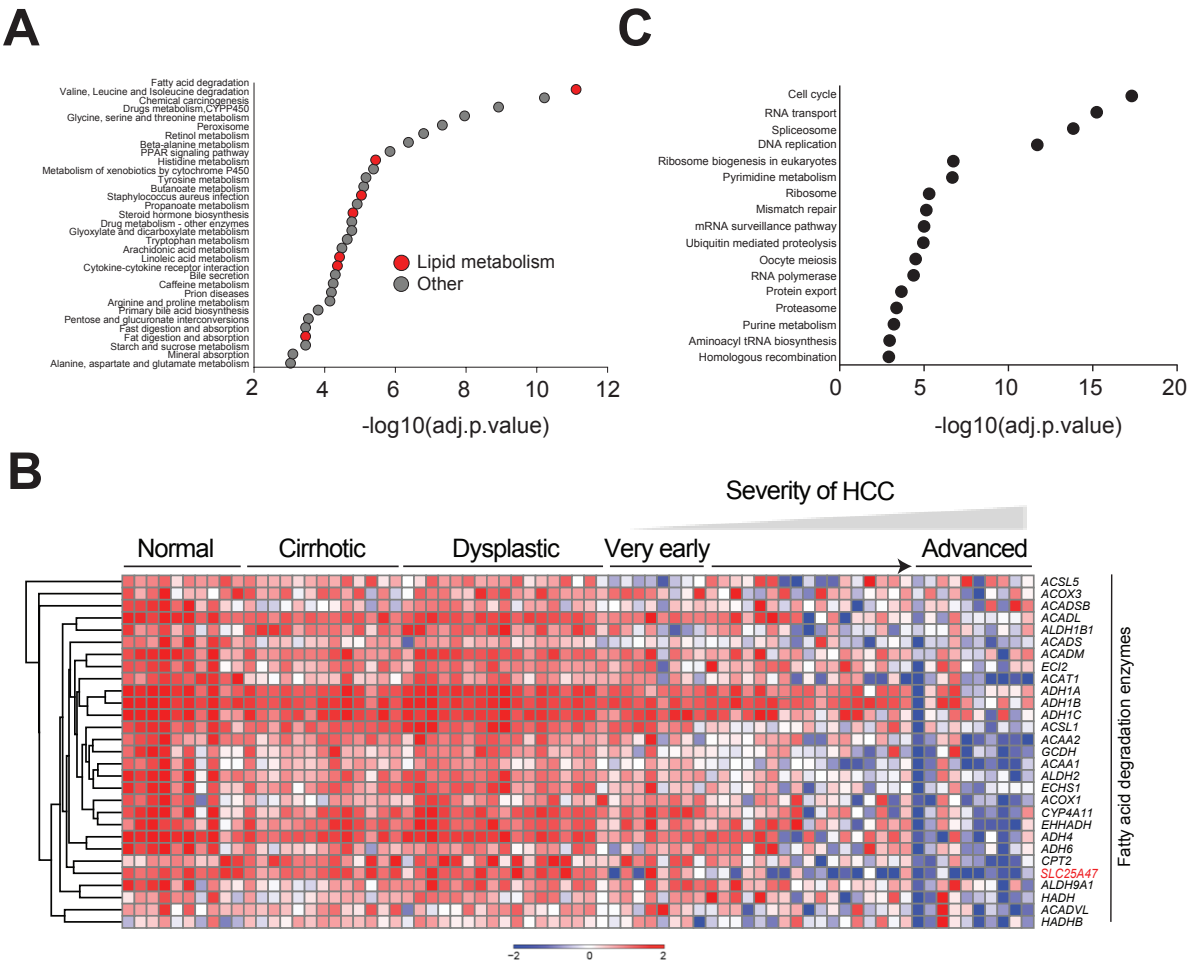

Figure VI.3 *Slc25a47* correlates positively with fatty acid degradation enzymes in hepatocellular carcinoma (HCC).

(**A**, **C**) KEGG pathway analysis of positive (**A**) and negative (**C**) correlating genes with *Slc25a47*. In **B**, a heat map displays the fatty acid degradation enzymes that correlate positively with *Slc25a47* and present a similar pattern of expression upon progression of HCC.

Chapter VII

General conclusion and future perspectives

Chapter VII General conclusion and future perspectives

The work presented here intended to establish the role of LRH-1 in fatty acid metabolism and NAFLD. To achieve this, we characterized the metabolic phenotype of both loss-of-function (*Lrh-1* $^{hep-/-}$) and gain-of-function (K289R) of LRH-1 upon different nutritional challenges or in the context of a setting that favors the development of hepatic steatosis. During the transition of the fasted to the fed state, the rise in blood glucose triggers insulin secretion and activates DNL in the liver. Upon fasting, the shift from insulin to glucagon triggers robust changes in hepatic metabolism, being the most prominent effect increased fatty acid delivery to the liver and enhanced mitochondrial fatty acid breakdown. In turn, a dysregulation of any of these processes can contribute to fat deposition within the liver. Here we showed that LRH-1 regulates multiple aspects of hepatic lipid homeostasis. In particular, we demonstrated that, upon refeeding, LRH-1 selective gain-of-function presented enhanced DNL rates. Consequently, under a lipogenic diet, LRH-1 K289R developed a more severe NAFLD phenotype. Moreover, loss of LRH-1 in the hepatocytes impaired mitochondrial fatty acid oxidation leading to exacerbated fasting-induced steatosis.

In this thesis, we also identified two novel proteins to counteract NAFLD, i.e. OSBPL3 and SLC25A47, and identified these as direct transcriptional targets of LRH-1. Most notably, these two proteins behave differently, playing a diverse role in NAFLD. OSBPL3, which is upregulated in LRH-1 K289R mice, is also a constant elevated presence in the liver of mouse and humans with NAFLD. A normal liver represses the expression of this oxysterol-binding protein, which hints at the fact that an abnormal overexpression of this protein is deleterious for liver function. On the other hand, SLC25A47 is highly and only expressed in the liver, which highlights its importance and possible therapeutic relevance for treating liver diseases. In accordance, this transporter is downregulated in *Lrh-1* $^{hep-/-}$ mice and in mouse models of NAFLD and its upregulation protects from the overload of lipids in the liver. The analysis of available datasets further emphasized the beneficial role of SLC25A47 in the liver. Additionally, we demonstrated how the loss of SLC25A47 relates significantly with the loss of liver morphology and function towards a tumorigenic state as in HCC. More importantly, we showed that overexpressing SLC25A47 in the liver improved mitochondrial function without causing any adverse and systemic effects. The development of compounds to target OSBPL3 and SLC25A47 will help determine the druggability

of these proteins and protection against this so common but so far not treatable disease.

Currently, we are conducting additional studies to determine the physiological role of SLC25A47 by using the liver-specific knockout mouse model (*Slc25a47* $^{hep-/-}$ mice). Transcriptomics, proteomics and metabolomics will be used to fully characterize both loss- (*Slc25a47* $^{hep-/-}$) and gain-of-function (AAV8-Slc25a47) of SLC25A47. Further studies will also help to unravel the regulation of SLC25A47 activity by PKA and SIRT3.

“A single experiment can prove me wrong“

Albert Einstein

References

References

1. Rinella, M.D., and Charlton, M. 2016. The globalization of nonalcoholic fatty liver disease: Prevalence and impact on world health. *Hepatology* 64(1):19-22.
2. Cohen, J.C., Horton, J.D., and Hobbs, H.H. 2011. Human fatty liver disease: old questions and new insights. *Science* 332:1519-1523.
3. Villanueva, A., and Llovet, J.M. 2014. Liver cancer in 2013: Mutational landscape of HCC--the end of the beginning. *Nat Rev Clin Oncol* 11:73-74.
4. Angulo, P. 2002. Nonalcoholic fatty liver disease. *N Engl J Med* 346:1221-1231.
5. Browning, J.D., Szczepaniak, L.S., Dobbins, R., Nuremberg, P., Horton, J.D., Cohen, J.C., Grundy, S.M., and Hobbs, H.H. 2004. Prevalence of hepatic steatosis in an urban population in the United States: impact of ethnicity. *Hepatology* 40:1387-1395.
6. Romeo, S., Kozlitina, J., Xing, C., Pertsemlidis, A., Cox, D., Pennacchio, L.A., Boerwinkle, E., Cohen, J.C., and Hobbs, H.H. 2008. Genetic variation in PNPLA3 confers susceptibility to nonalcoholic fatty liver disease. *Nat Genet* 40:1461-1465.
7. Schwimmer, J.B., Celedon, M.A., Lavine, J.E., Salem, R., Campbell, N., Schork, N.J., Shiehmorteza, M., Yokoo, T., Chavez, A., Middleton, M.S., et al. 2009. Heritability of nonalcoholic fatty liver disease. *Gastroenterology* 136:1585-1592.
8. Tappy, L., and Le, K.A. 2010. Metabolic effects of fructose and the worldwide increase in obesity. *Physiol Rev* 90:23-46.
9. Vos, M.B., and Lavine, J.E. 2013. Dietary fructose in nonalcoholic fatty liver disease. *Hepatology* 57:2525-2531.
10. Basaranoglu, M., Basaranoglu, G., and Bugianesi, E. 2015. Carbohydrate intake and nonalcoholic fatty liver disease: fructose as a weapon of mass destruction. *Hepatobiliary Surg Nutr* 4:109-116.
11. Machado, M., Marques-Vidal, P., and Cortez-Pinto, H. 2006. Hepatic histology in obese patients undergoing bariatric surgery. *J Hepatol* 45:600-606.
12. Targher, G., Bertolini, L., Padovani, R., Rodella, S., Tessari, R., Zenari, L., Day, C., and Arcaro, G. 2007. Prevalence of nonalcoholic fatty liver disease and its association with cardiovascular disease among type 2 diabetic patients. *Diabetes Care* 30:1212-1218.
13. de Alwis, N.M., and Day, C.P. 2008. Non-alcoholic fatty liver disease: the mist gradually clears. *J Hepatol* 48 Suppl 1:S104-112.
14. Vernon, G., Baranova, A., and Younossi, Z.M. 2011. Systematic review: the epidemiology and natural history of non-alcoholic fatty liver disease and non-alcoholic steatohepatitis in adults. *Aliment Pharmacol Ther* 34:274-285.
15. Williams, C.D., Stengel, J., Asike, M.I., Torres, D.M., Shaw, J., Contreras, M., Landt, C.L., and Harrison, S.A. 2011. Prevalence of nonalcoholic fatty liver disease and nonalcoholic steatohepatitis among a largely middle-aged population utilizing ultrasound and liver biopsy: a prospective study. *Gastroenterology* 140:124-131.
16. Caballeria, L., Pera, G., Auladell, M.A., Toran, P., Munoz, L., Miranda, D., Aluma, A., Casas, J.D., Sanchez, C., Gil, D., et al. 2010. Prevalence and factors associated with the presence of nonalcoholic fatty liver disease in an adult population in Spain. *Eur J Gastroenterol Hepatol* 22:24-32.

17. Bedogni, G., Miglioli, L., Masutti, F., Tiribelli, C., Marchesini, G., and Bellentani, S. 2005. Prevalence of and risk factors for nonalcoholic fatty liver disease: the Dionysos nutrition and liver study. *Hepatology* 42:44-52.
18. Ioannou, G.N., Boyko, E.J., and Lee, S.P. 2006. The prevalence and predictors of elevated serum aminotransferase activity in the United States in 1999-2002. *Am J Gastroenterol* 101:76-82.
19. Ruhl, C.E., and Everhart, J.E. 2003. Determinants of the association of overweight with elevated serum alanine aminotransferase activity in the United States. *Gastroenterology* 124:71-79.
20. Patt, C.H., Yoo, H.Y., Dibadj, K., Flynn, J., and Thuluvath, P.J. 2003. Prevalence of transaminase abnormalities in asymptomatic, healthy subjects participating in an executive health-screening program. *Dig Dis Sci* 48:797-801.
21. Bedogni, G., Bellentani, S., Miglioli, L., Masutti, F., Passalacqua, M., Castiglione, A., and Tiribelli, C. 2006. The Fatty Liver Index: a simple and accurate predictor of hepatic steatosis in the general population. *BMC Gastroenterol* 6:33.
22. Bedogni, G., Kahn, H.S., Bellentani, S., and Tiribelli, C. 2010. A simple index of lipid overaccumulation is a good marker of liver steatosis. *BMC Gastroenterol* 10:98.
23. Calle, E.E., Rodriguez, C., Walker-Thurmond, K., and Thun, M.J. 2003. Overweight, obesity, and mortality from cancer in a prospectively studied cohort of U.S. adults. *N Engl J Med* 348:1625-1638.
24. Lambert, J.E., and Parks, E.J. 2012. Postprandial metabolism of meal triglyceride in humans. *Biochim Biophys Acta* 1821:721-726.
25. Anstee, Q.M., and Goldin, R.D. 2006. Mouse models in non-alcoholic fatty liver disease and steatohepatitis research. *Int J Exp Pathol* 87:1-16.
26. Karpe, F., Dickmann, J.R., and Frayn, K.N. 2011. Fatty acids, obesity, and insulin resistance: time for a reevaluation. *Diabetes* 60:2441-2449.
27. Li, S., Brown, M.S., and Goldstein, J.L. 2010. Bifurcation of insulin signaling pathway in rat liver: mTORC1 required for stimulation of lipogenesis, but not inhibition of gluconeogenesis. *Proc Natl Acad Sci U S A* 107:3441-3446.
28. Horton, J.D., Goldstein, J.L., and Brown, M.S. 2002. SREBPs: activators of the complete program of cholesterol and fatty acid synthesis in the liver. *J Clin Invest* 109:1125-1131.
29. Uyeda, K., and Repa, J.J. 2006. Carbohydrate response element binding protein, ChREBP, a transcription factor coupling hepatic glucose utilization and lipid synthesis. *Cell Metab* 4:107-110.
30. Oosterveer, M.H., and Schoonjans, K. 2014. Hepatic glucose sensing and integrative pathways in the liver. *Cell Mol Life Sci* 71:1453-1467.
31. Dentin, R., Tomas-Cobos, L., Foufelle, F., Leopold, J., Girard, J., Postic, C., and Ferre, P. 2012. Glucose 6-phosphate, rather than xylulose 5-phosphate, is required for the activation of ChREBP in response to glucose in the liver. *J Hepatol* 56:199-209.
32. Donnelly, K.L., Smith, C.I., Schwarzenberg, S.J., Jessurun, J., Boldt, M.D., and Parks, E.J. 2005. Sources of fatty acids stored in liver and secreted via lipoproteins in patients with nonalcoholic fatty liver disease. *J Clin Invest* 115:1343-1351.
33. Lambert, J.E., Ramos-Roman, M.A., Browning, J.D., and Parks, E.J. 2014. Increased de novo lipogenesis is a distinct characteristic of individuals with nonalcoholic fatty liver disease. *Gastroenterology* 146:726-735.
34. Benhamed, F., Denechaud, P.D., Lemoine, M., Robichon, C., Moldes, M., Bertrand-Michel, J., Ratziu, V., Serfaty, L., Housset, C., Capeau, J., et al.

2012. The lipogenic transcription factor ChREBP dissociates hepatic steatosis from insulin resistance in mice and humans. *J Clin Invest* 122:2176-2194.

35. Dentin, R., Benhamed, F., Hainault, I., Fauveau, V., Foufelle, F., Dyck, J.R., Girard, J., and Postic, C. 2006. Liver-specific inhibition of ChREBP improves hepatic steatosis and insulin resistance in ob/ob mice. *Diabetes* 55:2159-2170.
36. Kohjima, M., Higuchi, N., Kato, M., Kotoh, K., Yoshimoto, T., Fujino, T., Yada, M., Yada, R., Harada, N., Enjoji, M., et al. 2008. SREBP-1c, regulated by the insulin and AMPK signaling pathways, plays a role in nonalcoholic fatty liver disease. *Int J Mol Med* 21:507-511.
37. Zimmermann, R., Strauss, J.G., Haemmerle, G., Schoiswohl, G., Birner-Gruenberger, R., Riederer, M., Lass, A., Neuberger, G., Eisenhaber, F., Hermetter, A., et al. 2004. Fat mobilization in adipose tissue is promoted by adipose triglyceride lipase. *Science* 306:1383-1386.
38. Kawano, Y., and Cohen, D.E. 2013. Mechanisms of hepatic triglyceride accumulation in non-alcoholic fatty liver disease. *J Gastroenterol* 48:434-441.
39. Doege, H., Baillie, R.A., Ortegon, A.M., Tsang, B., Wu, Q., Punreddy, S., Hirsch, D., Watson, N., Gimeno, R.E., and Stahl, A. 2006. Targeted deletion of FATP5 reveals multiple functions in liver metabolism: alterations in hepatic lipid homeostasis. *Gastroenterology* 130:1245-1258.
40. Greco, D., Kotronen, A., Westerbacka, J., Puig, O., Arkkila, P., Kiviluoto, T., Laitinen, S., Kolak, M., Fisher, R.M., Hamsten, A., et al. 2008. Gene expression in human NAFLD. *Am J Physiol Gastrointest Liver Physiol* 294:G1281-1287.
41. Hooper, A.J., Adams, L.A., and Burnett, J.R. 2011. Genetic determinants of hepatic steatosis in man. *J Lipid Res* 52:593-617.
42. Lomonaco, R., Ortiz-Lopez, C., Orsak, B., Webb, A., Hardies, J., Darland, C., Finch, J., Gastaldelli, A., Harrison, S., Tio, F., et al. 2012. Effect of adipose tissue insulin resistance on metabolic parameters and liver histology in obese patients with nonalcoholic fatty liver disease. *Hepatology* 55:1389-1397.
43. Romeo, S., Huang-Doran, I., Baroni, M.G., and Kotronen, A. 2010. Unravelling the pathogenesis of fatty liver disease: patatin-like phospholipase domain-containing 3 protein. *Curr Opin Lipidol* 21:247-252.
44. Jha, P., Claudel, T., Baghdasaryan, A., Mueller, M., Halilbasic, E., Das, S.K., Lass, A., Zimmermann, R., Zechner, R., Hoefler, G., et al. 2014. Role of adipose triglyceride lipase (PNPLA2) in protection from hepatic inflammation in mouse models of steatohepatitis and endotoxemia. *Hepatology* 59:858-869.
45. Tanoli, T., Yue, P., Yablonskiy, D., and Schonfeld, G. 2004. Fatty liver in familial hypobetalipoproteinemia: roles of the APOB defects, intra-abdominal adipose tissue, and insulin sensitivity. *J Lipid Res* 45:941-947.
46. Fujita, K., Nozaki, Y., Wada, K., Yoneda, M., Fujimoto, Y., Fujitake, M., Endo, H., Takahashi, H., Inamori, M., Kobayashi, N., et al. 2009. Dysfunctional very-low-density lipoprotein synthesis and release is a key factor in nonalcoholic steatohepatitis pathogenesis. *Hepatology* 50:772-780.
47. Walker, A.K. 2017. 1-Carbon Cycle Metabolites Methylate Their Way to Fatty Liver. *Trends Endocrinol Metab* 28:63-72.
48. Caballero, F., Fernandez, A., Matias, N., Martinez, L., Fucho, R., Elena, M., Caballeria, J., Morales, A., Fernandez-Checa, J.C., and Garcia-Ruiz, C. 2010. Specific contribution of methionine and choline in nutritional nonalcoholic

steatohepatitis: impact on mitochondrial S-adenosyl-L-methionine and glutathione. *J Biol Chem* 285:18528-18536.
49. Nassir, F., and Ibdah, J.A. 2014. Role of mitochondria in nonalcoholic fatty liver disease. *Int J Mol Sci* 15:8713-8742.
50. Koliaki, C., Szendroedi, J., Kaul, K., Jelenik, T., Nowotny, P., Jankowiak, F., Herder, C., Carstensen, M., Krausch, M., Knoefel, W.T., et al. 2015. Adaptation of hepatic mitochondrial function in humans with non-alcoholic fatty liver is lost in steatohepatitis. *Cell Metab* 21:739-746.
51. Saudubray, J.M., Martin, D., de Lonlay, P., Touati, G., Poggi-Travert, F., Bonnet, D., Jouvet, P., Boutron, M., Slama, A., Vianey-Saban, C., et al. 1999. Recognition and management of fatty acid oxidation defects: a series of 107 patients. *J Inherit Metab Dis* 22:488-502.
52. Lane, N., and Martin, W. 2010. The energetics of genome complexity. *Nature* 467:929-934.
53. Nunnari, J., and Suomalainen, A. 2012. Mitochondria: in sickness and in health. *Cell* 148:1145-1159.
54. Sato, M., and Sato, K. 2011. Degradation of paternal mitochondria by fertilization-triggered autophagy in C. elegans embryos. *Science* 334:1141-1144.
55. Hamanaka, R.B., and Chandel, N.S. 2010. Mitochondrial reactive oxygen species regulate cellular signaling and dictate biological outcomes. *Trends Biochem Sci* 35:505-513.
56. Calvo, S.E., and Mootha, V.K. 2010. The mitochondrial proteome and human disease. *Annu Rev Genomics Hum Genet* 11:25-44.
57. Koopman, W.J., Willems, P.H., and Smeitink, J.A. 2012. Monogenic mitochondrial disorders. *N Engl J Med* 366:1132-1141.
58. Szendroedi, J., Phielix, E., and Roden, M. 2011. The role of mitochondria in insulin resistance and type 2 diabetes mellitus. *Nat Rev Endocrinol* 8:92-103.
59. Lin, M.T., and Beal, M.F. 2006. Mitochondrial dysfunction and oxidative stress in neurodegenerative diseases. *Nature* 443:787-795.
60. Wallace, D.C. 2012. Mitochondria and cancer. *Nat Rev Cancer* 12:685-698.
61. Balaban, R.S., Nemoto, S., and Finkel, T. 2005. Mitochondria, oxidants, and aging. *Cell* 120:483-495.
62. Bratic, A., and Larsson, N.G. 2013. The role of mitochondria in aging. *J Clin Invest* 123:951-957.
63. Harbauer, A.B., Zahedi, R.P., Sickmann, A., Pfanner, N., and Meisinger, C. 2014. The protein import machinery of mitochondria-a regulatory hub in metabolism, stress, and disease. *Cell Metab* 19:357-372.
64. Ballard, J.W., and Whitlock, M.C. 2004. The incomplete natural history of mitochondria. *Mol Ecol* 13:729-744.
65. Murphy, M.P. 2009. How mitochondria produce reactive oxygen species. *Biochem J* 417:1-13.
66. Oyewole, A.O., and Birch-Machin, M.A. 2015. Mitochondria-targeted antioxidants. *FASEB J* 29:4766-4771.
67. Grimm, A., and Eckert, A. 2017. Brain aging and neurodegeneration: from a mitochondrial point of view. *J Neurochem*.
68. Elustondo, P., Martin, L.A., and Karten, B. 2017. Mitochondrial cholesterol import. *Biochim Biophys Acta* 1862:90-101.
69. Keilin, D., and Hartree, E.F. 1947. Activity of the cytochrome system in heart muscle preparations. *Biochem J* 41:500-502.
70. Chance, B., Estabrook, R.W., and Lee, C.P. 1963. Electron Transport in the Oxysome. *Science* 140:379-380.

71. Hackenbrock, C.R., Chazotte, B., and Gupte, S.S. 1986. The random collision model and a critical assessment of diffusion and collision in mitochondrial electron transport. *J Bioenerg Biomembr* 18:331-368.
72. Lamantea, E., Carrara, F., Mariotti, C., Morandi, L., Tiranti, V., and Zeviani, M. 2002. A novel nonsense mutation (Q352X) in the mitochondrial cytochrome b gene associated with a combined deficiency of complexes I and III. *Neuromuscul Disord* 12:49-52.
73. Enriquez, J.A. 2016. Supramolecular Organization of Respiratory Complexes. *Annu Rev Physiol* 78:533-561.
74. Schagger, H., and Pfeiffer, K. 2000. Supercomplexes in the respiratory chains of yeast and mammalian mitochondria. *EMBO J* 19:1777-1783.
75. Milenkovic, D., Blaza, J.N., Larsson, N.G., and Hirst, J. 2017. The Enigma of the Respiratory Chain Supercomplex. *Cell Metab* 25:765-776.
76. Wu, M., Gu, J., Guo, R., Huang, Y., and Yang, M. 2016. Structure of Mammalian Respiratory Supercomplex I1III2IV1. *Cell* 167:1598-1609 e1510.
77. Maranzana, E., Barbero, G., Falasca, A.I., Lenaz, G., and Genova, M.L. 2013. Mitochondrial respiratory supercomplex association limits production of reactive oxygen species from complex I. *Antioxid Redox Signal* 19:1469-1480.
78. Lapuente-Brun, E., Moreno-Loshuertos, R., Acin-Perez, R., Latorre-Pellicer, A., Colas, C., Balsa, E., Perales-Clemente, E., Quiros, P.M., Calvo, E., Rodriguez-Hernandez, M.A., et al. 2013. Supercomplex assembly determines electron flux in the mitochondrial electron transport chain. *Science* 340:1567-1570.
79. Comte, J., Maisterrena, B., and Gautheron, D.C. 1976. Lipid composition and protein profiles of outer and inner membranes from pig heart mitochondria. Comparison with microsomes. *Biochim Biophys Acta* 419:271-284.
80. Paradies, G., Paradies, V., De Benedictis, V., Ruggiero, F.M., and Petrosillo, G. 2014. Functional role of cardiolipin in mitochondrial bioenergetics. *Biochim Biophys Acta* 1837:408-417.
81. Palmieri, F., and Monne, M. 2016. Discoveries, metabolic roles and diseases of mitochondrial carriers: A review. *Biochim Biophys Acta* 1863:2362-2378.
82. Abrams, A.J., Hufnagel, R.B., Rebelo, A., Zanna, C., Patel, N., Gonzalez, M.A., Campeanu, I.J., Griffin, L.B., Groenewald, S., Strickland, A.V., et al. 2015. Mutations in SLC25A46, encoding a UGO1-like protein, cause an optic atrophy spectrum disorder. *Nat Genet* 47:926-932.
83. Robinson, A.J., Kunji, E.R., and Gross, A. 2012. Mitochondrial carrier homolog 2 (MTCH2): the recruitment and evolution of a mitochondrial carrier protein to a critical player in apoptosis. *Exp Cell Res* 318:1316-1323.
84. Agrimi, G., Russo, A., Scarcia, P., and Palmieri, F. 2012. The human gene SLC25A17 encodes a peroxisomal transporter of coenzyme A, FAD and NAD+. *Biochem J* 443:241-247.
85. Gutiérrez-Aguilar, M., and Baines, C.P. 2013. Physiological and pathological roles of mitochondrial SLC25 carriers. *Biochemical Journal* 454:371–386.
86. Schrum, J.P., Zhu, T.F., and Szostak, J.W. 2010. The origins of cellular life. *Cold Spring Harb Perspect Biol* 2:a002212.
87. Palmieri, F. 2013. The mitochondrial transporter family SLC25: Identification, properties and physiopathology. *Molecular Aspects of Medicine* 34:465–484.

88. Cesar-Razquin, A., Snijder, B., Frappier-Brinton, T., Isserlin, R., Gyimesi, G., Bai, X., Reithmeier, R.A., Hepworth, D., Hediger, M.A., Edwards, A.M., et al. 2015. A Call for Systematic Research on Solute Carriers. *Cell* 162:478-487.
89. Fauman, E.B., Rai, B.K., and Huang, E.S. 2011. Structure-based druggability assessment--identifying suitable targets for small molecule therapeutics. *Curr Opin Chem Biol* 15:463-468.
90. Sunny, N.E., Bril, F., and Cusi, K. 2017. Mitochondrial Adaptation in Nonalcoholic Fatty Liver Disease: Novel Mechanisms and Treatment Strategies. *Trends Endocrinol Metab* 28:250-260.
91. Miele, L., Grieco, A., Armuzzi, A., Candelli, M., Forgione, A., Gasbarrini, A., and Gasbarrini, G. 2003. Hepatic mitochondrial beta-oxidation in patients with nonalcoholic steatohepatitis assessed by 13C-octanoate breath test. *Am J Gastroenterol* 98:2335-2336.
92. Iozzo, P., Bucci, M., Roivainen, A., Nagren, K., Jarvisalo, M.J., Kiss, J., Guiducci, L., Fielding, B., Naum, A.G., Borra, R., et al. 2010. Fatty acid metabolism in the liver, measured by positron emission tomography, is increased in obese individuals. *Gastroenterology* 139:846-856, 856 e841-846.
93. Sunny, N.E., Parks, E.J., Browning, J.D., and Burgess, S.C. 2011. Excessive hepatic mitochondrial TCA cycle and gluconeogenesis in humans with nonalcoholic fatty liver disease. *Cell Metab* 14:804-810.
94. Patterson, R.E., Kalavalapalli, S., Williams, C.M., Nautiyal, M., Mathew, J.T., Martinez, J., Reinhard, M.K., McDougall, D.J., Rocca, J.R., Yost, R.A., et al. 2016. Lipotoxicity in steatohepatitis occurs despite an increase in tricarboxylic acid cycle activity. *Am J Physiol Endocrinol Metab* 310:E484-494.
95. Gariani, K., Menzies, K.J., Ryu, D., Wegner, C.J., Wang, X., Ropelle, E.R., Moullan, N., Zhang, H., Perino, A., Lemos, V., et al. 2016. Eliciting the mitochondrial unfolded protein response by nicotinamide adenine dinucleotide repletion reverses fatty liver disease in mice. *Hepatology* 63:1190-1204.
96. Gariani, K., Ryu, D., Menzies, K.J., Yi, H.S., Stein, S., Zhang, H., Perino, A., Lemos, V., Katsyuba, E., Jha, P., et al. 2017. Inhibiting poly ADP-ribosylation increases fatty acid oxidation and protects against fatty liver disease. *J Hepatol* 66:132-141.
97. Musso, G., and Gambino, R. 2017. Targeting mitochondrial pyruvate carrier (MPC) in NASH: Growing evidence and future challenges. *Hepatology*.
98. Satapati, S., Kucejova, B., Duarte, J.A., Fletcher, J.A., Reynolds, L., Sunny, N.E., He, T., Nair, L.A., Livingston, K.A., Fu, X., et al. 2015. Mitochondrial metabolism mediates oxidative stress and inflammation in fatty liver. *J Clin Invest* 125:4447-4462.
99. Perry, R.J., Zhang, D., Zhang, X.M., Boyer, J.L., and Shulman, G.I. 2015. Controlled-release mitochondrial protonophore reverses diabetes and steatohepatitis in rats. *Science* 347:1253-1256.
100. Perry, R.J., Kim, T., Zhang, X.M., Lee, H.Y., Pesta, D., Popov, V.B., Zhang, D., Rahimi, Y., Jurczak, M.J., Cline, G.W., et al. 2013. Reversal of hypertriglyceridemia, fatty liver disease, and insulin resistance by a liver-targeted mitochondrial uncoupler. *Cell Metab* 18:740-748.
101. Sablin, E.P., Krylova, I.N., Fletterick, R.J., and Ingraham, H.A. 2003. Structural basis for ligand-independent activation of the orphan nuclear receptor LRH-1. *Mol Cell* 11:1575-1585.
102. Solomon, I.H., Hager, J.M., Safi, R., McDonnell, D.P., Redinbo, M.R., and Ortlund, E.A. 2005. Crystal structure of the human LRH-1 DBD-DNA

complex reveals Ftz-F1 domain positioning is required for receptor activity. *J Mol Biol* 354:1091-1102.
103. Feige, J.N., and Auwerx, J. 2007. Transcriptional coregulators in the control of energy homeostasis. *Trends Cell Biol* 17:292-301.
104. Fayard, E., Auwerx, J., and Schoonjans, K. 2004. LRH-1: an orphan nuclear receptor involved in development, metabolism and steroidogenesis. *Trends Cell Biol* 14:250-260.
105. Nakajima, T., Takase, M., Miura, I., and Nakamura, M. 2000. Two isoforms of FTZ-F1 messenger RNA: molecular cloning and their expression in the frog testis. *Gene* 248:203-212.
106. Ellinger-Ziegelbauer, H., Hihi, A.K., Laudet, V., Keller, H., Wahli, W., and Dreyer, C. 1994. FTZ-F1-related orphan receptors in Xenopus laevis: transcriptional regulators differentially expressed during early embryogenesis. *Mol Cell Biol* 14:2786-2797.
107. Galarneau, L., Pare, J.F., Allard, D., Hamel, D., Levesque, L., Tugwood, J.D., Green, S., and Belanger, L. 1996. The alpha1-fetoprotein locus is activated by a nuclear receptor of the Drosophila FTZ-F1 family. *Mol Cell Biol* 16:3853-3865.
108. Kudo, T., and Sutou, S. 1997. Molecular cloning of chicken FTZ-F1-related orphan receptors. *Gene* 197:261-268.
109. Liu, D., Le Drean, Y., Ekker, M., Xiong, F., and Hew, C.L. 1997. Teleost FTZ-F1 homolog and its splicing variant determine the expression of the salmon gonadotropin IIbeta subunit gene. *Mol Endocrinol* 11:877-890.
110. Boerboom, D., Pilon, N., Behdjani, R., Silversides, D.W., and Sirois, J. 2000. Expression and regulation of transcripts encoding two members of the NR5A nuclear receptor subfamily of orphan nuclear receptors, steroidogenic factor-1 and NR5A2, in equine ovarian cells during the ovulatory process. *Endocrinology* 141:4647-4656.
111. Becker-Andre, M., Andre, E., and DeLamarter, J.F. 1993. Identification of nuclear receptor mRNAs by RT-PCR amplification of conserved zinc-finger motif sequences. *Biochem Biophys Res Commun* 194:1371-1379.
112. Galarneau, L., Drouin, R., and Belanger, L. 1998. Assignment of the fetoprotein transcription factor gene (FTF) to human chromosome band 1q32.11 by in situ hybridization. *Cytogenet Cell Genet* 82:269-270.
113. Li, M., Xie, Y.H., Kong, Y.Y., Wu, X., Zhu, L., and Wang, Y. 1998. Cloning and characterization of a novel human hepatocyte transcription factor, hB1F, which binds and activates enhancer II of hepatitis B virus. *J Biol Chem* 273:29022-29031.
114. Nitta, M., Ku, S., Brown, C., Okamoto, A.Y., and Shan, B. 1999. CPF: an orphan nuclear receptor that regulates liver-specific expression of the human cholesterol 7alpha-hydroxylase gene. *Proc Natl Acad Sci U S A* 96:6660-6665.
115. Lee, M.B., Lebedeva, L.A., Suzawa, M., Wadekar, S.A., Desclozeaux, M., and Ingraham, H.A. 2005. The DEAD-box protein DP103 (Ddx20 or Gemin-3) represses orphan nuclear receptor activity via SUMO modification. *Mol Cell Biol* 25:1879-1890.
116. Lee, Y.K., Choi, Y.H., Chua, S., Park, Y.J., and Moore, D.D. 2006. Phosphorylation of the hinge domain of the nuclear hormone receptor LRH-1 stimulates transactivation. *J Biol Chem* 281:7850-7855.
117. Chalkiadaki, A., and Talianidis, I. 2005. SUMO-dependent compartmentalization in promyelocytic leukemia protein nuclear bodies prevents the access of LRH-1 to chromatin. *Mol Cell Biol* 25:5095-5105.
118. Venteclef, N., Jakobsson, T., Ehrlund, A., Damdimopoulos, A., Mikkonen, L., Ellis, E., Nilsson, L.M., Parini, P., Janne, O.A., Gustafsson, J.A., et al.

2010. GPS2-dependent corepressor/SUMO pathways govern anti-inflammatory actions of LRH-1 and LXRbeta in the hepatic acute phase response. *Genes Dev* 24:381-395.

119. Stein, S., Oosterveer, M.H., Mataki, C., Xu, P., Lemos, V., Havinga, R., Dittner, C., Ryu, D., Menzies, K.J., Wang, X., et al. 2014. SUMOylation-Dependent LRH-1/PROX1 Interaction Promotes Atherosclerosis by Decreasing Hepatic Reverse Cholesterol Transport. *Cell Metab* 20:603-613.
120. Sablin, E.P., Blind, R.D., Uthayaruban, R., Chiu, H.J., Deacon, A.M., Das, D., Ingraham, H.A., and Fletterick, R.J. 2015. Structure of Liver Receptor Homolog-1 (NR5A2) with PIP3 hormone bound in the ligand binding pocket. *J Struct Biol* 192:342-348.
121. Wang, W., Zhang, C., Marimuthu, A., Krupka, H.I., Tabrizizad, M., Shelloe, R., Mehra, U., Eng, K., Nguyen, H., Settachatgul, C., et al. 2005. The crystal structures of human steroidogenic factor-1 and liver receptor homologue-1. *Proc Natl Acad Sci U S A* 102:7505-7510.
122. Krylova, I.N., Sablin, E.P., Moore, J., Xu, R.X., Waitt, G.M., MacKay, J.A., Juzumiene, D., Bynum, J.M., Madauss, K., Montana, V., et al. 2005. Structural analyses reveal phosphatidyl inositols as ligands for the NR5 orphan receptors SF-1 and LRH-1. *Cell* 120:343-355.
123. Musille, P.M., Pathak, M.C., Lauer, J.L., Hudson, W.H., Griffin, P.R., and Ortlund, E.A. 2012. Antidiabetic phospholipid-nuclear receptor complex reveals the mechanism for phospholipid-driven gene regulation. *Nat Struct Mol Biol* 19:532-537, S531-532.
124. Lee, J.M., Lee, Y.K., Mamrosh, J.L., Busby, S.A., Griffin, P.R., Pathak, M.C., Ortlund, E.A., and Moore, D.D. 2011. A nuclear-receptor-dependent phosphatidylcholine pathway with antidiabetic effects. *Nature* 474:506-510.
125. Corzo, C.A., Mari, Y., Chang, M.R., Khan, T., Kuruvilla, D., Nuhant, P., Kumar, N., West, G.M., Duckett, D.R., Roush, W.R., et al. 2015. Antiproliferation activity of a small molecule repressor of liver receptor homolog 1. *Mol Pharmacol* 87:296-304.
126. Benod, C., Carlsson, J., Uthayaruban, R., Hwang, P., Irwin, J.J., Doak, A.K., Shoichet, B.K., Sablin, E.P., and Fletterick, R.J. 2013. Structure-based Discovery of Antagonists of Nuclear Receptor LRH-1. *The Journal of biological chemistry* 288:19830-19844.
127. Rey, J., Hu, H., Kyle, F., Lai, C.F., Buluwela, L., Coombes, R.C., Ortlund, E.A., Ali, S., Snyder, J.P., and Barrett, A.G. 2012. Discovery of a new class of liver receptor homolog-1 (LRH-1) antagonists: virtual screening, synthesis and biological evaluation. *ChemMedChem* 7:1909-1914.
128. Whitby, R.J., Stec, J., Blind, R.D., Dixon, S., Leesnitzer, L.M., Orband-Miller, L.A., Williams, S.P., Willson, T.M., Xu, R., Zuercher, W.J., et al. 2011. Small molecule agonists of the orphan nuclear receptors steroidogenic factor-1 (SF-1, NR5A1) and liver receptor homologue-1 (LRH-1, NR5A2). *Journal of medicinal chemistry* 54:2266-2281.
129. Whitby, R.J., Dixon, S., Maloney, P.R., Delerive, P., Goodwin, B.J., Parks, D.J., and Willson, T.M. 2006. Identification of small molecule agonists of the orphan nuclear receptors liver receptor homolog-1 and steroidogenic factor-1. *J Med Chem* 49:6652-6655.
130. Stein, S., and Schoonjans, K. 2015. Molecular basis for the regulation of the nuclear receptor LRH-1. *Curr Opin Cell Biol* 33:26-34.
131. Heng, J.C., Feng, B., Han, J., Jiang, J., Kraus, P., Ng, J.H., Orlov, Y.L., Huss, M., Yang, L., Lufkin, T., et al. 2010. The nuclear receptor Nr5a2 can replace Oct4 in the reprogramming of murine somatic cells to pluripotent cells. *Cell Stem Cell* 6:167-174.

132. Wang, W., Yang, J., Liu, H., Lu, D., Chen, X., Zenonos, Z., Campos, L.S., Rad, R., Guo, G., Zhang, S., et al. 2011. Rapid and efficient reprogramming of somatic cells to induced pluripotent stem cells by retinoic acid receptor gamma and liver receptor homolog 1. *Proceedings of the National Academy of Sciences of the United States of America* 108:18283-18288.
133. Wagner, R.T., Xu, X., Yi, F., Merrill, B.J., and Cooney, A.J. 2010. Canonical Wnt/beta-catenin regulation of liver receptor homolog-1 mediates pluripotency gene expression. *Stem Cells* 28:1794-1804.
134. Stergiopoulos, A., and Politis, P.K. 2016. Nuclear receptor NR5A2 controls neural stem cell fate decisions during development. *Nat Commun* 7:12230.
135. Holmstrom, S.R., Deering, T., Swift, G.H., Poelwijk, F.J., Mangelsdorf, D.J., Kliewer, S.A., and MacDonald, R.J. 2011. LRH-1 and PTF1-L coregulate an exocrine pancreas-specific transcriptional network for digestive function. *Genes Dev* 25:1674-1679.
136. Kim, J.W., Havelock, J.C., Carr, B.R., and Attia, G.R. 2005. The orphan nuclear receptor, liver receptor homolog-1, regulates cholesterol side-chain cleavage cytochrome p450 enzyme in human granulosa cells. *J Clin Endocrinol Metab* 90:1678-1685.
137. Liu, D.L., Liu, W.Z., Li, Q.L., Wang, H.M., Qian, D., Treuter, E., and Zhu, C. 2003. Expression and functional analysis of liver receptor homologue 1 as a potential steroidogenic factor in rat ovary. *Biol Reprod* 69:508-517.
138. Peng, N., Kim, J.W., Rainey, W.E., Carr, B.R., and Attia, G.R. 2003. The role of the orphan nuclear receptor, liver receptor homologue-1, in the regulation of human corpus luteum 3beta-hydroxysteroid dehydrogenase type II. *J Clin Endocrinol Metab* 88:6020-6028.
139. Saxena, D., Escamilla-Hernandez, R., Little-Ihrig, L., and Zeleznik, A.J. 2007. Liver receptor homolog-1 and steroidogenic factor-1 have similar actions on rat granulosa cell steroidogenesis. *Endocrinology* 148:726-734.
140. Duggavathi, R., Volle, D.H., Mataki, C., Antal, M.C., Messaddeq, N., Auwerx, J., Murphy, B.D., and Schoonjans, K. 2008. Liver receptor homolog 1 is essential for ovulation. *Genes Dev* 22:1871-1876.
141. Zhang, C., Large, M.J., Duggavathi, R., DeMayo, F.J., Lydon, J.P., Schoonjans, K., Kovanci, E., and Murphy, B.D. 2013. Liver receptor homolog-1 is essential for pregnancy. *Nat Med* 19:1061-1066.
142. Chand, A.L., Wijayakumara, D.D., Knower, K.C., Herridge, K.A., Howard, T.L., Lazarus, K.A., and Clyne, C.D. 2012. The orphan nuclear receptor LRH-1 and ERalpha activate GREB1 expression to induce breast cancer cell proliferation. *PLoS One* 7:e31593.
143. Benod, C., Vinogradova, M.V., Jouravel, N., Kim, G.E., Fletterick, R.J., and Sablin, E.P. 2011. Nuclear receptor liver receptor homologue 1 (LRH-1) regulates pancreatic cancer cell growth and proliferation. *Proceedings of the National Academy of Sciences of the United States of America* 108:16927-16931.
144. Botrugno, O.A., Fayard, E., Annicotte, J.S., Haby, C., Brennan, T., Wendling, O., Tanaka, T., Kodama, T., Thomas, W., Auwerx, J., et al. 2004. Synergy between LRH-1 and beta-catenin induces G1 cyclin-mediated cell proliferation. *Mol Cell* 15:499-509.
145. Coste, A., Dubuquoy, L., Barnouin, R., Annicotte, J.S., Magnier, B., Notti, M., Corazza, N., Antal, M.C., Metzger, D., Desreumaux, P., et al. 2007. LRH-1-mediated glucocorticoid synthesis in enterocytes protects against inflammatory bowel disease. *Proc Natl Acad Sci U S A* 104:13098-13103.
146. Mamrosh, J.L., Lee, J.M., Wagner, M., Stambrook, P.J., Whitby, R.J., Sifers, R.N., Wu, S.P., Tsai, M.J., Demayo, F.J., and Moore, D.D. 2014. Nuclear

receptor LRH-1/NR5A2 is required and targetable for liver endoplasmic reticulum stress resolution. *Elife (Cambridge)* 3:e01694.
147. Schoonjans, K., Dubuquoy, L., Mebis, J., Fayard, E., Wendling, O., Haby, C., Geboes, K., and Auwerx, J. 2005. Liver receptor homolog 1 contributes to intestinal tumor formation through effects on cell cycle and inflammation. *Proc Natl Acad Sci U S A* 102:2058-2062.
148. Xu, P., Oosterveer, M.H., Stein, S., Demagny, H., Ryu, D., Moullan, N., Wang, X., Can, E., Zamboni, N., Comment, A., et al. 2016. LRH-1-dependent programming of mitochondrial glutamine processing drives liver cancer. *Genes Dev* 30:1255-1260.
149. Russell, D.W. 2003. The enzymes, regulation, and genetics of bile acid synthesis. *Annu Rev Biochem* 72:137-174.
150. Chiang, J.Y. 2013. Bile acid metabolism and signaling. *Compr Physiol* 3:1191-1212.
151. del Castillo-Olivares, A., and Gil, G. 2000. Alpha 1-fetoprotein transcription factor is required for the expression of sterol 12alpha -hydroxylase, the specific enzyme for cholic acid synthesis. Potential role in the bile acid-mediated regulation of gene transcription. *J Biol Chem* 275:17793-17799.
152. Lu, T.T., Makishima, M., Repa, J.J., Schoonjans, K., Kerr, T.A., Auwerx, J., and Mangelsdorf, D.J. 2000. Molecular basis for feedback regulation of bile acid synthesis by nuclear receptors. *Mol Cell* 6:507-515.
153. Goodwin, B., Jones, S.A., Price, R.R., Watson, M.A., McKee, D.D., Moore, L.B., Galardi, C., Wilson, J.G., Lewis, M.C., Roth, M.E., et al. 2000. A regulatory cascade of the nuclear receptors FXR, SHP-1, and LRH-1 represses bile acid biosynthesis. *Mol Cell* 6:517-526.
154. Shin, D.J., and Osborne, T.F. 2008. Peroxisome proliferator-activated receptor-gamma coactivator-1alpha activation of CYP7A1 during food restriction and diabetes is still inhibited by small heterodimer partner. *J Biol Chem* 283:15089-15096.
155. Mataki, C., Magnier, B.C., Houten, S.M., Annicotte, J.S., Argmann, C., Thomas, C., Overmars, H., Kulik, W., Metzger, D., Auwerx, J., et al. 2007. Compromised intestinal lipid absorption in mice with a liver-specific deficiency of liver receptor homolog 1. *Mol Cell Biol* 27:8330-8339.
156. Lee, Y.K., Schmidt, D.R., Cummins, C.L., Choi, M., Peng, L., Zhang, Y., Goodwin, B., Hammer, R.E., Mangelsdorf, D.J., and Kliewer, S.A. 2008. Liver receptor homolog-1 regulates bile acid homeostasis but is not essential for feedback regulation of bile acid synthesis. *Mol Endocrinol* 22:1345-1356.
157. Out, C., Hageman, J., Bloks, V.W., Gerrits, H., Sollewijn Gelpke, M.D., Bos, T., Havinga, R., Smit, M.J., Kuipers, F., and Groen, A.K. 2011. Liver receptor homolog-1 is critical for adequate up-regulation of Cyp7a1 gene transcription and bile salt synthesis during bile salt sequestration. *Hepatology* 53:2075-2085.
158. Song, X., Kaimal, R., Yan, B., and Deng, R. 2008. Liver receptor homolog 1 transcriptionally regulates human bile salt export pump expression. *J Lipid Res* 49:973-984.
159. Bohan, A., Chen, W.S., Denson, L.A., Held, M.A., and Boyer, J.L. 2003. Tumor necrosis factor alpha-dependent up-regulation of Lrh-1 and Mrp3(Abcc3) reduces liver injury in obstructive cholestasis. *J Biol Chem* 278:36688-36698.
160. Schoonjans, K., Annicotte, J.S., Huby, T., Botrugno, O.A., Fayard, E., Ueda, Y., Chapman, J., and Auwerx, J. 2002. Liver receptor homolog 1 controls the expression of the scavenger receptor class B type I. *EMBO Rep* 3:1181-1187.

161. Freeman, L.A., Kennedy, A., Wu, J., Bark, S., Remaley, A.T., Santamarina-Fojo, S., and Brewer, H.B., Jr. 2004. The orphan nuclear receptor LRH-1 activates the ABCG5/ABCG8 intergenic promoter. *J Lipid Res* 45:1197-1206.
162. Delerive, P., Galardi, C.M., Bisi, J.E., Nicodeme, E., and Goodwin, B. 2004. Identification of liver receptor homolog-1 as a novel regulator of apolipoprotein AI gene transcription. *Mol Endocrinol* 18:2378-2387.
163. Venteclef, N., Haroniti, A., Tousaint, J.J., Talianidis, I., and Delerive, P. 2008. Regulation of anti-atherogenic apolipoprotein M gene expression by the orphan nuclear receptor LRH-1. *J Biol Chem* 283:3694-3701.
164. Ducker, G.S., and Rabinowitz, J.D. 2017. One-Carbon Metabolism in Health and Disease. *Cell Metab* 25:27-42.
165. Wagner, M., Choi, S., Panzitt, K., Mamrosh, J.L., Lee, J.M., Zaufel, A., Xiao, R., Wooton-Kee, R., Stahlman, M., Newgard, C.B., et al. 2016. Liver receptor homolog-1 is a critical determinant of methyl-pool metabolism. *Hepatology* 63:95-106.
166. Moshage, H. 1997. Cytokines and the hepatic acute phase response. *J Pathol* 181:257-266.
167. Venteclef, N., Smith, J.C., Goodwin, B., and Delerive, P. 2006. Liver receptor homolog 1 is a negative regulator of the hepatic acute-phase response. *Mol Cell Biol* 26:6799-6807.
168. Venteclef, N., and Delerive, P. 2007. Interleukin-1 receptor antagonist induction as an additional mechanism for liver receptor homolog-1 to negatively regulate the hepatic acute phase response. *J Biol Chem* 282:4393-4399.
169. Oosterveer, M.H., Mataki, C., Yamamoto, H., Harach, T., Moullan, N., van Dijk, T.H., Ayuso, E., Bosch, F., Postic, C., Groen, A.K., et al. 2012. LRH-1-dependent glucose sensing determines intermediary metabolism in liver. *J Clin Invest* 122:2817-2826.
170. Matsukuma, K.E., Wang, L., Bennett, M.K., and Osborne, T.F. 2007. A key role for orphan nuclear receptor liver receptor homologue-1 in activation of fatty acid synthase promoter by liver X receptor. *J Biol Chem* 282:20164-20171.
171. Hattori, T., Iizuka, K., Horikawa, Y., and Takeda, J. 2014. LRH-1 heterozygous knockout mice are prone to mild obesity. *Endocr J* 61:471-480.
172. Corbin, K.D., and Zeisel, S.H. 2012. Choline metabolism provides novel insights into nonalcoholic fatty liver disease and its progression. *Curr Opin Gastroenterol* 28:159-165.
173. Walker, A.K., Jacobs, R.L., Watts, J.L., Rottiers, V., Jiang, K., Finnegan, D.M., Shioda, T., Hansen, M., Yang, F., Niebergall, L.J., et al. 2011. A conserved SREBP-1/phosphatidylcholine feedback circuit regulates lipogenesis in metazoans. *Cell* 147:840-852.
174. Oosterveer, M.H., Mataki, C., Yamamoto, H., Harach, T., Moullan, N., van Dijk, T.H., Ayuso, E., Bosch, F., Postic, C., Groen, A.K., et al. 2012. LRH-1-dependent glucose sensing determines intermediary metabolism in liver. *The Journal of clinical investigation* 122:2817-2826.
175. Ayuso, E., Mingozzi, F., Montane, J., Leon, X., Anguela, X.M., Haurigot, V., Edmonson, S.A., Africa, L., Zhou, S., High, K.A., et al. 2010. High AAV vector purity results in serotype- and tissue-independent enhancement of transduction efficiency. *Gene Ther* 17:503-510.
176. Lock, M., McGorray, S., Auricchio, A., Ayuso, E., Beecham, E.J., Blouin-Tavel, V., Bosch, F., Bose, M., Byrne, B.J., Caton, T., et al. 2010. Characterization

of a recombinant adeno-associated virus type 2 Reference Standard Material. *Hum Gene Ther* 21:1273-1285.
177. Williams, E.G., Wu, Y., Jha, P., Dubuis, S., Blattmann, P., Argmann, C.A., Houten, S.M., Amariuta, T., Wolski, W., Zamboni, N., et al. 2016. Systems proteomics of liver mitochondria function. *Science* 352:aad0189.
178. Wu, Y., Williams, E.G., Dubuis, S., Mottis, A., Jovaisaite, V., Houten, S.M., Argmann, C.A., Faridi, P., Wolski, W., Kutalik, Z., et al. 2014. Multilayered genetic and omics dissection of mitochondrial activity in a mouse reference population. *Cell* 158:1415-1430.
179. Shannon, P., Markiel, A., Ozier, O., Baliga, N.S., Wang, J.T., Ramage, D., Amin, N., Schwikowski, B., and Ideker, T. 2003. Cytoscape: a software environment for integrated models of biomolecular interaction networks. *Genome Res* 13:2498-2504.
180. Huang da, W., Sherman, B.T., and Lempicki, R.A. 2009. Systematic and integrative analysis of large gene lists using DAVID bioinformatics resources. *Nat Protoc* 4:44-57.
181. Huang da, W., Sherman, B.T., and Lempicki, R.A. 2009. Bioinformatics enrichment tools: paths toward the comprehensive functional analysis of large gene lists. *Nucleic Acids Res* 37:1-13.
182. Kearse, M., Moir, R., Wilson, A., Stones-Havas, S., Cheung, M., Sturrock, S., Buxton, S., Cooper, A., Markowitz, S., Duran, C., et al. 2012. Geneious Basic: an integrated and extendable desktop software platform for the organization and analysis of sequence data. *Bioinformatics* 28:1647-1649.
183. Kapushesky, M., Emam, I., Holloway, E., Kurnosov, P., Zorin, A., Malone, J., Rustici, G., Williams, E., Parkinson, H., and Brazma, A. 2010. Gene expression atlas at the European bioinformatics institute. *Nucleic Acids Res* 38:D690-698.
184. Frezza, C., Cipolat, S., and Scorrano, L. 2007. Organelle isolation: functional mitochondria from mouse liver, muscle and cultured fibroblasts. *Nat Protoc* 2:287-295.
185. Arnoult, D., Soares, F., Tattoli, I., Castanier, C., Philpott, D.J., and Girardin, S.E. 2009. An N-terminal addressing sequence targets NLRX1 to the mitochondrial matrix. *J Cell Sci* 122:3161-3168.
186. Jha, P., Wang, X., and Auwerx, J. 2016. Analysis of Mitochondrial Respiratory Chain Supercomplexes Using Blue Native Polyacrylamide Gel Electrophoresis (BN-PAGE). *Curr Protoc Mouse Biol* 6:1-14.
187. Hirschey, M.D., Shimazu, T., Goetzman, E., Jing, E., Schwer, B., Lombard, D.B., Grueter, C.A., Harris, C., Biddinger, S., Ilkayeva, O.R., et al. 2010. SIRT3 regulates mitochondrial fatty-acid oxidation by reversible enzyme deacetylation. *Nature* 464:121-125.
188. Bligh, E.G., and Dyer, W.J. 1959. A rapid method of total lipid extraction and purification. *Canadian journal of biochemistry and physiology* 37:911-917.
189. Oosterveer, M.H., van Dijk, T.H., Tietge, U.J., Boer, T., Havinga, R., Stellaard, F., Groen, A.K., Kuipers, F., and Reijngoud, D.J. 2009. High fat feeding induces hepatic fatty acid elongation in mice. *PLoS One* 4:e6066.
190. Houtkooper, R.H., Argmann, C., Houten, S.M., Canto, C., Jeninga, E.H., Andreux, P.A., Thomas, C., Doenlen, R., Schoonjans, K., and Auwerx, J. 2011. The metabolic footprint of aging in mice. *Sci Rep* 1:134.
191. Chung, J., Torta, F., Masai, K., Lucast, L., Czapla, H., Tanner, L.B., Narayanaswamy, P., Wenk, M.R., Nakatsu, F., and De Camilli, P. 2015. INTRACELLULAR TRANSPORT. PI4P/phosphatidylserine countertransport at ORP5- and ORP8-mediated ER-plasma membrane contacts. *Science* 349:428-432.

192. Moser von Filseck, J., Copic, A., Delfosse, V., Vanni, S., Jackson, C.L., Bourguet, W., and Drin, G. 2015. INTRACELLULAR TRANSPORT. Phosphatidylserine transport by ORP/Osh proteins is driven by phosphatidylinositol 4-phosphate. *Science* 349:432-436.
193. Maeda, K., Anand, K., Chiapparino, A., Kumar, A., Poletto, M., Kaksonen, M., and Gavin, A.C. 2013. Interactome map uncovers phosphatidylserine transport by oxysterol-binding proteins. *Nature* 501:257-261.
194. Yan, D., Lehto, M., Rasilainen, L., Metso, J., Ehnholm, C., Yla-Herttuala, S., Jauhiainen, M., and Olkkonen, V.M. 2007. Oxysterol binding protein induces upregulation of SREBP-1c and enhances hepatic lipogenesis. *Arterioscler Thromb Vasc Biol* 27:1108-1114.
195. Holmstrom, S.R., Deering, T., Swift, G.H., Poelwijk, F.J., Mangelsdorf, D.J., Kliewer, S.A., and MacDonald, R.J. 2011. LRH-1 and PTF1-L coregulate an exocrine pancreas-specific transcriptional network for digestive function. *Genes & Development* 25:1674-1679.
196. Chong, H.K., Biesinger, J., Seo, Y.K., Xie, X., and Osborne, T.F. 2012. Genome-wide analysis of hepatic LRH-1 reveals a promoter binding preference and suggests a role in regulating genes of lipid metabolism in concert with FXR. *BMC Genomics* 13:51.
197. Cha, J.Y., and Repa, J.J. 2007. The liver X receptor (LXR) and hepatic lipogenesis. The carbohydrate-response element-binding protein is a target gene of LXR. *J Biol Chem* 282:743-751.
198. Joseph, S.B., Laffitte, B.A., Patel, P.H., Watson, M.A., Matsukuma, K.E., Walczak, R., Collins, J.L., Osborne, T.F., and Tontonoz, P. 2002. Direct and indirect mechanisms for regulation of fatty acid synthase gene expression by liver X receptors. *J Biol Chem* 277:11019-11025.
199. Huang, J., Iqbal, J., Saha, P.K., Liu, J., Chan, L., Hussain, M.M., Moore, D.D., and Wang, L. 2007. Molecular characterization of the role of orphan receptor small heterodimer partner in development of fatty liver. *Hepatology* 46:147-157.
200. Duval, C., Thissen, U., Keshtkar, S., Accart, B., Stienstra, R., Boekschoten, M.V., Roskams, T., Kersten, S., and Muller, M. 2010. Adipose tissue dysfunction signals progression of hepatic steatosis towards nonalcoholic steatohepatitis in C57BL/6 mice. *Diabetes* 59:3181-3191.
201. Moylan, C.A., Pang, H., Dellinger, A., Suzuki, A., Garrett, M.E., Guy, C.D., Murphy, S.K., Ashley-Koch, A.E., Choi, S.S., Michelotti, G.A., et al. 2014. Hepatic gene expression profiles differentiate presymptomatic patients with mild versus severe nonalcoholic fatty liver disease. *Hepatology* 59:471-482.
202. Ahrens, M., Ammerpohl, O., von Schonfels, W., Kolarova, J., Bens, S., Itzel, T., Teufel, A., Herrmann, A., Brosch, M., Hinrichsen, H., et al. 2013. DNA methylation analysis in nonalcoholic fatty liver disease suggests distinct disease-specific and remodeling signatures after bariatric surgery. *Cell Metab* 18:296-302.
203. Yin, C., Evason, K.J., Asahina, K., and Stainier, D.Y. 2013. Hepatic stellate cells in liver development, regeneration, and cancer. *J Clin Invest* 123:1902-1910.
204. Krycer, J.R., Sharpe, L.J., Luu, W., and Brown, A.J. 2010. The Akt-SREBP nexus: cell signaling meets lipid metabolism. *Trends Endocrinol Metab* 21:268-276.
205. Yecies, J.L., Zhang, H.H., Menon, S., Liu, S., Yecies, D., Lipovsky, A.I., Gorgun, C., Kwiatkowski, D.J., Hotamisligil, G.S., Lee, C.H., et al. 2011. Akt stimulates hepatic SREBP1c and lipogenesis through parallel mTORC1-dependent and independent pathways. *Cell Metab* 14:21-32.

206. Haas, J.T., Miao, J., Chanda, D., Wang, Y., Zhao, E., Haas, M.E., Hirschey, M., Vaitheesvaran, B., Farese, R.V., Jr., Kurland, I.J., et al. 2012. Hepatic insulin signaling is required for obesity-dependent expression of SREBP-1c mRNA but not for feeding-dependent expression. *Cell Metab* 15:873-884.
207. Leavens, K.F., Easton, R.M., Shulman, G.I., Previs, S.F., and Birnbaum, M.J. 2009. Akt2 is required for hepatic lipid accumulation in models of insulin resistance. *Cell Metab* 10:405-418.
208. Ricoult, S.J., Yecies, J.L., Ben-Sahra, I., and Manning, B.D. 2016. Oncogenic PI3K and K-Ras stimulate de novo lipid synthesis through mTORC1 and SREBP. *Oncogene* 35:1250-1260.
209. Kandutsch, A.A., and Shown, E.P. 1981. Assay of oxysterol-binding protein in a mouse fibroblast, cell-free system. Dissociation constant and other properties of the system. *J Biol Chem* 256:13068-13073.
210. Dawson, P.A., Ridgway, N.D., Slaughter, C.A., Brown, M.S., and Goldstein, J.L. 1989. cDNA cloning and expression of oxysterol-binding protein, an oligomer with a potential leucine zipper. *J Biol Chem* 264:16798-16803.
211. Dawson, P.A., Van der Westhuyzen, D.R., Goldstein, J.L., and Brown, M.S. 1989. Purification of oxysterol binding protein from hamster liver cytosol. *J Biol Chem* 264:9046-9052.
212. Ridgway, N.D. 2010. Oxysterol-binding proteins. *Subcell Biochem* 51:159-182.
213. Olkkonen, V.M., and Li, S. 2013. Oxysterol-binding proteins: sterol and phosphoinositide sensors coordinating transport, signaling and metabolism. *Prog Lipid Res* 52:529-538.
214. Weber-Boyvat, M., Kentala, H., Lilja, J., Vihervaara, T., Hanninen, R., Zhou, Y., Peranen, J., Nyman, T.A., Ivaska, J., and Olkkonen, V.M. 2015. OSBP-related protein 3 (ORP3) coupling with VAMP-associated protein A regulates R-Ras activity. *Exp Cell Res* 331:278-291.
215. Lehto, M., Hynynen, R., Karjalainen, K., Kuismanen, E., Hyvarinen, K., and Olkkonen, V.M. 2005. Targeting of OSBP-related protein 3 (ORP3) to endoplasmic reticulum and plasma membrane is controlled by multiple determinants. *Exp Cell Res* 310:445-462.
216. Lehto, M., Mayranpaa, M.I., Pellinen, T., Ihalmo, P., Lehtonen, S., Kovanen, P.T., Groop, P.H., Ivaska, J., and Olkkonen, V.M. 2008. The R-Ras interaction partner ORP3 regulates cell adhesion. *J Cell Sci* 121:695-705.
217. Cave, M.C., Clair, H.B., Hardesty, J.E., Falkner, K.C., Feng, W., Clark, B.J., Sidey, J., Shi, H., Aqel, B.A., McClain, C.J., et al. 2016. Nuclear receptors and nonalcoholic fatty liver disease. *Biochim Biophys Acta* 1859:1083-1099.
218. Neuschwander-Tetri, B.A., Loomba, R., Sanyal, A.J., Lavine, J.E., Van Natta, M.L., Abdelmalek, M.F., Chalasani, N., Dasarathy, S., Diehl, A.M., Hameed, B., et al. 2015. Farnesoid X nuclear receptor ligand obeticholic acid for non-cirrhotic, non-alcoholic steatohepatitis (FLINT): a multicentre, randomised, placebo-controlled trial. *Lancet* 385:956-965.
219. Sanyal, A.J., Chalasani, N., Kowdley, K.V., McCullough, A., Diehl, A.M., Bass, N.M., Neuschwander-Tetri, B.A., Lavine, J.E., Tonascia, J., Unalp, A., et al. 2010. Pioglitazone, vitamin E, or placebo for nonalcoholic steatohepatitis. *N Engl J Med* 362:1675-1685.
220. Jin, X., Yang, Y., Chen, K., Lv, Y., Zheng, L., Liu, Y., Chen, S., Yu, C., Jiang, X., Zhang, C., et al. 2009. HDMCP uncouples yeast mitochondrial respiration and alleviates steatosis in L02 and hepG2 cells by decreasing ATP and H2O2 levels: A novel mechanism for NAFLD. *Journal of Hepatology* 50:1019–1028.

221. Pebay-Peyroula, E., Dahout-Gonzalez, C., Kahn, R., Trezeguet, V., Lauquin, G.J., and Brandolin, G. 2003. Structure of mitochondrial ADP/ATP carrier in complex with carboxyatractyloside. *Nature* 426:39-44.
222. Sobel, J.A., Krier, I., Andersin, T., Raghav, S., Canella, D., Gilardi, F., Kalantzi, A.S., Rey, G., Weger, B., Gachon, F., et al. 2017. Transcriptional regulatory logic of the diurnal cycle in the mouse liver. *PLoS Biol* 15:e2001069.
223. Murakami, M., Tognini, P., Liu, Y., Eckel-Mahan, K.L., Baldi, P., and Sassone-Corsi, P. 2016. Gut microbiota directs PPARgamma-driven reprogramming of the liver circadian clock by nutritional challenge. *EMBO Rep* 17:1292-1303.
224. Ubersax, J.A., and Ferrell, J.E., Jr. 2007. Mechanisms of specificity in protein phosphorylation. *Nat Rev Mol Cell Biol* 8:530-541.
225. Alasbahi, R.H., and Melzig, M.F. 2012. Forskolin and derivatives as tools for studying the role of cAMP. *Pharmazie* 67:5-13.
226. Rui, L. 2014. Energy metabolism in the liver. *Compr Physiol* 4:177-197.
227. Lavine, R.L., Voyles, N., Perrino, P.V., and Recant, L. 1975. The effect of fasting on tissue cyclic cAMP and plasma glucagon in the obese hyperglycemic mouse. *Endocrinology* 97:615-620.
228. Geisler, C.E., Hepler, C., Higgins, M.R., and Renquist, B.J. 2016. Hepatic adaptations to maintain metabolic homeostasis in response to fasting and refeeding in mice. *Nutr Metab (Lond)* 13:62.
229. Nsiah-Sefaa, A., and McKenzie, M. 2016. Combined defects in oxidative phosphorylation and fatty acid beta-oxidation in mitochondrial disease. *Biosci Rep* 36.
230. Sekoguchi, E., Sato, N., Yasui, A., Fukada, S., Nimura, Y., Aburatani, H., Ikeda, K., and Matsuura, A. 2003. A novel mitochondrial carnitine-acylcarnitine translocase induced by partial hepatectomy and fasting. *J Biol Chem* 278:38796-38802.
231. Indiveri, C., Iacobazzi, V., Tonazzi, A., Giangregorio, N., Infantino, V., Convertini, P., Console, L., and Palmieri, F. 2011. The mitochondrial carnitine/acylcarnitine carrier: function, structure and physiopathology. *Mol Aspects Med* 32:223-233.
232. Porcelli, V., Fiermonte, G., Longo, A., and Palmieri, F. 2014. The human gene SLC25A29, of solute carrier family 25, encodes a mitochondrial transporter of basic amino acids. *J Biol Chem* 289:13374-13384.
233. Pfaff, E., Klingenberg, M., and Heldt, H.W. 1965. Unspecific permeation and specific exchange of adenine nucleotides in liver mitochondria. *Biochim Biophys Acta* 104:312-315.
234. Heldt, H.W., Jacobs, H., and Klingenberg, M. 1965. Endogenous Adp of Mitochondria, an Early Phosphate Acceptor of Oxidative Phosphorylation as Disclosed by Kinetic Studies with C14 Labelled Adp and Atp and with Atractyloside. *Biochem Biophys Res Commun* 18:174-179.
235. Aquila, H., Misra, D., Eulitz, M., and Klingenberg, M. 1982. Complete amino acid sequence of the ADP/ATP carrier from beef heart mitochondria. *Hoppe Seylers Z Physiol Chem* 363:345-349.
236. Tan, M.G.K., and Ooi, L.L.P.J. 2004. Cloning and Identification of Hepatocellular Carcinoma Down-regulated Mitochondrial Carrier Protein, a Novel Liver-specific Uncoupling Protein *J. Biol. Chem.* 279:45235-45244.
237. Jin, X., Liu, J., Chen, Y.P., Xiang, Z., Ding, J.X., and Li, Y.M. 2017. Effect of miR-146 targeted HDMCP up-regulation in the pathogenesis of nonalcoholic steatohepatitis. *PLoS One* 12:e0174218.

238. Palikaras, K., Lionaki, E., and Tavernarakis, N. 2015. Coordination of mitophagy and mitochondrial biogenesis during ageing in C. elegans. *Nature* 521:525-528.
239. Correia, J.C., Massart, J., de Boer, J.F., Porsmyr-Palmertz, M., Martinez-Redondo, V., Agudelo, L.Z., Sinha, I., Meierhofer, D., Ribeiro, V., Bjornholm, M., et al. 2015. Bioenergetic cues shift FXR splicing towards FXRalpha2 to modulate hepatic lipolysis and fatty acid metabolism. *Mol Metab* 4:891-902.
240. Halpern, K.B., Shenhav, R., Matcovitch-Natan, O., Toth, B., Lemze, D., Golan, M., Massasa, E.E., Baydatch, S., Landen, S., Moor, A.E., et al. 2017. Single-cell spatial reconstruction reveals global division of labour in the mammalian liver. *Nature* 542:352-356.
241. Acin-Perez, R., Salazar, E., Kamenetsky, M., Buck, J., Levin, L.R., and Manfredi, G. 2009. Cyclic AMP produced inside mitochondria regulates oxidative phosphorylation. *Cell Metab* 9:265-276.
242. Cogliati, S., Frezza, C., Soriano, M.E., Varanita, T., Quintana-Cabrera, R., Corrado, M., Cipolat, S., Costa, V., Casarin, A., Gomes, L.C., et al. 2013. Mitochondrial cristae shape determines respiratory chain supercomplexes assembly and respiratory efficiency. *Cell* 155:160-171.
243. Ntambi, J.M., Miyazaki, M., Stoehr, J.P., Lan, H., Kendziorski, C.M., Yandell, B.S., Song, Y., Cohen, P., Friedman, J.M., and Attie, A.D. 2002. Loss of stearoyl-CoA desaturase-1 function protects mice against adiposity. *Proc Natl Acad Sci U S A* 99:11482-11486.
244. Fujimoto, T., Miyasaka, K., Koyanagi, M., Tsunoda, T., Baba, I., Doi, K., Ohta, M., Kato, N., Sasazuki, T., and Shirasawa, S. 2009. Altered energy homeostasis and resistance to diet-induced obesity in KRAP-deficient mice. *PLoS One* 4:e4240.
245. Battle, M.A., Konopka, G., Parviz, F., Gaggl, A.L., Yang, C., Sladek, F.M., and Duncan, S.A. 2006. Hepatocyte nuclear factor 4alpha orchestrates expression of cell adhesion proteins during the epithelial transformation of the developing liver. *Proc Natl Acad Sci U S A* 103:8419-8424.
246. Jeong, J.W., Kwak, I., Lee, K.Y., White, L.D., Wang, X.P., Brunicardi, F.C., O'Malley, B.W., and DeMayo, F.J. 2006. The genomic analysis of the impact of steroid receptor coactivators ablation on hepatic metabolism. *Mol Endocrinol* 20:1138-1152.
247. Hayhurst, G.P., Lee, Y.H., Lambert, G., Ward, J.M., and Gonzalez, F.J. 2001. Hepatocyte nuclear factor 4alpha (nuclear receptor 2A1) is essential for maintenance of hepatic gene expression and lipid homeostasis. *Mol Cell Biol* 21:1393-1403.
248. Wurmbach, E., Chen, Y.B., Khitrov, G., Zhang, W., Roayaie, S., Schwartz, M., Fiel, I., Thung, S., Mazzaferro, V., Bruix, J., et al. 2007. Genome-wide molecular profiles of HCV-induced dysplasia and hepatocellular carcinoma. *Hepatology* 45:938-947.
249. Vander Heiden, M.G., Cantley, L.C., and Thompson, C.B. 2009. Understanding the Warburg effect: the metabolic requirements of cell proliferation. *Science* 324:1029-1033.

Supplementary Material

University of Zurich[UZH]

Center for Molecular Cardiology

Wagistrasse 12
CH-8952 Schlieren

Sokrates Stein, PhD
SNSF-Ambizione Group Leader
Center for Molecular Cardiology
Tel.: +41 44 635 5094
E-mail: sokrates.stein@uzh.ch

Zurich, 06.06.2017

Critérios para a inclusão, em dissertações académicas, de trabalhos científicos publicados por vários coautores

To whom it may concern,

It is my pleasure to confirm that Vera Lemos significantly contributed to our common studies. I was working as a postdoctoral scientist at the time when Vera joined the laboratory of Professor Schoonjans at the École Polytechnique Fédérale de Lausanne. Vera quickly integrated herself into the team that studied the different functions of liver receptor homolog-1 (LRH-1) in metabolism. Kristina Schoonjans directly supervised all the studies mentioned below.

Right at the beginning Vera helped us to finalize a study in which we explored the role of a LRH-1 mutant in atherosclerosis, which was in revision and later published in Cell Metabolism (Stein et al, *Cell Metab* 2014).

At the same time we worked together on another study focusing on the function of this same mutant LRH-1 in nonalcoholic fatty liver disease. Vera was involved in all basic and crucial experiments linked to the work, including mouse breeding, cohort set up and planning of sacrifices, tissue collection and processing, phenotyping of the mice, identification of a new LRH-1 target gene, lipid quantification, in vivo VLDL secretion assessment, Glucose-6-phosphate quantification, RNA and protein preparation, qPCRs and Western blots, liver histology, microarrays and statistical analyses. Our common study was finally published in the Journal of Clinical Investigation (Stein, Lemos et al., *J Clin Invest* 2017). I declare that the work was performed with equal contribution, and therefore I fully authorize Vera to use our manuscript on her PhD thesis.

The interest of Vera in fatty liver disease and mitochondrial function went beyond our common studies. She carried out completely independent studies working on other aspects of LRH-1 biology using different mouse models, and is currently submitting another manuscript as a first author.

Sincerely yours,

Sokrates Stein

Impaired SUMOylation of nuclear receptor LRH-1 promotes nonalcoholic fatty liver disease

Sokrates Stein,[1,2] Vera Lemos,[1,3] Pan Xu,[1] Hadrien Demagny,[1] Xu Wang,[4] Dongryeol Ryu,[4] Veronica Jimenez,[5] Fatima Bosch,[5] Thomas F. Lüscher,[2] Maaike H. Oosterveer,[6] and Kristina Schoonjans[1]

[1]Laboratory of Metabolic Signaling, Institute of Bioengineering, School of Life Sciences, École Polytechnique Fédérale de Lausanne, Lausanne, Switzerland. [2]Center for Molecular Cardiology, University of Zurich, Zurich, Switzerland. [3]Abel Salazar Biomedical Sciences Institute, University of Porto, Porto, Portugal. [4]Laboratory of Integrative and Systems Physiology, Institute of Bioengineering, School of Life Sciences, École Polytechnique Fédérale de Lausanne, Lausanne, Switzerland. [5]Center of Animal Biotechnology and Gene Therapy and Department of Biochemistry and Molecular Biology, School of Veterinary Medicine, Universitat Autònoma de Barcelona, Bellaterra, and Centro de Investigación Biomédica en Red de Diabetes y Enfermedades Metabólicas Asociadas (CIBERDEM), Barcelona, Spain. [6]Department of Pediatrics, Center for Liver Digestive and Metabolic Diseases, University of Groningen, University Medical Center Groningen, Groningen, The Netherlands.

Hepatic steatosis is caused by metabolic imbalances that could be explained in part by an increase in de novo lipogenesis that results from increased sterol element binding protein 1 (SREBP-1) activity. The nuclear receptor liver receptor homolog 1 (LRH-1) is an important regulator of intermediary metabolism in the liver, but its role in regulating lipogenesis is not well understood. Here, we have assessed the contribution of LRH-1 SUMOylation to the development of nonalcoholic fatty liver disease (NAFLD). Mice expressing a SUMOylation-defective mutant of LRH-1 (LRH-1 K289R mice) developed NAFLD and early signs of nonalcoholic steatohepatitis (NASH) when challenged with a lipogenic, high-fat, high-sucrose diet. Moreover, we observed that the LRH-1 K289R mutation induced the expression of oxysterol binding protein-like 3 (OSBPL3), enhanced SREBP-1 processing, and promoted de novo lipogenesis. Mechanistically, we demonstrated that ectopic expression of OSBPL3 facilitates SREBP-1 processing in WT mice, while silencing hepatic *Osbpl3* reverses the lipogenic phenotype of LRH-1 K289R mice. These findings suggest that compromised SUMOylation of LRH-1 promotes the development of NAFLD under lipogenic conditions through regulation of OSBPL3.

Introduction

Hepatic steatosis is characterized by the excessive accumulation of triglycerides as a consequence of an imbalance between the acquisition and disposal of fatty acids. Increased hepatic uptake of adipose tissue–derived fatty acids, defective breakdown via β-oxidation, reduced VLDL-triglyceride secretion, and induced activity of master regulators of de novo lipogenesis, such as sterol element binding protein 1 (SREBP-1, encoded by *Srebf1*), are factors that contribute to the development of steatosis (1). Nonalcoholic fatty liver disease (NAFLD) comprises a spectrum of disorders, of which the earliest stage is characterized by the deposition of lipid droplets within the cytoplasm of the hepatocytes. NAFLD increases the susceptibility to hepatocyte damage and inflammation, a condition termed nonalcoholic steatohepatitis (NASH), and can ultimately progress to cirrhosis and hepatocellular carcinoma (HCC) (1–4).

Liver receptor homolog 1 (LRH-1) is a nuclear receptor with diverse biological functions ranging from cell cycle regulation to the control of steroid homeostasis. In the liver, LRH-1 is an important regulator of glucose, cholesterol, and bile acid metabolism (5). Liver-specific *Lrh-1* knockout mice display reduced glycolytic flux and de novo lipogenesis secondary to impaired glucokinase activity (6). On the other hand, treatment of mice with the LRH-1 agonist 1,2-dilauroyl-*sn*-glycero-3-phosphocholine (DLPC) protects animals from developing NAFLD and insulin resistance in genetic and dietary models of diabesity (7, 8). To address this apparent contradictory role of LRH-1 in hepatic triglyceride metabolism, we chose to study lipogenesis in our recently described *Lrh-1* K289R knockin mouse model (LRH-1 K289R mice), which displays selective gain of function of LRH-1 as a result of impaired SUMOylation at K289 (9).

In this study, we demonstrate that LRH-1 K289R induces the expression of oxysterol binding protein-like 3 (OSBPL3, encoded by *Osbpl3*, also known as *Orp3*), which in turn promotes the posttranslational activation of SREBP-1. As a consequence, LRH-1 K289R mice display increased de novo lipogenesis upon refeeding in comparison with WT mice. In fact, compared with what is seen in LRH-1 WT mice, this chronic lipogenic stress promotes NAFLD in LRH-1 K289R mice accompanied by early signs of NASH when mice are exposed to a lipogenic, high-fat, high-sucrose (HFHS) diet.

Results

Increased hepatic SREBP-1 processing in LRH-1 K289R mice. In order to evaluate the role of an LRH-1 SUMO–defective pathway on intermediary liver metabolism, we subjected LRH-1 K289R mice, which exhibit partial gain of function of LRH-1, and control LRH-1 WT mice (9) to fasting-refeeding challenges in which mice were fasted and then refed for a period of 6 hours. We then evaluated the expression of metabolic genes in refed livers of both genotypes using microarray analysis. Interestingly, the expression of

Authorship note: S. Stein and V. Lemos contributed equally to this work.
Conflict of interest: The authors have declared that no conflict of interest exists.
Submitted: November 11, 2015; **Accepted:** November 22, 2016.
Reference information: *J Clin Invest*.
https://doi.org/10.1172/JCI85499.

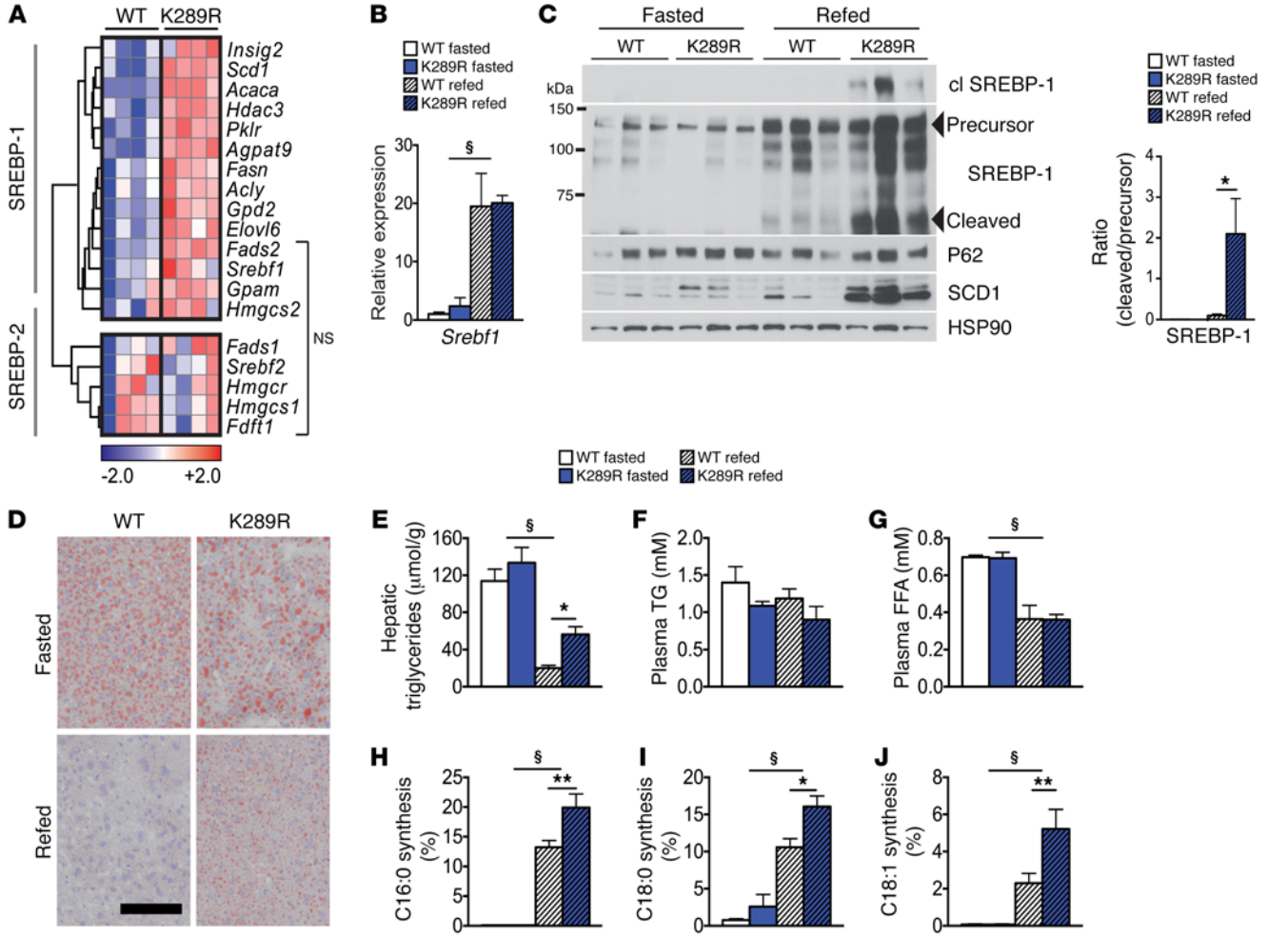

Figure 1. LRH-1 K289R mice display increased de novo lipogenesis. (**A**) Heat map showing the expression of genes involved in de novo fatty acid and cholesterol synthesis in refed WT and K289R mice. Normalized expression values are in $\log_2$ scale. SREBP-1, depicting mainly SREBP-1 target genes; SREBP-2, mostly SREBP-2 target genes; NS, transcripts that are not significantly changed between the indicated genotypes. For all other transcripts $P < 0.05$. (**B**) Hepatic mRNA expression of *Srebf1* in K289R and WT mice. $n = 10$ per genotype. (**C**) Left, immunoblots of precursor and cleaved (cl) SREBP-1, SCD1, HSP90, and P62 in hepatic lysates of WT or K289R livers. Right, graph displaying the ratio of cleaved to precursor SREBP-1. (**D**) Representative images of liver sections of K289R or WT mice stained with oil red O to visualize neutral lipids. Scale bar: 200 μm. (**E**) Quantification of hepatic triglyceride content in WT and K289R mice. $n = 10$ per group. (**F** and **G**) Plasma triglyceride (TG) and free fatty acid (FFA) contents in WT and K289R mice. $n = 10$ per group. (**H**–**J**) Fractional de novo synthesis rates of palmitate (**H**), stearate (**I**), and oleate (**J**) in WT and K289R mice. $n = 6$ per group. Error bars represent mean ± SEM. $^*P < 0.05$, $^{**}P < 0.01$ relative to WT within each nutritional state; $^{§}P < 0.001$ refed relative to fasted mice, as determined by unpaired Student's *t* test (**A**) or 2-way ANOVA with Bonferroni's post-hoc test (**B**, **C**, **E**–**J**). WT, LRH-1 WT; K289R, LRH-1 K289R mice.

many SREBP-1 target genes was increased in 6-hour–refed LRH-1 K289R compared with LRH-1 WT livers, whereas SREBP-2 targets were not altered (Figure 1A). Although no changes in *Srebf1* mRNA (Figure 1B) or uncleaved precursor SREBP-1 (Figure 1C) could be observed between both genotypes, refed LRH-1 K289R livers displayed significantly more of the cleaved and transcriptionally active SREBP-1 protein in comparison with the LRH-1 WT livers (Figure 1C), indicating that the posttranslational processing and maturation of SREBP-1 is increased in LRH-1 K289R mice. We then performed acute insulin challenges as well as shorter 2-hour refeeding experiments to analyze whether early signaling events could explain the increased SREBP-1 activity. Insulin did not induce an additional increase in AKT phosphorylation or a consistent induction of early response genes, such as activating transcription factor 3 (*Atf3*) or early growth response 1 (*Egr1*) (Supplemental Figure 1, A and B; supplemental material available online with this article; https://doi.org/10.1172/JCI85499DS1) (10, 11), in LRH-1 K289R versus LRH-1 WT livers. Similarly, we did not observe differences in *Srebf1a* and *Srebf1c* expression in 2-, 6-, or 12-hour–refed LRH-1 K289R and LRH-1 WT mice (Supplemental Figure 1C). Taken together, these data suggest that LRH-1 K289R induces SREBP-1 signaling primarily at the posttranscriptional level independently of early insulin-AKT signaling.

Enhanced de novo lipogenesis in LRH-1 K289R mice. To verify whether the increased expression of lipogenic genes is accompanied by hepatic fat accumulation, we next quantified hepatic triglyceride content in LRH-1 K289R and LRH-1 WT mice. The content of neutral lipids and triglycerides was significantly increased in LRH-1 K289R compared with LRH-1 WT livers upon refeeding (Figure 1, D and E). Of note, plasma triglycerides and free fatty

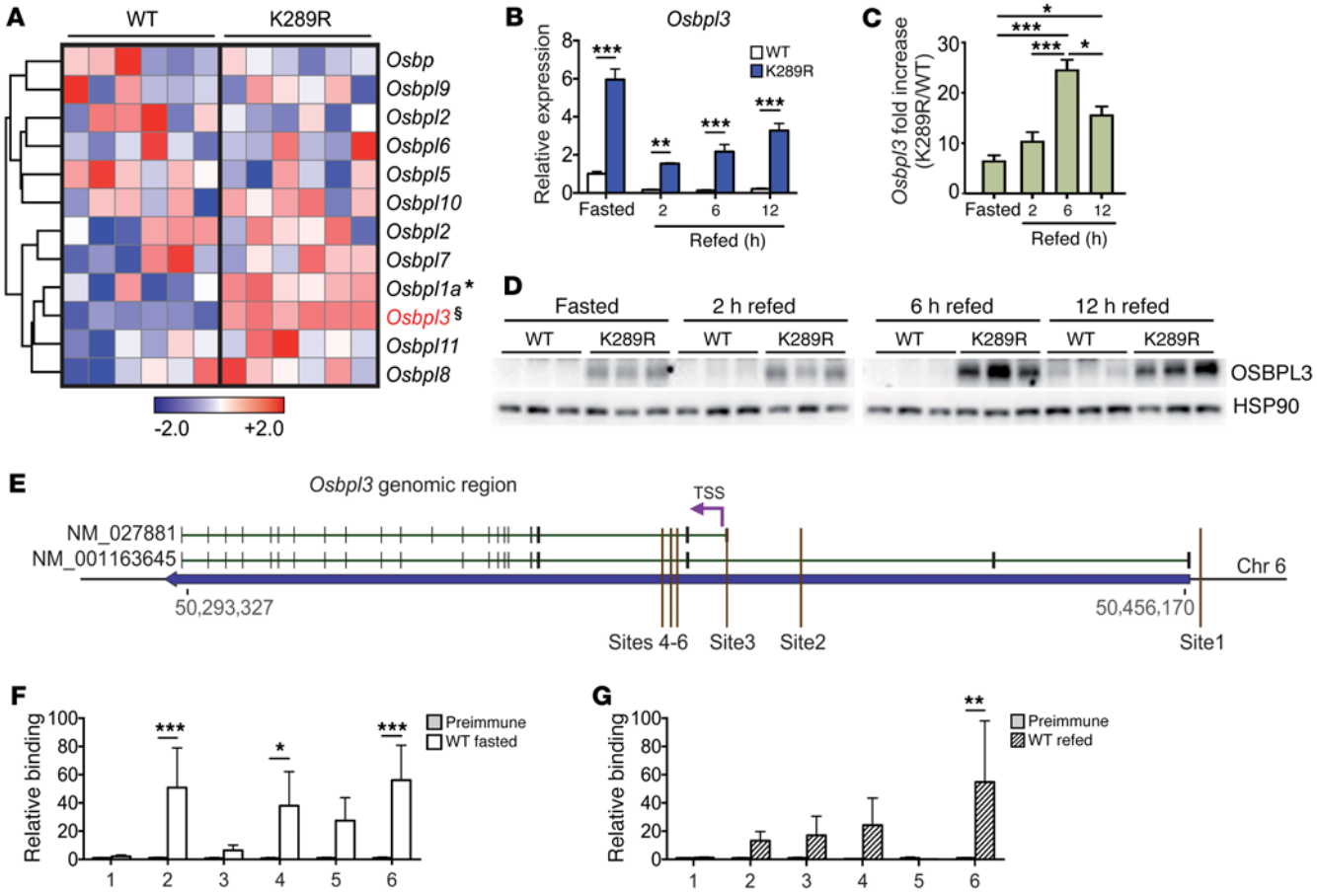

Figure 2. *Osbpl3* is a direct LRH-1 target gene and overexpressed in LRH-1 K289R mice. (**A**) Heat map showing the hepatic expression of oxysterol-binding protein family members in WT and K289R mice. Normalized expression values are in $\log_2$ scale. (**B** and **C**) Expression of *Osbpl3* mRNA in hepatic lysates of fasted and refed WT and K289R mice (**B**) and the fold change between the genotypes (**C**). n = 4 per fasted, 2-hour–, or 12-hour–refed groups, and n = 5 per 6-hour–refed groups. (**D**) Expression levels of OSBPL3 protein in hepatic lysates of fasted and refed WT and K289R mice. (**E**) Schematic showing the genomic area containing the *Osbpl3* gene and the sites used for ChIP-qPCR experiments (mouse genome assembly mm10). (**F** and **G**) Binding of LRH-1 to the different *Osbpl3* promoter sites assessed by ChIP analysis using genomic DNA from fasted WT (**F**) and refed WT livers (**G**). n = 5 WT fasted, n = 5 WT refed. Error bars represent mean ± SEM. $^*P < 0.05$, $^{**}P < 0.01$, $^{***}P < 0.001$, $^{§}P = 2 \times 10^{-7}$ relative to WT, as determined by unpaired Student's t test (**A**), or 1-way (**C**) or 2-way (**B**, **F**, **G**) ANOVA with Bonferroni post-hoc test. TSS, transcription start site.

acids did not show significant alterations between LRH-1 K289R and LRH-1 WT mice (Figure 1, F and G). To verify whether the enhanced expression of lipogenic genes translates into increased de novo lipogenesis, animals received ^{13}C-acetate prior to sacrifice to quantify de novo lipogenesis (6). In line with the increased lipogenic gene expression, de novo synthesis of palmitate (C16:0), stearate (C18:0), and oleate (C18:1) was significantly higher in LRH-1 K289R compared with LRH-1 WT livers (Figure 1, H–J). Of note, chain elongation of preexisting fatty acids was not altered between the 2 genotypes (Supplemental Figure 1, D and E). Collectively, these data show that LRH-1 K289R mice display increased de novo lipogenesis and that enhanced activation of SREBP-1 likely contributes to this process.

SUMOylation-defective LRH-1 drives the expression of Osbpl3. We next analyzed the transcriptome of livers from refed LRH-1 K289R and LRH-1 WT mice and searched for transcripts that are linked to SREBP-1 processing. One of the top hits on the list of genes that was increased in LRH-1 K289R compared with LRH-1 WT livers corresponded to *Osbpl3*, a member of a class of lipid transfer proteins recently implicated in the shuttling of lipids between the plasma and endoplasmic reticulum membrane (12–14). The expression of *Osbpl3*, and to a lesser extent *Osbpl1a*, was robustly induced in LRH-1 K289R livers, while that of most other OSBP family members did not differ between the 2 genotypes (Figure 2A). Of interest, overexpression of certain oxysterol-binding proteins has been suggested as increasing SREBP-1 processing and hepatic lipogenesis (15). Analysis of livers of LRH-1 K289R versus LRH-1 WT mice confirmed the enhanced expression of *Osbpl3* mRNA during fasting and refeeding (Figure 2B), while the expression of other OSBP family members did not differ between the 2 genotypes (Supplemental Figure 2A). Notably, the expression of *Osbpl3* was high during fasting and then reduced upon refeeding (Figure 2B). This postprandial suppression of *Osbpl3* mRNA expression was also observed upon overexpression of *Osbpl3* in mice using an adenovirus (Supplemental Figure 2B), suggesting that during the refed state, *Osbpl3* is regulated by posttranscriptional mechanisms occurring independently of LRH-1. Despite this feeding-dependent regulation of the mRNA, hepatic *Osbpl3* mRNA levels were consistently higher in the LRH-1 K289R

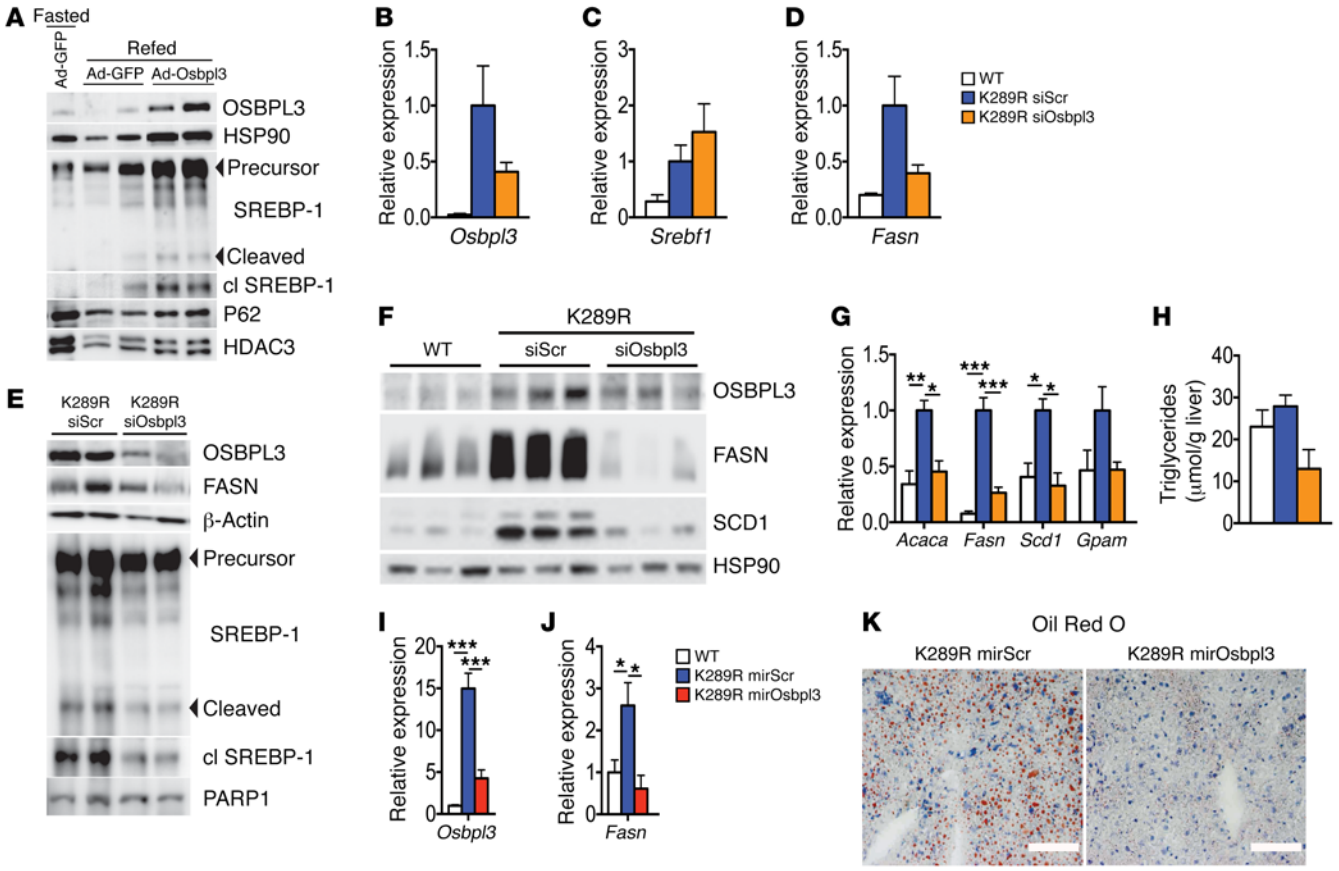

Figure 3. *Osbpl3* silencing rescues the lipogenic phenotype of LRH-1 K289R mice. (**A**) Immunoblots of OSBPL3, HSP90, precursor and cleaved SREBP-1, P62, and HDAC3 in hepatic lysates of fasted or refed WT plus Ad-GFP or refed WT plus Ad-OSBPL3 livers. (**B**–**D**) Hepatic mRNA expression of *Osbpl3* (**B**), *Srebf1* (**C**), and *Fasn* (**D**) in refed K289R and WT mice. WT, $n = 3$; K289R siScr or K289R siOsbpl3, $n = 9$ per genotype. (**E**) Immunoblots of OSBPL3, FASN, β-actin, precursor and cleaved SREBP-1, and PARP1 in hepatic lysates of refed K289R siScr or K289R siOsbpl3 livers. (**F**) Hepatic expression of OSBPL3, FASN, SCD1, and HSP90 in livers of ad libitum–fed WT, K289R siScr, and K289R siOsbpl3 mice. (**G**) Hepatic mRNA expression of genes involved in de novo lipogenesis in ad libitum–fed WT, K289R siScr, and K289R siOsbpl3 mice. $n = 3$ per genotype. (**H**) Quantification of hepatic triglycerides in hepatic lipid extracts from ad libitum–fed WT, K289R siScr, and K289R siOsbpl3 mice. $n = 3$ per genotype. (**I** and **J**) Hepatic mRNA expression of *Osbpl3* (**I**) and *Fasn* (**J**) in 6-hour–refed WT, K289R, or K289R mirOsbpl3 mice. $n = 3$ per genotype. (**K**) Representative oil red O staining in liver cryosections from refed K289R mirScrambled or K289R mirOsbpl3 mice. Scale bars: 100 μm. Error bars represent mean ± SEM. $^*P < 0.05$, $^{**}P < 0.01$, $^{***}P < 0.001$ relative to K289R siScr, as determined by 1-way ANOVA with Bonferroni's post-hoc test (**B**–**D**, **G**–**J**). WT, LRH-1 WT; K289R siOsbpl3, LRH-1 K289R mice injected with Osbpl3-siRNA complexes; K289R siScr, LRH-1 K289R mice injected with scrambled-siRNA complexes; K289R mirOsbpl3, LRH-1 K289R mice injected with AAV8 viral vectors containing an miRNA targeting *Osbpl3*.

mice in all nutritional states, but were particularly high under 6-hour–refeeding conditions (Figure 2C), and these differences were translated into similar changes at the protein level (Figure 2D).

To investigate whether *Osbpl3* is directly controlled by LRH-1, we first analyzed the *Osbpl3* genomic region in available ChIP-Seq data for potential LRH-1–binding sites (16, 17). We identified 3 main sites from the ChIP-Seq data from Holmstrom et al. (sites 1–3; ref. 16), and 3 additional sites with an LRH-1 consensus sequence close to one of the transcription start sites of the *Osbpl3* gene (sites 4–6) were identified by computational analysis (Figure 2E). We then performed site-specific ChIP analysis to evaluate whether these sites are bound by LRH-1 in fasted and refed mice. LRH-1 was recruited at different sites under both nutritional conditions (Figure 2, F and G), suggesting that *Osbpl3* is a direct LRH-1 target gene.

Based on the fact that LRH-1 and the nuclear receptor liver X receptor (LXR) have been shown to crosstalk in the regulation of hepatic acute-phase response proteins (18, 19) and that various LRH-1 target genes, including lipogenic genes, are coregulated by members of the LXR subfamily (20–22), we assessed the possibility that the LRH-1 mutant may modulate the recruitment of LXRα to its target genes, *Abca1*, *Chrebp*, and *Srebf1*. Although recruitment of LXRα was detected on these promoters in the genomic lysates of LRH-1 K289R and LRH-1 WT livers, no differences were observed between both genotypes, suggesting that LXRα binding is not altered due to the LRH-1 K289R mutation (Supplemental Figure 3A). Furthermore, Hepa 1.6 and AML-12 cells treated with the LXR agonist GW3965 did not alter *Osbpl3* expression (Supplemental Figure 3, B and C), indicating that *Osbpl3* expression is not regulated by LXR.

Osbpl3 silencing rescues the steatotic phenotype of LRH-1 K289R mice. To establish whether the increased expression of OSBPL3 in LRH-1 K289R livers is causatively linked to exacerbated de novo lipogenesis, we performed in vivo overexpression and silencing experiments. Adenoviral overexpression of OSBPL3 increased

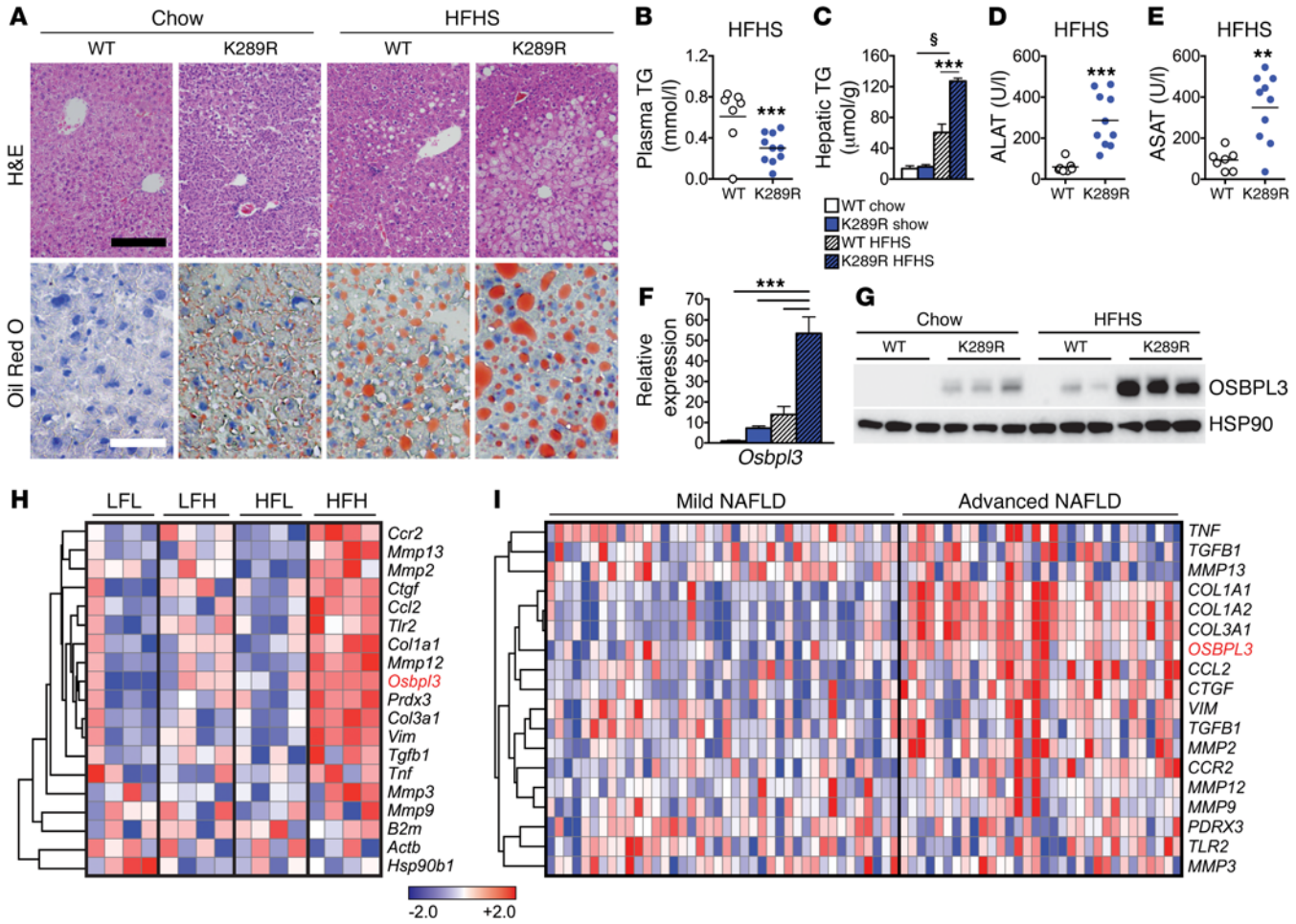

Figure 4. LRH-1 K289R mice develop NAFLD upon HFHS diet feeding. (**A**) Representative images of liver sections of K289R or WT mice stained with H&E or oil red O to visualize the tissue structure and neutral lipids, respectively. Black scale bar: 200 μm; white scale bar: 50 μm. (**B** and **C**) Quantification of triglyceride content in plasma (**B**) and in hepatic lipid extracts (**C**) in WT and K289R mice. WT, $n = 7$; K289R, $n = 10$. (**D** and **E**) Plasma levels of ALAT (**D**) and ASAT (**E**) in mice fed a HFHS diet. WT, $n = 7$; K289R, $n = 10$. (**F** and **G**) Expression of *Osbpl3* mRNA (**F**) and protein (**G**) levels in livers of WT and K289R mice fed chow and HFHS diets. $n = 9$ per genotype. (**H**) Heat map displaying the expression of *Osbpl3* as well as markers of matrix degradation, fibrosis, and inflammation in mice that were classified as LFL responders, LFH responders, HFL responders, and HFH responders according to the development of NAFLD/NASH upon chow or high-fat diet feeding (24). (**I**) Expression of *OSBPL3* and markers of matrix degradation, fibrosis, and inflammation in transcriptomic data from human patients that were categorized for mild or advanced NAFLD (25). Normalized expression values are in $\log_2$ scale. Error bars represent mean ± SEM. $^{**}P < 0.01$, $^{***}P < 0.001$ relative to WT; $^{§}P < 0.001$ refed relative to fasted mice, as determined by unpaired Student's *t* test (**B**, **D**, **E**) or 2-way ANOVA with Bonferroni's post-hoc test (**C**, **F**).

SREBP-1 cleavage in refed LRH-1 WT mice (Figure 3A), suggesting that elevated OSBPL3 levels promote SREBP-1 activation. We next silenced *Osbpl3* in LRH-1 K289R mice using siRNAs in LRH-1 K289R mice under fast-refeeding conditions. The hepatic mRNA expression of *Osbpl3* showed a clear trend of effective silencing (Figure 3B), while *Srebf1* expression was not altered (Figure 3C). Importantly, we observed a robust decrease in OSBPL3 protein along with a reduction in the maturation of SREBP-1 and a blunted expression of the fatty acid synthase (FASN) transcript and protein in the livers of refed LRH-1 K289R mice treated with siOsbpl3 (Figure 3, D and E). We next assessed the effect of *Osbpl3* silencing under normal-fed conditions. Western blot analysis revealed reduced OSBPL3 expression (Figure 3F) and a robust decrease in the lipogenic proteins FASN and stearoyl–coenzyme A desaturase 1 (SCD-1) in ad libitum–fed LRH-1 K289R mice treated with siOsbpl3 compared with control mice (Figure 3F). Of interest, mRNA expression levels of the lipogenic enzymes acetyl–coenzyme A carboxylase alpha (*Acaca*), *Fasn*, *Scd1*, and glycerol-3-phosphate acyltransferase (*Gpam)* were often normalized to values observed in LRH-1 WT mice (Figure 3G), suggesting that *Osbpl3* silencing rescues the lipogenic phenotype of LRH-1 K289R mice. In line with the reduced expression of lipogenic genes, *Osbpl3* silencing also decreased hepatic triglyceride and neutral lipid content (Figure 3H). As an additional approach to silence *Osbpl3*, we injected mice with an AAV8 viral vector containing an miRNA targeting *Osbpl3* in the liver. Here again, we observed a robust silencing of *Osbpl3,* which was accompanied by the suppression of *Fasn* and a striking reduction of hepatic lipid droplets (Figure 3, I–K).

Finally, we also examined whether other mechanisms, directly or indirectly regulated by LRH-1, may contribute to the lipogenic phenotype. Of interest, both hepatic glucose-6-phosphate content (6) and VLDL secretion (23) were unchanged between

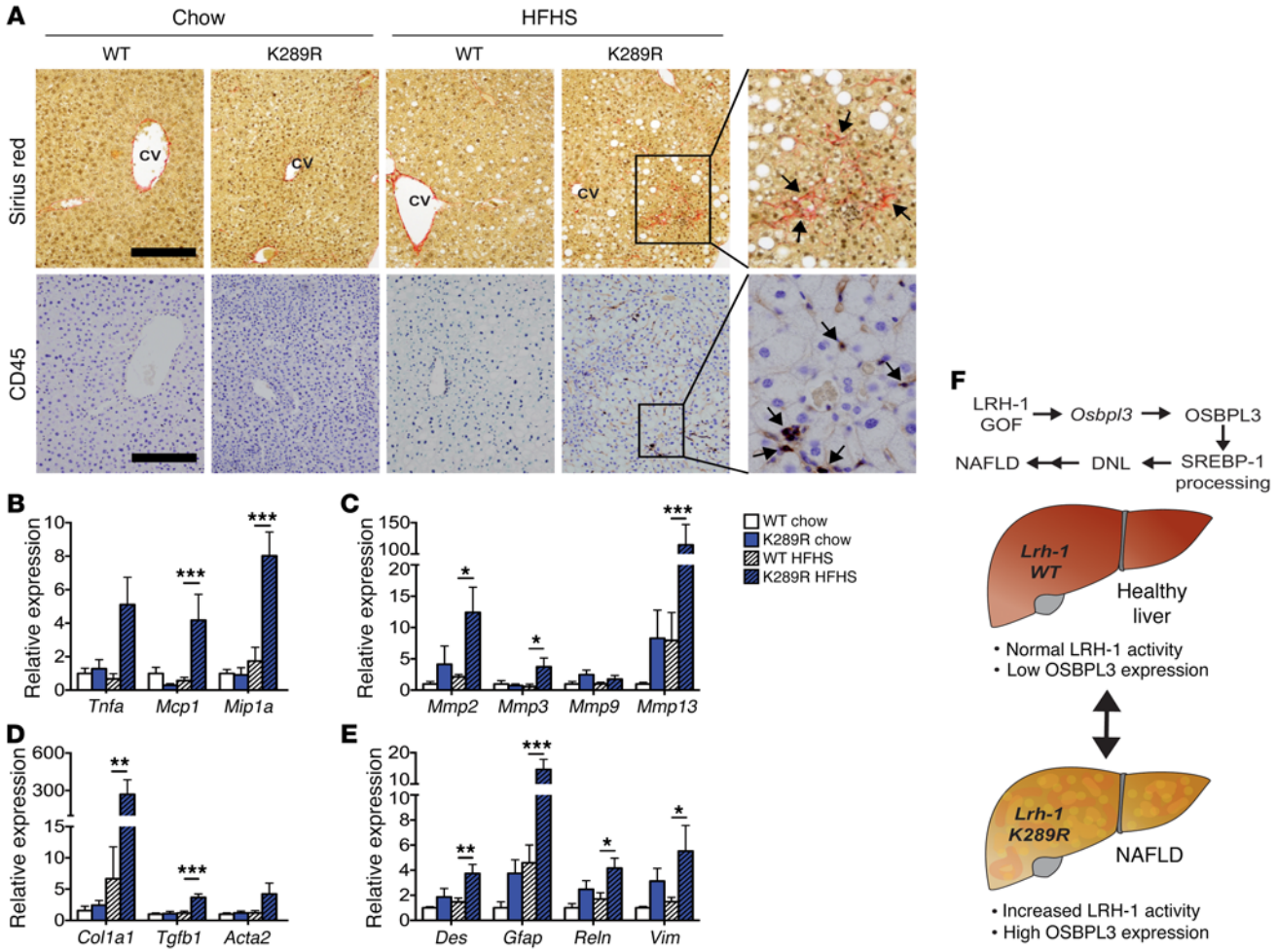

Figure 5. LRH-1 K289R mice display increased inflammation and early signs of fibrosis upon HFHS diet feeding. (**A**) Representative images of liver sections of K289R or WT mice stained with sirius red or CD45 to visualize collagen depositions and CD45-positive cells, respectively. Scale bars: 200 μm. CV, central vein. (**B**–**E**) Hepatic mRNA expression of genes involved in inflammation (**B**), matrix degradation (**C**), fibrosis (**D**), and stellate cells (**E**) in K289R and WT mice. n = 9 per genotype. (**F**) Graphical presentation showing how the LRH-1/OSBPL3 axis drives the accumulation of hepatic lipids. Error bars represent mean ± SEM. $^*P < 0.05$, $^{**}P < 0.01$, $^{***}P < 0.001$ relative to WT within each diet, as determined by 2-way ANOVA with Bonferroni's post-hoc test (**B**–**E**).

LRH-1 K289R and LRH-1 WT mice (Supplemental Figure 4, A–C), making it unlikely that these processes account for the exacerbated lipid accumulation in liver.

Together, these data suggest that the LRH-1-OSBPL3 signaling axis contributes to the increased maturation of SREBP-1, the induction of lipogenic enzymes, and the hepatic accumulation of triglycerides observed in LRH-1 K289R mice.

LRH-1 K289R mice are prone to developing NAFLD upon lipogenic diet feeding. Excessive de novo lipogenesis contributes to the development of NAFLD, a condition that can eventually progress to NASH (1, 3). In order to investigate whether LRH-1 affects the development of NAFLD, LRH-1 K289R and LRH-1 WT mice were fed a highly lipogenic HFHS diet or a chow diet for 17 weeks, and then sacrificed under normal-fed conditions. Stainings of hepatic sections with H&E and oil red O revealed that LRH-1 K289R mice developed a stronger steatotic phenotype compared with LRH-1 WT mice fed a HFHS diet (Figure 4A). While plasma cholesterol levels were unchanged (Supplemental Figure 5A), triglyceride content in plasma (Figure 4B) or in VLDL fractions (Supplemental Figure 5B) was reduced in HFHS-fed LRH-1 K289R mice. This reduction was accompanied with a robust accumulation of hepatic triglycerides (Figure 4C) as well as an induction of plasma levels of the enzymes alanine transaminase (ALAT) and aspartate aminotransferase (ASAT) in the HFHS-challenged LRH-1 K289R mice (Figure 4, D and E). Similar to our earlier observations in normal chow diet conditions (Figure 2, A–D), *Osbpl3* mRNA and OSBPL3 protein were significantly induced in LRH-1 K289R compared with LRH-1 WT mice fed a HFHS diet (Figure 4, F and G), while the expression of other *Osbp* genes did not differ between the genotypes (Supplemental Figure 5C).

The development of hepatic steatosis in mice is known to be highly heterogeneous (24). Therefore, we analyzed the data from a study in which mice were fed a chow or high-fat diet and then classified according to the development of NAFLD/NASH into low-fat low (LFL) responders, low-fat high (LFH) responders, high-fat low (HFL) responders, and high-fat high (HFH) responders (24). Interestingly, the expression of *Osbpl3* was significantly induced in the HFH responders along with markers of inflammation and

necrosis (Figure 4H) and was by far the most strikingly increased *Osbp* among all family members (Supplemental Figure 5D). We also analyzed *OSBPL3* expression in 2 cohorts of NAFLD/NASH patients. In the first cohort, livers were categorized as showing mild or advanced NAFLD (25). In the second study, subjects had livers ranging from healthy controls to showing steatosis and further to NASH (26). *OSBPL3* expression was low in healthy livers, but increased in advanced stages of NAFLD/NASH and clustered with markers of fibrosis (Figure 4I and Supplemental Figure 6), suggesting that OSBPL3 could be a novel biomarker for advanced liver diseases, such as NASH. Taken together, these data show that *Osbpl3* is markedly increased in LRH-1 K289R mice as well as in mice and humans with NAFLD/NASH.

LRH-1 K289R mice display increased inflammation and early signs of fibrosis in response to lipogenic diet feeding. Given the strong steatotic phenotype and the high levels of ALAT and ASAT markers in LRH-1 K289R mice fed a HFHS diet as well as the clustering of *Osbpl3* with genes involved in inflammation and fibrosis in mice and humans with NAFLD, we next analyzed inflammatory and fibrotic markers in LRH-1 K289R and LRH-1 WT mice. Stainings of hepatic sections with sirius red and CD45 revealed that, in contrast with LRH-1 WT mice, LRH-1 K289R mice developed small fibrotic lesions and accumulated CD45-positive immune cells upon HFHS feeding (Figure 5A). Moreover, LRH-1 K289R livers displayed higher levels of the inflammatory genes *Tnfα*, monocyte chemoattractant protein-1 (*Mcp1* or *Ccl2*), and macrophage inflammatory protein-1 α (Mip1α or *Ccl3*) (Figure 5B), indicating increased inflammation in livers of HFHS-fed LRH-1 K289R mice. The expression of MMPs, such as *Mmp2* and *Mmp13*, as well as early markers of fibrosis, such as α-1 type I collagen (*Col1a1*) and *Tgfb1*, was also elevated in LRH-1 K289R in comparison with LRH-1 WT mice fed a HFHS diet (Figure 5, C and D). Hepatic stellate cells are the primary hepatic cell type promoting fibrogenesis (27). The expression of different hepatic stellate cell markers, such as desmin (*Des*), glial fibrillary acidic protein (*Gfap*), and reelin (*Reln*), was also increased in HFHS-fed LRH-1 K289R compared with LRH-1 WT mice (Figure 5E), suggesting that HFHS-treated LRH-1 K289R mice exhibit early signs of NASH.

Previous studies showed that LRH-1 and the SUMOylation machinery might affect the hepatic acute phase response (APR) (18, 19, 28). While induction of the APR by short exposure of LPS led to reduced hepatic expression of *Crp* and *Tnf* in LRH-1 K289R compared with LRH-1 WT mice, it did not alter the hepatic expression of other APR and inflammatory genes (Supplemental Figure 7A). Moreover, no difference in plasma IL-6, MCP-1 (also known as CCL-2), or TNF-α could be observed in LPS-challenged LRH-1 K289R and LRH-1 WT mice (Supplemental Figure 7B), suggesting that the APR is likely not driving the observed inflammatory phenotype in our NAFLD-model.

Taken together, these data show that SUMOylation-defective LRH-1 promotes the development of NAFLD and displays early signs of NASH in mice fed a HFHS diet. This process is at least partially driven by the LRH-1-OSBPL3 signaling axis, which contributes to increased maturation of SREBP-1, the induction of lipogenic enzyme expression, and hepatic triglyceride accumulation in LRH-1 K289R mice (Figure 5F).

Discussion

In this study, we analyzed the contribution of a selective LRH-1 gain of function on hepatic de novo lipogenesis and fatty liver development and identified *Osbpl3* as a critical component in the regulation of this process. While the hepatic expression of *Osbpl3* is normally low in mice under basal conditions, LRH-1 K289R mice express high levels of this specific OSBP family member. Consistent with our observations, the analyses of independent mouse and human transcriptomic data sets revealed that *Osbpl3* expression is often induced in NAFLD/NASH. Our work furthermore strengthens the putative role of OSBPL3 in SREBP-1 maturation. As a consequence, LRH-1 K289R mice display increased de novo lipogenesis and accumulation of triglycerides upon refeeding in a manner that is independent of enhanced LXRα recruitment or activity. Importantly, silencing of OSBPL3 in vivo reverts the increased lipogenesis observed in these animals. Moreover, when exposed to a lipogenic HFHS diet, LRH-1 K289R mice develop NAFLD accompanied by early signs of NASH, most likely as a consequence of chronic fat accumulation (1, 3).

The excessive accumulation of hepatic lipids and increased de novo lipogenesis could also have other causes. A previous study using liver-specific *Lrh-1* knockout mice showed that LRH-1 promotes glucokinase expression, hence regulating glycolysis and de novo lipogenesis (6). However, we did not observe a difference in hepatic glucose-6-phosphate content between LRH-1 WT and LRH-1 K289R mice, suggesting that the selective gain of function of LRH-1 driven by the K289R mutation does not increase substrate availability for the glycolytic pathway. Based on the finding that the primary corepressor of LRH-1 affects microsomal triglyceride transfer protein levels and consequently hepatic VLDL-triglyceride secretion (23), we also performed in vivo VLDL-secretion assays, but could not detect any difference between refed LRH-1 K289R and LRH-1 WT mice. Finally, LRH-1 SUMOylation has been linked to the induction of the hepatic APR (18, 19, 28), which could explain the excessive inflammation observed in the livers of mice receiving a chronic HFHS diet. To study the APR in vivo, we challenged LRH-1 WT and LRH-1 K289R mice with lipopolysaccharide for 2.5 hours. Besides the reduction in *Crp* and *Tnf*, the inflammatory signature was comparable between the genotypes, suggesting that the exacerbated inflammatory phenotype of the LRH-1 K289R mice is most likely not driven by changes in the APR.

While the induction of SREBP-2 processing has been well described, the mechanisms that trigger SREBP-1 processing are less well understood (29). Insulin receptor/AKT/mTOR signaling is considered one of the main pathways triggering SREBP-1 signaling (30). A recent study showed that insulin promotes SREBP-1 activation and de novo lipogenesis via mTORC1-dependent and -independent mechanisms (31). Others proposed that while insulin signaling is required for SREBP-1 activation in insulin-resistant conditions, it is not critical for inducing the feeding-dependent induction of SREBP-1 under physiological conditions (32, 33). In breast epithelial cells, the expression of oncogenic forms of the PI3K or K-Ras are sufficient to induce SREBP-1 maturation and de novo lipogenesis through induction of mTOR signaling (34). Whereas these and many other studies demonstrate that the expression of *Srebf1* and the posttranslational maturation of SREBP-1 can be triggered by insulin signaling, other downstream

or parallel pathways exist. One recent example is the induction of SREBP-1 processing upon depletion of phosphatidylcholine, whose synthesis is dependent on S-adenosylmethionine, a methionine derivative that is generated in the one-carbon cycle (35). We did not observe a difference in AKT phosphorylation between LRH-1 WT and LRH-1 K289R mice, suggesting other signaling pathways to induce the processing of SREBP-1. Indeed, our current study highlights the existence of an alternative mechanism of SREBP-1 activation involving a SUMO-dependent LRH-1/OSBPL3 pathway.

The first oxysterol-binding proteins were identified, purified, and cloned in the 1980s (36–38). Recent studies suggest that OSBPs act as sterol transfer and/or sensor proteins that may also play important roles in cell signaling (39, 40). OSBPL3, a member of subfamily III, contains a conserved sterol-binding OSBP homology domain (OHD) as well as a phosphatidylinositol lipid species–binding pleckstrin homology (PH) domain and two 2-phenylalanines in an acidic tract (FFAT) domains that bind to the vesicle-associated membrane protein–associated (VAMP-associated) protein (VAP) (39, 41, 42). Recently, it has been shown that this last interaction can activate R-RAS, thus reorganizing the actin cytoskeleton and affecting cell polarity and cell-cell adhesion (43). Future studies will be necessary to dissect the exact mechanisms by which OSBPL3 modulates SREBP-1 processing, but its association with the ER could indicate a possible site of regulation.

In addition to the identification of OSBPL3 as a target of LRH-1, our study also highlights the existence of complex regulatory mechanisms to which OSBPL3 is subjected. We observed a discrepancy between mRNA and protein levels of OSBPL3 between fasting and refed conditions despite its persistent increase in LRH-1 K289R mice. The marked reduction in mRNA levels upon refeeding was also noticed when OSBPL3 was overexpressed using an adenovirus, indicating that additional posttranscriptional mechanisms independent of LRH-1 regulate the expression of OSBPL3. Moreover, while the expression of OSBPL3 is low in healthy livers, it is increased in NAFLD, suggesting that this protein could be a novel biomarker for NAFLD.

In this study, we described a function of LRH-1 in the development of fatty liver disease. It is noteworthy that other nuclear receptors also contribute to the development of NAFLD by affecting steatosis, glucose homeostasis, inflammation, and/or fibrosis in the liver. For instance, while activation of LXRs or pregnane x receptor (PXR) promotes lipogenesis and the development of NAFLD, activation of other nuclear receptors such as PPARs or farnesoid X-activated receptor (FXR) has opposite effects (reviewed in ref. 44). Clinical trials performed in NASH patients using PPARγ or FXR agonists showed that the beneficial effects observed on hepatic steatosis and inflammation were accompanied by adverse effects on obesity and hypercholesterolemia, respectively (45, 46), highlighting the functional complexity of nuclear receptors (44). Therefore, the development of drugs targeting specific nuclear receptor targets, such as OSBPL3, might provide alternative therapeutic options for treating NAFLD.

Methods

Animal studies. Congenic C57BL/6J LRH-1 WT or LRH-1 K289R (9) as well as C57BL/6J *Lrh-1*$^{hep-/-}$ and *Lrh-1*$^{hep+/+}$ mice (6) were kept under normal housing conditions. For fast-refeeding protocols, 12- to 16-week-old male mice were initially fasted for 24 hours, followed by refeeding for 12 hours (8 pm to 8 am), 6 hours (2 am to 8 am), or 2 hours (6 am to 8 am), and finally sacrificed together at 8 am to avoid confounding effects of the circadian rhythm. To induce a chronic hepatic steatosis, male mice were fed ad libitum with a HFHS diet (TD.08811, Harlan Laboratories) for 17 weeks and sacrificed at 9 am. To study the APR, male mice fed a chow diet received an intraperitoneal injection of either 500 μl PBS or 40 μg LPS dissolved in 500 μl PBS. Mice were sacrificed 2.5 hours after injection and tissues collected.

Subcellular fractionation of liver tissues and Western blotting. From 50 to 100 mg of liver pieces were incubated in 400 μl of hypotonic buffer (10 mM HEPES-KOH, pH 7.4, 10 mM KCl, 1.5 mM $MgCl_2$, 0.5 mM DTT, protease and phosphatase inhibitor cocktails; Roche) and lysed with 10 strokes in a Dounce homogenizer. The supernatant fraction containing mainly cytoplasmic proteins was collected after centrifugation (14,000 *g* for 5 minutes, 4°C), and the pellets were washed twice with hypotonic buffer. The pellets were resuspended in 100 to 200 μl of hypertonic buffer (50 mM Tris-HCl pH 7.4, 150 mM NaCl, 0.1 % NP-40, protease and phosphatase inhibitor cocktails) for 30 minutes on ice. The supernatant containing mainly nucleoplasm and membrane fractions was collected by centrifugation (2,000 *g* for 5 minutes, 4°C), and the remaining insoluble pellet containing mainly chromatin was resuspended in 100 μl of hypertonic buffer and sonicated. Before running SDS-PAGE, protein lysates were boiled for 5 minutes at 95°C. The following proteins were used for Western blotting: anti-Hsp90, anti–SREBP-1, and anti-P62 (BD Biosciences catalog 610418, 557036, and 610497); anti-OSBPL3 (Novus Biologicals, catalog NBP-155151), anti-FASN (Abcam, catalog ab22759), anti-SCD1 (Thermo Fisher, catalog A13996), anti–α-tubulin, anti-PARP1, and anti–β-actin (Santa Cruz Biotechnology Inc., catalog sc-5286, sc-7150, and sc-47778). Anti–SREBP-1, anti-P62, and anti-PARP1 were blotted on nuclear/membrane fractions and all other antibodies on cytoplasmic fractions.

Gene expression and analysis. RNA was extracted from the livers of mice that were fasted for 24 hours followed by 6 hours of refeeding, LRH-1 WT ($n = 6$) and LRH-1 K289R ($n = 6$). Extraction was performed using TRIZOL (Invitrogen) and purified with the RNeasy Cleanup Kit for Microarray Analysis (QIAGEN). For quantitative reverse-transcription PCR (RT-qPCR), cDNA was generated using the QuantiTect Reverse Transcription Kit (QIAGEN) and analyzed by qPCR using a LightCycler 480 Real-Time PCR System (Roche) and the primers listed in Supplemental Table 1. Expression data were normalized to *36b4* or *B2m* mRNA levels. Microarray analysis was performed using the Affymetrix MouseGene 1.0 ST array and normalized using the robust multi-array average (RMA) method. All original microarray data were deposited in the NCBI's Gene Expression Omnibus (GEO GSE89877). Heat maps were generated using GENE-E (http://www.broadinstitute.org/cancer/software/GENE-E/index.html), and rows were clustered using the one minus Pearson correlation metric.

ChIP-PCR. ChIP analysis was performed as described previously, with minor modifications (9). ChIPed DNA was purified using the PCR Clean-up Extraction Kit (Macherey-Nagel), after which qPCR was performed as described previously (47). Data were normalized to the input (fold differences = $2^{-(Ct\text{-}sample - Ct\text{-}input)}$). ChIP primer sequences are listed in Supplemental Table 2. For LXR ChIP assays, an anti-LXRα antibody (Abcam, catalog ab41902) was used. For LRH-1 ChIP experiments, a custom LRH-1 antibody was generated. A synthetic peptide ([H]-QEQSNRNRQEKLSAFG-[NH2]) was used to immunize 2 rab-

bits (AbFRONTIER). The antiserum with the highest ELISA titer was selected and used in ChIP experiments. The preimmunization serum from the same rabbit was used as a negative control.

LXR agonist treatment. Hepa 1.6 (ATCC, catalog CRL1830) or AML-12 (ATCC, catalog CRL2254) cells were treated with 1 μM of GW3965 (Selleckchem), a dual LXRα and LXRβ agonist, for 6 hours in full medium.

In vivo siRNA transfection. siRNA sequences are listed in Supplemental Table 4. HPLC-purified siRNAs (3 nmol, Microsynth) were tail-vein injected into each recipient mouse using in vivo-JetPEI (Polyplus) according to the manufacturer's instructions. Mice were fast-refed as described above and sacrificed 2 days after injection.

Adenoviral infection. *Osbpl3* cDNA was cloned into a pENTR/D-TOPO plasmid (Invitrogen; the Topo primer is listed in Supplemental Table 3) and then subcloned in the pAd/CMV-DEST plasmid (Invitrogen). After linearization with *PacI*, the construct was transfected into HEK 293A cells to produce the adenoviruses. Mice were tail-vein injected with Ad-*gfp* or Ad-*Osbpl3*, 2.5×10^9 PFU, fast-refed as described above, and sacrificed 3 days after injection.

AAV8 miRNA injection. The *Osbpl3*-siRNA sequence (Supplemental Table 4) was engineered to create a pre-miRNA sequence targeting *Osbpl3*, which was cloned into an AAV vector construct driven by the liver-specific *hAAT* promoter. AAV8 mirOsbpl3 viral vectors were generated and titrated as described previously (48, 49) and injected into jugular vein under isoflurane anesthesia (5×10^{11} vg). Two weeks after the injection, mice were fasted for 24 hours followed by 6 hours refeeding, then sacrificed, and tissues were snap-frozen.

Lipid analyses and plasma parameters. Hepatic lipids were extracted according to the Bligh and Dyer protocol (50). Triglycerides, free fatty acids, and cholesterol contents in plasma and/or hepatic lipid fractions were quantified using enzymatic assays (Roche). To asses fatty acid synthesis rates in vivo, mice received sodium [1-^{13}C] acetate via their drinking water (2%) 24 hours prior to sacrifice. Fatty acids derived from hepatic lipid extracts were liberated, derivatized, and subjected to gas chromatography–mass spectrometry (GC-MS) analysis in order to calculate the fractional synthesis rates from the incorporation of ^{13}C-acetate as described previously (51). ASAT and ALAT concentrations in blood were determined using standard clinical chemistry methods.

VLDL secretion assay and glucose-6-phosphate quantification. The VLDL secretion assay was performed as described previously (51). Thirteen-week-old male LRH-1 K289R or LRH-1 WT mice were subjected to the fasting-refeeding protocol and treated with 50 mg/ml poloxamer 407 (Sigma-Aldrich, catalog 16758) 8 hours after refeeding was initiated. Blood samples were collected once before and every hour after poloxamer treatment to determine the triglyceride content. Glucose-6-phosphate content was determined using enzymatic assays as described previously (6).

Immunohistochemistry. Liver sections were cut into 5-μm–thick serial cryosections for oil red O staining to visualize neutral lipids or paraffin cryosections to stain collagen with sirius red, CD45-positive cells using rat anti-CD45 antibody (eBioscience, catalog 30-F11), or H&E.

Statistics. Data are expressed as mean ± SEM. Comparison of differences between 2 groups was assessed using unpaired 2-tailed Student's *t* tests. Multiple group comparisons were assessed by ANOVA and Bonferroni's post-hoc *t* tests. $P < 0.05$ was considered statistically significant.

Study approval. All animal procedures were approved by the Swiss authorities (Canton of Vaud, animal protocols ID 2380, 2561, and 2768) and performed in accordance with École Polytechnique Fédérale de Lausanne institutional guidelines.

Author contributions

SS and VL designed and carried out most of the experiments, analyzed data, prepared the figures, and wrote the manuscript. PX and DR helped with Western blotting, histology, adenovirus production, and/or in vivo experiments. HD carried out the ChIP-qPCR experiments. XW helped with bioinformatic analyses. VJ and FB designed and generated the AAV8 constructs. MHO performed GC-MS analysis and quantification of fatty acids. TFL and MHO provided useful advice on the experimental procedures. KS supervised all aspects of the work.

Acknowledgments

We thank Vasco de Campos and Norman Moullan for help with tail-vein and jugular-vein injections and Theo van Dijk, Theo Boer, Sara Oppi, Thibaud Clerc, Sabrina Bichet, and Soline Odouard for technical help. This study was funded by École Polytechnique Fédérale de Lausanne and the Swiss National Science Foundation (31003A_1666695 and CRSII3_160798/1). SS was supported by postdoctoral fellowships from the German Academy of Sciences Leopoldina (LPDS 2011-6) and the Novartis Consumer Health Foundation and an Ambizione grant from the Swiss National Science Foundation (PZOOP3_161521). VL was supported by a PhD grant from the Portuguese Foundation for Science and Technology (SFRH/BD/52046/2012) through the Graduate Program in Basic and Applied Biology (GABBA) PhD program. MHO holds a Rosalind Franklin Fellowship from the University of Groningen. FB is an ICREA Academia recipient, Generalitat de Catalunya, Spain. AAV vector generation and production were funded by the Ministerio de Economía y Competitividad, Plan Nacional I+D+I (SAF2014-54886-R), Spain.

Address correspondence to: Kristina Schoonjans, Institute of Bioengineering, School of Life Sciences, École Polytechnique Fédérale de Lausanne, EPFL SV SSV-GE, AI 1149 (Bâtiment AI), Station 19, CH-1015 Lausanne, Switzerland. Phone: 41.21.693.18.91; E-mail: kristina.schoonjans@epfl.ch.

1. Cohen JC, Horton JD, Hobbs HH. Human fatty liver disease: old questions and new insights. *Science*. 2011;332(6037):1519–1523.
2. Villanueva A, Llovet JM. Liver cancer in 2013: Mutational landscape of HCC--the end of the beginning. *Nat Rev Clin Oncol*. 2014;11(2):73–74.
3. Angulo P. Nonalcoholic fatty liver disease. *N Engl J Med*. 2002;346(16):1221–1231.
4. Perry RJ, Samuel VT, Petersen KF, Shulman GI. The role of hepatic lipids in hepatic insulin resistance and type 2 diabetes. *Nature*. 2014;510(7503):84–91.
5. Stein S, Schoonjans K. Molecular basis for the regulation of the nuclear receptor LRH-1. *Curr Opin Cell Biol*. 2015;33:26–34.
6. Oosterveer MH, et al. LRH-1-dependent glucose sensing determines intermediary metabolism in liver. *J Clin Invest*. 2012;122(8):2817–2826.
7. Lee JM, et al. A nuclear-receptor-dependent phosphatidylcholine pathway with antidiabetic effects. *Nature*. 2011;474(7352):506–510.
8. Musille PM, Pathak MC, Lauer JL, Hudson WH, Griffin PR, Ortlund EA. Antidiabetic phospholipid-nuclear receptor complex reveals the mech-

anism for phospholipid-driven gene regulation. *Nat Struct Mol Biol*. 2012;19(5):532–537.
9. Stein S, et al. SUMOylation-dependent LRH-1/PROX1 interaction promotes atherosclerosis by decreasing hepatic reverse cholesterol transport. *Cell Metab*. 2014;20(4):603–613.
10. Keeton AB, Bortoff KD, Bennett WL, Franklin JL, Venable DY, Messina JL. Insulin-regulated expression of Egr-1 and Krox20: dependence on ERK1/2 and interaction with p38 and PI3-kinase pathways. *Endocrinology*. 2003;144(12):5402–5410.
11. Keeton AB, Bortoff KD, Franklin JL, Messina JL. Blockade of rapid versus prolonged extracellularly regulated kinase 1/2 activation has differential effects on insulin-induced gene expression. *Endocrinology*. 2005;146(6):2716–2725.
12. Chung J, et al. Intracellular transport. PI4P/phosphatidylserine countertransport at ORP5- and ORP8-mediated ER-plasma membrane contacts. *Science*. 2015;349(6246):428–432.
13. Moser von Filseck J, et al. Intracellular transport. Phosphatidylserine transport by ORP/Osh proteins is driven by phosphatidylinositol 4-phosphate. *Science*. 2015;349(6246):432–436.
14. Maeda K, et al. Interactome map uncovers phosphatidylserine transport by oxysterol-binding proteins. *Nature*. 2013;501(7466):257–261.
15. Yan D, et al. Oxysterol binding protein induces upregulation of SREBP-1c and enhances hepatic lipogenesis. *Arterioscler Thromb Vasc Biol*. 2007;27(5):1108–1114.
16. Holmstrom SR, et al. LRH-1 and PTF1-L coregulate an exocrine pancreas-specific transcriptional network for digestive function. *Genes Dev*. 2011;25(16):1674–1679.
17. Chong HK, Biesinger J, Seo YK, Xie X, Osborne TF. Genome-wide analysis of hepatic LRH-1 reveals a promoter binding preference and suggests a role in regulating genes of lipid metabolism in concert with FXR. *BMC Genomics*. 2012;13:51.
18. Venteclef N, Smith JC, Goodwin B, Delerive P. Liver receptor homolog 1 is a negative regulator of the hepatic acute-phase response. *Mol Cell Biol*. 2006;26(18):6799–6807.
19. Venteclef N, et al. GPS2-dependent corepressor/SUMO pathways govern anti-inflammatory actions of LRH-1 and LXRbeta in the hepatic acute phase response. *Genes Dev*. 2010;24(4):381–395.
20. Cha JY, Repa JJ. The liver X receptor (LXR) and hepatic lipogenesis. The carbohydrate-response element-binding protein is a target gene of LXR. *J Biol Chem*. 2007;282(1):743–751.
21. Joseph SB, et al. Direct and indirect mechanisms for regulation of fatty acid synthase gene expression by liver X receptors. *J Biol Chem*. 2002;277(13):11019–11025.
22. Matsukuma KE, Wang L, Bennett MK, Osborne TF. A key role for orphan nuclear receptor liver receptor homologue-1 in activation of fatty acid synthase promoter by liver X receptor. *J Biol Chem*. 2007;282(28):20164–20171.
23. Huang J, et al. Molecular characterization of the role of orphan receptor small heterodimer partner in development of fatty liver. *Hepatology*. 2007;46(1):147–157.
24. Duval C, et al. Adipose tissue dysfunction signals progression of hepatic steatosis towards nonalcoholic steatohepatitis in C57BL/6 mice. *Diabetes*. 2010;59(12):3181–3191.
25. Moylan CA, et al. Hepatic gene expression profiles differentiate presymptomatic patients with mild versus severe nonalcoholic fatty liver disease. *Hepatology*. 2014;59(2):471–482.
26. Ahrens M, et al. DNA methylation analysis in nonalcoholic fatty liver disease suggests distinct disease-specific and remodeling signatures after bariatric surgery. *Cell Metab*. 2013;18(2):296–302.
27. Yin C, Evason KJ, Asahina K, Stainier DY. Hepatic stellate cells in liver development, regeneration, and cancer. *J Clin Invest*. 2013;123(5):1902–1910.
28. Venteclef N, Delerive P. Interleukin-1 receptor antagonist induction as an additional mechanism for liver receptor homolog-1 to negatively regulate the hepatic acute phase response. *J Biol Chem*. 2007;282(7):4393–4399.
29. Horton JD, Goldstein JL, Brown MS. SREBPs: activators of the complete program of cholesterol and fatty acid synthesis in the liver. *J Clin Invest*. 2002;109(9):1125–1131.
30. Krycer JR, Sharpe LJ, Luu W, Brown AJ. The Akt-SREBP nexus: cell signaling meets lipid metabolism. *Trends Endocrinol Metab*. 2010;21(5):268–276.
31. Yecies JL, et al. Akt stimulates hepatic SREBP1c and lipogenesis through parallel mTORC1-dependent and independent pathways. *Cell Metab*. 2011;14(1):21–32.
32. Haas JT, et al. Hepatic insulin signaling is required for obesity-dependent expression of SREBP-1c mRNA but not for feeding-dependent expression. *Cell Metab*. 2012;15(6):873–884.
33. Leavens KF, Easton RM, Shulman GI, Previs SF, Birnbaum MJ. Akt2 is required for hepatic lipid accumulation in models of insulin resistance. *Cell Metab*. 2009;10(5):405–418.
34. Ricoult SJ, Yecies JL, Ben-Sahra I, Manning BD. Oncogenic PI3K and K-Ras stimulate de novo lipid synthesis through mTORC1 and SREBP. *Oncogene*. 2016;35(10):1250–1260.
35. Walker AK, et al. A conserved SREBP-1/phosphatidylcholine feedback circuit regulates lipogenesis in metazoans. *Cell*. 2011;147(4):840–852.
36. Kandutsch AA, Shown EP. Assay of oxysterol-binding protein in a mouse fibroblast, cell-free system. Dissociation constant and other properties of the system. *J Biol Chem*. 1981;256(24):13068–13073.
37. Dawson PA, Ridgway ND, Slaughter CA, Brown MS, Goldstein JL. cDNA cloning and expression of oxysterol-binding protein, an oligomer with a potential leucine zipper. *J Biol Chem*. 1989;264(28):16798–16803.
38. Dawson PA, Van der Westhuyzen DR, Goldstein JL, Brown MS. Purification of oxysterol binding protein from hamster liver cytosol. *J Biol Chem*. 1989;264(15):9046–9052.
39. Ridgway ND. Oxysterol-binding proteins. *Subcell Biochem*. 2010;51:159–182.
40. Olkkonen VM, Li S. Oxysterol-binding proteins: sterol and phosphoinositide sensors coordinating transport, signaling and metabolism. *Prog Lipid Res*. 2013;52(4):529–538.
41. Weber-Boyvat M, et al. OSBP-related protein 3 (ORP3) coupling with VAMP-associated protein A regulates R-Ras activity. *Exp Cell Res*. 2015;331(2):278–291.
42. Lehto M, Hynynen R, Karjalainen K, Kuismanen E, Hyvärinen K, Olkkonen VM. Targeting of OSBP-related protein 3 (ORP3) to endoplasmic reticulum and plasma membrane is controlled by multiple determinants. *Exp Cell Res*. 2005;310(2):445–462.
43. Lehto M, et al. The R-Ras interaction partner ORP3 regulates cell adhesion. *J Cell Sci*. 2008;121(Pt 5):695–705.
44. Cave MC, et al. Nuclear receptors and nonalcoholic fatty liver disease. *Biochim Biophys Acta*. 2016;1859(9):1083–1099.
45. Neuschwander-Tetri BA, et al. Farnesoid X nuclear receptor ligand obeticholic acid for non-cirrhotic, non-alcoholic steatohepatitis (FLINT): a multicentre, randomised, placebo-controlled trial. *Lancet*. 2015;385(9972):956–965.
46. Sanyal AJ, et al. Pioglitazone, vitamin E, or placebo for nonalcoholic steatohepatitis. *N Engl J Med*. 2010;362(18):1675–1685.
47. Mataki C, et al. Compromised intestinal lipid absorption in mice with a liver-specific deficiency of liver receptor homolog 1. *Mol Cell Biol*. 2007;27(23):8330–8339.
48. Ayuso E, et al. High AAV vector purity results in serotype- and tissue-independent enhancement of transduction efficiency. *Gene Ther*. 2010;17(4):503–510.
49. Lock M, et al. Characterization of a recombinant adeno-associated virus type 2 Reference Standard Material. *Hum Gene Ther*. 2010;21(10):1273–1285.
50. Bligh EG, Dyer WJ. A rapid method of total lipid extraction and purification. *Can J Biochem Physiol*. 1959;37(8):911–917.
51. Oosterveer MH, et al. High fat feeding induces hepatic fatty acid elongation in mice. *PLoS One*. 2009;4(6):e6066.

Supplemental Information for

A SUMO-dependent LRH-1/OSBP pathway promoting nonalcoholic fatty liver disease

Sokrates Stein[§], Vera Lemos[§], Pan Xu, Hadrien Demagny, Xu Wang, Dongryeol Ryu, Veronica Jimenez, Fatima Bosch, Thomas F. Lüscher, Maaike H. Oosterveer and Kristina Schoonjans*

*E-mail: kristina.schoonjans@epfl.ch

[§]S. Stein and V. Lemos contributed equally to this work

Figure S1

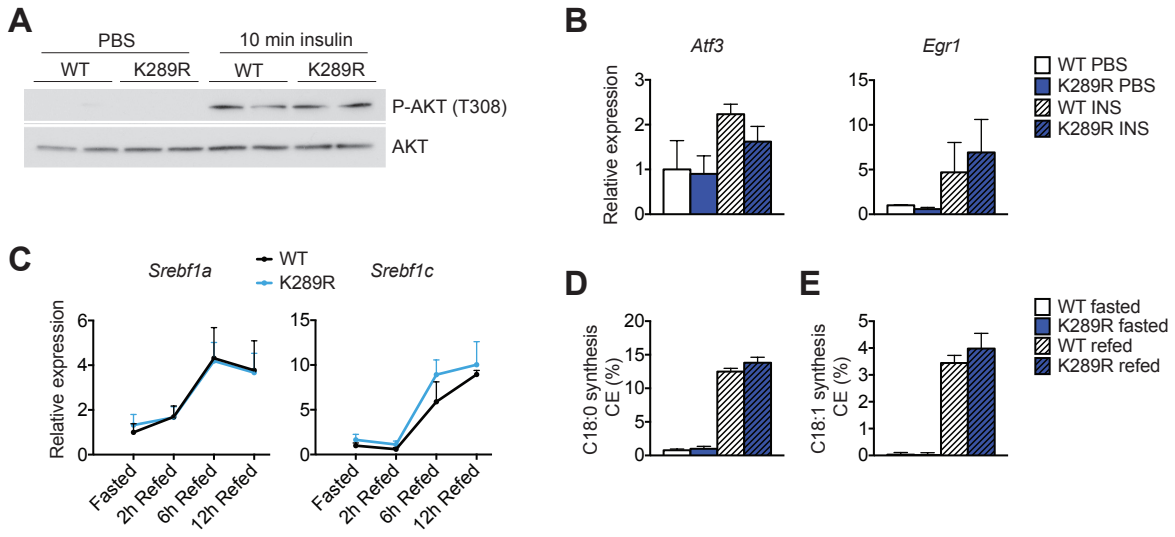

Figure S1. *Lrh-1 K289R* mice do not show changes in the early insulin response. (A, B) Phospho and total AKT immunoblots (A), and mRNA expression of early response genes (B) in livers from fasted WT or K289R mice that were injected with PBS or insulin 10 min prior to sacrifice. n = 3 for PBS groups, 4 for insulin groups. (C) Hepatic expression of the two *Srebf1* isoforms, *Srebf1a* and *Srebf1c*, in fasted and refed WT and K289R mice. n = 4 per genotype. (D, E) Fractional chain elongation (CE) of pre-existing palmitate to hepatic stearate (D) and oleate (E). n = 6 per genotype. Error bars represent means ± S.E.M. WT, *Lrh-1 WT;* K289R, *Lrh-1 K289R* mice.

Figure S2

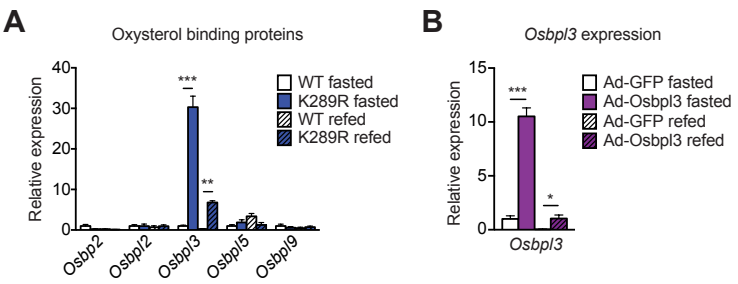

Figure S2. *Osbpl3* is a direct transcriptional target of LRH-1. (A) Hepatic mRNA expression of oxysterol binding protein family members in fasted or 6-hour-refed K289R and WT mice. n = 10 per genotype. (B) *Osbpl3* expression in hepatic lysates of fasted or refed mice infected with Ad-GFP or Ad-OSBPL3. n = 2 per fasted group, n = 5 for refed group. Error bars represent means ± S.E.M. *p<0.05, **p<0.01 and ***p<0.001 relative to WT, as determined by two-way ANOVA with Bonferroni post-hoc test (A, B). WT, *Lrh-1 WT;* K289R, *Lrh-1 K289R* mice.

Figure S3.

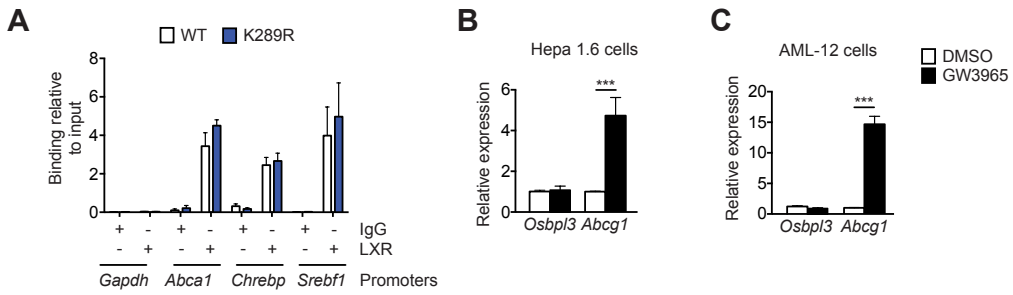

Figure S3. Crosstalk between LXR and LRH-1 pathways. (A) LXR chromatin immunoprecipitation on hepatic lysates from WT and K289R mice. n = 6 per genotype. (B, C) Expression of *Osbpl3* and *Abcg1* in Hepa 1.6 (B) or AML-12 (C) cells upon treatment with the LXR agonist GW3965. n = 3 per treatment. Error bars represent means ± S.E.M. ***p<0.001 relative to WT, as determined by unpaired Student's *t*-test (B, C). WT, *Lrh-1 WT;* K289R, *Lrh-1 K289R* mice.

Figure S4

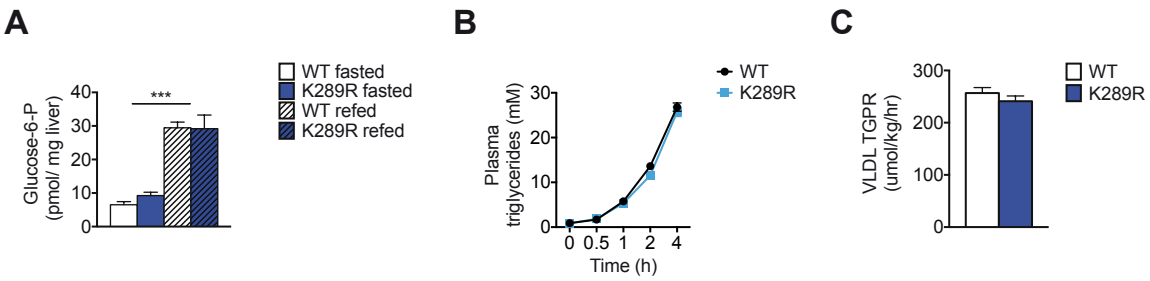

Figure S4. No change in glucose-6-phosphate production and VLDL secretion in *Lrh-1 K289R* mice. (A) Quantification of glucose-6-phosphate (glucose-6-P) in hepatic lysates of fasted or refed WT and K289R mice. n = 4 WT fasted, 7 K289R fasted, 7 WT refed, and 6 K289R refed. (B, C) Plasma triglyceride synthesis over time (B), and triglyceride production rate (TGPR) in WT and K289R mice (C). n = 7 per genotype. Error bars represent means ± S.E.M. ***p<0.001 refed mice relative to fasted mice, as determined by two-way ANOVA with Bonferroni post-hoc test (A). WT, *Lrh-1 WT;* K289R, *Lrh-1 K289R* mice.

Figure S5

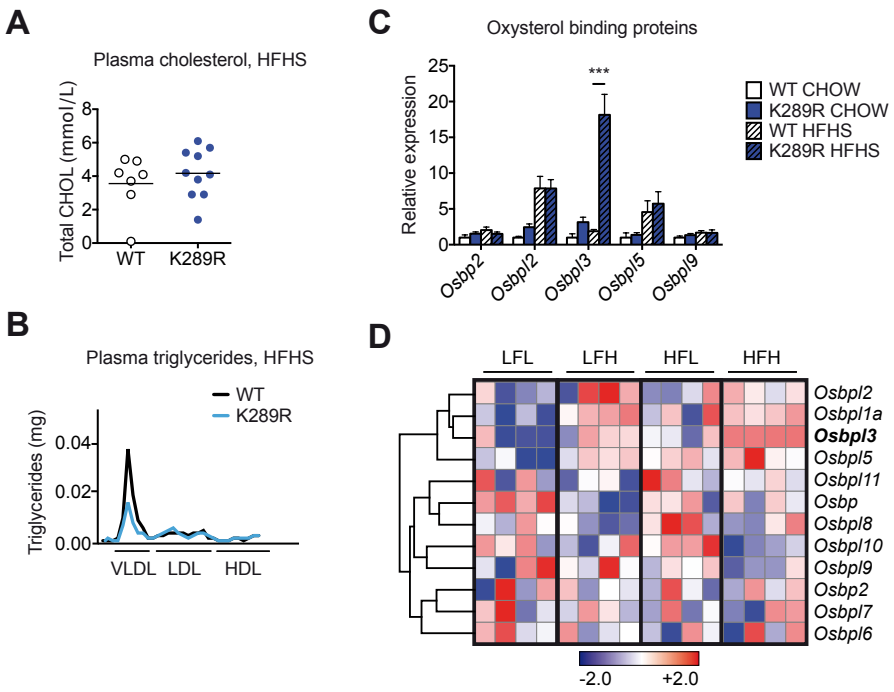

Figure S5. *Lrh-1 K289R* mice develop NAFLD upon HFHS diet feeding. (A) Plasma cholesterol levels in WT and K289R mice fed a HFHS diet. WT, n = 7; K289R, n = 10 per genotype. (B) Triglyceride (TG) content in lipoprotein subfractions. VLDL, very-low density lipoprotein; LDL, low-density lipoprotein; HDL, high-density lipoprotein. n = 1 pooled sample from 7 mice per genotype. (C) Hepatic mRNA expression of oxysterol binding protein family members in K289R and WT mice upon chow or HFHS feeding. n = 9 per genotype. (D) Heatmap displaying the expression of oxysterol binding protein family members as well as markers of matrix degradation, fibrosis, and inflammation in mice that were classified as low-fat low (LFL) responders, low-fat high (LFH) responders, high-fat low (HFL) responders, and high fat high (HFH) responders according to the development of NAFLD/NASH upon chow or high-fat diet feeding (1). Normalized expression values are in Log_2 scale. Error bars represent means ± S.E.M. ***p<0.001 relative to WT, as determined by two-way ANOVA with Bonferroni post-hoc test (C). WT, *Lrh-1 WT;* K289R, *Lrh-1 K289R* mice.

Figure S6

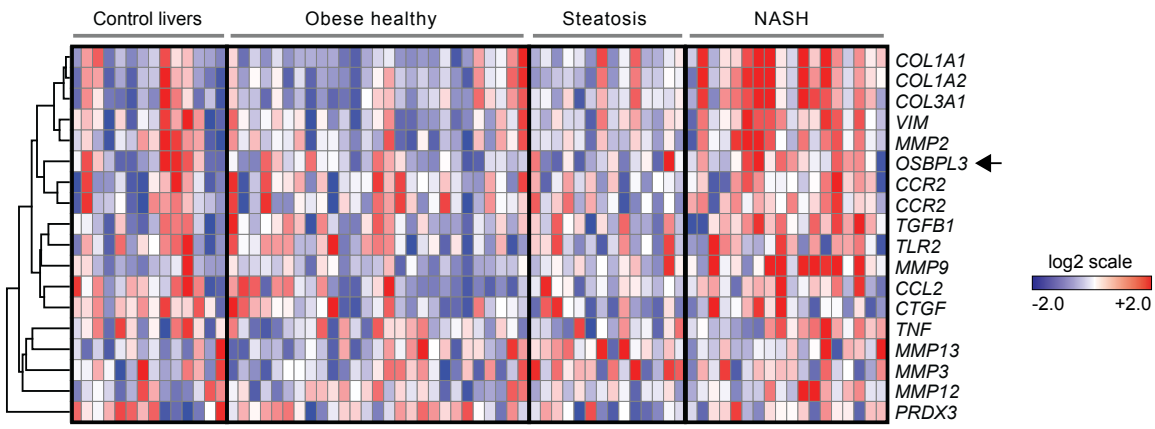

Figure S6. Expression of *OSBPL3* in NASH patients. Expression of *OSBPL3* and markers of matrix degradation, fibrosis, and inflammation in transcriptomic data from human subjects that had livers ranging from healthy controls to steatosis and further to NASH (2). Arrow indicates *OSBPL3*. Normalized expression values are in Log_2 scale.

Figure S7

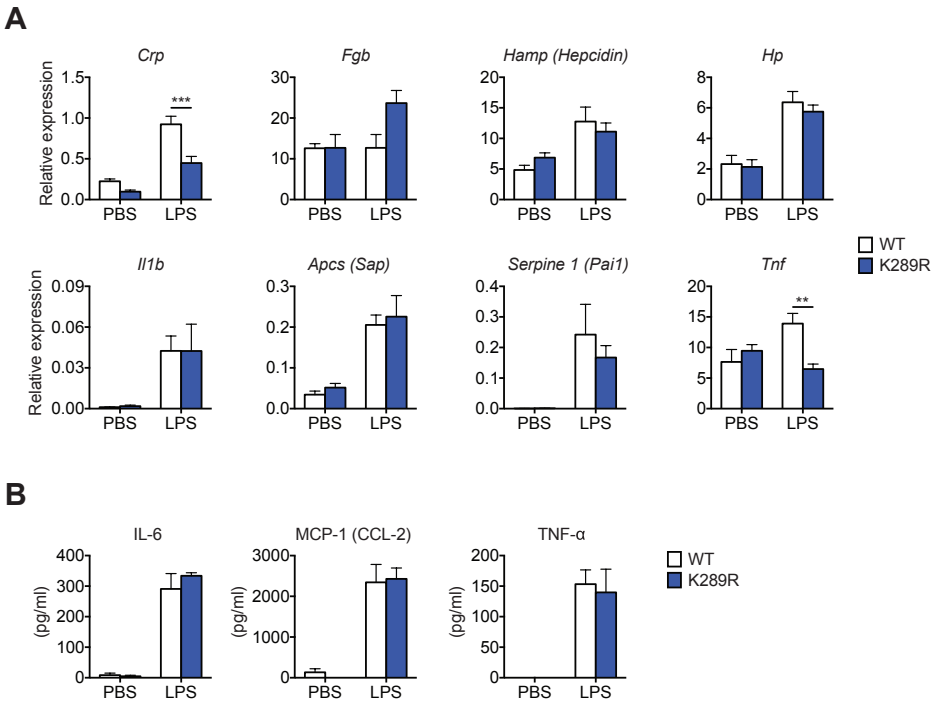

Figure S7. Hepatic acute phase response in *Lrh-1 WT* and *K289R* mice. (A) Hepatic expression of the indicated acute phase response genes in WT and K289R mice that were challenged with either PBS or lipopolysaccharide (LPS) for 2.5 hours. n = 5 PBS-treated groups, n = 6 LPS-treated groups. (B) ELISA assays to determine the plasma content of IL-6, MCP-1 or TNF-α. n = 5 PBS-treated groups, n= 6 LPS-treated groups. **<0.01 and ***p<0.001 relative to WT, as determined by two-way ANOVA with Bonferroni post-hoc test (A). WT, *Lrh-1 WT;* K289R, *Lrh-1 K289R* mice.

Table S1. Q-PCR primer table.

Gene	Forward (5' to 3' sequence)	Reverse (5' to 3' sequence)
36B4	AGATTCGGGATATGCTGTTGG	AAAGCCTGGAAGAAGGAGGTC
Acaca	CCATCCAAACAGAGGGAACATC	CTACATGAGTCATGCCATAGTGGTT
Acly	GCCAGCGGGAGCACATC	CTTTGCAGGTGCCACTTCATC
Acta2	CCCAGACATCAGGGAGTAATGG	TCTATCGGATACTTCAGCGTCA
Apcs	GGACCAAGCATGGACAAGCTA	TGTCTGACAAAAGGCTTCTGAAAG
Atf3	GGTCGCACTGACTTCTGAGG	CTCTGGCCGTTCTCTGGA
B2m	TTCTGGTGCTTGTCTCACTG	TATGTTCGGCTTCCCATTCT
Col1a1	TGTTCAGCTTTGTGGACCTC	TCAAGCATACCTCGGGTTTC
Col1a1	AACCCTGCCCGCACATG	CAGACGGCTGAGTAGGGAACA
Crp	CCCTCTTCAGATCCTTTCCT	GCCCTCCTGATAGATTATCC
Des	CTCGGAAGTTGAGAGCAGAGA	GTGAAGATGGCCTTGGATGT
Egr1	TGGGATAACTCGTCTCCACC	GAGCGAACAACCCTATGAGC
Elovl6	AACTTGGCTCGCTTGTTCAT	CCAATGGATGCAGGAAAACT
Fasn	AGCTTCGGCTGCTGTTGGAAGT	TCGGATGCCTCTGAACCACTCACA
Fgb	GTATCTCATCCAGCCTGACA	CATCCTGACGGTTCTGTATG
Gfap	CCTTCTGACACGGATTTGGT	ACATCGAGATCGCCACCTAC
Gpam	GCTATCATGTCCACCCACATTG	ACTTCCTCCTTCATCACAAAGAAGTC
Hamp	GCTGCCTGTCTCCTGCTTCT	AGCTCTGTAGTCTGTCTCATCTGTTG
Hp	GAAGCAATGGGTGAACACAG	TGCCTTTGGCATCCATAGAG
Il1b	CAACCAACAAGTGATATTCTCCATG	GATCCACACTCTCCAGCTGCA
Mcp1/Ccl2	AGGTCCCTGTCATGCTTCTG	GCTGCTGGTGATCCTCTTGT
Mip1a/Ccl3	GTGGAATCTTCCGGCTGTAG	ACCATGACACTCTGCAACCA
Mmp13	CTTCTTCTTGTTGAGCTGGACTC	CTGTGGAGGTCACTGTAGACT
Mmp2	CAAGTTCCCCGGCGATGTC	TTCTGGTCAAGGTCACCTGTC
Mmp3	ACATGGAGACTTTGTCCCTTTTG	TTGGCTGAGTGGTAGAGTCCC
Mmp9	CTGGACAGCCAGACACTAAAG	CTCGCGGCAAGTCTTCAGAG
Osbp2	TGTGGTGGAGTTCACTGTTG	CAAGGCTATCCGTGTGATGA
Osbpl2	TCTATATTTATGTTGAAGTTGTGTGGA	CTTGGGTGTCAGAGGGTTG
Osbpl3	TCAATCCTTCCACGACTTCC	CGGTGTGTCTCAAAAGTTGGT
Osbpl5	AGAAAGGCCTCCTCCTTCAT	GGCCCTGAGCATCTTGTCT
Osbpl9	TCCAAGGGACTAGGCTGGTA	CAACAAATAGCATGGTAGAATCAA
Ppib	CAGGGGAGATGGCACAGGAG	CGGCTGTCTGTCTTGGTGCTCTCC
Reln	ACATGAGAGGCCACCACACT	CTTCTCAGAGCATTGGAGGC
Scd1	CCGGAGACCCCTTAGATCGA	TAGCCTGTAAAAGATTTCTGCAAACC
Scd1	CTGTACGGGATCATACTGGTTCCC	CAGCCGAGCCTTGTAAGTTCTGTG
Serpine 1	TGGCTCAGAGCAACAAGTTCAA	TCAAAGGGTGCAGCGATGAACA
Srebf1a	GCCGGCGCCATGGACGAGCTGGCC	CAGGAAGGCTTCCAGAGAGGAGGC
Srebf1c	GGAGCCATGGATTGCACATT	GGCCCGGGAAGTCACTGT
Tgfb1	TGACGTCACTGGAGTTGTACGG	GGTTCATGTCATGGATGGTGC
Tnf	GTAGCCCACGTCGTAGCAAAC	AGTTGGTTGTCTTTGAGATCCATG
Vim	GGATTCCACTTTCCGTTCAA	GAAATTGCAGGAGGAGATGC

Table S2. ChIP primer table.

Gene	Forward (5' to 3' sequence)	Reverse (5' to 3' sequence)	Refe-rence
Abca1	GCTTTCTGCTGAGTGACTGAACTAC	GAATTACTGCTTTTTGCCGCG	(3)
Actin	GCGGCCAACGCCAAAACTCTCC	GGCCCCGCGCCGCTCACTCAC	
Chrebp	TCTGTGGATCGTGAACCCTATTT	TTCGTCCTCGGGTGGCAACGGGGGACA	(4)
Gapdh	AGTGCCAGCCTCGTCCCGTAGACAAAATG	AAGTGGGCCCCGGCCTTCTCCAT	
Osbpl3-site1	ATTTGCCAGGCACTACCAAC	TCCCCGGAAAGGTAAGAGTT	
Osbpl3-site2	TCCTCTACCCCACACTTTGAG	CCTTCCCATCTCCCATGCTCC	
Osbpl3-site3	TTGGCATCCAAAACACACTG	ACATTTCCCCGACTTCATCA	
Osbpl3-site4	TCATGTGTGGCAGGTTTTGT	ATAAAAGCCACCCCTTCCAT	
Osbpl3-site5	CCCAGCTTCTCAGCATCTTC	CTCAATCCTCTTGCCTCTGC	
Osbpl3-site6	CCTTCTCCCCTTTTCTCTGC	ACGGATCTTGACTGGAGCAC	
Srebf1	GAACCAGCGGTGGGAACACAGAGC	GACGGCGGCAGCTCGGGTTTCTC	(3)

Table S3. Cloning primer table.

Gene	Forward (5' to 3' sequence)	Reverse (5' to 3' sequence)
Osbpl3 Topo	CACCATGAGTGACGAGAAGAATCTCG	TCACCATAAGACGGGATGGT

Table S4. siRNA table (HPLC purified).

Gene	Sense sequence (5' to 3' sequence)	Overhangs
Osbpl3 siRNA	AAG UUG GUU UCA CCU UCA ATT	dTdT
Scrambled siRNA	ACA GAC GGA GAC GCA CAC CTT	dTdT

Supplemental references

1. Duval, C., Thissen, U., Keshtkar, S., Accart, B., Stienstra, R., Boekschoten, M.V., Roskams, T., Kersten, S., and Muller, M. 2010. Adipose tissue dysfunction signals progression of hepatic steatosis towards nonalcoholic steatohepatitis in C57BL/6 mice. *Diabetes* 59:3181-3191.

2. Ahrens, M., Ammerpohl, O., von Schonfels, W., Kolarova, J., Bens, S., Itzel, T., Teufel, A., Herrmann, A., Brosch, M., Hinrichsen, H., et al. 2013. DNA methylation analysis in nonalcoholic fatty liver disease suggests distinct disease-specific and remodeling signatures after bariatric surgery. *Cell Metab* 18:296-302.

3. Wagner, B.L., Valledor, A.F., Shao, G., Daige, C.L., Bischoff, E.D., Petrowski, M., Jepsen, K., Baek, S.H., Heyman, R.A., Rosenfeld, M.G., et al. 2003. Promoter-

specific roles for liver X receptor/corepressor complexes in the regulation of ABCA1 and SREBP1 gene expression. *Mol Cell Biol* 23:5780-5789.

4. Cha, J.Y., and Repa, J.J. 2007. The liver X receptor (LXR) and hepatic lipogenesis. The carbohydrate-response element-binding protein is a target gene of LXR. *J Biol Chem* 282:743-751.

Title: Fasting-induced steatosis driven by loss of LRH-1 in the liver is rescued by SLC25A47

Authors: Vera Lemos[1,2], Norman Moullan[3], Alessia Perino[1], Tatjana Sajic[4], Pooja Jha[3], Veronica Jimenez[5], Ruedi Aebersold[4], Fatima Bosch[5], and Kristina Schoonjans[1]*

Affiliations:

[1]*Laboratory of Metabolic Signaling, Institute of Bioengineering, School of Life Sciences, Ecole Polytechnique Fédérale de Lausanne, CH-1015 Lausanne, Switzerland.*

[2]*Abel Salazar Biomedical Sciences Institute, University of Porto, PT-4050-313 Porto, Portugal.*

[3]*Laboratory of Integrative and Systems Physiology, Institute of Bioengineering, School of Life Sciences, Ecole Polytechnique Fédérale de Lausanne, CH-1015 Lausanne, Switzerland.*

[4]Department of Biology, Institute of Molecular Systems Biology, ETH Zurich, CH-8093, Zurich, Switzerland.

[5]*Center of Animal Biotechnology and Gene Therapy and Department of Biochemistry and Molecular Biology, School of Veterinary Medicine, Universitat Autònoma de Barcelona, Bellaterra, and Centro de Investigación Biomédica en Red de Diabetes y Enfermedades Metabólicas Asociadas (CIBERDEM), Barcelona, Spain.*

***Corresponding author:**

Kristina Schoonjans

Laboratory of Metabolic Signaling, Institute of Bioengineering, School of Life Sciences, Ecole Polytechnique Fédérale de Lausanne, CH-1015 Lausanne, Switzerland

Phone: +41 21 693 18 91; E-mail: kristina.schoonjans@epfl.ch.

Abstract

During fasting, adipose tissue-derived fatty acids overload the liver and activate pathways for their utilization and systemic re-distribution. When the oxidative capacity of the liver is compromised, fat builds up inside hepatocytes and the liver becomes steatotic. The nuclear receptor homolog-1 (LRH-1, NR5A2) is a pivotal regulator of hepatic intermediary metabolism, however, very little is known about its role in coordinating fasting-induced responses to coordinate fatty acid metabolism. Here, we have assessed the biological consequences of a loss of function of LRH-1 in livers subjected to an overnight fasting. Mice with a specific deletion of LRH-1 in hepatocytes (*Lrh-1* $^{hep-/-}$ mice) developed fasting-induced steatosis. This condition was accompanied by mitochondrial dysfunction with consequent reduction in fatty acid oxidation. Moreover, we observed that an as of yet uncharacterized liver-specific mitochondrial solute carrier (SLC25A47), is downregulated in *Lrh-1* $^{hep-/-}$ livers. These changes were attributed to direct transcriptional regulation of *Slc25a47* by LRH-1. Restoring *Slc25a47* expression in hepatocytes significantly improved mitochondrial function, increased fatty acid degradation, and rescued the steatotic phenotype of LRH-1 deficient livers. These findings suggest that LRH-1 is important for the coordination of nutritional responses in the liver and point to a putative role of SLC25A47 in fasting-induced mobilization of energy.

Conflict of interest statement

The authors declare that no conflict of interest exists.

Author Contributions

VL designed and carried out most of the experiments, data analysis, prepared the figures, and wrote the manuscript. NM helped with all the AAV8 injections. AP helped with the fresh tissue high-resolution respirometry. PJ performed the *ex vivo* lipolysis. TS and RA performed and analyzed the proteomics. VJ and FB designed and generated the AAV8 constructs. KS supervised all aspects of the work.

Acknowledgments

We thank T. Clerc, S. Bichet, A. Fouassier, R. Pasquettaz for technical help. VL was supported by a PhD grant from the Portuguese Foundation for Science and Technology (SFRH/BD/52046/2012) through the GABBA (Graduate Program in Basic and Applied Biology) PhD program. KS is supported by EPFL funding and a Sinergia grant from the SNSF (CRSII3_160798/1).

Figure legends

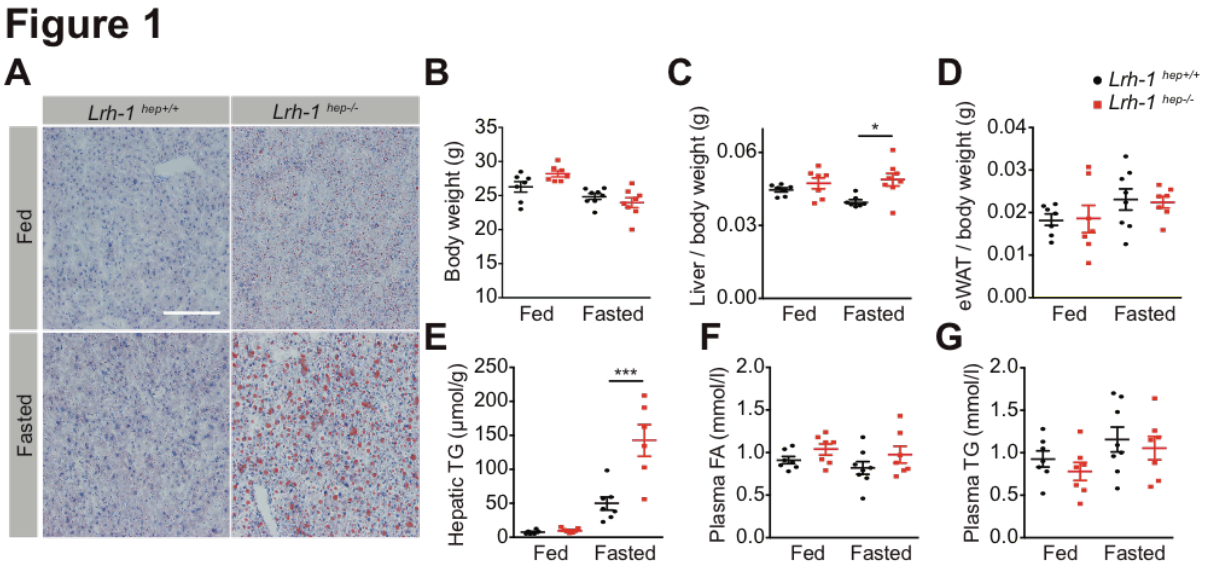

Figure 1. ***Lrh-1 $^{hep-/-}$ mice display fasting-induced steatosis.*** (**A**) Representative oil red O stainings of *Lrh-1 $^{hep+/+}$* and *Lrh-1 $^{hep-/-}$* mice in fed and fasted conditions to visualize neutral lipids. Scale bar: 200 µm. (**B**) Body weight of fed and fasted *Lrh-1 $^{hep+/+}$* and *Lrh-1 $^{hep-/-}$* mice. (**C**, **D**) Liver (**C**) and epididymal white adipose tissue (**D**) mass normalized to body weight of *Lrh-1 $^{hep+/+}$* and *Lrh-1 $^{hep-/-}$* mice in both fed and fasted conditions. (**E**) Quantification of hepatic triglyceride (TG) in lipid extracts of fed and fasted *Lrh-1 $^{hep+/+}$* and *Lrh-1 $^{hep-/-}$* mice. (**F**, **G**) Plasma free fatty acids (FA, **F**) and TG (**G**) levels in fed and fasted *Lrh-1 $^{hep+/+}$* and *Lrh-1 $^{hep-/-}$* mice. Error bars represent mean ± S.E.M. *p<0.05 and ***p<0.001 relative to *Lrh-1 $^{hep+/+}$* mice, as determined by one-way ANOVA with Bonferroni post-hoc test.

Figure 2

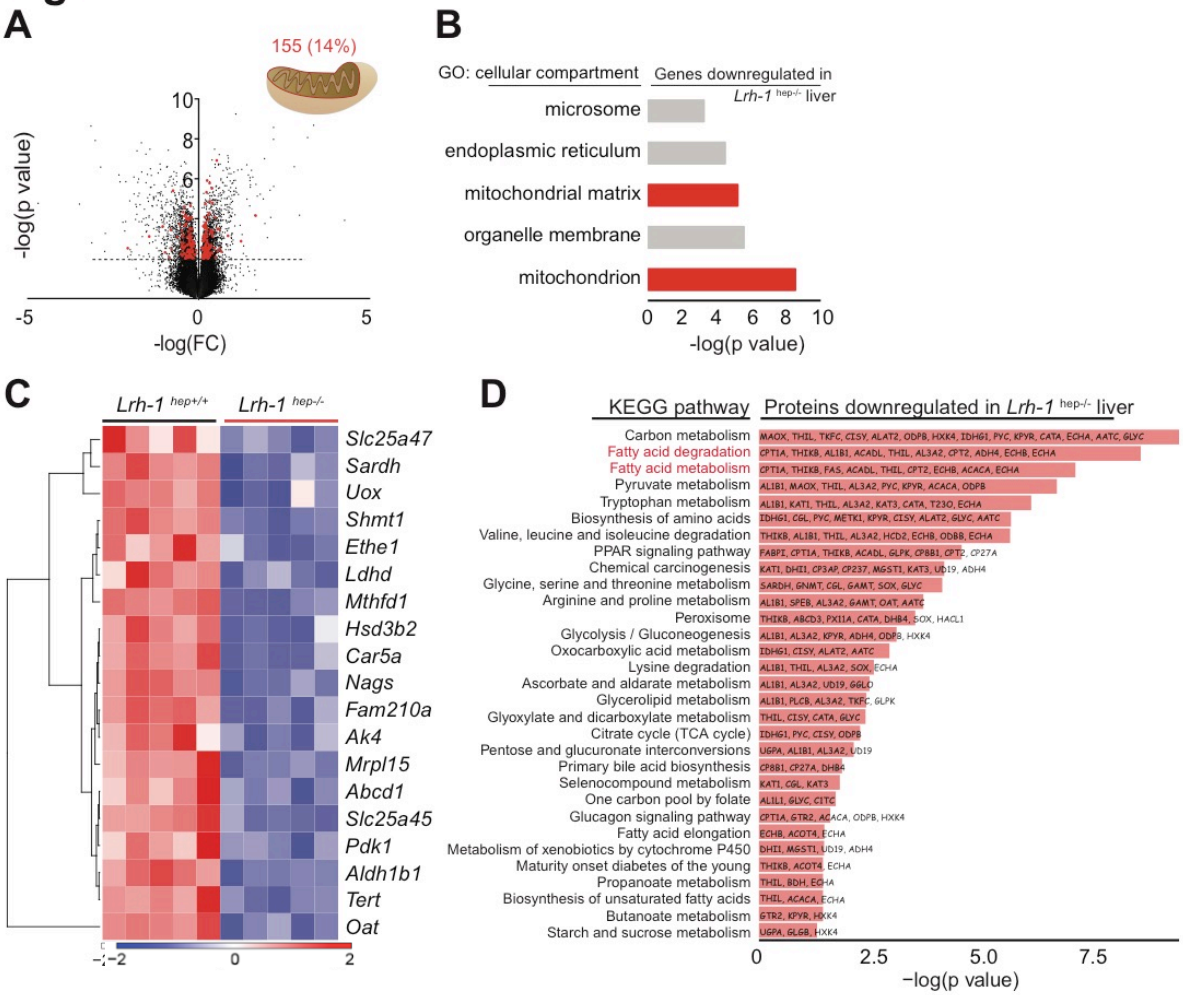

Figure 2. LRH-1 regulates mitochondrial transcripts. (**A**) Vulcano plot depicting in red the significant representation of mitochondrial transcripts among all genes in fasted *Lrh-1* $^{hep+/+}$ and *Lrh-1* $^{hep-/-}$ mice liver microarray. FC, fold change. (**B**) Gene ontology (GO, cellular compartment) of genes downregulated in livers from fasted *Lrh-1* $^{hep-/-}$ in comparison with *Lrh-1* $^{hep+/+}$ mice. (**C**) Heat map of the most significant downregulated mitochondrial genes (from **B**) in fasted *Lrh-1* $^{hep-/-}$ livers, FC > 1.4 (WT/KO) and $P< 1x10^4$. (**D**) Pathway enrichment analysis (KEGG) of proteins downregulated in *Lrh-1* $^{hep-/-}$ livers

Figure 3

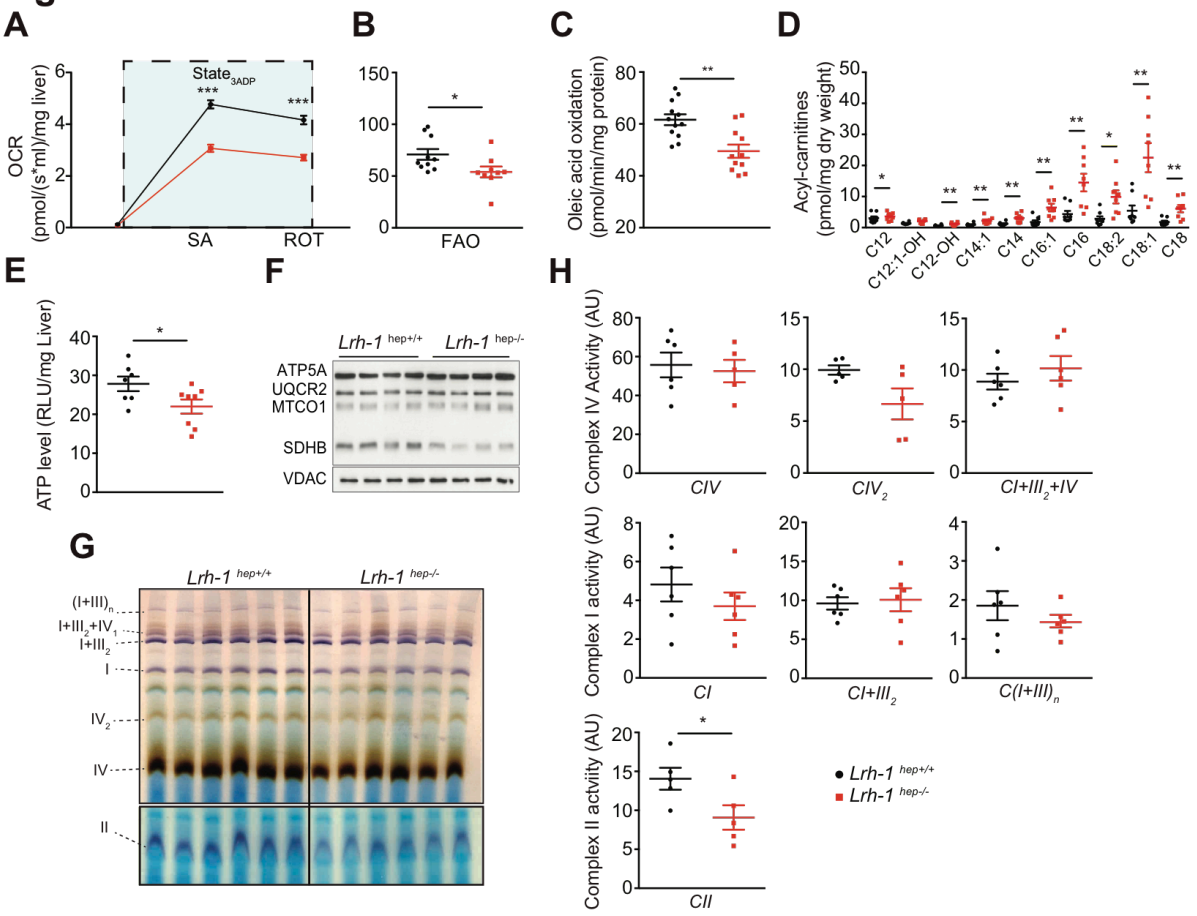

Figure 3. ***Lrh-1$^{hep-/-}$ mice present mitochondrial dysfunction.*** (**A**) Oxygen consumption rate (OCR) of fresh liver homogenates from fasted *Lrh-1* $^{hep+/+}$ and *Lrh-1* $^{hep-/-}$ mice by high-resolution respirometry in the presence of succinate, ADP (SA) and rotenone (ROT) – state$_{3ADP}$. (**B**) OCR of fresh liver homogenates from fasted *Lrh-1* $^{hep+/+}$ and *Lrh-1* $^{hep-/-}$ mice in the presence of fatty acid oxidation (FAO) substrates, palmitoyl- and octanolyl-carnitine, and ADP. (**C**) Oleic acid oxidation assay in the liver of fasted *Lrh-1* $^{hep+/+}$ and *Lrh-1* $^{hep-/-}$ mice. (**D**) Liver acyl-carnitines content in fasted *Lrh-1* $^{hep+/+}$ and *Lrh-1* $^{hep-/-}$ mice. (**E**) Hepatic ATP level of fasted *Lrh-1* $^{hep+/+}$ and *Lrh-1* $^{hep-/-}$ mice. (**F**) Immunoblots of mitochondrial complexes subunits ATP5A (CV), UQCRC2 (CIII), MTCO1 (CIV), SDHB (CII) and VDAC as a loading control in isolated mitochondria from fasted *Lrh-1* $^{hep+/+}$ and *Lrh-1* $^{hep-/-}$ livers. (**G**) *In-gel* activity of mitochondrial complexes (I, II and IV) from *Lrh-1* $^{hep+/+}$ and *Lrh-1* $^{hep-/-}$ fasted liver mitochondria. Complex I (purple); Complex IV (brown); complex II (blue). (**H**) Quantification of the bands in (**G**) normalized to coomassie blue staining bands. Error bars represent mean ± S.E.M. and *p<0.05, **p<0.01 relative to *Lrh-1* $^{hep+/+}$ mice, as determined by Student's t-test.

Figure 4

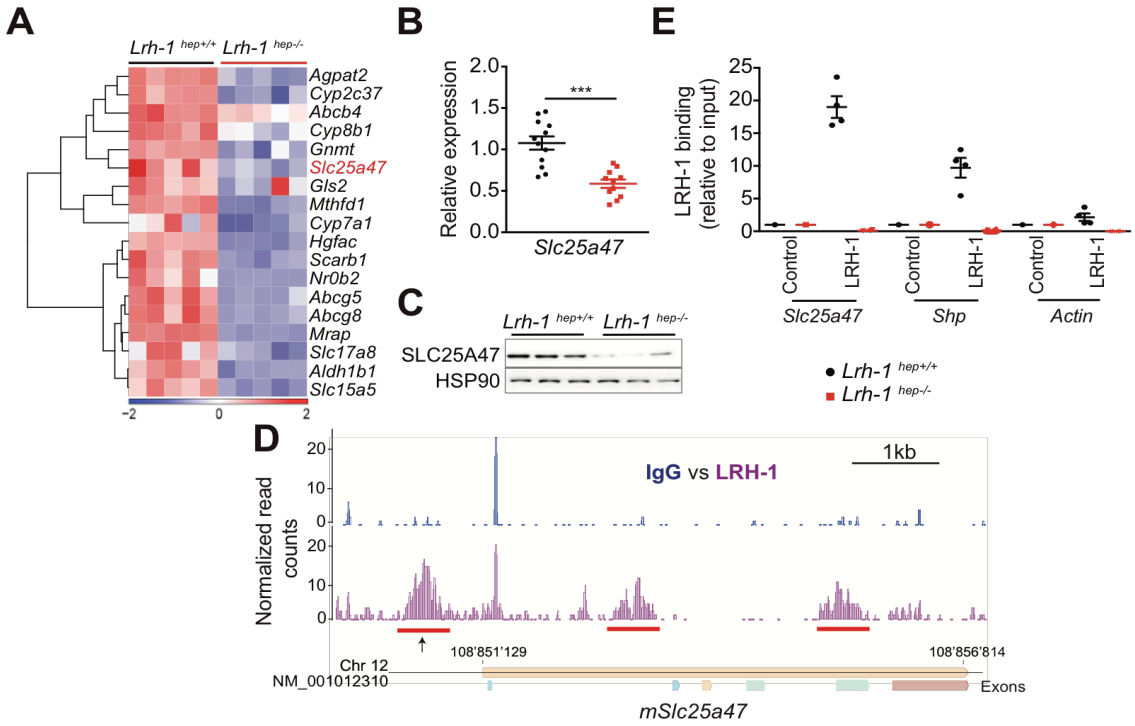

Figure 4. *Slc25a47* is a direct transcriptional target of LRH-1. (**A**) Heat map depicting LRH-1 target genes expression between fasted *Lrh-1* $^{hep+/+}$ and *Lrh-1* $^{hep-/-}$ livers. Normalized values are in log_2 scale. (**B**, **C**) *Slc25a47* gene (**B**) and protein (**C**) expression levels in the liver of fasted *Lrh-1* $^{hep+/+}$ and *Lrh-1* $^{hep-/-}$ mice. (**D**) University of California at Santa Cruz (UCSC) genome browser (mm9) view displaying the occupancy of mouse *Slc25a47* by LRH-1 and IgG. Significant peaks are underlined in red. (**E**) Binding of LRH-1 to *Slc25a47* promoter region as assessed by Chip analysis using genomic DNA from *Lrh-1* $^{hep+/+}$ and *Lrh-1* $^{hep-/-}$ livers. Error bars represent mean ± S.E.M. ***p<0.001 relative to *Lrh-1* $^{hep+/+}$ mice, as determined by student's t-test.

Figure 5

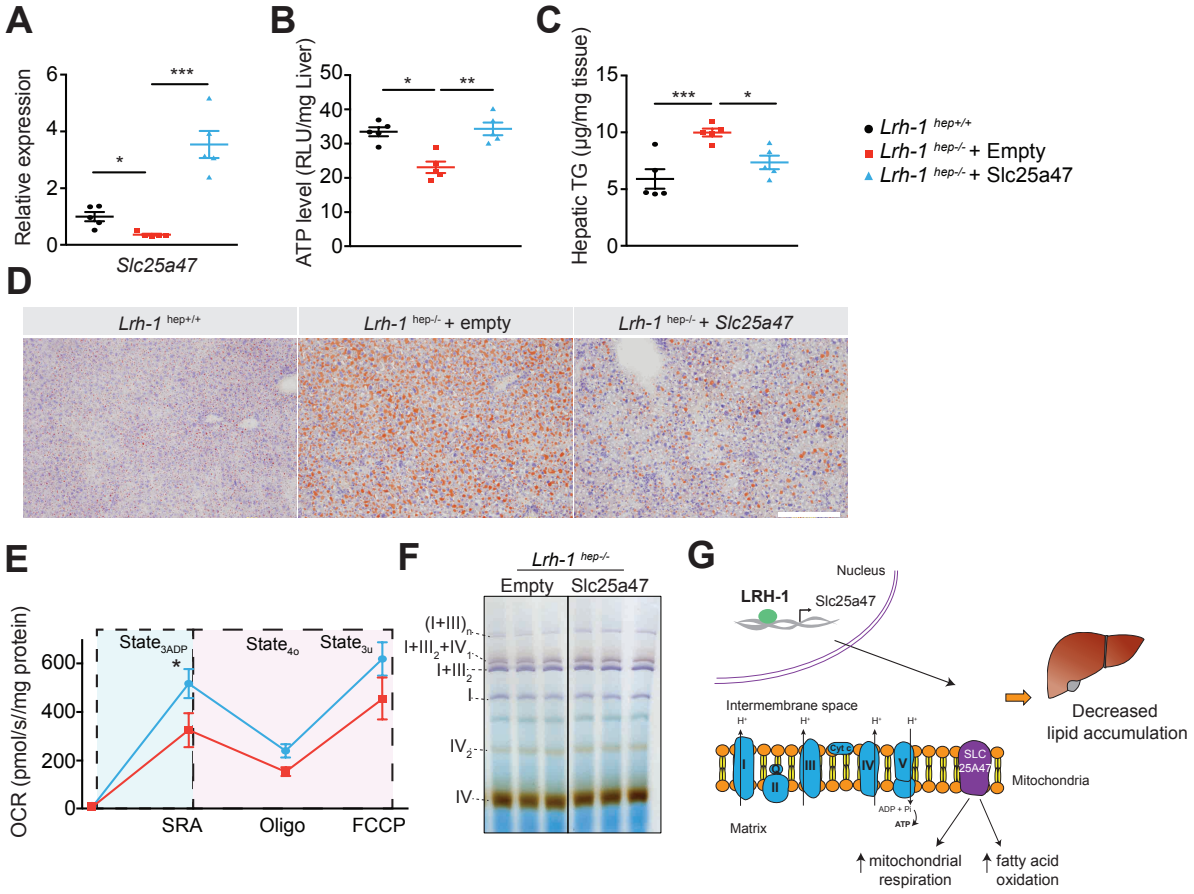

Figure 5. ***Slc25a47 rescues the steatotic phenotype of the Lrh-1$^{hep-/-}$ fasted livers.*** (**A**) Gene expression of *Slc25a47* in *Lrh-1* $^{hep+/+}$ and *Lrh-1* $^{hep-/-}$ mice transduced with AAV8-Empty or AAV8-Slc25a47. (**B**, **C**) Hepatic ATP level (**B**) and triglyceride (TG) content (**C**) in *Lrh-1* $^{hep+/+}$ and *Lrh-1* $^{hep-/-}$ mice transduced with AAV8-Empty or AAV8-Slc25a47. (**D**) Representative oil red O stainings in the liver of *Lrh-1* $^{hep+/+}$ and *Lrh-1* $^{hep-/-}$ mice transduced with AAV8-Empty or AAV8-Slc25a47. (**E**) Oxygen consumption rate (OCR) in liver mitochondria of *Lrh-1* $^{hep-/-}$ transduced with AAV8-Empty or AAV8-Slc25a47 by high-resolution respirometry in response to substrates (succinate, rotenone and ADP – SRA, State$_{3ADP}$), oligomycin (Oligo, State$_{4o}$) and the uncoupler carbonyl cyanide-4-(trifluoromethoxy)phenylhydrazone (FCCP, State$_{3u}$) in freshly isolated liver mitochondria from AAV8-empty and AAV8-Slc25a47 transduced *Lrh-1* $^{hep-/-}$ mice. (**F**) *In-gel* activity of mitochondrial complexes (I, II and IV) from *Lrh-1* $^{hep+/+}$ and *Lrh-1* $^{hep-/-}$ fasted liver mitochondria. Complex I (purple); Complex IV (brown). (**G**) Graphical presentation showing how LRH-1 regulates *Slc25a47* leading to normalization of lipid accumulation by enhancing the breakdown of fatty acids. Error bars represent mean ± S.E.M. *p<0.05, **p<0.01, and ***p<0.001 relative to *Lrh-1* $^{hep+/+}$ or *Lrh-1* $^{hep-/-}$ mice as indicated; determined by student's t-test.

Figure S1

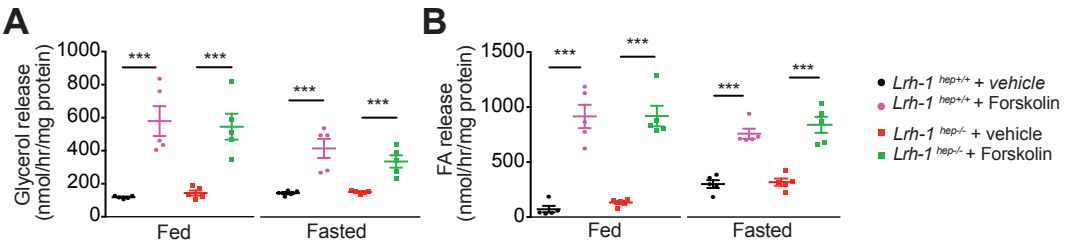

Figure S1. *Lrh-1* $^{hep-/-}$ mice do not present different white adipose tissue lipolysis rate. (**A**, **B**) Ex vivo lipolysis-associated glycerol (**A**) and free fatty acids (FA) (**B**) released from *Lrh-1* $^{hep+/+}$ and *Lrh-1* $^{hep-/-}$ white adipose tissue explants. Error bars represent mean ± S.E.M. ***p<0.001 relative to Forskolin-treated group.

Figure S2

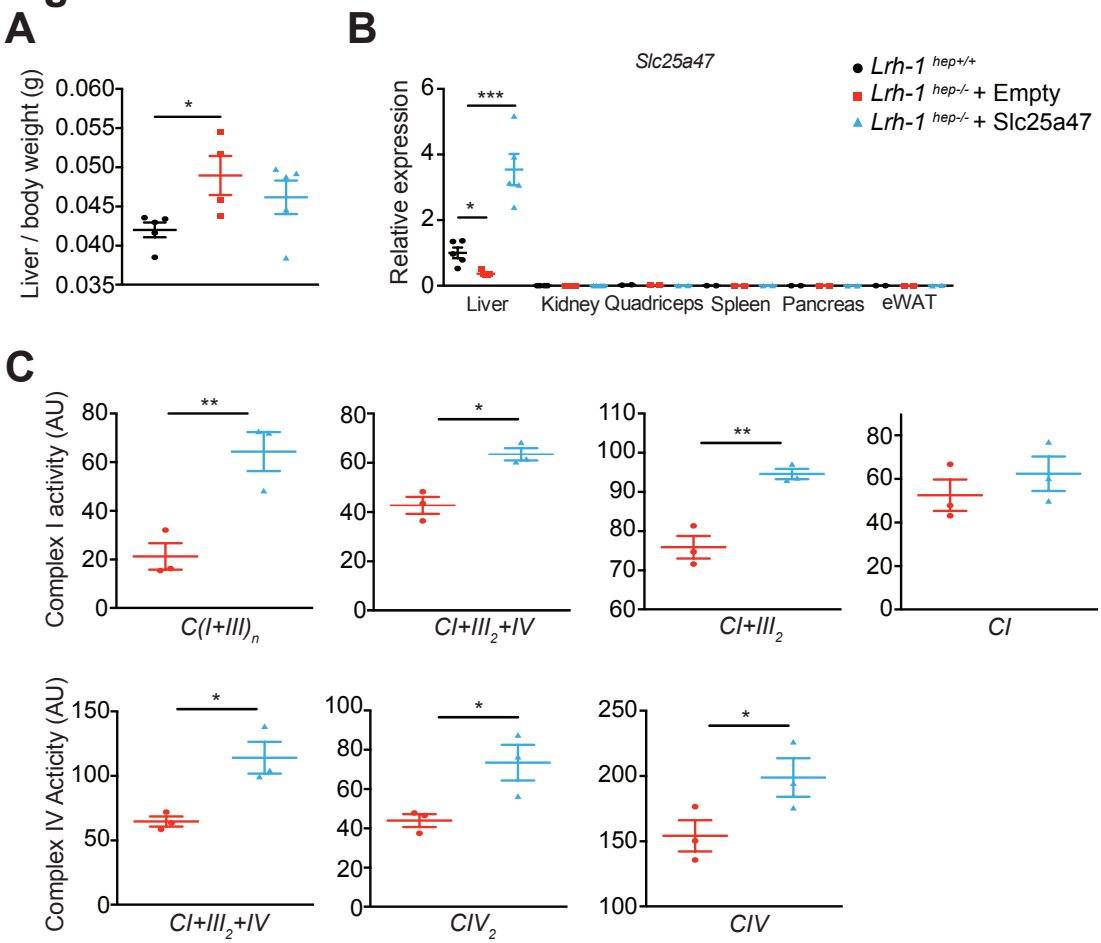

Figure S2. *Slc25a47*-overexpression in the liver of *Lrh-1* $^{hep-/-}$ mice increases mitochondrial complexes activity. (**A**) Gene expression of *Slc25a47* in *Lrh-1* $^{hep+/+}$ and *Lrh-1* $^{hep-/-}$ mice transduced with AAV8-Empty or AAV8-Slc25a47. (**B**) Liver weight of *Lrh-1* $^{hep+/+}$ and *Lrh-1* $^{hep-/-}$ mice transduced with AAV8-Empty or AAV8-Slc25a47. (**C**) Quantification of the bands in Figure 5G normalized by coomassie blue staining bands. Error bars represent mean ± S.E.M. *p<0.05, **p<0.01, ***p<0.001 relative to *Lrh-1* $^{hep/-}$ + AAV8-Empty.

Supplemental Table 1: Sequence of primers used

Gene	Forward (5' to 3' sequence)	Reverse (5' to 3' sequence)
36b4	AGATTCGGGATATGCTGTTGG	AAAGCCTGGAAGAAGGAGGTC
B2m	TTCTGGTGCTTGTCTCACTG	TATGTTCGGCTTCCCATTCT
Slc25a47	GGGCCATTGGAGGAGTCTG	CTCTTGACGATACGTGTCCCG
16S (gDNA)	CCGCAAGGGAAAGATGAAAGAC	TCGTTTGGTTTCGGGGTTTC
HK2 (gDNA)	GCCAGCCTCTCCTGATTTTAGTGT	GGGAACACAAAAGACCTCTTCTGG

Supplemental Table 2: Chip-qPCR primer sequences

Gene	Forward (5' to 3' sequence)	Reverse (5' to 3' sequence)
Slc25a47prom #1	CCAGATGTCACAAAGCCAGA	TCGCCCTGACAGTTTGTCTA
Slc25a47prom #2	CGAGGGGTCATCCCTAGTTT	CAGTTCAGGGGCTCAAAGAC

Title: Liver-specific mitochondrial carrier SLC25A47 enhances fatty acid oxidation and is downregulated in NAFLD

Authors: Vera Lemos[1,2], Norman Moullan[3], Alessia Perino[1], Nuria Cirauqui[4], Veronica Jimenez[5], Matteo Dal Peraro[4], Fatima Bosch[5], and Kristina Schoonjans[1]*

Affiliations:

[1]*Laboratory of Metabolic Signaling, Institute of Bioengineering, School of Life Sciences, Ecole Polytechnique Fédérale de Lausanne, CH-1015 Lausanne, Switzerland.*

[2]Abel Salazar Biomedical Sciences Institute, University of Porto, PT-4050-313 Porto, Portugal.

[3]*Laboratory of Integrative and Systems Physiology, Institute of Bioengineering, School of Life Sciences, Ecole Polytechnique Fédérale de Lausanne, CH-1015 Lausanne, Switzerland.*

[4]*Laboratory of Biomolecular Modeling, Institute of Bioengineering, School of Life Sciences, Ecole Polytechnique Fédérale de Lausanne, 1015 Lausanne, Switzerland.*

[5]*Center of Animal Biotechnology and Gene Therapy and Department of Biochemistry and Molecular Biology, School of Veterinary Medicine, Universitat Autònoma de Barcelona, Bellaterra, and Centro de Investigación Biomédica en Red de Diabetes y Enfermedades Metabólicas Asociadas (CIBERDEM), Barcelona, Spain.*

***Corresponding author:**

Kristina Schoonjans

Laboratory of Metabolic Signaling, Institute of Bioengineering, School of Life Sciences, Ecole Polytechnique Fédérale de Lausanne, CH-1015 Lausanne, Switzerland

Phone: +41 21 693 18 91; E-mail: kristina.schoonjans@epfl.ch.

Abstract

Mitochondria are the hub of intermediary metabolism. SLC25 family of mitochondrial transporters are the dictators of mitochondrial metabolic pathways by controlling almost all metabolites that go in and out of the mitochondria. Here, we have assessed the function of an uncharacterized SLC25 family member, SLC25A47, and evaluated its potential therapeutical role in a pathological condition such as nonalcoholic fatty liver disease (NAFLD). From all the members of the SLC25 family, SLC25A47 is the one that holds the highest expression in the liver and furthermore it is liver-specific. We found that SLC25A47 is significantly different in both sequence and structure from the closest members of the family, presenting a new loop in the matrix, possible site of regulation. Of note, SLC25A47 is induced upon fasting and correlates with fatty acid degradation. Increasing its expression *in vivo* by AAV8 transduction improves significantly mitochondrial function. Overexpression of SLC25A47 in the liver of a mouse model of NAFLD decreased lipid accumulation by enhancing mitochondrial fatty acid oxidation. Collectively, our study confirms the importance of SLC25 family by characterizing the function of SLC25A47 whose liver specificity strengthens it as a very relevant target for liver diseases such as NAFLD minimizing possible side effects.

Conflict of interest statement

The authors have declared that no conflict of interest exists.

Author Contributions

VL designed and carried out most of the experiments, data analysis, prepared the figures, and wrote the manuscript. NM helped with all the AAV8 injections. AP helped with the fresh tissue high-resolution respirometry. VJ and FB designed and generated the AAV8 constructs. NC and MDP performed the structural biology analysis. KS supervised all aspects of the work.

Acknowledgments

We thank T. Clerc, S. Bichet, A. Fouassier, R. Pasquettaz for technical help. VL was supported by a PhD grant from the Portuguese Foundation for Science and Technology (SFRH/BD/52046/2012) through the GABBA (Graduate Program in Basic and Applied Biology) PhD program. KS is supported by EPFL funding and a Sinergia grant from the SNSF (CRSII3_160798/1).

Figure legends

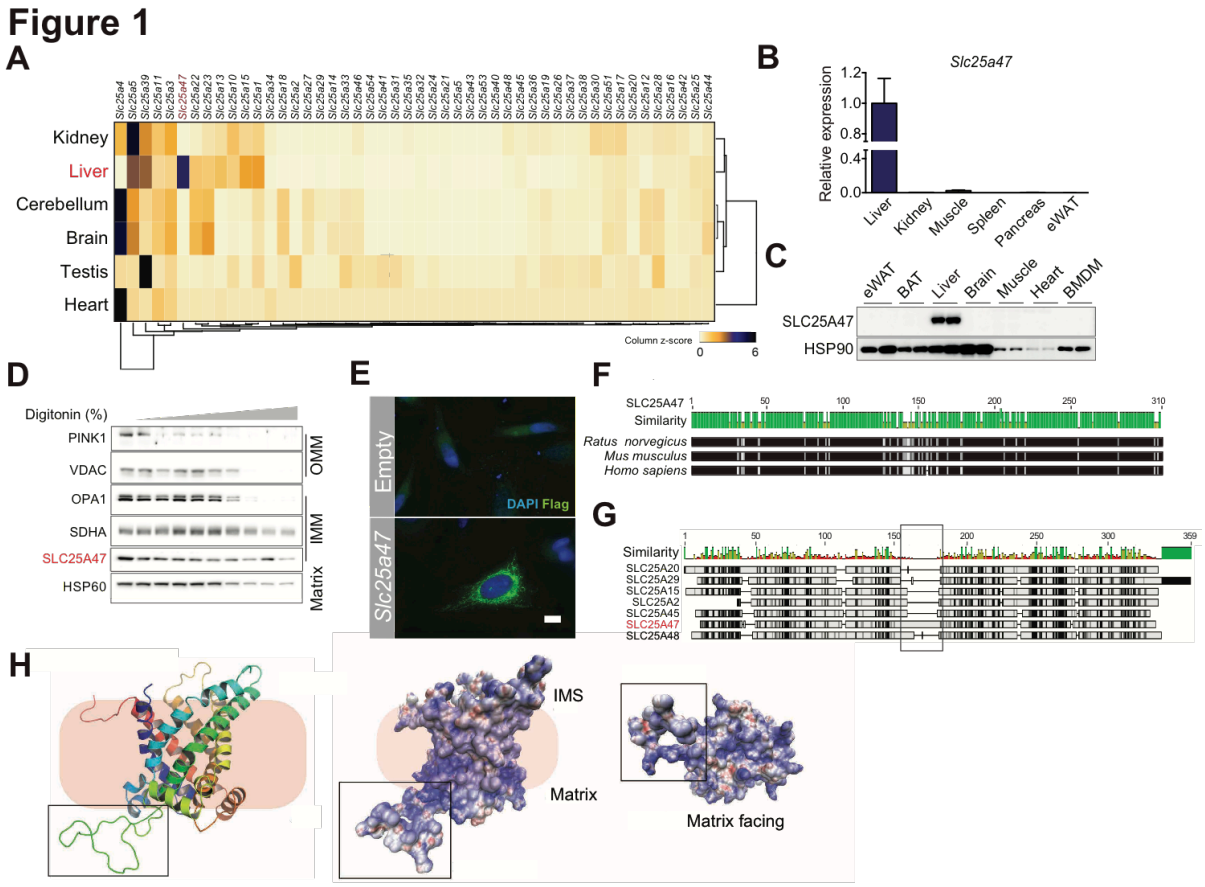

Figure 1. *Slc25a47* is a liver-specific mitochondrial inner membrane carrier. (**A**) Heat map depicting the relative mouse *Slc25* family transcripts abundance in heart, testis, brain, cerebellum, liver and kidney. (**B**, **C**) Expression level of *Slc25a47* transcript (**B**) and protein (**C**) levels in different mouse tissues. (**D**) Immunoblots of SLC25A47 in liver mitochondria lysates after permeabilization with increasing amount of digitonin. PINK1 and VDAC for the OMM, OPA1 and SDHA for the IMM and HSP60 for the matrix are used as controls. (**E**) FLAG immunofluorescence staining of alpha mouse liver 12 (AML12) cells overexpressing FLAG-tagged SLC25A47. DAPI is used to stain nuclei. Scale bar: 10 µm. (**F**, **G**) Protein alignment of SLC25A47 within species (**F**) and between SLC25A47 and its closest homologs (**G**). Similarity color code: green, high homology; red, low homology. (**H**) 3-D structure of SLC25A47 depicting the new loop. Color code of the amino acids charge (right panel): blue, positive; white, neutral; red, negative. Rectangle emphasizes the loop specific to SLC25A47. Error bars represent mean ± S.E.M.

Figure 2

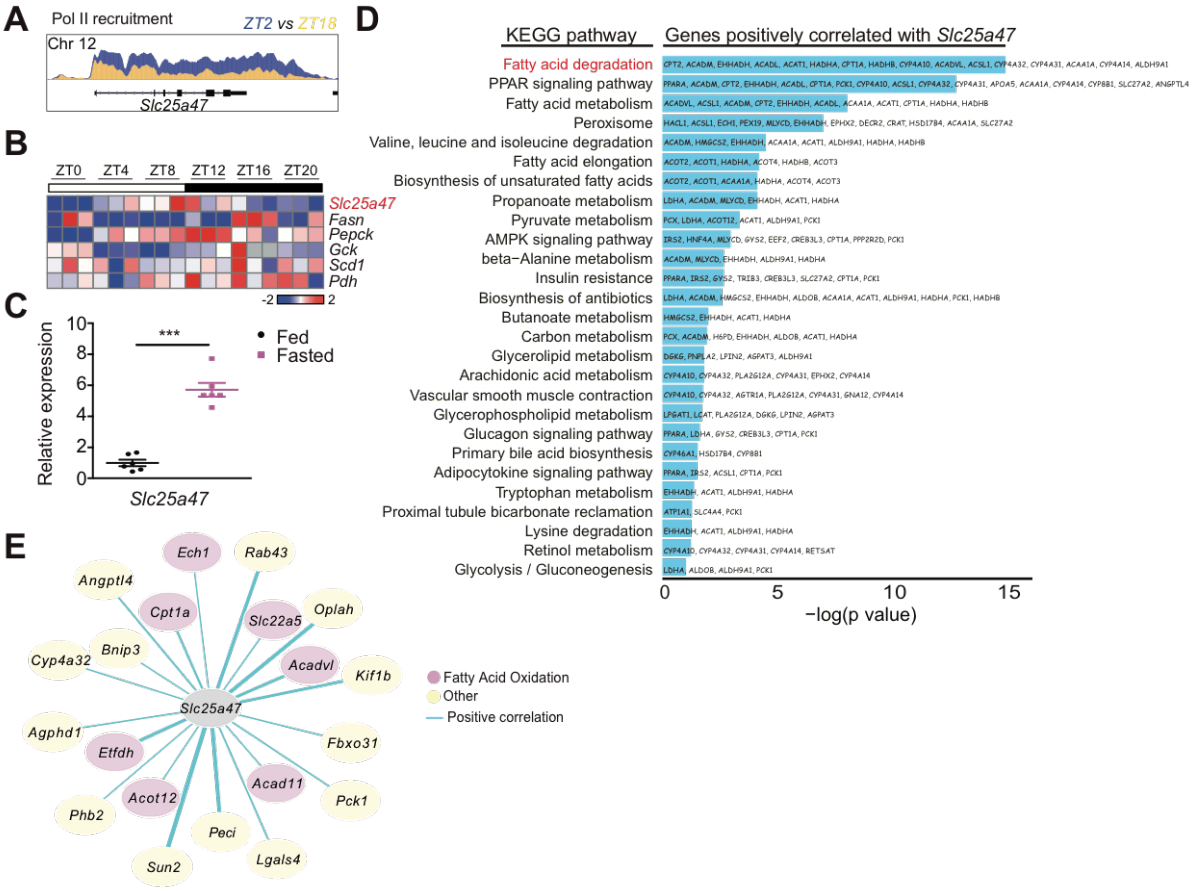

Figure 2. *Slc25a47* is induced upon fasting. (**A**) Representation of *Slc25a47* genomic area binding/occupancy by Pol II assessed by Chip-seq at ZT2 (9am) and ZT18 (1am). (**B**) Heat map displaying the expression of genes important under fed and fasted conditions during circadian rhythm. (**C**) Gene expression analysis of *Slc25a47* in the liver of fed and 24h-fasted mice (7am - 7am). (**D**) Pathway enrichment (KEGG) of genes positively correlating with *Slc25a47* in 42 BXD mouse strains. BXD mouse strains were fed CD and sacrificed under fasting conditions. (**E**) Correlation network (pearson's r) between *Slc25a47* and top 20 most significant positively correlating genes. Thickness of the line is associated with higher significance. Error bars represent mean ± S.E.M. ***p<0.001 relative to Fed condition, as determined by Student's t-test.

Figure 3

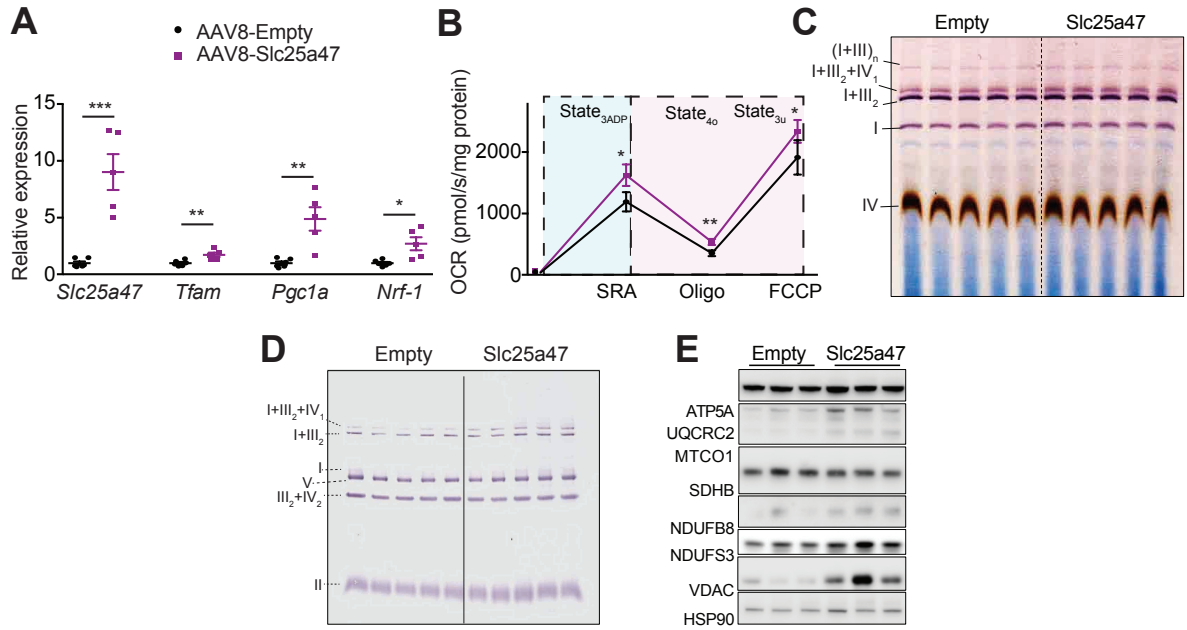

Figure 3. *Slc25a47* improves mitochondrial function *in vivo*. (**A**) Gene expression of mitochondria-related genes, *Tfam*, *Pgc1a*, *Nrf-1* in AAV8-Empty and AAV8-Slc25a47 transduced livers. (**B**) Oxygen consumption rate (OCR) in response to substrates (succinate, rotenone and ADP – SRA, State$_{3ADP}$), oligomycin (Oligo, State$_{4o}$) and the uncoupler carbonyl cyanide-4-(trifluoromethoxy)phenylhydrazone (FCCP, State$_{3u}$) in freshly isolated liver mitochondria from AAV8-Empty and AAV8-Slc25a47 transduced mice. (**C**) *In-gel* activity of mitochondrial complexes (CIV+CI) in AAV8-Empty and AAV8-Slc25a47 transduced liver mitochondria. CI activity (purple); CIV activity (brown). (**D**) Immunoblot of mitochondrial complexes after blue-native polyacrylamide gel electrophoresis (BN-PAGE) fasted AAV8-Empty and AAV8-Slc25a47 transduced liver mitochondria. (**E**) Immunoblots of mitochondrial complexes subunits ATP5A (CV), UQCR2 (CIII), MTCO1 (CIV), SDHB (CII), NDUFB8 and NDUFS3 (CI), and mitochondrial protein VDAC. HSP90 was used as loading control. Error bars represent mean ± S.E.M. *p<0.05, **p<0.01 and ***p<0.001, as determined by Student's t-test.

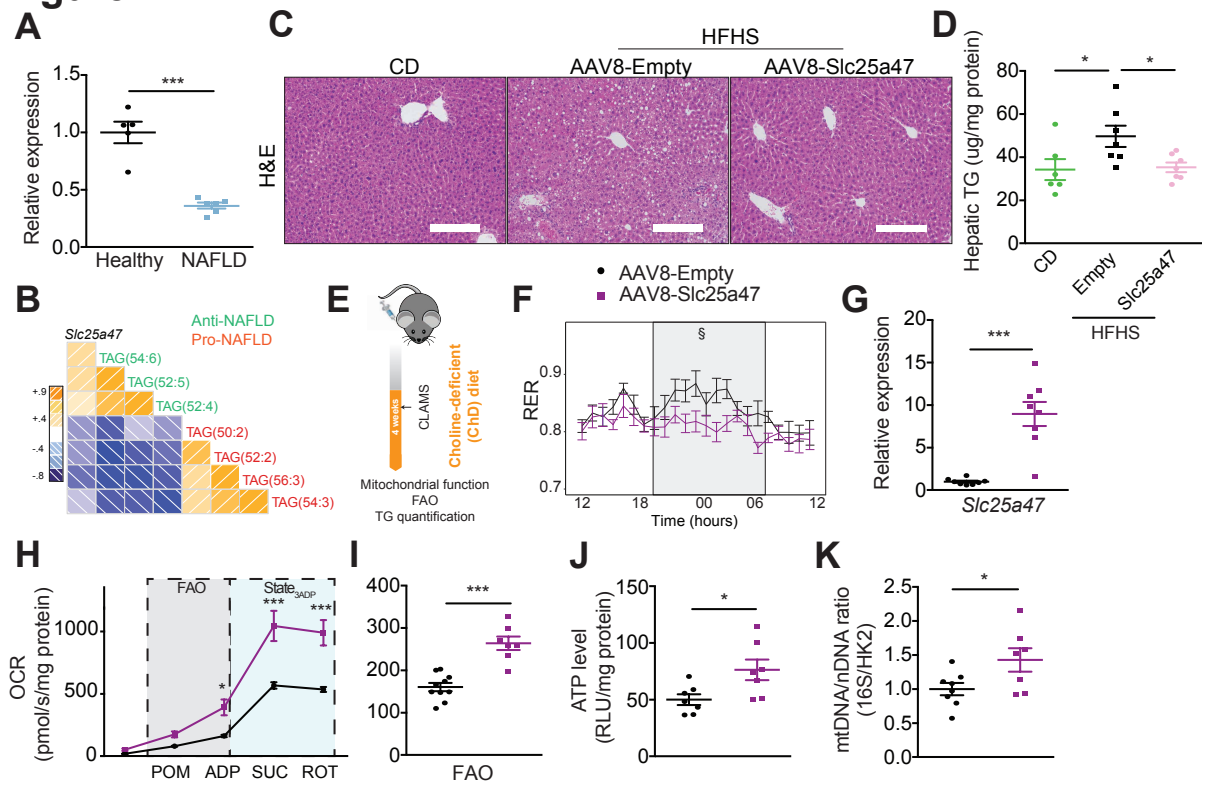

Figure 4. *Slc25a47* is downregulated in NAFLD and its recovery rescues hepatic steatosis. (**A**) Liver gene expression of *Slc25a47* in diet-induced NAFLD model (high-fat, high-sucrose diet – HFHS - for 18 weeks). Mice fed a chow diet are depicted as "healthy". (**B**) Corrgram (pearson's r) of *Slc25a47* with hepatic lipid species assigned as anti-NAFLD and pro-NAFLD markers. (**C**) Representative images of liver sections of AAV8-Empty and AAV8-Slc25a47 transduced mice fed HFHS for 7 weeks stained with hematoxylin and eosin (H&E) to visualize tissue structure. Scale bar: 200 µm. (**D**) Hepatic triglyceride (TG) content of HFHS-fed AAV8-Empty and AAV8-Slc25a47 transduced mice. (**E**) Scheme demonstrating experimental design for AAV8-Empty and AAV8-Slc25a47 *in vivo* transduction in mice fed choline-deficient diet (ChD) for 4 weeks. (**F**) Respiratory exchange ratio (RER) measured through indirect calorimetry (24h) in ChD-fed AAV8-Empty and AAV8-Slc25a47 transduced mice. (**G**) Hepatic mRNA expression of *Slc25a47* in ChD-fed AAV8-Empty and AAV8-Slc25a47 transduced mice. (**H**) Oxygen consumption rate (OCR) of fresh liver homogenates from ChD- AAV8-Empty and AAV8-Slc25a47 transduced mice. Fatty acid oxidation (FAO) substrates (palmitoyl-, octanoyl-carnitine with malate - POM) were added in the presence of ADP, followed by succinate (SUC) and rotenone (ROT) to achieve State$_{3ADP}$. (**I**) Quantification of FAO-driven respiration assessed in (**H**). (**J**) Hepatic ATP level of ChD-fed AAV8-Empty and AAV8-Slc25a47 transduced mice. (**K**) Hepatic mtDNA/nDNA (16S/HK2) ratio of ChD-fed AAV8-Empty and AAV8-Slc25a47 transduced mice. Error bars represent mean ± S.E.M. *p<0.05 and ***p<0.001 relative AAV8-Empty, as determined by Student's *t*-test. §adjusted p-value<0.05, relative to the night period.

Figure S1

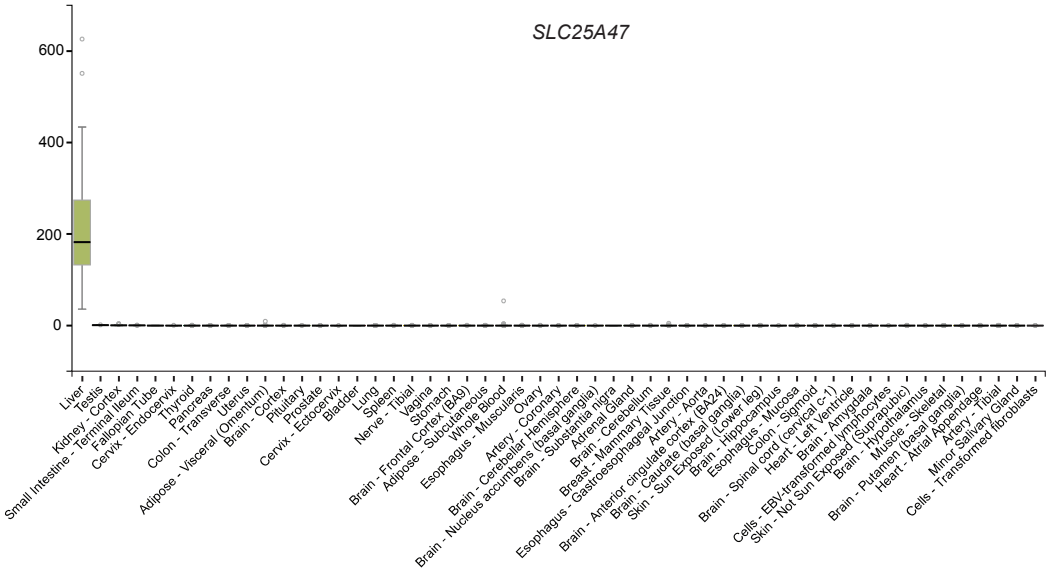

Figure S1. *SLC25A47* is a liver-specific mitochondrial carrier also in humans. Human tissue expression profile of *SLC25A47* from https://www.gtexportal.org/home/.

Figure S2

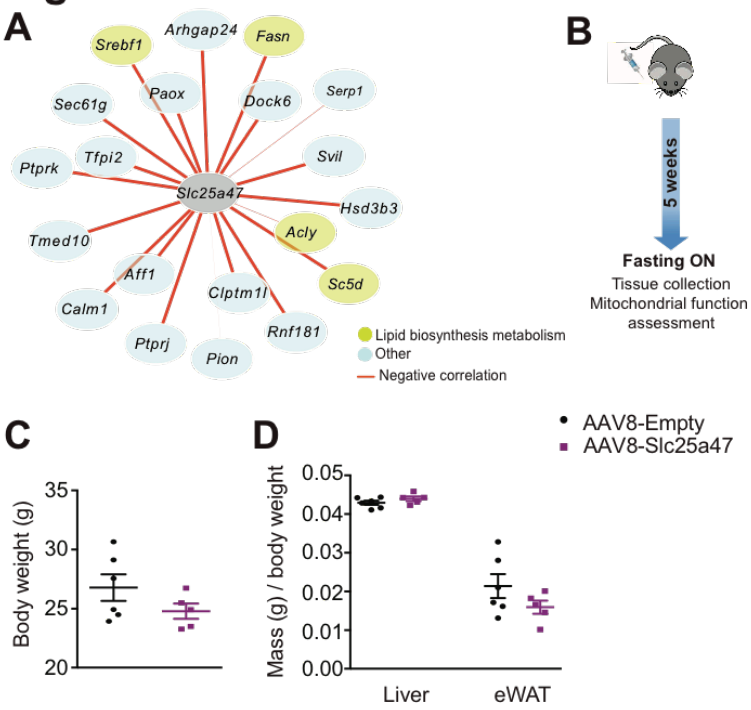

Figure S2. *Slc25a47* is conserved between species and increases mitochondrial complexes expression. (**A**) Correlation network (pearson's r) between *Slc25a47* and top 20 most significant negatively correlating genes found in BXD mouse strains liver microarray. Thickness of the line is associated with higher significance. (**B**) Scheme showing experimental design for *in vivo* AAV8-mediated gain-of-function of SLC25A47 in mice. (**C**, **D**) No changes in body weight (**C**) as well as liver and epididymal white adipose tissue (eWAT) mass (**D**) of fasted AAV8-Empty and AAV8-Slc25a47 transduced mice. Error bars represent mean ± S.E.M.

Figure S3

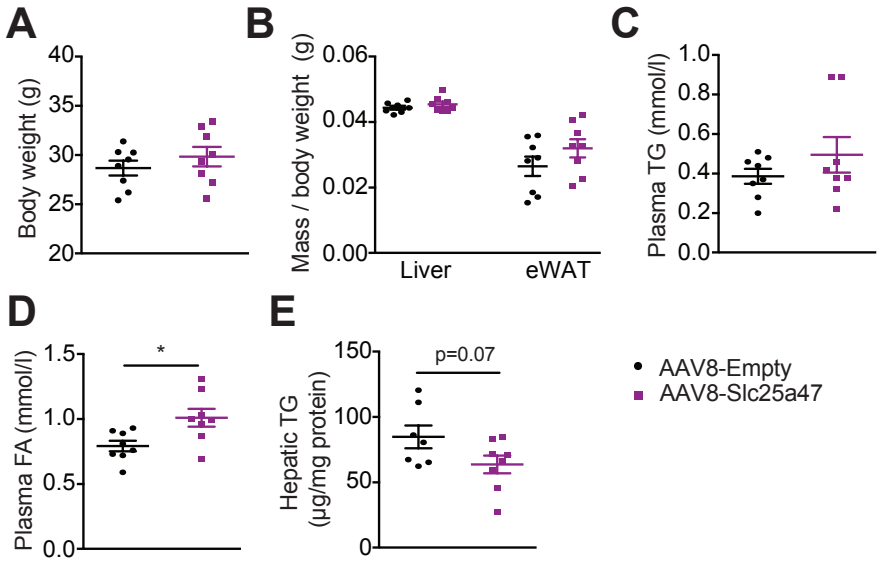

Figure S3. Overexpression of *Slc25a47* in the liver doesn't affect body mass. (**A**, **B**) Body weight (**A**) and liver and epididymal white adipose tissue (eWAT) mass (**B**) in choline-deficient diet (ChD)-fed AAV8-Empty and AAV8-Slc25a47 transduced mice. (**C**, **D**) Plasma triglyceride (TG, **C**) and free fatty acids (FA, **D**) content in ChD-fed AAV8-Empty and AAV8-Slc25a47 transduced mice. (**E**) Hepatic triglyceride (TG) content of ChD-fed AAV8-Empty and AAV8-Slc25a47 transduced mice. Error bars represent mean ± S.E.M. *p<0.05 relative to AAV8-Empty.

Supplemental Table 1: Sequence of primers used

Gene	Forward (5' to 3' sequence)	Reverse (5' to 3' sequence)
36b4	AGATTCGGGATATGCTGTTGG	AAAGCCTGGAAGAAGGAGGTC
B2m	TTCTGGTGCTTGTCTCACTG	TATGTTCGGCTTCCCATTCT
Slc25a47	GGGCCATTGGAGGAGTCTG	CTCTTGACGATACGTGTCCCG
Tfam	AAGTGTTTTTCCAGCATGGG	GGCTGCAATTTTCCTAACCA
Pgc1a	AGCCGTGACCACTGACAACGAG	GCTGCATGGTTCTGAGTGCTAAG
Nrf-1	CGGAGTGACCCAAACTGAAC	TGCCGTGGAGTTGAGGATGT
16S (gDNA)	CCGCAAGGGAAAGATGAAAGAC	TCGTTTGGTTTCGGGGTTTC
HK2 (gDNA)	GCCAGCCTCTCCTGATTTTAGTGT	GGGAACACAAAAGACCTCTTCTGG